Faculty of Science and Engineering

WA School of Mines: Minerals, Energy and Chemical Engineering

Computational fluid dynamics-based evaluation and optimisation of feed spacer design parameters for reverse osmosis membrane modules

Omid Kavianipour

This thesis is presented for the Degree of
Doctor of Philosophy
of
Curtin University

January 2023

Declaration

To the best of my knowledge and belief:

- This thesis has been substantially accomplished during enrolment in the degree.
- This thesis does not contain material which has been accepted for the award of any other degree or diploma in my name, in any university or other tertiary institution.
- No part of this work will, in the future, be used in a submission in my name, for any other degree or diploma in any university or other tertiary institution without the prior approval of Curtin University.
- This thesis does not contain any material previously published or written by another person, except where due reference has been made in the text.
- This thesis contains some parts that has been published and/or prepared for publication.

Signature :

Date :

Authorship Declaration: Co-Authored Publications

This thesis contains the following works, arising from this research that were co-authored by my supervisors, and have been published or submitted for publication:

Details of the work: **Investigation into the effectiveness of feed spacer configurations for Reverse Osmosis membrane modules using Computational Fluid Dynamics** Kavianipour, O., Ingram, G. D., Vuthaluru, H. B. Published by Elsevier in the *Journal of Membrane Science* 525, 156-171 and online on 20 December 2016 at https://doi.org/10.1016/j.memsci.2016.12.034
Location in thesis: Chapter 4

Details of the work: **Studies into the mass transfer and energy consumption of commercial feed spacers for RO membrane modules using CFD: Effectiveness of performance measures** Kavianipour, O., Ingram, G. D., Vuthaluru, H. B. Published by Elsevier in the *Chemical Engineering Research and Design* 141, 328-338 and online on 6 November 2018 at https://doi.org/10.1016/j.cherd.2018.10.041
Location in thesis: Chapter 5

Details of the work: **A detailed approach for the analysis and prediction of SWM feed spacer performance based on CFD results** Kavianipour, O., Ingram, G. D., Vuthaluru, H. B. Submitted to *Chemical Engineering Science* and currently under review for publication.
Location in thesis: Chapter 6

Publications

These publications derived from this research:

Kavianipour, O., Ingram, G. D., Vuthaluru, H. B., *Investigation into the effectiveness of feed spacer configurations for reverse osmosis membrane modules using Computational Fluid Dynamics.* Journal of Membrane Science 2017; 526:156–171.

Kavianipour, O., Ingram, G. D., Vuthaluru, H. B., *Studies into the mass transfer and energy consumption of commercial feed spacers for RO membrane modules using CFD: Effectiveness of performance measures.* Chemical Engineering Research and Design. 2019; 141:328–338.

Kavianipour, O., Ingram, G. D., Vuthaluru, H. B., *A detailed approach for the analysis and prediction of SWM feed spacer performance based on CFD results*. Submitted to Desalination, currently under review.

Conference presentation:

Kavianipour, O., Ingram, G. D., Vuthaluru, H. B., *Novel approach for effectiveness prediction of feed spacer configurations for RO modules*. Oral presentation in 3rd International Conference on Desalination using Membrane Technology 2017

Acknowledgements

I would like to acknowledge and express appreciation for all the help and support that made it possible for me to produce this thesis. I shall begin with expressing my sincere gratitude to my supervisors, Associate Professor Hari Vuthaluru and Dr Gordon Ingram, who provided me with invaluable guidance and suggestions, and led me through this course with absolute patience.

I also would like to express my heartfelt gratitude to some very special people, Mohammad Ali Faripour, and Professor Fattola Farhadi, who taught and encouraged me to be curious, and my beloved parents, for their eternal and unconditional love.

This research is supported by an Australian Government Research Training Program (RTP) Scholarship. I would also like to acknowledge Curtin University and Western Australian School of Mines for providing me with research scholarships that helped me to focus on my research, and the Pawsey Supercomputing Research Centre (with funding from the Australian Government and the Government of Western Australia), for providing an extensive allocation on their supercomputing facilities that allowed me to run my CFD model, within a practical timeframe.

I would like to acknowledge the help that I received from Dr Kayt Davis for proof-reading and improving the language, completeness, and consistency of this thesis.

And last, but not least, I also would like to specially thank my own family for their support and endless love throughout this course.

Abstract

Reverse osmosis (RO) is one of the methods available for water desalination, in a world experiencing worsening water scarcity. However, similar to other membrane operations, it presents challenges including the need for frequent maintenance operations to address material build-up and rejuvenate the membrane surfaces. There are different possible preventive methods available to reduce the need for membrane maintenance, such as enhanced feed pre-treatment or improvement in membrane properties. Another alternative method is to manipulate the fluid's flow patterns on the feed side to reduce the tendency for scale build-up.

From the early years of conceptual development of RO desalination units, flow promoters, or as they have been named more recently, feed spacers, have been put in place to serve that purpose, as well as improving mass transfer and the permeation rate.

A review of the literature on the topic uncovered numerous studies focusing on feed spacers, aiming to evaluate and compare their performance through a variety of measures, and to optimise design parameters, such as filament size, the gap between filaments, and the angle of attack. Other research has studied the impact of manufacturing imperfections on spacer performance and assessed the result of using different filament shapes and arrangements.

In addition, several models were introduced for estimating the performance of feed spacers and the economics of RO units, based on research results. However, these were mainly developed from the researchers' own data sets. Questions about the validity of their assumptions and their choices of configurations restrict the extent to which these models can be reused, and in most cases attempts to increase the accuracy of these models has led to the development of more complex models with more parameters and stricter limits on their application. Overall, this body of research has revealed that more complicated mathematical models are more beneficial for calculation purposes, but less practical to help us to understand the logic behind the numbers.

The main objective of this thesis is to investigate the impact of changing selected parameters on feed spacer performance, to look for possible trends and correlations, and to explain the observed patterns, in order to enhance the understanding of feed spacers in RO modules.

To achieve this goal, different ANSYS modules were used to develop a three-dimensional Computational Fluid Dynamics (CFD) model, which showed good agreement with previous experimental and numerical results. The model was then used to simulate various cases and

predict the hydrodynamic and mass transport behaviour in the spacer-filled feed channels of RO desalination units.

In the present work, nineteen geometries were considered: four commercial spacers, designated 45-PP, 60-PP, 90-PP, and 90-HDPE, and five non-commercial spacers, termed Submerged, Ladder, Triple, Wavy, and Woven, with three filament gap sizes for each non-commercial spacer (3.6 mm, 4.1 mm, and 4.6 mm), and for six Reynolds number (Re) values (25, 50, 75, 100, 150, and 200) for each geometry.

The results were used to investigate the impact of changing parameters on the spacer performance, and CFD post-processing was used to visualise the flow patterns inside the feed channel. In addition, MATLAB was used to investigate the correlation between spacer parameters and spacer performance, and to generate equations to predict spacer performance over a range of flowrates.

Most of the studied performance measures – all, except spacer performance ratio (SPMP) – showed a strong correlation with Re through a power-law equation – with R^2 values higher than 0.974 for Sherwood number (Sh) and 0.999 for pressure drop per unit length ($\Delta P/L$), power number (Pn), Specific Power Consumption (SPC), and Spacer Configuration Efficacy (SCE). For all the spacers and throughout the range of flowrates studied, increasing the flowrate resulted in a stronger response in power-related measures (pressure drop, power number and SPC) compared to Sh. This was also seen in the negative exponents of the SCE equations.

For all performance measures, the equation parameters were affected by the spacer configuration. However, this study did not find any correlation between the power-law equation parameters, namely the coefficient and exponent, and the spacers' geometrical parameters of porosity and characteristic length (hydraulic diameter divided by cell length) for any of the four equation types studied (linear, exponential, logarithmic, and power-law).

This study showed that selecting the best-performing spacer is not only related to the performance measure selected for comparison, but is also affected by other operational parameters, like flowrate and the concentration of salt in the feed stream. In addition, the performance of the feed spacer is heavily connected to the operational parameters and any change in feed conditions could affect the unit's performance, which emphasises the practical importance of frequent and regular optimisation. As an example, the following figures compare the spacer ranking (higher is better) for nine spacers (four commercial spacers, and five non-commercial spacers with a gap of 4.1 mm) using five performance measures ($\Delta P/L$, SPC, Pn,

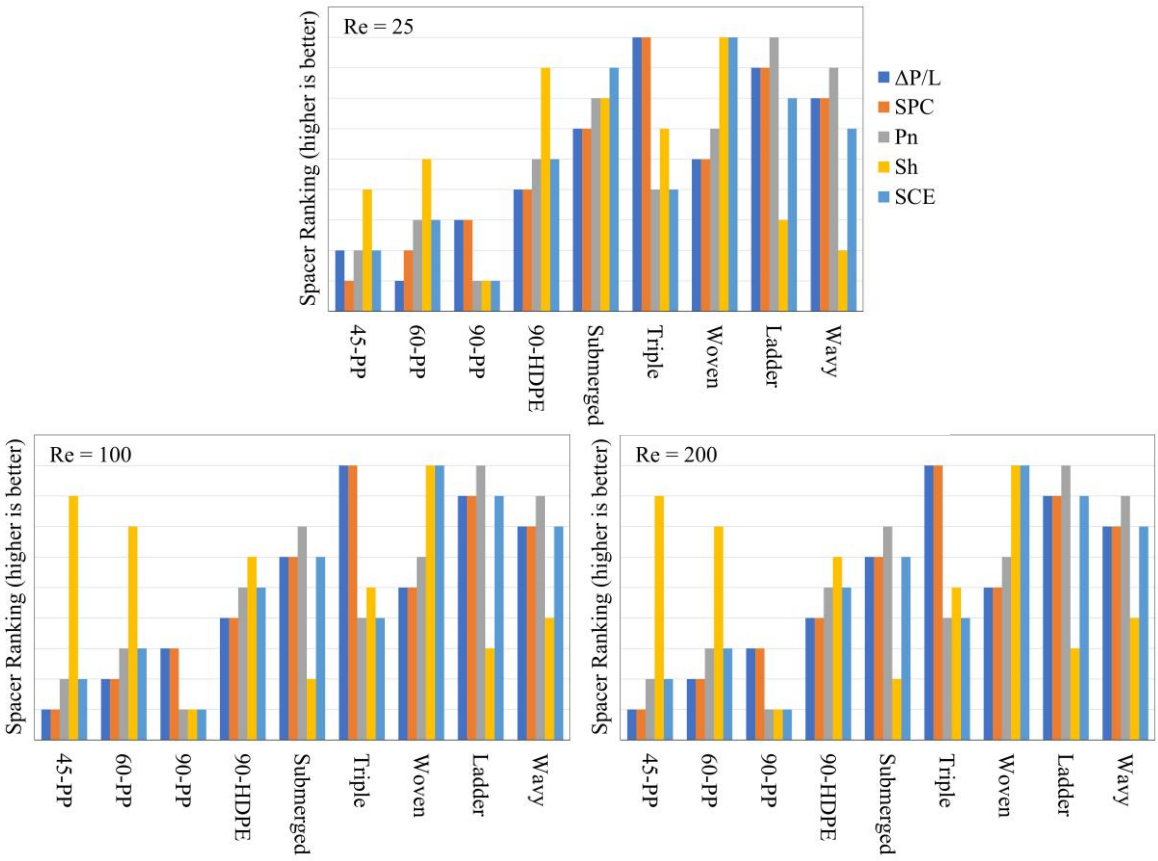

Sh, and SCE), and for three Re values (25, 100 and 200). There is no consistent agreement between the measures, which makes selecting the best spacer a matter of deciding which performance measure to use. In addition, it is clear that the best-performing spacer at the design flowrate is not necessarily performing the best at any other flowrate.

Considering SCE as the chosen performance measure, the results indicate that the Woven configuration has the best performance among the nineteen spacers studied, with Ladder and Wavy as runners-up, both having about 33% lower SCE values.

This study also revealed the impact and importance of secondary flows in enhancing mass transfer and the shear stress at the membrane, which is an important indicator of fouling tendency. The secondary flows were divided into three categories, namely, backwash (normally appearing after latitudinal filaments), forward-wash (normally appearing before latitudinal filaments), and side-wash (normally appearing before and after latitudinal filaments when the spacer's longitudinal filaments are sinusoidal). The backwash streams have a notable impact on the performance of Triple, Ladder, Wavy and Woven configurations, and the role of forward-washing is significant in Submerged, Ladder and Wavy. However, the presence of all three types in Wavy and Woven configurations, and the stronger side-wash streams in Woven could be the key, not only to explain the better performance of Woven, but also to understand and justify the changes in equation parameters for different filament gap sizes.

Table of Contents

List of Figures

List of Tables

Chapter 1. Introduction

1.1 Background

In the current world, human demand for fresh water is growing, but only 3% of the world's water is fresh water, and 5/6 of that fresh water is frozen and locked up in Antarctica, the Arctic, and glaciers, thus inaccessible to human beings. That leaves just 0.5% of the planet's water fresh and available, but not all of it is located in the places where it is needed (1, 2).

Drawing on the other 97% of the planet's water, the seawater, to address the demand for fresh water is another option. However, addressing the need for more fresh water by using seawater through available desalination technologies leads to a major challenge: energy demand, which is responsible for more than half of the operational costs of desalination (3).

Over the last century, human demand for water grew by a factor of six and is expected to grow further by about 1% per year for next three decades. In addition to that, it is predicted that climate change will intensify the water scarcity by 2050 (4).

Growing needs for water and higher levels of water scarcity are driving demand for desalination plants. By the February 2020, the world's installed desalination capacity was about 97.2 million m^3/day showing a growth rate of 6.8% p.a. through 2010-2019. A further 17.7 million m^3/day of already contracted desalination projects demonstrates the continuity and steadiness of the industry expansion (5).

1.2 Water desalination technologies

Desalination is the process of separating dissolved impurities from water sources to a level that makes it match the expected requirements for that purpose (e.g., for potable water). Water desalination can proceed by thermal-based or membrane-based methods (6).

In the thermal-based method, a phase change is essential, as the phase interface provides a selective barrier which limits impurities from progressing forward. Thermal-based desalination uses a simple process of evaporation-condensation, or sometimes freezing-melting, but as the phase change enthalpy (energy requirement) of water is significant – at 2257 kJ/kg vaporisation enthalpy and 333.5 kJ/kg for fusion enthalpy, both at standard pressure (7) – other desalination methods have been developed in order to increase the efficiency of the process, or use lower-valued forms of energy, like recoverable waste heat sources.

For instance, multi-effect desalination (MED) and multi-stage flash (MSF) methods employ multiple stages that are arranged in series configuration and the pressure of each stage is less than its predecessor and more than its successor. This translates to a gradual decrease in the water's boiling point, while it proceeds through the stages. This gradient in boiling temperature is the essential key of MED and MSF operations. Every stage in the process includes an evaporation and a condensation step and the gradient in boiling temperature allows the use of one stage's condensate as the energy source for boiling in the next stage (6).

In small-scale units, mechanical vapour compression (MVC) and thermal vapour compression (TVC) methods can be employed. These processes use the hot compressed vapour extracted from the unit as the source of heat for the initial evaporation. These methods can be used in conjunction with MED, MSF or as just a single-stage evaporating unit. Other main alternative thermal-based methods are those that using solar energy for initial evaporation or co-generation concepts (6).

In co-generation, the desalination plant is coupled with a power plant (most commonly a closed-cycle steam power plant using once-through seawater as the heat sink). In this concept, medium pressure steam from a high-pressure turbine's output, or extracted from the middle stages of a turbine, can be used as the heat source for initial evaporation. In addition to that, the seawater stream returning to the sea, which is already warmed up after condensing the low pressure steam, can be used as desalination plant's feed water. This concept is wide-spreading, as its capital and operational costs are very competitive, due to its use of a low-cost heat-source, reducing required energy by using warm seawater, and elimination of the need for a significant portion of the infrastructures and utility units that are required for a conventional thermal-based desalination plant (8).

On the other hand, in membrane-based methods, a membrane plays the role of the barrier for impurities. The drive for water to pass through the membrane can be pressure (reverse osmosis, RO), electric potential (electrodialysis, ED) or thermal (membrane distillation, MD), among which, RO is by far the most common and widely commercialised option (3, 8).

Among available methods and technologies for RO desalination, spiral wound modules (SWM) have become the major and sole trusted option since the 1990s (9). In the SWM configuration, sandwiches of (feed-channel/membrane/permeate-channel) are rolled around a

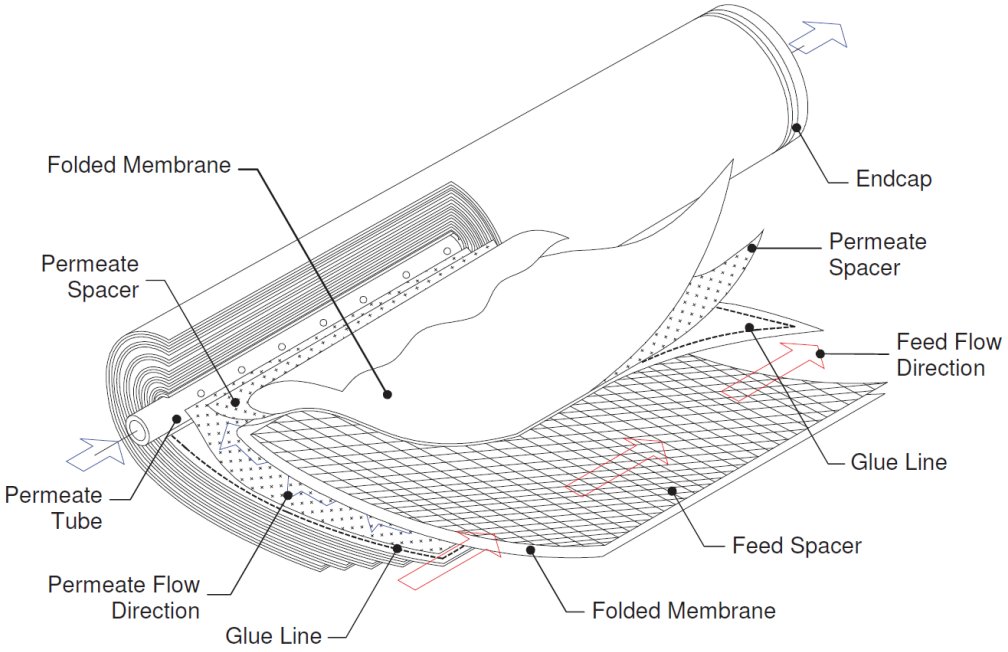

Figure 1-1. Configuration of a typical SWM

(Source: (11), © copyright [2010], reprinted by permission of Informa UK Limited, trading as Taylor & Taylor & Francis Group, http://www.tandfonline.com)

permeate collection tube to form a cylindrical-shaped module (Figure 1-1). This arrangement mechanically enables the membrane to withstand higher pressure differences that increases the permeate flowrate. Moreover, the condensed arrangement of layers minimises the size and footprint of the module and significantly reduces the designing, manufacturing, distribution, capital, and maintenance expenses. This also provides greater flexibility in desalination plant design to accommodate a variety of feed water specifications, permeate specifications and plant capacity requirements. (6, 9).

Among available technologies for desalination, RO is by far the most successful and trusted one. It is used in 84% of the currently in-operation plants and produces 69% of global desalinated water (10).

1.3 Plants around the world

The Middle East and North Africa (MENA) is home to about half of the world's desalination plants. This region has a well-established oil and gas industry that results in a significant growth in the water demand. This region have a notable number of new desalination projects as well, followed by the East Asia / Pacific, and North America regions, which have 18.4% and 11.9% of the world's desalination capacity, respectively. While 71% of the global capacity is located in high-income countries, low-income countries benefit from less than 0.1% of desalination

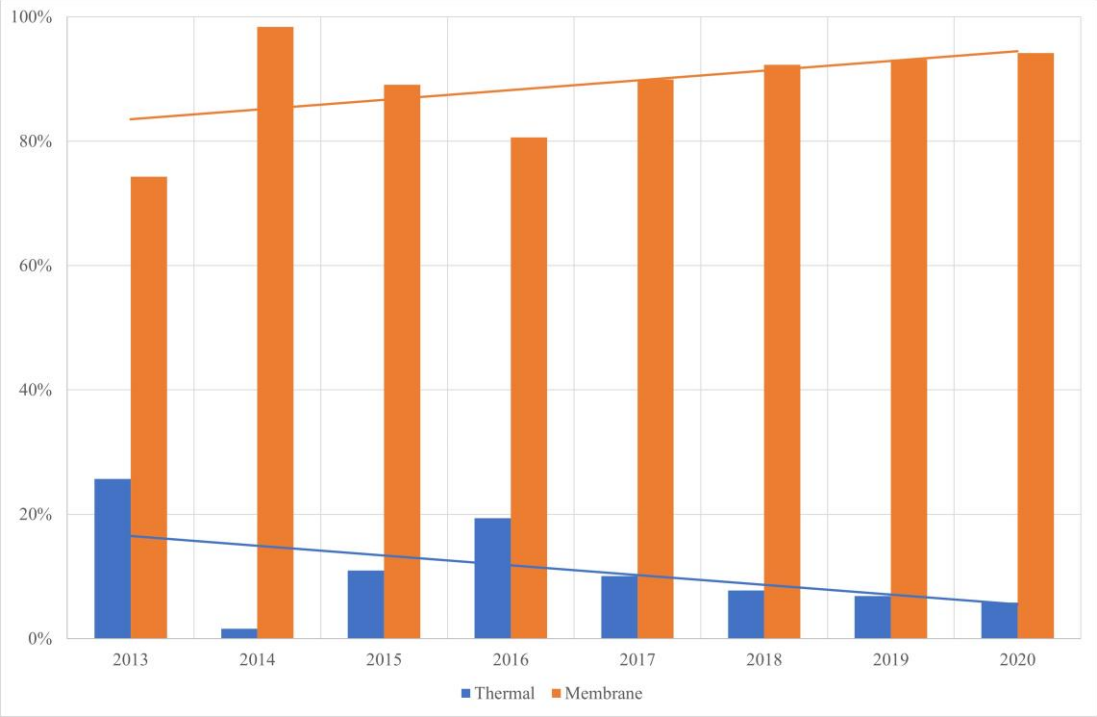

Figure 1-2. Trends in selected separation method, based on new projects' capacity of desalination

capacity. This is probably because desalination plants are hunger for energy that makes them an exorbitant option for smaller economies (10).

Analysing the capacity of desalination plants over the past two decades indicates a growing tendency in favouring RO over its competitors. For example, during 2000-2009, the ratio of RO capacity in new plants was 52% in MENA and 75% globally, while in 2014-2015, 92% (MENA) and 94% (globally) of new contracts' capacity was provided by RO plants (8). Figure 1-2 shows the global trend in selected desalination methods, based on new project capacity over the past few years.

A comparison of the Capital Expenditures (CAPEX) and Operating Expenses (OPEX) for different technologies with a focus on MENA, revealed that while RO plants are the most competitive plants for the locations near the Mediterranean Sea, their advantage diminishes rapidly in higher salinity waters, and they only outperforms MED units in the Red Sea and Persian Gulf by a small margin. However, it has been posited that implementing a hybrid approach (1/3 RO and 2/3 MED) in high salinity locations could result in a further 24% reduction in the production costs (8).

1.4 Spiral Wound Module RO units

The SWM is made of repeated sandwiches of flat membrane sheets separated by a thin mesh spacer material (Figure 1-1). The spacer on feed side is called feed spacer and its main purpose

is to act as a flow enhancer, while the spacer on the product side is called permeate spacer and is in place to prevent higher pressure of feed side, blocking the permeate channel. This combination is rolled around a central tube and fitted into a cylindrical body. As the feed stream flows through the module, a portion passes through the membrane surface, leaving behind a rich brine, and producing permeate that flows into the central collecting tube. This design is a compact and cheap option for RO designs that offers a high mass transfer area to volume ratio, which results in high volumetric throughput and moderate energy consumption.

RO operations consume less energy per unit product than other desalination processes, such as MSF, MED and MVC (8). However, RO operations in practice still consume about three times the minimum theoretical required energy, which provides opportunities for optimisation in this area (11).

There is scope for this optimisation to be achieved via improved design and manufacturing of the membrane or through optimisation of feed spacer configurations, leading to enhanced mass transfer and lower energy consumption (9, 12). This thesis is mainly focused on feed spacers and their performance in a range of different flowrates, and the impact of variations in the filament arrangements and configurations on their performance.

1.5 Performance measures

Different approaches have been reported in the literature that aim to improve the performance of RO desalination plant operations, attempting to make the desalination process more efficient. However, it should be noted that there is no commonly agreed method for measuring feed spacer's performance. Common concepts currently used consider energy consumption (in the form of pressure drop, dimensionless pressure drop, specific power consumption and power number, as in (13-24)); mass transfer (in the form of Sherwood number, mass transfer coefficient or local and/or average sheer stress over the membrane, as in (17-37)); or a combination of both (mostly in the form of Spacer Configuration Efficacy) to indicate a spacer's performance. But none of these performance measures are capable of evaluating the actual plants' production costs in a simple step.

1.6 Research gap

The extent of current and the forecast future trends in the capacity of RO plants and their energy consumption is a significant motivation to improve our understanding of their performance and their response to variations in operational parameters. Progress in this area

will help to maintain the unit operation at its optimal point, and minimise energy consumption and maintenance costs.

Many approaches have been employed to enhance our understanding of the SWMs feed spacers with the aim of comparing and identifying optimum designs. These include visualising flow characteristics in the channel (14-16, 20-22, 24, 25, 28, 29, 38); calculating and reporting different performance measures from data sourced through experimental or Computational Fluid Dynamics (CFD) models (17-19); providing equations that describe energy consumption or mass transfer as a function of flow (13, 25, 26); and reporting the effect of spacers' geometrical parameters on performance measures (16, 21, 28). Some have also tried to introduce predictive equations that describes either the pressure drop or the mass transfer as a function of flow and the spacers' geometry, with limited success (39, 40).

Some studies have emphasised the well-known and frequently discussed analogy between mass transfer and heat transfer (41, 42). These efforts to establish an equation that predicts the mass transfer, based on the flowrate and geometrical characteristics, can be linked to the studies focused on this problem in late 1800s and early 1900s. Later in this thesis, some of the most important works that aimed to provide such equation has been summarised, with the geometry limited to the flow inside a circular hollow tube. The extent of time and work that has been invested in solving this problem for such a basic geometry can explain the magnitude of complexity that is involved in this phenomenon, and hence the gap that is still available in our understanding of this topic.

The present study aims to extend our insight about SWM feed spacers and prepare a foundation for further investigations into them and improvements in their performance.

1.7 Scope of work

CFD tools, including but not limited to ANSYS DesignModeler, ANSYS SpaceClaim, ANSYS Mesh, ANSYS Fluent mesh engine, ANSYS Fluent, and ANSYS CFD-Post are used in this thesis to simulate the fluid dynamic and mass transfer through spacer filled narrow channels that representing SWMs feed side, to generate data for further analysis. This thesis focuses on the feed channel in steady-state, with $25 \leq Re \leq 200$ and a water solution of 5%w/w NaCl as the feed-stream. This present study takes the following steps to achieve its goals.

- Develop a 3D-CFD model to study the effect of fluid flowrate on fluid behaviour and mass transfer for different basic and commercial feed spacers.

- Use the model to study the effect of spacers' mesh length, porosity, and hydraulic diameter on fluid behaviour and mass transfer.
- Use the model results to provide equations for predicting different performance measures, based on other parameters, e.g., Re, dP, Pn and SPC.
- Investigate the correlation between the equation parameters and the spacers' characteristics, e.g., porosity and D_h/L.
- Use the model results to compare the studied spacers and pick the best configuration, based on energy consumption and mass transfer performance.
- Use the flow visualisation at micro-level to explain the observed changes and trends in the feed spacer performance at macro-level.

1.8 Thesis structure

Including the current introductory chapter, this thesis comprises of seven chapters that address the objectives mentioned in Section 1.7, where:

Chapter 1 provides a snapshot of the background, motivations, and objectives of the current research.

Chapter 2 includes a detailed literature review, with a focus on the research that aims to provide better understanding of SWMs and analyse their behaviours.

Chapter 3 provides the details of the research methodology that has been used to achieve the research objectives, including the details of the High Performance Environment (HPE) infrastructure, CFD software, assumptions, and detailed steps taken in pre-processing, solution and post-processing stages, to ensure replicability of the present work.

Chapter 4 presents a CFD-based numerical study that investigates the effectiveness of four simple feed spacers over four different flowrates and compares them with an unobstructed domain, using six different performance measures.

Chapter 5 extends the work and includes a further four commercial feed spacers. This chapter not only compares the performance of commercial spacers with simple spacers for different flowrates, but also discusses the influence of the selected performance measures on the comparison outcome.

Chapter 6 aims to improve our understanding of the feed side's fluid behaviour by examining the correlation between various performance measures and the spacers' geometrical characteristics. It also investigates the response of a simple spacer arrangement to variations in

the filament gap, by observing the spacer performance at the macro level and providing justification for the observations based on comprehensive post-processing at the micro level.

Chapter 7 summarises the major outcomes of research and provides some suggestions for future work in this area.

References

1. Gleick PH. Water in crisis: A guide to the world's fresh water resources. New York: Oxford University Press; 1993.

2. Water facts and trends. World Business Council for Sustainable Development; 2005. Available from: https://docs.wbcsd.org/2005/08/WaterFactsAndTrends.pdf.

3. Voutchkov N. Desalination-past, present and future. 2016. Available from: https://iwa-network.org/desalination-past-present-future/.

4. Burek P, Satoh Y, Fischer G, Kahil MT, Scherzer A, Tramberend S, et al. Water futures and solution - fast track initiative (final report). IIASA Working Paper. IIASA, Laxenburg, Austria; 2016.

5. Eke J, Yusuf A, Giwa A, Sodiq A. The global status of desalination: An assessment of current desalination technologies, plants and capacity. Desalination. 2020; 495:114633.

6. Voutchkov N. Desalination engineering: Planning and design. U.S.: McGraw Hill Professional; 2012.

7. Perry's chemical engineers' handbook. 9th ed. Green DW, Southard MZ, editors. New York: McGraw-Hill Education; 2019.

8. Desalination technologies and economics: Capex, opex & technological game changers to come. Mediterranean Regional Technical Meeting; 2016; Marseille: Centre of Mediterranean Integration.

9. Johnson J, Busch M. Engineering aspects of reverse osmosis module design. Desalination and Water Treatment. 2010; 15(1-3):236-48.

10. Jones E, Qadir M, van Vliet MTH, Smakhtin V, Kang SM. The state of desalination and brine production: A global outlook. Science of The Total Environment. 2019; 657:1343-56.

11. Dashtpour R, Al-Zubaidy S. Energy efficient reverse osmosis desalination process. International Journal of Environmental Science and Development. 2012; 3(4):339-45.

12. Abid HS, Johnson DJ, Hashaikeh R, Hilal N. A review of efforts to reduce membrane fouling by control of feed spacer characteristics. Desalination. 2017; 420:384-402.

13. Karode SK, Kumar A. Flow visualization through spacer filled channels by computational fluid dynamics i. Pressure drop and shear rate calculations for flat sheet geometry. Journal of Membrane Science. 2001; 193(1):69-84.

14. Cao Z, Wiley DE, Fane AG. Cfd simulations of net-type turbulence promoters in a narrow channel. Journal of Membrane Science. 2001; 185(2):157-76.

15. Schwinge J, Wiley DE, Fletcher DF. A cfd study of unsteady flow in narrow spacer-filled channels for spiral-wound membrane modules. Desalination. 2002; 146(1-3):195-201.

16. Schwinge J, Wiley DE, Fletcher DF. Simulation of the flow around spacer filaments between narrow channel walls. 1. Hydrodynamics. Industrial & Engineering Chemistry Research. 2002; 41(12):2977-87.

17. Li F, Meindersma W, de Haan AB, Reith T. Optimization of commercial net spacers in spiral wound membrane modules. Journal of Membrane Science. 2002; 208(1-2):289-302.

18. Li F, Meindersma GW, de Haan AB, Reith T. Optimization of non-woven spacers by cfd and validation by experiments. Desalination. 2002; 146(1-3):209-12.

19. Li F, Meindersma W, de Haan AB, Reith T. Experimental validation of cfd mass transfer simulations in flat channels with non-woven net spacers. Journal of Membrane Science. 2004; 232(1-2):19-30.

20. Koutsou CP, Yiantsios SG, Karabelas AJ. Numerical simulation of the flow in a plane-channel containing a periodic array of cylindrical turbulence promoters. Journal of Membrane Science. 2004; 231(1-2):81-90.

21. Ranade VV, Kumar A. Fluid dynamics of spacer filled rectangular and curvilinear channels. Journal of Membrane Science. 2006; 271(1-2):1-15.

22. Santos JLC, Geraldes V, Velizarov S, Crespo JG. Investigation of flow patterns and mass transfer in membrane module channels filled with flow-aligned spacers using computational fluid dynamics (cfd). Journal of Membrane Science. 2007; 305(1-2):103-17.

23. Li YL, Tung KL. Cfd simulation of fluid. Flow through spacer-filled membrane module: Selecting suitable cell types for periodic boundary conditions. Desalination. 2008; 233(1-3):351-8.

24. Haaksman VA, Siddiqui A, Schellenberg C, Kidwell J, Vrouwenvelder JS, Picioreanu C. Characterization of feed channel spacer performance using geometries obtained by x-ray computed tomography. Journal of Membrane Science. 2017; 522:124-39.

25. In Seok K, Ho Nam C. The effect of turbulence promoters on mass transfer—numerical analysis and flow visualization. International Journal of Heat and Mass Transfer. 1982; 25(8):1167-81.

26. Schock G, Miquel A. Mass-transfer and pressure loss in spiral wound modules. Desalination. 1987; 64(C):339-52.

27. DaCosta AR, Fane AG. Net-type spacers: Effect of configuration on fluid flow path and ultrafiltration flux. Industrial and Engineering Chemistry Research. 1994; 33(7):1845-51.

28. Schwinge J, Wiley DE, Fletcher DF. Simulation of the flow around spacer filaments between channel walls. 2. Mass-transfer enhancement. Industrial & Engineering Chemistry Research. 2002; 41(19):4879-88.

29. Fimbres-Weihs GA, Wiley DE. Numerical study of mass transfer in three-dimensional spacer-filled narrow channels with steady flow. Journal of Membrane Science. 2007; 306(1-2):228-43.

30. Cipollina A, Di Miceli A, Koschikowski J, Micale G, Rizzuti L. Cfd simulation of a membrane distillation module channel. Desalination and Water Treatment. 2009; 6(1-3):177-83.

31. Cipollina A, Micale G, Rizzuti L. Membrane distillation heat transfer enhancement by cfd analysis of internal module geometry. Desalination and Water Treatment. 2011; 25(1-3):195-209.

32. Qureshi M, Shakaib M. Cfd study for temperature and concentration profiles in membrane channels. International conference on Energy and Sustainability: NED University of Engineering & Technology; 2013. Karachi, Pakistan.

33. Saeed A. Effect of feed channel spacer geometry on hydrodynamics and mass transport in membrane modules [Ph.D Thesis]. Perth, Australia: Curtin University; 2012.

34. Saeed A, Vuthaluru R, Yang YW, Vuthaluru HB. Effect of feed spacer arrangement on flow dynamics through spacer filled membranes. Desalination. 2012; 285:163-9.

35. Saeed A, Vuthaluru R, Vuthaluru H. Concept of spacer configuration efficacy (sce) applied to optimize ladder type feed spacer filament spacing in narrow channels. International Conference On Water Desalination, Treatment and Management & Indian Desalination Association Annual Congress; 2013. Jaipur, India: The Malaviya National Institute of Technology.

36. Saeed A, Vuthaluru R, Vuthaluru HB. Investigations into the effects of mass transport and flow dynamics of spacer filled membrane modules using cfd. Chemical Engineering Research & Design. 2015; 93:79-99.

37. Saeed A, Vuthaluru R, Vuthaluru HB. Impact of feed spacer filament spacing on mass transport and fouling propensities of ro membrane surfaces. Chemical Engineering Communications. 2015; 202(5):634-46.

38. Shakaib M, Hasani SMF, Mahmood M. Study on the effects of spacer geometry in membrane feed channels using three-dimensional computational flow modeling. Journal of Membrane Science. 2007; 297(1-2):74-89.

39. DaCosta AR. Fluid flow and mass transfer in spacer-filled channels for ultrafiltration [Ph.D thesis]. Sydney, Australia: University of New South Wales; 1993.

40. DaCosta AR, Fane AG, Wiley DE. Spacer characterization and pressure drop modelling in spacer-filled channels for ultrafiltration. Journal of Membrane Science. 1994; 87(1-2):79-98.

41. Lienhard IV JH, Lienhard V JH. A heat transfer textbook. 5th ed. Mineola, NY: Dover Publications; 2020.

42. Holman JP. Heat transfer. 10th ed. Boston: McGraw Hill Higher Education; 2010.

Chapter 2. Literature review

2.1 The discovery of osmosis

For the first time in 1748, Nollet (1) described and documented an observation that was later named 'Osmosis'. He wrote:

> Before I finish this memoir, I think I must give an account of a fact which I owe to chance, and which first appeared to me... unusual... I had filled a cylindrical flask, five inches long, and an inch in diameter or about; and having covered it with a piece of damp bladder and tied to the neck of the flask, I immersed it in a large container full of water, to be sure that there was no air in the alcohol. At the end of five or six hours, I was quite surprised to see that the flask was fuller than at the time of its immersion, although it was then as full as its edges could permit; the bladder which served as a lid, had become convex and so stretched, that by pricking it with a pin, it let out a jet of alcohol which rose more than a foot in height [1].

Assume that in a container, a separating permeable membrane is placed between the two sides that are filled with mixture(s) that have at least one common component and the membrane is semi-permeable only for the common component(s). Being more specific, in Nollet's experiment, water is the common component, the bladder is the semi-permeable membrane and ethanol is the component that cannot pass through the divider. Osmosis can be defined as the movement of water (common component / solvent) through the membrane, from the side with higher concentration (pure water that is placed in the bigger container) to the side

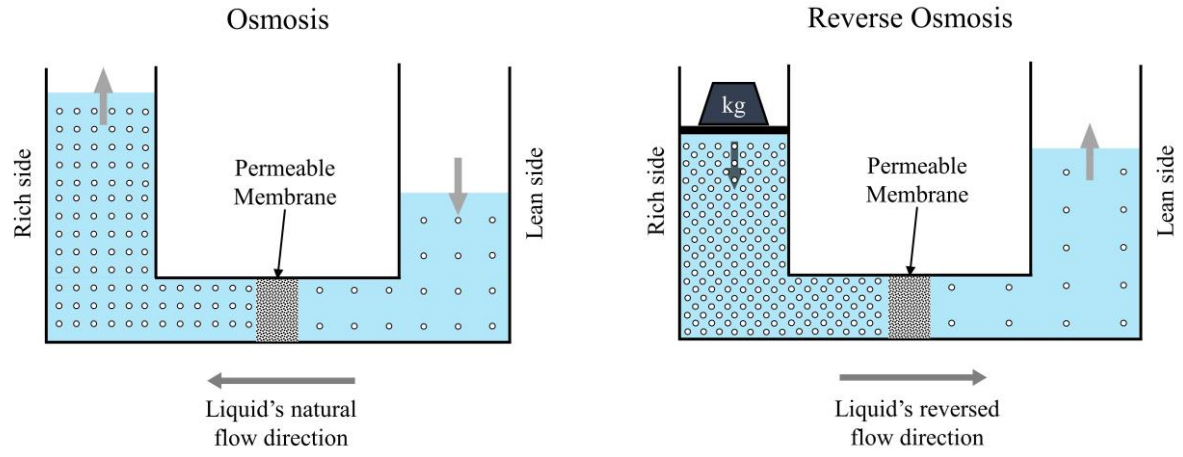

Figure 2-1. Osmotic (left) and reverse osmotic flow (right).

[1] The quote extracted from https://gallica.bnf.fr/ark:/12148/bpt6k3546r/f247.item, accessed on 3/11/2022, and translated from French to English, with the aid of Google Translate and Cambridge French to English Dictionary.

with lower concentration (ethanol solution in the flask). The movement is motivated by concentration difference that can be described by the second law of thermodynamics (see Figure 2-1 left). In the configuration presented in Figure 2-1 right, the rich side includes more solute and less solvent, while the lean side has less solute and more solvent. Thus, the solvent would flow from the lean side to the rich side. After a while, the osmotic flow would result in a change of the liquid column height that will eventually reach an equilibrium state, where the liquid column head/weight balances with and counteracts the force of concentration difference. This pressure, known as osmotic pressure, has been extensively studied, explained, and formulated by J.H. van't Hoff, (2) whose efforts on this topic were acknowledged with the award of the very first Nobel Prize in chemistry to him in 1901 (3). The key equation is

$$\Pi = icRT \tag{2-1}$$

where Π is osmotic pressure, i is the van't Hoff index that represents the number of dissolved particles per molecule of solvent, c is the solvent's molar concentration, R is the ideal gas constant, and T is the absolute temperature.

Understanding osmosis and osmotic pressure is crucial to understand reverse osmosis. As explained before, the osmotic flow will reach an equilibrium state, where the static pressure on the rich side of the membrane is equal to the osmotic pressure plus the membrane's lean side static pressure. This equilibrium can be shifted to the reverse direction (see Figure 2-1 right) by applying extra pressure on the rich side to make it exceed the sum of the osmotic pressure and the membrane's lean side static pressure. In such a situation, the solvent will pass through the membrane, from the rich side to the lean side, and leave the solute remaining on the rich side. This will continue to the point when the rich side concentration is raised enough to make a new equilibrium in which the external pressure plus the liquid head on the rich side is equal to the osmotic pressure plus the liquid head on the lean side.

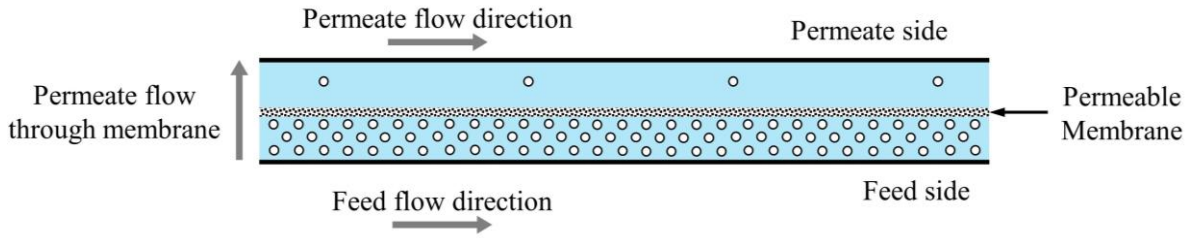

Figure 2-2. Reverse osmosis – continuous process

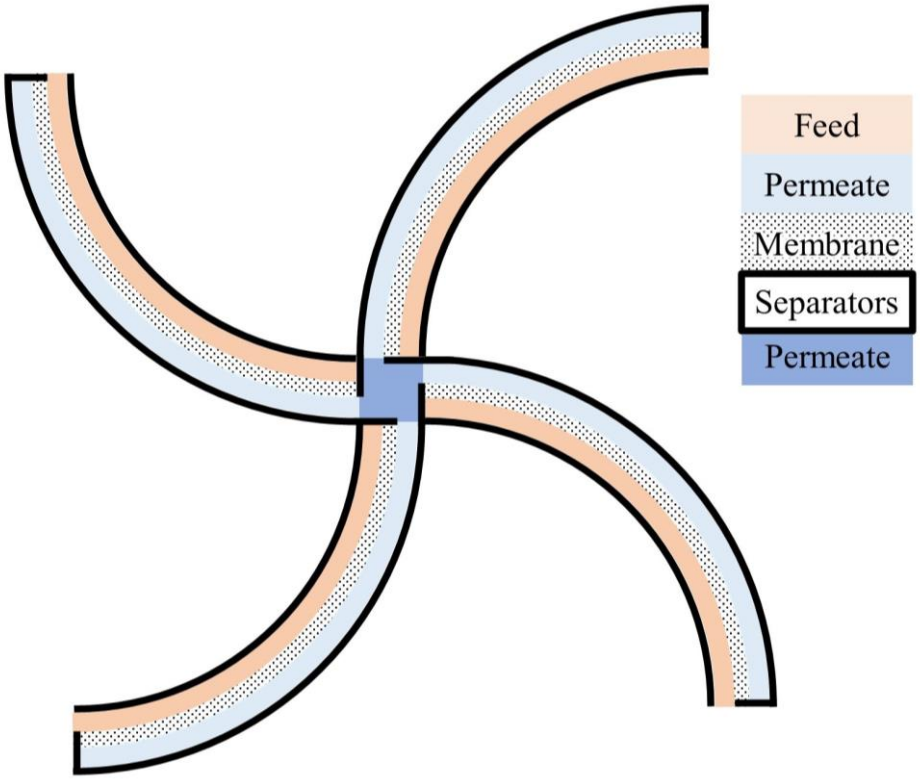

Figure 2-3. Reverse osmosis – Spiral wound concept with four leaves – cross section view

This is the foundation of a RO water desalination unit. However, to suit industrial practicalities, the batch operation should be converted to a continuous operation for easier scale-up. Figure 2-2 demonstrates a simple concept that can provide a continuous RO process. While the high-pressure feed stream passes from left to right along the domain, a portion of permeate/solvent penetrates through the membrane leaving the solute behind. The feed side outlet, also known as the reject flow, has a higher concentration of solute than the feed stream and exits the domain from right-hand side. The permeate stream, which is almost free of solute, is collected from the other side of the membrane.

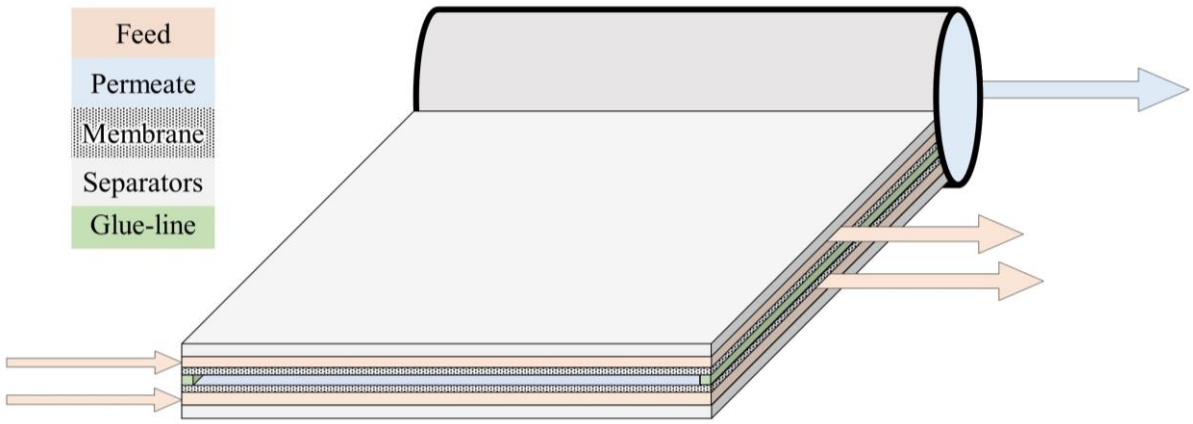

Figure 2-4. Reverse osmosis – Spiral wound arrangement with two leaves

2.2 Spiral wound modules

Preliminary investigations and engineering analyses revealed that the membrane and its containment is responsible for the largest share of the capital costs. RO unit designers mindful of the cost of materials, assembly, and installation labour, have developed various approaches to the general shape of the equipment;. these include ‘plate and frame’, and ‘shell and tube’ concepts. The additional need for easy replacement procedures, has led them to conclude that a modular approach with tubular-shaped pressure vessels that contain a repeated array of feed-membrane-permeate sandwiches, spirally twisted around an inner tube (see Figure 2-3 for a simplified cross-section or Figure 2-4 for another view) is the most feasible design (4, 5). The modular concept makes it possible to mass-produce the modules, reducing both engineering and manufacturing costs and making them available to be used in any desired configuration of series/parallel arrangements, in a quick and efficient process. It is also very easy to replace a low-performing module during maintenance periods, with minimum costs associated with pre-procurement, warehousing, and installation of new modules. These modules provide good area-to-volume ratios and have a relatively small footprint on the plant, which can reduce piping and land acquisition fees.

However, by continuing the process, the left-behind solute can develop a solute concentration gradient over the membrane surface. Equation (2-1) demonstrates the connection between the solute concentration and osmotic pressure, which can affect the permeate flux through the membrane. Therefore, it becomes necessary to disrupt the build-up of the solute concentration gradient, in order to avoid reduction of the unit’s productivity and maintain its performance (6-16). A recent study investigated this phenomenon and showed that a reduction of 5-12% in concentration polarisation improved the permeate flux by 0.5-1.5% (17).

Employing feed spacers is the main response to this challenge in RO units (11). Feed spacers are obstacles that can be placed on the feed side of the membrane sandwich to interfere with the stream flow pattern and increase turbulence on the feed side, mainly designed to break through concentration polarisation layer and enhance convective mass transfer. The correlation between pressure drop triggered by feed spacers, and mass transfer has been investigated through different studies (6-8, 12-36).

On the other hand, it should be noted that employing a feed spacer has some downsides. The most obvious undesired consequence of adding a feed spacer is the increase in pressure drop and unit’s energy consumption that is the first result of increasing turbulence on the feed side.

Adding a feed spacer to the domain can raise the feed side's pressure drop by almost an order of magnitude. However, it should be noted that the feed side's pressure drop is not necessarily responsible for the greater part of the energy bill. Generally, the feed side's pressure drop is about or just less than 10% of the inlet pressure (11).

In addition, having feed spacers in RO modules may lead to creating zones with very low velocity magnitude that are known as 'dead zones', specifically when close to the spacer filaments. The higher solute concentration in the dead zones not only reduces the permeate flux, but also make these zones more vulnerable to scale build-up that can increase the frequency of required maintenance, and the amount of off-production time (12).

Despite the fact that the Specified Energy Consumption[2] of seawater desalination plants has been reduced notably through the past decades, a typical desalination plant still uses 2.5 times the minimum theoretically required energy for desalination (37). This gap provides an opportunity for academic and industrial stakeholders to investigate and optimise SWMs, in order to improve performance and reduce maintenance requirements.

Several researchers have approached this challenge by comparing different feed spacers, introducing novel filament shapes, or optimising parameters, like filament gap and angle of attack. In addition to using some of these approaches, the main goal of the present study was to use CFD post-processing advantages at the micro level, to explain the spacers' behaviours at the macro level, in order to have a better understanding of causalities and to provide a better foundation for future research on this topic.

2.3 Definitions

Clarity and reproducibility are essential pillars of academic research, which make it necessary to define all parameters that are used or referred to in this study. The domain and spacer's geometrical characteristics that have been shown in Figure 2-5 are:

L is the cell's length, which is the distance between a latitudinal filament's centreline and the next latitudinal filament's centreline.

W is the cell's width, which is the distance between a longitudinal filament's centreline and the next longitudinal filament's centreline.

[2] The amount of energy that has been used to produce 1 m^3 of desalinated water.

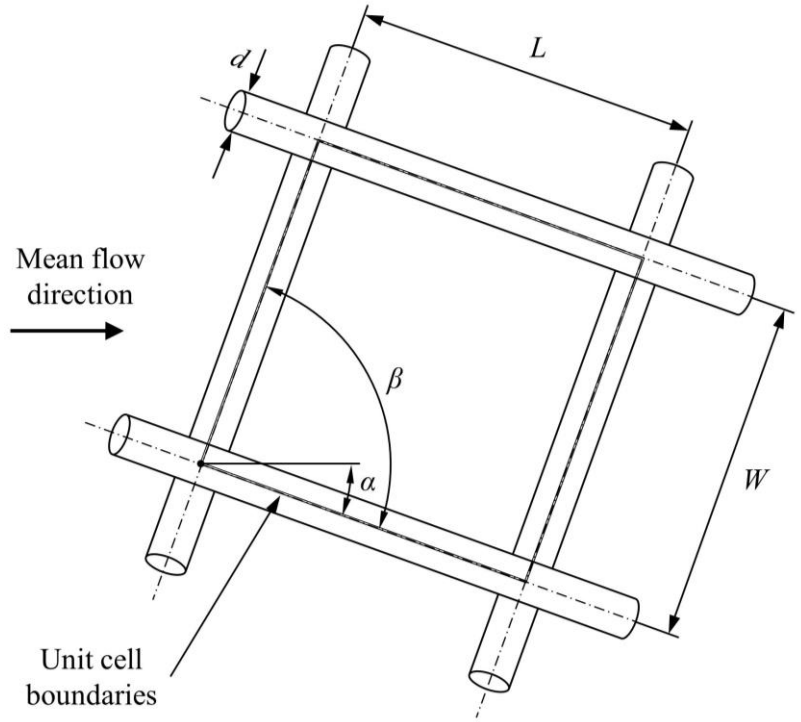

Figure 2-5. The domain cell and its parameters

β is the spacer's geometry angle, which is the angle between a latitudinal filament's centreline and its intersecting longitudinal filament's centreline.

α is the angle of attack, which is the angle between the main flow direction and the longitudinal filament's centreline.

d is the circular-shaped filament's diameter.

The unit cell is a part of the domain that is contained within the centrelines of two adjacent latitudinal filaments and two adjacent longitudinal filaments. A unit cell is the smallest individual component that when repeated, will build the domain.

H, which is not shown in the figure, is the channel height, which is the distance between top and bottom membranes.

Apart from the geometrical terms, various parameters have been incorporated in this study as well, including:

Hydraulic diameter (D_h)

The general definition for hydraulic diameter for obstructed channels is

$$D_h = \frac{4 \times volume\ occupied\ by\ fluid}{surface\ area\ of\ wetted\ walls} \tag{2-2}$$

which could be rearranged as

$$D_h = \frac{4 \times (channel\ volume - filament\ volume)}{membrane\ surface\ area + filament\ surface\ area} \quad (2\text{-}3)$$

Porosity (ϵ)

In the obstructed channels, that is, channels with spacers, porosity comes into account. It represents the amount of obstruction and defines as the ratio of available volume in the channel to the original volume of unobstructed channel, or

$$\epsilon = \frac{volume\ of\ the\ channel\ with\ obstruction}{volume\ of\ the\ channel\ without\ obstruction} \quad (2\text{-}4)$$

which could be rearranged as

$$\epsilon = 1 - \frac{volume\ of\ the\ obstruction}{volume\ of\ the\ channel\ without\ obstruction} \quad (2\text{-}5)$$

Effective area (A_{eff})

With an obstructed channel, the domain's cross-sectional area can variate as a function of length. The effective area represents the average value for the cross-sectional area and is defined as the amount of cross-sectional area for the unobstructed channel multiplied by the porosity of the channel, or

$$A_{eff} = WH\epsilon \quad (2\text{-}6)$$

Average velocity (u_{avg})

Conceptually, average velocity (u_{avg}) simply neglects the presence of obstructions and is defined as the amount of average velocity in an unobstructed channel, or

$$u_{avg} = \frac{\dot{V}}{WH} \quad (2\text{-}7)$$

where, $\dot{V}$ is the fluid's volumetric flow

Effective velocity (u_{eff})

With obstructions varying the cross-sectional area, the effective velocity comes into use to represent the average fluid flow and is defined as the volumetric flow divided by the effective area, or

$$u_{eff} = \frac{\dot{V}}{A_{eff}} \tag{2-8}$$

Reynolds number (Re)

The Reynolds number is defined as the ratio of inertial forces to viscous forces, or

$$Re = \frac{\rho u X}{\mu} \tag{2-9}$$

where ρ is fluid's density, u is velocity, μ is fluid's dynamic viscosity, and X represents the characteristic length. However, according to different approaches to include the obstructions' effect into u and D, different approaches are used in the literature to calculate the Reynolds number. For example, when filament diameter and average velocity are chosen to represent X and u, the calculated value is usually referred to as the cylinder Reynolds number, or

$$Re_{cyl} = \frac{\rho u_{avg} d}{\mu} \tag{2-10}$$

This approach is used by (9, 18, 38-40).

On the other hand, using the channel height and average velocity is normally referred to, as the channel Reynolds number Re_{ch}, or

$$Re_{ch} = \frac{\rho u_{avg} h}{\mu} \tag{2-11}$$

This method has been used by (18, 33, 41-43).

Another approach to incorporating obstructions into the velocity and characteristic length, which usually referred to as the hydraulic Reynolds number, is to use the effective velocity and hydraulic diameter, or

$$Re_h = \frac{\rho u_{eff} D_h}{\mu} \tag{2-12}$$

This approach has been used by (10, 12-15, 19, 21, 29, 31, 44, 45).

The current work uses the hydraulic Reynolds number and anywhere in this thesis, where the term Reynolds number or Re is used without any specification, it should be assumed to mean the hydraulic Reynolds number or Re_h.

Specific power consumption (SPC)

The concept of specific power consumption was introduced by (46) to represent the mechanical energy that is required to address the fluid's pressure drop per unit of length of the domain. It is defined as

$$SPC = \frac{\dot{V} \Delta P}{A_{eff} L} = \frac{u_{eff} \Delta P}{L} \tag{2-13}$$

where, ΔP is the difference in the static pressure at the domain's inlet and outlet. This performance measure is used to measure energy consumption in studies including (12, 14-16, 26-28, 47).

Dimensionless pressure drop (ΔP^*)

The dimensionless pressure drop is defined as

$$\Delta P^* = \frac{\Delta P}{L} \left(\frac{{D_h}^3}{Re_{cyl}^2 \rho {u_{eff}}^2} \right) \tag{2-14}$$

by Shakaib et al. (42) and was used in (12, 43).

Power number (Pn)

Power number is another approach to indicate the energy consumption. It was introduced by Li et al. (26), as the outcome of a dimensional analysis to investigate the effect of different parameters on energy consumption.

$$Pn = SPC \left(\frac{\rho^2 H^4}{\mu^3} \right) = \frac{\Delta P}{L} \left(\frac{v \rho^2 H^4}{\mu^3} \right) \tag{2-15}$$

Researchers showed interest in using power number as a performance measure and reported the power number values for different geometries and flowrates (10, 12, 13, 15, 16).

Sherwood number (Sh)

The Sherwood number is defined and widely accepted as a dimensionless number. It represents the ratio of convective mass transfer to diffusive mass transfer, or

$$Sh = \frac{kX}{\mathcal{D}} \tag{2-16}$$

where k is the mass transfer coefficient, $\mathcal{D}$ is the molecular diffusivity, and X represents the characteristic length. In the present study, in harmony with Re, D_h is used as the characteristic length.

Spacer performance ratio (SPMC)

SPMC was originally introduced by Schwinge et al. (48) as a dimensionless number to combine both mass transfer and energy consumption in one group. It is conceptually defined as the ratio of enhancement in mass transfer to the increase in energy consumption, resulting from adding a specific spacer to the channel, or

$$SPMP = \frac{\Delta C_{Spacer}/\Delta C_{Slit}}{\Delta P_{Spacer}/\Delta P_{Slit}} \tag{2-17}$$

where the 'Spacer' subscript indicates the value of the parameter with the spacer in the channel while the subscript 'Slit' reflects the value of the parameter in an unobstructed channel. The original article used a constant 'Re_{ch}' for both cases, in order to put the same flow through the domain, with and without spacer. However, the definition of Re_{ch} used in that article reveals that the authors used hydraulic diameter as the characteristic length, and the average velocity, which makes their interpretation of Reynolds number, dissimilar to the way other researchers refer to as Re_{ch}, but some approach between Re_{ch} and Re_h. This particular approach to calculating the Reynolds number not only allocates different mass flowrates for spacer-filled and open channels with the same Re, but also makes the reported results by Schwinge et al. (48) incomparable with other works' results.

Spacer configuration efficacy (SCE)

SCE is another attempt to combine both mass transfer and energy requirements in one dimensionless number, it was introduced by Saeed (12) and used in other studies (14-16, 49-52).

SCE is defined as the ratio of mass transfer to energy consumption where the power number represents the energy consumption and the Sherwood number represents mass transfer, or

$$SCE = \frac{Sh}{Pn} \tag{2-18}$$

2.4 Early studies into membrane desalination

While osmosis was first described in 1748, for the next couple of centuries, further studies were mainly focused on gaining more information about the phenomenon itself. While WWII had devastating effects on parts of Europe, it also resulted in rapid growth in several industries and agriculture sector in the rest of the world. In the US, this rapid expansion put unsustainable pressure on overground and underground water resources. The limits applied to the industrial water usage, rapid falling water table levels, and seawater flowing into underground domestic water resources slowed the industrial and economic growth, and threatened the liveability of metropolitan areas (53). To address the challenge, in 1949, US Senator George O'Mahoney proposed a bill named *Conversion of seawater for industrial and irrigation uses* (53). A year later, the bill was amended and renamed the *Conservation and increase of water resources* (54) and finally in 1952, under *Public Law 448*, it led to the allocation of $2,000,000 for funding research into the production of fresh water from seawater. The funding continued under the Office of Saline Water (OSW) until the mid-1970s. In 1953, a group from the University of Florida started to investigate the use of synthetic osmotic membranes and then developed a desalination method based on osmotic membranes. The results were astonishing, as they successfully tested a pilot plant operating at about 700 psi for over a month that resulted in 95-99.5% of salt rejection (55, 56). Their work attracted a lot of interest and over the next fifteen years, OSW alone funded more than a hundred research programmes about RO, to boost the industrialisation of RO desalination plants.

2.5 Feed spacers

In earlier studies, the presence and impact of concentration polarisation were not completely agreed on. For example, while some research suggested it was better to employ no spacer on the feed side and assume the solute concentration at the membrane was equal to the bulk concentration (5), others were trying to investigate, formulate, and control the concentration polarisation (57-60). Meanwhile, from 1964, the OSW funded two different companies, General Atomic, (which was renamed to Gulf General Atomic Inc. during the project) and Universal Oil Products (UOP), to develop, test, and commercialise the spiral wound concept for RO desalination, and both companies arrived at the necessity of feed spacers (61, 62).

Working on the mass transfer, pressure loss, and the performance of SWMs started from the early stages of their development. In those early stages, studies (63, 64) proposed equations that would predict the performance of RO operation in an open channel because of its simplicity, however, in another work Strathmann (57) mainly focused on obstructed channels and improving the performance of feed spacers compared RO units with thin channels in the laminar region; thin channels with longitudinal grooved spacers; and non-stirred turbulent arrangements to investigate concentration polarisation. They concluded that neither the presence of longitudinal obstructors nor a flow distributor can significantly help with controlling concentration polarisation. In addition, turbulent flow in either stirred or non-stirred systems cannot eliminate the concentration polarisation phenomenon. They concluded that a thin channel that operates in the laminar region would be the best option among the studied arrangements (57).

While focusing on brackish water electrodialysis, A. Sonin and S. Isaacson (65) found that in terms of production costs, spacers with no longitudinal filaments might perform slightly better than arrangements with a longitudinal filaments, and both can easily outperform an open channel. They also predict that improving the spacer configuration can result in a further 30% cost reduction for lower saline concentrations, while the opportunity diminishes for higher concentrations. In addition, they showed that the system would perform at its best when the gap between the filaments is about five times the channel height, as larger gaps leave more of the flow unaffected from the filaments and smaller gaps cause unnecessary pressure drop with limited permeate flow enhancement (65, 66).

2.6 Performance measures – optimising feed spacer design

In the early 1980s, In Seok et al. (18) demonstrated the influence of the spacers as turbulence promoters in enhancing mass transfer. In their experiments, they visualised and compared the flow patterns for two types of obstruction configurations, cavity and zigzag, among a range of flowrates that covers laminar, transitional, and turbulent regimes. A few years later, in 1987, Schock et al. (19) not only showed the impact of operating pressure, feed flowrate, and feed spacer (mainly its height in their case) on the modules' performance, but also re-emphasised the effect of the number of leaves and the glue-line[3] width, on the modules' performance.

A few years later, DaCosta et al. (6) started to investigate the optimal feed spacer for SWMs among some commercial spacers, based on their own experimental results (6, 20), and expanded their work to provide an equation to predict the feed side's pressure drop for a parallelogram-shaped spacer, based on the spacer's dimensions (21). They also recommended a modification of the Gröber equation (67) for predicting mass transfer in SWMs, based on their experimental results (7, 21).

2.7 Use of CFD to enhance spacer investigations

A notable work from Schwinge et al. (23) investigated the effect of employing a zigzag feed spacer and compared it with an open channel configuration. In their experiments they used dextran, silica and reconstituted whey protein concentrate solutions, and velocity ranging between 0.1 and 0.8 m/s. They observed up to three times enhancement in permeate flux and up to 65% reduction in costs per unit product (23). Additionally, they extended their work by using 2D and 3D CFD models to investigate flowrate and spacer geometry on the flow patterns and mass transfer (48, 68, 69). They also suggested using the 'spacer performance ratio' (SPMP) as defined in equation (2-17), a dimensionless group to evaluate and compare the performance of different spacers (48).

In another CFD-based study, Karode et al. (44) emphasised the influence of loss of momentum in the feed side pressure drop and the undesired effect of using spacers with unequal filament sizes, on mass transfer (44). Furthermore, and in agreement with (57), they concluded that developing a bulk turbulent flow would not necessarily provide a benefit overall.

[3] As shown in Figure 2-4, the glue-line is the binding line, where two immediate membranes are fused together to seal the permeate channel, at both ends of the module.

Santos et al. (10) used a CFD model, with results validated by their own experimental rig, to investigate and compare the performance of twelve different spacers, with two highlighted outcomes. First, and in accordance with (57, 65, 66), they concluded that the longitudinal filaments' impact on performance of the module is notably less than the latitudinal filaments, and second, there was a direct connection between the wall shear stress and the Sherwood number.

In another CFD-based study, Shakaib et al. (42) stressed the effect of the filament's thickness compared to the spacing gap, on the feed side's pressure drop. They also reiterated the significance of latitudinal filaments compared to the longitudinal ones (42).

In a study based on a CFD model and backed up by their own experimental data, focusing on the correlation between the spacer's geometrical characteristics and mass transfer, Koutsou et al. (38) proposed an equation to predict mass transfer in a commercial spacer with $L/D \sim 10$ and $\beta = 90°$: $Sh = 0.2\, Re^{0.575} Sc^{0.41}$, subject to further testing with more datapoints. While they outlined the direct impact of L/D and β on the mass transfer, they were not able to incorporate these parameters into their proposed equation (38, 39).

Another important work in this field was accomplished by Saeed (12), who aimed to optimise both the latitudinal and longitudinal spacer gap in ladder-type feed spacers with straight latitudinal filaments on the bottom membrane and longitudinal ones on the top. As expected, and in agreement with previous studies, they demonstrated that increasing the gap between the filaments in either direction consistently decreased the pressure drop. A similar pattern was reported for the average top and bottom membranes' shear stress. However, they also noted that the reported values for Sherwood number seemed to increase in configurations with longer gaps in either direction. Based on the limited significant figures of reported results and Sh being reported only for selected configurations, this conclusion should be considered as tentative (12-16). On the other hand, the coefficient values for the average top and bottom membranes' mass transfer showed a generally decreasing pattern with a local maximum at $W = 4H$, for all the studied latitudinal gaps, which is in agreement with what has been reported in other studies (65, 66). An interesting part of their work was introducing and using the SCE that was defined in equation **(5-1)**. As SCE includes Sh and Pn, representing mass transfer and energy consumption, it is expected to be an indication of the product's unit price. However, that correlation has not yet been investigated.

2.8 Recent studies

In another study, Haaksman et al. (35) used X-ray CT-scans to generate a precise geometry for their 3D CFD model and found that the commercial spacers' filaments suffered from a highly variable cross-section size and shape, which was found to have a significant impact on the spacers' performance. In their work, in contrast with the majority of other studies, they decided to use a tetrahedral meshing approach with prism-type inflation layers. This decision indicates that they doubted the validity of the simplifying assumption that the fluid mainly enters the domain cells from one face and exits from the opposite face, in alignment with the bulk flow direction and that recommends to use a hexahedral mesh-type. Their study concluded that using a simplified geometry for feed spacers and neglecting the effect of actual spacers' imperfections might reduce the credibility of CFD results for quantitative prediction of commercial spacers' performance. They also proposed a spacer geometry with alternating strand thickness, which resulted in lower pressure drop and better yield in mass transfer. Their findings were corroborated by Horstmeyer et al. (36), who reported the influence of imperfections and the advantages of accurate X-ray CT-scanning in comparison with simplified cylindrical geometries and microscopic measurements, which result in overestimation of both pressure drop and concentration polarisation at the membrane surface. They also demonstrated that among three CT-scan resolutions they investigated (22μm, 11μm, and 5.5 μm), 22 μm was enough to achieve adequately precise results and increasing the CT-scan resolution did not result in notable benefits. It can be noted that similar to (35), they chose to use tetrahedral cells for meshing the bulk volume of the domain.

Liang et al. (70) investigated the influence of adding a third layer of filaments to a ladder-type feed spacer configuration on mass transfer, friction factor, and production costs. In their study, the added layer of filaments was laid in the middle of the feed channel, without increasing the channel height and it went through the top and bottom filaments. The authors observed that adding the third layer resulted in an increase of up to 12% in Sh and 140% in friction factor. However, the extent of these impacts may not necessarily translate to the same level of changes in the processing cost. The authors used a very simplified economical model for evaluating the impact of introducing the third layer of filaments. It involved a constant feed volumetric flowrate over a range of filament sizes, flow angle of attack, and retentate pressure recovery efficiency values. Their economic model reported a reduction of 2-4% in production costs of desalinated water. However, their model was founded on several simplifying assumptions, including neglecting the changes in parameters like feed spacer manufacturing

costs, maintenance costs, recovery rates, etc., that would notably affect their model's accuracy. In another study, they investigated the impact of employing the third layer of filaments in Wavy and Woven arrangements, with Re values ranging from 50 to 200, for $L=4H$ (50). They found that while the benefits of adding the third layer to the Wavy arrangement could result in up to 20% higher Sh, the improvements are far smaller for the Woven arrangement. Examining their equations for Sh, as a function of Re indicates that:

- For all arrangements, Sh can be defined as a function of Re with reasonable accuracy, using a power-law equation.
- For conventional 2-layer arrangements, while both Wavy and Woven had almost similar power exponents (0.61 and 0.60, respectively), the Woven's coefficient was about 20% higher than Wavy's (2.44 and 2.97, respectively).
- For the new 3-layer arrangements, notwithstanding that the power exponent differences were still very small (0.50 and 0.49 for Wavy and Woven, respectively), the difference between coefficients reduced to less than 3% (4.78 and 4.92 for Wavy and Woven, respectively) and the two arrangements had Sh values much closer at same flowrate, with Wavy having the lead.
- In the study's conclusion, they reported that the wall shear stress would increase at least one order of magnitude by implementing the third layer of filaments, however, the figure presented in their work shows that the value would be increased by three-fold in all cases. If either situation were true, further investigation into the possible benefits of this approach for reducing the fouling and scale build-up is warranted (50).

In another study, this team used their previously developed techno-economic model to investigate the influence of changes in membrane permeance and comparing its benefits, comparing to using an improved feed spacer. Based on their model's results, increasing the membrane's permeability by a factor of ten without changing the plant's feed flowrate, while assuming no changes in the membrane's life expectancy and scaling tendency that might affect the permeance, along with neglecting the change in manufacturing, installation, and maintenance costs, could reduce the operational costs of water desalination up to 32% for brackish and 7.5% for seawater plants. Using similar assumptions for a unit where the feed flow is adjusted to maintain the product flowrate was predicted to result in up to 35% reduction of operational costs for brackish and 8% for seawater-fed plants (51).

In addition, they also considered the effect of a hypothetical spacer that is able to double the Sh and halve the pressure drop on the operational costs. They found that the impact of using the advanced spacer would be strongly weakened for longer modules and suggested consideration of smaller tapered-array modules for both high-performing spacers and membranes (51).

In another study, Mansouri et al. (49) employed the response surface methodology (RSM) to post-process their CFD results, in order to optimise pressure dop, permeate flux and SCE, by altering a set of design parameters, namely, angle of attack (α), spacer's geometry angle (β), and feed flowrate, according to Latin Hypercube Sampling (LHS). Sensitivity analysis revealed that among the three investigated parameters, flowrate was the most important while angle of attack was ranked as the least impacting parameter. Their method can be applied to any other filament shape for optimisation purposes (49).

To expand the capabilities in design parameter optimisation, Binger et al. (52) used a six-D matrix of varying design parameters to develop and run their CFD model for 321 different cases to obtain the *dP*, *k*, Pn, Sh, and SCE as spacer performance measures. They then used the results to find the best configuration of an artificial neural network to train a machine learning (ML) model. After finding the best ML model setup, they used the trained model to calculate the abovementioned performance measures and found that their ML model was capable of predicting them, where in the worst case, the deviation was less than 20%. Using this surrogate model for optimising the design parameters and finding the best-performing spacer could reduce the required computational power by several orders of magnitude and be easily used to narrow down the range of cases that need to be accurately modelled through CFD (52).

2.9 Summary

Feed spacers have travelled a long way and faced a lot of mutations, before arriving at present state and the models for predicting them, from simple empirical equations to complex ML models derived by neural networks, became more trustable and accurate, but also increasingly complicated. Despite the unquestionable benefits of more accurate models as a simple and easy-to-use tool for evaluating the design cases, their intricacy would make them less understandable by the design engineers. On the other hand, design engineers would need a concrete foundation of knowledge to be able to step ahead of try-and-error and found-by-luck approaches and creating the new design cases, intentionally.

The present work focuses on this topic, by looking for simple but general patterns that can explain the spacers' behaviours and make them more understandable for the readers.

References

1. Nollet J-A. Recherches sur les causes du bouillonnement des liquides. Histoire de l'Académie royale des sciences. 1752; 1:57-104.

2. van't Hoff JH. The function of osmotic pressure in the analogy between solutions and gases. Proceedings of the Physical Society of London. 1887; 9(1):307-334.

3. van't Hoff JH. Osmotic pressure and chemical equilibrium. Nobel Lecture. 1901.

4. Saline water conversion report. Washington, D.C.: United States Office of Saline Water; 1964.

5. Vos KD, Riley RL, Lonsdale HK, Merten U. Reverse osmosis for water desalination. Research and development progress report, no. 208. Washington, D.C.: United States Office of Saline Water; 1966.

6. DaCosta AR, Fane AG, Fell CJD, Franken ACM. Optimal channel spacer design for ultrafiltration. Journal of Membrane Science. 1991; 62(3):275-291.

7. DaCosta AR. Fluid flow and mass transfer in spacer-filled channels for ultrafiltration [Ph.D thesis]. Sydney, Australia: University of New South Wales; 1993.

8. Cao Z, Wiley DE, Fane AG. CFD simulations of net-type turbulence promoters in a narrow channel. Journal of Membrane Science. 2001; 185(2):157-176.

9. Koutsou CP, Yiantsios SG, Karabelas AJ. Numerical simulation of the flow in a plane-channel containing a periodic array of cylindrical turbulence promoters. Journal of Membrane Science. 2004; 231(1-2):81-90.

10. Santos JLC, Geraldes V, Velizarov S, Crespo JG. Investigation of flow patterns and mass transfer in membrane module channels filled with flow-aligned spacers using computational fluid dynamics (CFD). Journal of Membrane Science. 2007; 305(1-2):103-117.

11. Johnson J, Busch M. Engineering aspects of reverse osmosis module design. Desalination and Water Treatment. 2010; 15(1-3):236-248.

12. Saeed A. Effect of feed channel spacer geometry on hydrodynamics and mass transport in membrane modules [Ph.D Thesis]. Perth, Australia: Curtin University; 2012.

13. Saeed A, Vuthaluru R, Yang YW, Vuthaluru HB. Effect of feed spacer arrangement on flow dynamics through spacer filled membranes. Desalination. 2012; 285:163-169.

14. Saeed A, Vuthaluru R, Vuthaluru H. Concept of spacer configuration efficacy (sce) applied to optimize ladder type feed spacer filament spacing in narrow channels. International Conference On Water Desalination, Treatment and Management & Indian Desalination Association Annual Congress, 2013. Jaipur, India: The Malaviya National Institute of Technology.

15. Saeed A, Vuthaluru R, Vuthaluru HB. Investigations into the effects of mass transport and flow dynamics of spacer filled membrane modules using CFD. Chemical Engineering Research & Design. 2015; 93:79-99.

16. Saeed A, Vuthaluru R, Vuthaluru HB. Impact of feed spacer filament spacing on mass transport and fouling propensities of ro membrane surfaces. Chemical Engineering Communications. 2015; 202(5):634-646.

17. Taherinejad M, Afrouzan A, Derakhshan S. CFD investigation of near-membrane slippery condition effects on water/salt transport in a reverse osmosis feed channel. Arabian Journal for Science and Engineering. 2021; 46(7):6673-6685.

18. In Seok K, Ho Nam C. The effect of turbulence promoters on mass transfer—numerical analysis and flow visualization. International Journal of Heat and Mass Transfer. 1982; 25(8):1167-1181.

19. Schock G, Miquel A. Mass-transfer and pressure loss in spiral wound modules. Desalination. 1987; 64(C):339-352.

20. DaCosta AR, Fane AG. Net-type spacers: Effect of configuration on fluid flow path and ultrafiltration flux. Industrial and Engineering Chemistry Research. 1994; 33(7):1845-1851.

21. DaCosta AR, Fane AG, Wiley DE. Spacer characterization and pressure drop modelling in spacer-filled channels for ultrafiltration. Journal of Membrane Science. 1994; 87(1-2):79-98.

22. Fane AG, DaCosta AR, Cao Z, Wiley DE. Factors affecting performance of membrane processes: The spiral wound element design and operation. Australian Journal of Dairy Technology. 1997; 52(1):71-72.

23. Schwinge J, Wiley DE, Fane AG, Guenther R. Characterization of a zigzag spacer for ultrafiltration. Journal of Membrane Science. 2000; 172(1-2):19-31.

24. Geraldes V, Semião V, De Pinho MN. Flow and mass transfer modelling of nanofiltration. Journal of Membrane Science. 2001; 191(1-2):109-128.

25. Geraldes V, Semiao V, Norberta De Pinho M. The effect on mass transfer of momentum and concentration boundary layers at the entrance region of a slit with a nanofiltration membrane wall. Chemical Engineering Science. 2002; 57(5):735-748.

26. Li F, Meindersma W, de Haan AB, Reith T. Optimization of commercial net spacers in spiral wound membrane modules. Journal of Membrane Science. 2002; 208(1-2):289-302.

27. Li F, Meindersma GW, de Haan AB, Reith T. Optimization of non-woven spacers by CFD and validation by experiments. Desalination. 2002; 146(1-3):209-212.

28. Li F, Meindersma W, de Haan AB, Reith T. Experimental validation of CFD mass transfer simulations in flat channels with non-woven net spacers. Journal of Membrane Science. 2004; 232(1-2):19-30.

29. Fimbres-Weihs GA, Wiley DE. Numerical study of mass transfer in three-dimensional spacer-filled narrow channels with steady flow. Journal of Membrane Science. 2007; 306(1-2):228-243.

30. Cipollina A, Di Miceli A, Koschikowski J, Micale G, Rizzuti L. CFD simulation of a membrane distillation module channel. Desalination and Water Treatment. 2009; 6(1-3):177-183.

31. Cipollina A, Micale G, Rizzuti L. Membrane distillation heat transfer enhancement by CFD analysis of internal module geometry. Desalination and Water Treatment. 2011; 25(1-3):195-209.

32. Fane AG, Tang CY, Wang R. Membrane technology for water: Microfiltration, ultrafiltration, nanofiltration, and reverse osmosis. Treatise on water science. Vol. 4: Elsevier; 2011. p.301-335.

33. Qureshi M, Shakaib M. CFD study for temperature and concentration profiles in membrane channels. International conference on Energy and Sustainability, 2013. Karachi, Pakistan: NED University of Engineering & Technology.

34. Karabelas AJ, Kostoglou M, Koutsou CP. Modeling of spiral wound membrane desalination modules and plants: Review and research priorities. Desalination. 2015; 356:165-186.

35. Haaksman VA, Siddiqui A, Schellenberg C, Kidwell J, Vrouwenvelder JS, Picioreanu C. Characterization of feed channel spacer performance using geometries obtained by x-ray computed tomography. Journal of Membrane Science. 2017; 522:124-139.

36. Horstmeyer N, Lippert T, Schön D, Schlederer F, Picioreanu C, Achterhold K, et al. Ct scanning of membrane feed spacers – impact of spacer model accuracy on hydrodynamic and solute transport modeling in membrane feed channels. Journal of Membrane Science. 2018; 564:133-145.

37. Dashtpour R, Al-Zubaidy S. Energy efficient reverse osmosis desalination process. International Journal of Environmental Science and Development. 2012; 3(4):339-345.

38. Koutsou CP, Yiantsios SG, Karabelas AJ. Direct numerical simulation of flow in spacer-filled channels: Effect of spacer geometrical characteristics. Journal of Membrane Science. 2007; 291(1-2):53-69.

39. Koutsou CP, Yiantsios SG, Karabelas AJ. A numerical and experimental study of mass transfer in spacer-filled channels: Effects of spacer geometrical characteristics and schmidt number. Journal of Membrane Science. 2009; 326(1):234-251.

40. Koutsou CP, Karabelas AJ, Goudoulas TB. Characteristics of permeate-side spacers of spiral wound membrane modules. Desalination. 2013; 322:131-136.

41. Ranade VV, Kumar A. Fluid dynamics of spacer filled rectangular and curvilinear channels. Journal of Membrane Science. 2006; 271(1-2):1-15.

42. Shakaib M, Hasani SMF, Mahmood M. Study on the effects of spacer geometry in membrane feed channels using three-dimensional computational flow modeling. Journal of Membrane Science. 2007; 297(1-2):74-89.

43. Shakaib M, Hasani SMF, Ahmed I, Yunus RM. A CFD study on the effect of spacer orientation on temperature polarization in membrane distillation modules. Desalination. 2012; 284:332-340.

44. Karode SK, Kumar A. Flow visualization through spacer filled channels by computational fluid dynamics i. Pressure drop and shear rate calculations for flat sheet geometry. Journal of Membrane Science. 2001; 193(1):69-84.

45. Li YL, Tung KL. CFD simulation of fluid. Flow through spacer-filled membrane module: Selecting suitable cell types for periodic boundary conditions. Desalination. 2008; 233(1-3):351-358.

46. Storck A, Hutin D. Energetic aspects of turbulence promotion applied to electrolysis processes. Canadian Journal of Chemical Engineering. 1980; 58(1):92-102.

47. Lau KK, Abu Bakar MZ, Ahmad AL, Murugesan T. Feed spacer mesh angle: 3d modeling, simulation and optimization based on unsteady hydrodynamic in spiral wound membrane channel. Journal of Membrane Science. 2009; 343(1-2):16-33.

48. Schwinge J, Wiley DE, Fletcher DF. Simulation of the flow around spacer filaments between channel walls. 2. Mass-transfer enhancement. Industrial & Engineering Chemistry Research. 2002; 41(19):4879-4888.

49. Mansouri N, Moghimi M, Taherinejad M. Investigation on hydrodynamics and mass transfer in a feed channel of a spiral-wound membrane element using response surface methodology. Chemical Engineering Research and Design. 2019; 149:147-157.

50. Toh KY, Liang YY, Lau WJ, Fimbres Weihs GA. 3d CFD study on hydrodynamics and mass transfer phenomena for swm feed spacer with different floating characteristics. Chemical Engineering Research and Design. 2020; 159:36-46.

51. Toh KY, Liang YY, Lau WJ, Weihs GAF. The techno-economic case for coupling advanced spacers to high-permeance ro membranes for desalination. Desalination. 2020; 491:114534.

52. Binger ZM, Achilli A. Surrogate modeling of pressure loss & mass transfer in membrane channels via coupling of computational fluid dynamics and machine learning. Desalination. 2023; 548:116241.

53. U.S. Congressional record – senate. Washington, D.C.: Library of Congress; 1949. p. 2574-2575.

54. U.S. Congressional record – senate. Washington, D.C.: Library of Congress; 1950. p. 67.

55. Saline water conversion report. Washington, D.C.: United States Office of Saline Water; 1955.

56. Reid CE, Breton EJ. Water and ion flow across cellulosic membranes. Journal of Applied Polymer Science. 1959; 1(2):133-143.

57. Strathmann H. Control of concentration polarization in reverse osmosis desalination of water. Research and development progress report; no. 336. Washington, D.C.: United States Office of Saline Water; 1968.

58. Bixler HJ, Cross RA. Final report on control of concentration polarization in reverse osmosis desalination of water. Research and development progress report; no. 469. Washington, D.C.: United States Office of Saline Water; 1969.

59. Goldsmith H, Lolachi H. Test cell for measuring the concentration polarization boundary layer in a reverse osmosis system. Research and development progress report; no. 527. Washington, D.C.: United States Office of Saline Water; 1970.

60. Goldsmith H, Lolachi H. Measurements of concentration polarization boundary layer in reverse osmosis desalinating systems. Research and development progress report; no. 727. Washington, D.C.: United States Office of Saline Water; 1971.

61. Ohya H, Taniguchi Y. An analysis of reverse osmotic characteristics of roga-4000 spiral-wound module. Desalination. 1975; 16(3):359-373.

62. Taniguchi Y. An analysis of reverse osmosis characteristics of roga spiral-wound modules. Desalination. 1978; 25(1):71-88.

63. Kimura S, Sourirajan S. Mass transfer coefficients for use in reverse osmosis process design. Industrial & Engineering Chemistry Process Design and Development. 1968; 7(4):539-547.

64. Ohya H, Sourirajan S. Some general equations for reverse osmosis process design. Aiche Journal. 1969; 15(6):829-836.

65. A. Sonin A, S. Isaacson M. Optimization of flow design in forced flow electrochemical systems, with special application to electrodialysis. Industrial & Engineering Chemistry Process Design and Development 1974; 13(3):241-248.

66. Isaacson MS, Sonin AA. Sherwood number and friction factor correlations for electrodialysis systems, with application to process optimization. Industrial & Engineering Chemistry Process Design and Development. 1976; 15(2):313-321.

67. Gröber H, Erk S, Grigull U. Fundamentals of heat transfer. New York: McGraw-Hill, ; 1961.

68. Schwinge J, Wiley DE, Fletcher DF. A CFD study of unsteady flow in narrow spacer-filled channels for spiral-wound membrane modules. Desalination. 2002; 146(1-3):195-201.

69. Schwinge J, Wiley DE, Fletcher DF. Simulation of the flow around spacer filaments between narrow channel walls. 1. Hydrodynamics. Industrial & Engineering Chemistry Research. 2002; 41(12):2977-2987.

70. Liang YY, Toh KY, Weihs GAF. 3d CFD study of the effect of multi-layer spacers on membrane performance under steady flow. Journal of Membrane Science. 2019; 580:256-267.

Chapter 3. Methodology and numerical techniques

This study is based on the Computational Fluid Dynamics (CFD) approach as the main method for evaluating fluid motion and mass transfer through different configurations of spacer-filled channels. This chapter covers the details of what lies behind the scenes, namely, fundamental CFD concepts, simplifying assumptions, governing equations, boundary conditions, and numerical solver settings, to ensure the accuracy and reproducibility of the study's outcomes.

3.1 Introduction

Experiments are more expensive than CFD models to design, set-up and run and they need much more time and experienced human resources, but they provide a higher level of accuracy. As an alternative to experiments, the CFD approach can be used to numerically solve a model that in this case includes solving mass, energy and momentum equations that govern the fluid motion and solute mass transfer inside the domain. The precision and reliability of the results are founded on the accuracy of the governing equations, simplifying assumptions, boundary conditions, numerical solution parameters, and mesh suitability. CFD models can also have notable advantages as well. For example, compared to an experimental rig, it is much easier to replicate or transfer a CFD model to other researchers. This can enable other researchers to continue or expand a project. In addition, with the rapid growth in High Performance Computing (HPC) resources available to the academic and industrial sectors, it is easy to setup and run a CFD model for numerous scenarios at the same time, which is not possible for an experimental setup. In addition to the extent, ease of use, and quality of the post-processing options, the ability to gather data at any point and at any time without interfering with the fluid's motion is the other notable advantage of using a CFD approach.

In this study, a CFD model has been developed, validated, and used for generating data, which was employed to investigate the characteristics of different feed spacer arrangements and the effect of changing the flowrate, the gap between the spacer filaments, and some geometrical characteristics on the spacers' performance.

3.2 Basic elements of CFD

For successfully using CFD software, ANSYS User Guide (1) recommends that users proceed via these steps:

- Define the modelling goals.
- Create the model geometry and mesh.
- Set up the solver and physical models.
- Compute and monitor the solution.
- Examine and save the results.
- Consider revisions to the numerical or physical model parameters, if necessary.

To achieve a successful simulation, a workflow with three main stages should be followed, where the first and last stages have a more interactive nature, while the second stage is mainly governed and controlled by the software. The three stages are:

Pre-processing

- Setup the problem / getting the problem definition from the user

Solving

- Converting the problem to an appropriate set of equations/matrixes to be solved
- Assuming proper initial values, if applicable
- Splitting the work into partitions, if applicable
- Allocating each partition to a solver task
- Running the iteration and gathering the outcome from the solver task(s)
- Deciding whether the problem is solved
- If required, proceeding through another iteration
- When the problem solved, integrating the partitions, and creating a unified solution

Post-processing

- Facilitating the user's post-processing tasks, such as data extraction and visualisation

Generally, there are two main ways to interact with the software, Graphical User Interface (GUI) and Text User Interface (TUI). Based on its ease of use, the former can be a time-efficient option for small or unrepetitive problems and it is a better choice for less experienced users. The latter, however, can provide notable advantages in terms of decreasing the user's workload and the possibly adding of human-error, when the model runs several cases, especially in HPC environments.

In this study, the GUI was used for developing the geometries and a basic model, and then TUI scripts were used for the mesh generation phase and running all the cases. More details about this are discussed through the chapter. **Appendix III** includes an example script for meshing, and **Appendix IV** shows an example script for solving the model.

3.2.1 Hardware / software used

In the present study, different ANSYS versions (from 15.0 to 2021R1) and modules (ANSYS Design Modeler™, SpaceClaim™, ANSYS Meshing™, ANSYS Fluent™ and ANSYS Workbench™) were used to simulate the flow through the membrane feed channels.

In the initial stages, a PC equipped with one E5-1650v2 Intel Xeon CPU with 6/12 core/hyper-thread configuration was used for developing and running the model. It had a base clock speed of 3.5 GHz (100 MHz × 35) that was overclocked to 4.2 GHz (100 MHz × 42). The machine was equipped with 1×NVIDIA Quadro K2000 and 128 GB of ECC-Registered DDR3 memory (PC3-14900) running at 1866 MHz, in the form of 8 × 16 GB modules.

Since 2018, the Pawsey Supercomputing Centre[4] (Pawsey) provided the author with HPC infrastructure, which assisted in increasing the number of cases and enhanced the post-processing capabilities. In the meshing stage, up to two nodes were used that had two Intel Xeon E5-2680 v4 @ 2.4 GHz (Broadwell) with 14 physical cores per CPU, no hyper-threading, 128 GB DDR4 of memory. The nodes were connected via Intel 100 Gb/s Omni-Path interconnect. In the solving stage, the model was run via eight parallel Magnus nodes from the Pawsey, each equipped with two Intel Xeon E5-2690 v3 (Haswell) 12-core CPUs (192 physical cores in total, with no hyper-threading) and 64 GB DDR4 of memory, with Cray's Aries interconnect for inter-node communications and a Cray Sonexion 1600 Lustre filesystem connected through InfiniBand for storage. Intensive post-processing tasks were facilitated by using a single node, equipped with two Intel Xeon E5-2680 v4 @ 2.4 GHz (Broadwell) 14-core CPUs, 256 GB DDR4 and four NVIDIA Tesla P100 GPUs with 16 GB HBM2 per GPU. The Pawsey computing nodes used for both meshing and solving, used 'SUSE Linux Enterprise Server 12 SP3' as Operating System (OS), while the visualising nodes used for post-processing used 'CentOS 7'.

[4] Pawsey Supercomputing Centre with funding from the Australian Government and the Government of Western Australia

3.2.2 Assumptions

In the present study, several simplifying assumptions were used to keep the model's complexity at a manageable level, with minimum effect on its accuracy. This section explains the details of the employed assumptions.

The effect of lateral curvature of the channel

Coiling the feed / permeate sandwiches around the central permeate collection tube is the basis of SWMs and the effect of the lateral curvature has been fully investigated by Li and Tung (2). However, as this work is mainly focusing on the spacers' characteristics and their effects on the production rate and energy consumption in a comparative way, investigating the effect of lateral curvature is not part of current work's vision. In the present study, the top and bottom boundaries of the domain are assumed to be parallel flat planes, and the effect of the domain's curvature has been neglected.

Meshing the filament / membrane interface

In an ideal approach, a membrane would touch its nearby filament, as a tangential plane. Figure 3-1 shows two arcs (a 40° and a 1°arc) accompanied by their tangential lines, where the 1° arc can demonstrate the extent of difficulty involved in meshing the area between the arc and its tangential line. Meshing this part of the model will lead to a fractal structure, which means that regardless of the meshing method or the extent of reducing the minimum cell size, the mesh will have low quality and highly skewed faces close to the contact point.

In addition, in 3-D models, trying to subtract a cylinder touching the domain boundary (representing the spacer filament) from the domain will lead to an interface with no volume, which is problematic for some software as it would not be accepted as a valid domain.

Figure 3-1. 40° and 1° arcs, with tangential lines

There are a few approaches available to address this problem. In the next chapter, **Table 4-1** reviews the options that have been used in some of the previous studies. The details of the approach used in the present study, which is increasing the filament diameter by 1%, is discussed in Section **4.2.5**.

Fluid flow

The fluid is assumed to be Newtonian and the flow to be at a steady state in the laminar region, as the model is used for investigating Reynolds numbers below 200, in a fully wetted channel geometry. The fluid dynamic is also assumed to be fully developed in the measuring unit cell. As discussed in (3), the fluid dynamic can be considered fully developed, after 3–4 unit cells, however, it should be noted that the mass transfer will not become fully developed so quickly. In fact, for arriving at fully developed mass transfer, several thousands of unit cells need to be considered. This under-developed mass transfer can explain why the mass transfer performance measures are related to boundary conditions.

The inlet flow is defined as a '*mass flow inlet*' that enters the domain normal to the inlet face. The outlet is assumed to be a pressure outlet at ambient pressure.

The fluid's physical properties are assumed to be constant, regardless of the salt concentration.

Salinity

Notwithstanding the possibility of calculating the concentration at membrane faces based on the van't Hoff osmotic pressure equation, the salt concentration was assumed to be constant at the membrane, in order to keep the model results comparable with previous studies (3-11), and also to decrease the computational demand for solving the model.

3.3 Pre-processing

The main goal in the pre-processing stage is to define the problem and prepare the model for the solver, which can be done through the GUI or TUI. As discussed before, the GUI was used to prepare all geometries and the base CFD model in the present study, with the TUI used for more repetitive tasks, such as meshing different geometries or running the model for different flowrates and exporting the results, with example scripts provided in **Appendix III** and **Appendix IV**.

3.3.1 Geometry

More geometries have been included in each step of this study, starting from four basic filaments, and gradually expanding to nineteen at the end. The details of the geometries used for each stage are described in the relevant chapters.

In the present study, the domain covers several unit cells in length and one (or two, in the case of Woven) in width. A unit cell is a Cuboid region on the feed side of the module that is bounded by the membrane surfaces above and below, and by the filament centrelines at the inlet, end and both sides. Therefore, the unit cell includes the fluid and portions of feed spacers (as void), which can be repeated in both longitudinal and latitudinal directions to reconstruct the whole feed side geometry. Figure 3-2 shows a typical domain with nine unit cells, where the middle unit cell is highlighted, and a magnified view is provided to clarify its boundaries on the corner.

As it is impractical to mesh and model the interface between a cylinder and its tangential plane –see Section 3.2.2– the filament diameter, *d*, was increased by 1%, without changing the unit cell's height, width, or length, to make it possible to mesh and model the interface.

3.3.2 Mesh

There are different meshing approaches available for numerical solutions, with their own characteristics, advantages, and disadvantages. For example, hexahedral meshing, in structured and unstructured forms, has been used widely in the literature to model the spacer-filled feed channel of the SWMs (2, 3, 5, 6, 8-10, 12-17), as it needs considerably lower computational

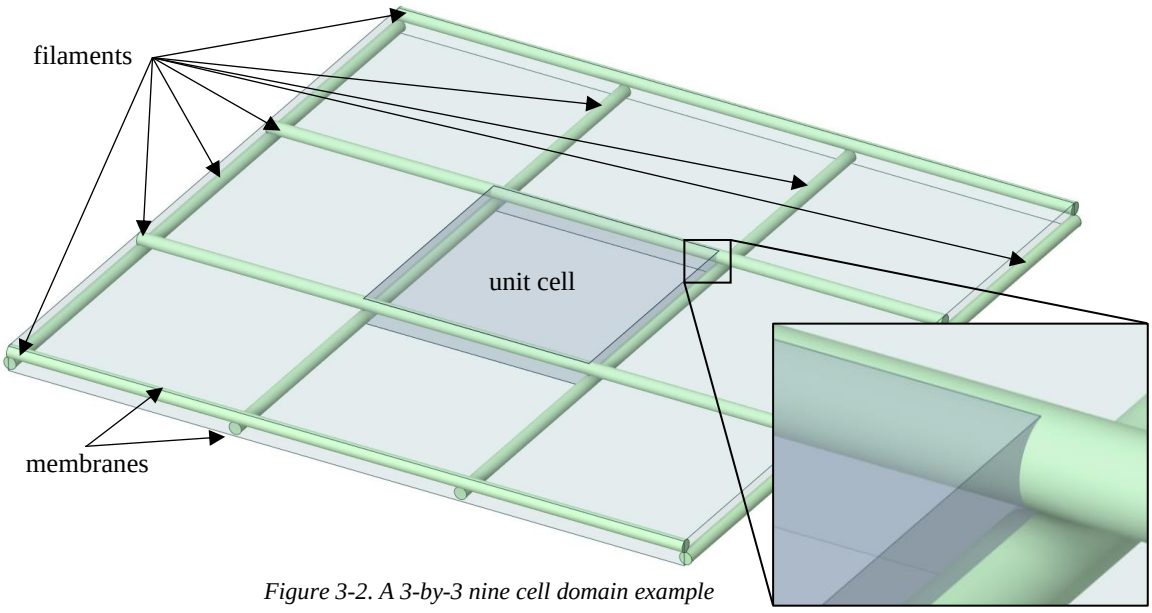

Figure 3-2. A 3-by-3 nine cell domain example

resources, comparing to tetrahedral meshing (18), but hexahedral meshing would be best acting where the fluid movement is mainly parallel with the bulk flow, which might raise doubts about if it is the best approach for modelling SWM feed channel. As explained in the next chapter, Section **4.2.5**, both tetrahedral and hexahedral methods were tried in the preliminary stages of this study and it was found that despite the fact that hexahedral meshing requires less time for each iteration, the tetrahedral mesh would require notably smaller number of iterations to converge, with residual errors reducing in a more consistent pattern. Therefore, the unstructured tetrahedral mesh approach was used for the model, in the first stage.

ANSYS Fluent introduced *poly-hex*, a different approach for meshing in its newer versions, which uses polyhedral cells at the domain boundaries and hexahedral in the bulk volume. This approach preserves the benefits of the polyhedral method where needed and uses a less computationally demanding approach for the rest of the domain, in order to minimise the resources required, while improving accuracy for capturing lateral flow patterns. Therefore, poly-hex meshing was used for the later stages of the present study. Details of the meshing approaches, including the meshing parameters are discussed for each chapter separately. Furthermore, **Appendix III** provides an example script for ANSYS Fluent meshing, including the meshing parameters, which have been used for the poly-hex mesh generation.

3.4 Solver setup and physical models

3.4.1 Governing equations

The liquid is assumed to be an incompressible Newtonian fluid and the Navier-Stokes set of equations used to describe the relevant conservation and transport processes are set out below (19, 20).

$$\frac{\partial u}{\partial x}+\frac{\partial v}{\partial y}+\frac{\partial w}{\partial z}=0 \tag{3-1}$$

$$u\frac{\partial u}{\partial x}+v\frac{\partial u}{\partial y}+w\frac{\partial u}{\partial z}=-\frac{1}{\rho}\frac{\partial P}{\partial x}+\frac{\mu}{\rho}\left[\frac{\partial^2 u}{\partial x^2}+\frac{\partial^2 u}{\partial y^2}+\frac{\partial^2 u}{\partial z^2}\right] \tag{3-2}$$

$$u\frac{\partial v}{\partial x}+v\frac{\partial v}{\partial y}+w\frac{\partial v}{\partial z}=-\frac{1}{\rho}\frac{\partial P}{\partial y}+\frac{\mu}{\rho}\left[\frac{\partial^2 v}{\partial x^2}+\frac{\partial^2 v}{\partial y^2}+\frac{\partial^2 v}{\partial z^2}\right] \tag{3-3}$$

$$u\frac{\partial w}{\partial x}+v\frac{\partial w}{\partial y}+w\frac{\partial w}{\partial z}=-\frac{1}{\rho}\frac{\partial P}{\partial z}+\frac{\mu}{\rho}\left[\frac{\partial^2 w}{\partial x^2}+\frac{\partial^2 w}{\partial y^2}+\frac{\partial^2 w}{\partial z^2}\right] \quad (3\text{-}4)$$

$$u\frac{\partial C}{\partial x}+v\frac{\partial C}{\partial y}+w\frac{\partial C}{\partial z}=\mathcal{D}\left[\frac{\partial^2 C}{\partial x^2}+\frac{\partial^2 C}{\partial y^2}+\frac{\partial^2 C}{\partial z^2}\right] \quad (3\text{-}5)$$

3.4.2 Material properties

The physical properties of the feed-side salt solution is assumed to be constant and to be the same as water, except the density, which was calculated as the weighted average of the component densities. The properties used in this work are provided in next chapter, **Table 4-3**. The salt-water diffusivity was assumed to be constant as suggested in (21).

3.4.3 Boundary conditions

Inlet

The inlet flow was defined as a mass-flow-inlet that enters the domain, normal to the surface, with constant mass flow representing the desired Reynolds number.

$$C|_{inlet}=C_i \quad (3\text{-}6)$$

$$u=\frac{\dot{m}}{\rho A_i} \quad (3\text{-}7)$$

$$v=w=0 \quad (3\text{-}8)$$

Outlet

The outlet face was assumed to be a pressure outlet.

$$P|_{outlet}=P_O \quad (3\text{-}9)$$

Membranes

Membranes were assumed to be non-slip walls with no permeation and a constant solute concentration.

$$C|_{membrane}=C_m \quad (3\text{-}10)$$

$$u = v = w = 0 \tag{3-11}$$

Filaments

Filaments were assumed to be non-slip walls with zero mass flux for water and salt.

$$\frac{\partial C}{\partial n} = 0 \tag{3-12}$$

$$u = v = w = 0 \tag{3-13}$$

Side walls

Side walls were assumed to be symmetry walls.

$$\frac{\partial C}{\partial z} = 0 \tag{3-14}$$

$$\frac{\partial u}{\partial z} = \frac{\partial v}{\partial z} = \frac{\partial w}{\partial z} = 0 \tag{3-15}$$

3.4.4 Numerical solution setup

In general, pressure-based absolute velocity and steady-state methods were used to define the CFD model. For the solver, the Coupled Scheme was chosen as it offers steady convergence and a minimum of fluctuation through the iterations. For spatial discretization, the Green-Gauss Node Base method was used for Gradient, Second Order for pressure and Third Order MUSCL for momentum and salinity calculations. The maximum accepted error was set to 10^{-5}.

3.4.5 Validation

Before using the developed model for simulating planned cases, the model results were compared with some similar cases covered in other studies, to ensure the model's validity.

The values reported for shear stress, pressure drop, Pn and ΔP^* from (22), (17), (8) and the present work are shown and compared in Table 3-1. The validity of the model is discussed in more details in the next chapter, Section **4.3.4**.

Table 3-1. Comparison of hydraulic results for Re = 100 with a Ladder-type spacer

Parameter	(22) [a]	(17) [b]	(8) [c]	Present study [d]
Average shear stress on top wall (N/m^2)	–	1	1.15	0.915
Average shear stress on bottom wall (N/m^2)	–	0.16	0.20	0.165
Pressure drop, $\Delta P/L$ (kPa/m)	–	5	6.29	3.859
Power number, Pn × 10^{-5}	1.7	–	1.80	2.946
Dimensionless pressure drop, ΔP^*	–	–	0.32	0.192

[a] Interpolated values, extracted from provided plot
[b] $L = 4\ H$
[c] $L = 4.1\ H$ and $H = 0.772$ mm
[d] $L = 4.1\ H$ and $H = 1$ mm

3.5 Solver

After validating the model, a general and common basis was used for all cases covered in this study to maintain maximum comparability and a minimum of inconsistency in the results.

The CFD solver, ANSYS Fluent, used in this study was run until it reached an acceptable convergence level. **Appendix IV** provides an example script for solving the model. The case and results were stored for post-processing.

3.6 Post-processing and interpreting the results

As described earlier, the solving script (see **Appendix IV**) also extracts the raw results, namely pressure drop and changes in solute concentration along the domain, from each case and stores them in text format for further calculations. Microsoft® Excel was used to calculate all other parameters for each case, according to their definitions as mentioned in Section 2.3.

MATLAB® version 9.9.0.1592791 (R2020b) Update 5 was used to perform further numerical tasks. To investigate possible correlations between different parameters, the 'fit' function was used, where the fitting type was limited to power ($y = ax^b$) format with the 'non-linear least square' method and 'Levenberg-Marquardt' algorithm, and exponential ($y = ae^{bx}$) format, with the 'non-linear least square' method and 'Trust-Region' algorithm.

References

1. Ansys® fluent academic research, release 2022r1, help system, getting started, 2.1. Steps in solving your CFD problem. 2022.

2. Li YL, Tung KL. The effect of curvature of a spacer-filled channel on fluid flow in spiral-wound membrane modules. Journal of Membrane Science. 2008; 319(1-2):286-297.

3. Saeed A. Effect of feed channel spacer geometry on hydrodynamics and mass transport in membrane modules [Ph.D Thesis]. Perth, Australia: Curtin University; 2012.

4. In Seok K, Ho Nam C. The effect of turbulence promoters on mass transfer—numerical analysis and flow visualization. International Journal of Heat and Mass Transfer. 1982; 25(8):1167-1181.

5. Schwinge J, Wiley DE, Fletcher DF. A CFD study of unsteady flow in narrow spacer-filled channels for spiral-wound membrane modules. Desalination. 2002; 146(1-3):195-201.

6. Schwinge J, Wiley DE, Fletcher DF. Simulation of the flow around spacer filaments between channel walls. 2. Mass-transfer enhancement. Industrial & Engineering Chemistry Research. 2002; 41(19):4879-4888.

7. Fimbres-Weihs GA, Wiley DE. Numerical study of mass transfer in three-dimensional spacer-filled narrow channels with steady flow. Journal of Membrane Science. 2007; 306(1-2):228-243.

8. Saeed A, Vuthaluru R, Yang YW, Vuthaluru HB. Effect of feed spacer arrangement on flow dynamics through spacer filled membranes. Desalination. 2012; 285:163-169.

9. Saeed A, Vuthaluru R, Vuthaluru H. Concept of spacer configuration efficacy (sce) applied to optimize ladder type feed spacer filament spacing in narrow channels. International Conference On Water Desalination, Treatment and Management & Indian Desalination Association Annual Congress; 2013. Jaipur, India: The Malaviya National Institute of Technology.

10. Saeed A, Vuthaluru R, Vuthaluru HB. Investigations into the effects of mass transport and flow dynamics of spacer filled membrane modules using CFD. Chemical Engineering Research & Design. 2015; 93:79-99.

11. Saeed A, Vuthaluru R, Vuthaluru HB. Impact of feed spacer filament spacing on mass transport and fouling propensities of ro membrane surfaces. Chemical Engineering Communications. 2015; 202(5):634-646.

12. Shakaib M, Hasani SMF, Ahmed I, Yunus RM. A CFD study on the effect of spacer orientation on temperature polarization in membrane distillation modules. Desalination. 2012; 284:332-340.

13. Karode SK, Kumar A. Flow visualization through spacer filled channels by computational fluid dynamics i. Pressure drop and shear rate calculations for flat sheet geometry. Journal of Membrane Science. 2001; 193(1):69-84.

14. Schwinge J, Wiley DE, Fletcher DF. Simulation of the flow around spacer filaments between narrow channel walls. 1. Hydrodynamics. Industrial & Engineering Chemistry Research. 2002; 41(12):2977-2987.

15. Ranade VV, Kumar A. Fluid dynamics of spacer filled rectangular and curvilinear channels. Journal of Membrane Science. 2006; 271(1-2):1-15.

16. Santos JLC, Geraldes V, Velizarov S, Crespo JG. Investigation of flow patterns and mass transfer in membrane module channels filled with flow-aligned spacers using computational fluid dynamics (CFD). Journal of Membrane Science. 2007; 305(1-2):103-117.

17. Shakaib M, Hasani SMF, Mahmood M. Study on the effects of spacer geometry in membrane feed channels using three-dimensional computational flow modeling. Journal of Membrane Science. 2007; 297(1-2):74-89.

18. Tomei GL, editor. Steam: Its generation and use. 42nd ed: Barberton, Ohio; Babcock &Wilcox; 2015.

19. Ansys® fluent academic research, release 17.0, help system, theory guide, 1.2. Continuity and momentum equations/1.2.1. The mass conservation equation/1.2.2. Momentum conservation equations.

20. Ansys® fluent academic research, release 17.0, help system, theory guide, 7.1.1. Species transport equations/ 7.1.1.1. Mass diffusion in laminar flows.

21. Capobianchi M, Irvine TF, Tutu NK, Greene GA. A new technique for measuring the fickian diffusion coefficient in binary liquid solutions. Experimental Thermal and Fluid Science. 1998; 18(1):33-47.

22. Li F, Meindersma W, de Haan AB, Reith T. Experimental validation of CFD mass transfer simulations in flat channels with non-woven net spacers. Journal of Membrane Science. 2004; 232(1-2):19-30.

Chapter 4. Investigation into the effectiveness of feed spacer configurations for Reverse Osmosis membrane modules using Computational Fluid Dynamics[5]

Abstract

Reverse osmosis operations for water treatment are usually energy intensive with power being responsible for most of the product price. Several studies used flow characteristics to compare different geometries of feed spacers, but these cannot completely explain the effectiveness of feed spacers for promoting mass transfer near membranes. A few recent studies introduced the concept of Spacer Configuration Efficacy (SCE) combining mass transfer and energy consumption, but SCE has been applied only to a limited extent.

The present study uses 3-dimensional steady state Computational Fluid Dynamics with mass transfer to compare four channels with feed spacer configurations (Ladder-type, Triple, Wavy and Submerged) and an empty plain channel using SCE and other performance measures. In contrast to previous studies, a saturated concentration boundary condition is employed at the membrane surface and optimised meshing of the domain is discussed. Power law correlations for SCE and other performance measures developed from the simulation results enable quick evaluation of the spacers.

Results indicated that the assumed saturated solute concentration at the membrane strongly affects the mass transfer coefficient. Based on SCE, the Wavy spacer configuration showed the highest performance for Re > 120 among the obstructed geometries considered, while Ladder-type was better for Re < 120.

[5] The content of this chapter has been published in Journal of Membrane Science 526 (2017), Q1, IF = 10.53

4.1 Introduction

Reverse osmosis (RO) is a common approach to water desalination, mostly used for brackish water in medium to large scale facilities as well as small scale home applications. It relies on an imposed pressure difference to drive the transfer of the desired permeate, water, through a semi-permeable membrane. The membrane is supposed to stop dissolved species and emulsified particles from passing through to the permeate side. Two of the main challenges in RO desalination are reducing energy consumption and the build-up of deposits on the membrane surface leading to frequent outages. Several studies have focussed on different RO membrane variations, helping the desalination industry to have a better understanding of RO modules and to minimize desalination costs.

RO plants require the minimum amount of energy per unit product among the different desalination technologies available today industrially: multi-stage flash, multi-effect distillation, mechanical vapour compression and reverse osmosis (1). One of the most readily available designs of RO systems is the Spiral Wound Module (SWM), which is made of repeated sandwiches of flat membrane sheets separated by a thin mesh spacer material (Figure 4-1). This combination is rolled around a central tube and fitted into a cylindrical body. As the feed flows through the module, a portion passes through the membrane surface, leaving behind a rich brine and producing permeate, which flows into the central collecting tube (2). SWMs are a compact and cheap option for RO designs offering a high mass transfer area to volume ratio, which leads to high volumetric throughput and moderate energy consumption. In the last few years, several studies have investigated mass transport phenomena or fluid flow to optimize the performance of SWMs. Most of them focused on temperature polarization (3), fluid flow patterns and characteristics (4-8), membrane performance (9) or particle deposition (10). Limited studies tried to optimize the performance of the modules by changing the spacer configuration to reduce energy consumption and particle deposition while also maximizing fluid mixing and recirculation zone effects. Good spacer configurations should minimize build-up of deposits and concentration polarization by keeping the concentration of the solute in the fluid layer in contact with membrane close to the bulk concentration (4, 5, 11-13). Table 4-1 presents a summary of studies conducted on selected SWM spacer configurations from the early 1980s to present.

In general, more mixing in the fluid and more effective recirculating zones will keep mass transfer resistance low and the membrane unblocked. Both effects are characterised by the

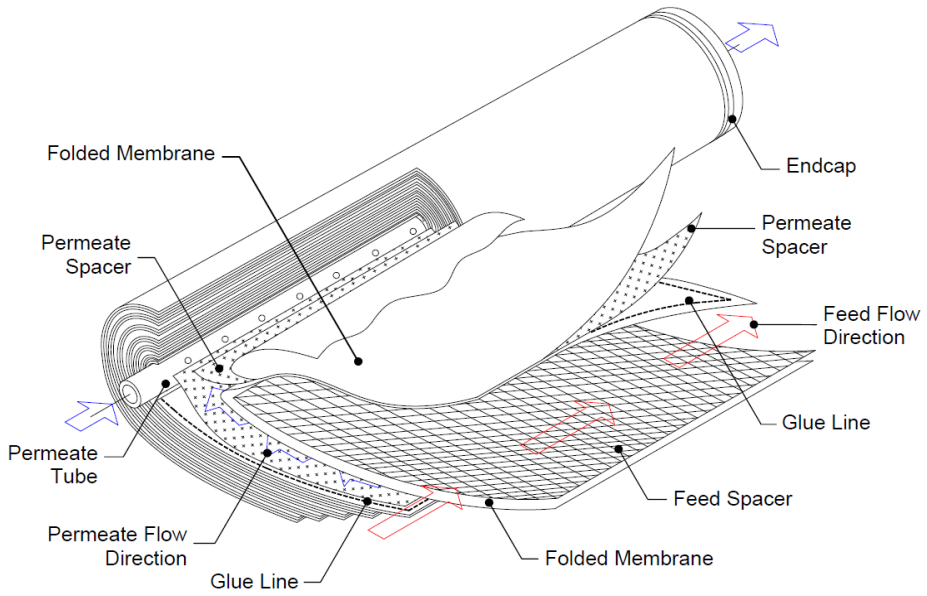

Figure 4-1. Configuration of a typical spiral wound module used for reverse osmosis desalination.

(Source: (1), © copyright [2010], reprinted by permission of Informa UK Limited, trading as Taylor & Taylor & Francis Group, http://www.tandfonline.com)

Sherwood number, Sh. On the other hand, more mixing and flow recirculation means more energy consumption. The final decision on membrane configuration and operating conditions is a trade-off between higher mass transfer rates and longer service intervals between cleaning on one hand, and greater energy costs on the other.

A recent study (12) proposed a dimensionless number that captures both mass transfer, in the form of the Sherwood number, and the energy required for flow, in the form of the Power number, Pn. This dimensionless number, the Spacer Configuration Efficacy (SCE) is defined as Sh/Pn. SCE quantifies mixing quality on the feed side of the membrane for different feed spacer arrangements. Due to its definition, a higher SCE represents a smaller solute concentration difference between the bulk fluid and that near the membrane surface, or a lower pumping energy requirement per unit of permeate. Both mixing quality and recirculating flows will directly influence a unit's energy consumption and increase the maintenance intervals. Saeed et al. (12) defined the SCE concept and also studied the effect of Re on Pn, Sh, SPC and SCE for Ladder-type spacers and suggested the best geometrical arrangement to use among the different Ladder-type cases studied, but this study needs to be extended to investigate the SCE concept for other spacer configurations.

The main goal of this study is to extend the application of SCE to other spacer geometries and to compare spacer behaviour for varying Reynolds numbers in the laminar regime, up to Re = 200, in terms of both flow characteristics and mass transfer phenomena. Computational

fluid dynamics (CFD) will be used to simulate the flow and mass transfer phenomena. Along with commonly reported measures like pressure drop, power consumption and Sherwood number, SCE will also be evaluated from the CFD results, which will allow SCE to be compared with those conventional measures of spacer performance.

Table 4-1. Summary of previous works focusing on spacer effectiveness in spacer filled RO modules.

Configuration	Investigation type	Reynolds number range	Key channel dimension	Number of cells for CFD studies	Geometrical approximation used for filament near membrane [a]	Boundary condition at membrane	Validation	Major findings	Reference
Zigzag Cavity	Numerical analysis for Re = 50 – 500; Experimental visualization for Re = 20 – 410	Re_{ch} = 20 – 500	L/H = 5 Centre to centre	Grid size = 67 × 21	Rectangular block	C = 0 (Electrodialysis case)	Original experiments	Visualized flow patterns $Sh = 0.519\ Sc^{0.376}\ Re^{0.475}$ (Zigzag) $Sh = 1.069\ Sc^{0.376}\ Re^{0.294}$ (Cavity)	(14)
Commercial geometries	Experimental	Re_h = 20 – 2000	Domain size: 2.5 × 40 in	N/A	N/A	N/A	Original experiments	$Sh = 0.065\ Sc^{0.25}\ Re^{0.875}$	(15)
Commercial geometries	Experimental	Re_h = 150 –1000	Domain size: 35 × 285 mm	N/A	N/A	N/A	Original experiments	They modify the Gröber equation for Sh by using a correction factor k_{dc} to increase accuracy: $Sh = 0.664\ k_{dc}\ Sc^{0.33}\ Re^{0.5}\left(\frac{2D_h}{L}\right)^{0.5}$ where $k_{dc} = 1.654\ (d/H)^{-0.039}\ \varepsilon^{0.75}\ (\sin\beta/2)^{0.086}$	(16)
Commercial geometries	CFD: 3D, steady state	Re_h = 300 – 1800	Domain size: 25 × 35 mm H = 1 – 2 mm	Not mentioned	Filament deformed to octagon	No mass transfer included	Using data provided by (16)	Ten equations for different commercial spacers for the spacer drag coefficient of the form $C_d = A\ /\ (Re)^n$ Velocity distribution reported for some cases.	(17)
Zigzag Cavity Submerged Plain	CFD: 2D, steady state	Re = 120 – 480	Domain size: 2 × 50 mm	15,000	Not mentioned	No mass transfer included	No validation	Flow patterns, shear stress and velocity contours, turbulent kinetic energy diagrams and overall pressure drop.	(18)
Zigzag Cavity Submerged Plain	CFD: 2D, steady state and transient flow	$Re_{ch} \leq 1000$	L/H = 4	Not mentioned	Cylinder cut	No mass transfer included	No validation	Flow patterns, velocity contours and effect of Re on flow disturbance.	(19)
Zigzag Cavity Submerged	CFD: 3D, steady state	Re_{ch} = 90 – 768	L/d = 1.4 – 75 Centre to centre	22,000	Cylinder cut	No mass transfer included	No validation	Flow patterns, velocity contours, effect of spacer geometry (H/d and L/H) on pressure drop and wall shear stress.	(20)
Zigzag Cavity Submerged	CFD: 2D, steady state	Re_{ch} = 100 – 400	L/H = 4 & 8 Centre to centre	Not mentioned	Cylinder cut	Constant unmentioned value set for membrane concentration	No validation	Concept of spacer performance ratio introduced as: $SPMP = \frac{\Delta C_{sp}/\Delta C_{slit}}{\Delta P_{sp}/\Delta P_{slit}}$ Zigzag shows the best SPMP.	(21)

Table 4-1. Summary of previous works focusing on spacer effectiveness in spacer filled RO modules.

Configuration	Investigation type	Reynolds number range	Key channel dimension	Number of cells for CFD studies	Geometrical approximation used for filament near membrane [a]	Boundary condition at membrane	Validation	Major findings	Reference
Ladder-type Woven	Experimental; CFD: 3D, steady state Angle of attack: 0, 15, 30 & 45°; filament angle: 60, 90 & 120°	Re = 80 – 550	L/H = 2 – 10 Side to side	Not mentioned	Not mentioned	Not mentioned	Original experiments	SPC, Pn and Sh number for different geometries and different Re.	(22-24)
Submerged	CFD: 2D, steady state, transient flow	$Re_{ch} \leq 200$	L/H = 3 Centre to centre	5,400	N/A	No mass transfer included	No validation	Velocity contours, shear stress and pressure drop for different Re; flow pattern stable at Re < 60; eddies appear at Re = 78.	(25)
Commercial geometries	CFD: 3D, steady state	Re_{ch} = 75 – 1500	ϵ = 0.52 – 0.875	150,000	Filament expanded by 7%	No mass transfer included	No validation	Pressure drop, dimensionless pressure drop and shear stress for different geometries and different Re; velocity contours.	(26)
Ladder-type	Experimental; CFD: 3D, transient flow	Re_h = 50 – 600 for experiment, Re_h = 67 – 336	L = 3.8, 7.6 & 11.4 mm H = 2 mm Domain size: 30 × 30 mm	500,000	Rectangular block	Not mentioned	Original experiments	Friction factor, flow regime, velocity profile, Reynolds stress tensor, local shear stress, Pn and local Sh for different geometries and Re. S1L0 (L = 3.8 mm, no longitudinal spacer) shows best results.	(27)
Submerged Ladder-type	CFD: 3D, steady state Angle of attack: 30, 45, 60 & 90°	Re_{ch} = 20 – 200	L/H = 2, 3, 4, 6 W/H = 2, 3, 4, 6 Centre to centre	105,000 – 230,000	Cylinder cut	No mass transfer included	± 10% of Li et al. +25% with Koutsou.	Velocity contours and vectors, pressure drop and shear stress for different geometries and Re.	(28)
Ladder-type	CFD: 2D / 3D, steady state Angle of attack: 45 & 90°	$Re_h \leq 1000$	L/H = 4	19×10^6	Filament expanded by 20%, rounded edges	Constant concentration at membrane, equal to average concentration result from 2D simulation	Using data provided by (15)	$\alpha = 45^o$ shows higher mass transfer. Friction factor, local friction factor, salinity, velocity, Sh, salinity contours with tangential velocity vectors and percentage of energy losses for different Re and geometries.	(29)
Ladder-type	Experimental; CFD: 3D	Re_h = 30 – 1000	L/H = 3 Centre to centre	Not mentioned	Not mentioned	No mass transfer included	Original experiments	Model developed agrees with experimental data within 7%. Velocity, shear stress and pressure drop for different lengths with different Re.	(30)
Commercial geometries	CFD: 3D	Re_h < 200 Fixed inlet flowrate	Different 2, 3 and 4-layer spacers	1,500,000 to 6,700,000	Filament expanded	Constant heat flux at membrane	No validation	Membrane distillation study. Multilayer spacers show higher performance and thinner polarization zones.	(31, 32)

Table 4-1. Summary of previous works focusing on spacer effectiveness in spacer filled RO modules.

Configuration	Investigation type	Reynolds number range	Key channel dimension	Number of cells for CFD studies	Geometrical approximation used for filament near membrane [a]	Boundary condition at membrane	Validation	Major findings	Reference
Cavity	CFD: 2D	Re_{ch} = 150 – 300	L/H = 3, 4	50,000	Cylinder cut	Constant heat flux and unspecified mass fraction at membrane	Using data provided by (15)	Membrane distillation study. Sh-Re results are similar to correlations from (15), but Nu values are underpredicted by 30–50%.	(33)
Ladder-type	CFD: 3D, steady state Angle of attack: 0, 45 & 90°	Re_h = 75 – 200	*L*/*H* = 2, 3, 4, 6 *W*/*H* = 2, 3, 4, 6 Side to side	750,000	Filament deformed by ~15% *d*	Mass fraction of salt at membrane equal to 1	Using data provided by (22, 28, 34)	Velocity, dimensionless pressure drop, pressure drop, shear stress, mass transfer coefficient, SPC, Pn, Sh and SCE contours with tangential velocity vectors for different Re and geometries. *L*/*H* and *W*/*H* optimized at 3.6.	(4, 5, 11-13)
Ladder-type	Experimental; CFD: 3D Angle of attack: 45°	Re_h = 100 – 1000	*L*/*H* = 2.1 Centre to centre	5,300,000	Cylinder cut	No mass transfer included	Original experiments	Steady laminar flow for at Re < 200. Unsteadiness appears at Re ~ 250. Fully turbulent at Re ~ 1000. Appearance of different primary and secondary vortices studied.	(35)
Ladder-type	Experimental; CFD: 3D Angle of attack: 45°	Re_h = ~20 – 200	*L*/*H* = 4.5 – 5.7	Not mentioned	Not mentioned	No mass transfer included	Original experiments	Shear stress, pressure drop, power number, friction factor and modified friction factor reported for five commercial spacers. X-ray computed tomography used for accurate determination of spacer geometry. Detailed geometries may lead to better local velocity and shear prediction, resulting in better estimation of fouling and concentration polarization.	(36)

a. Different approaches to geometrical approximation of filament near membrane:

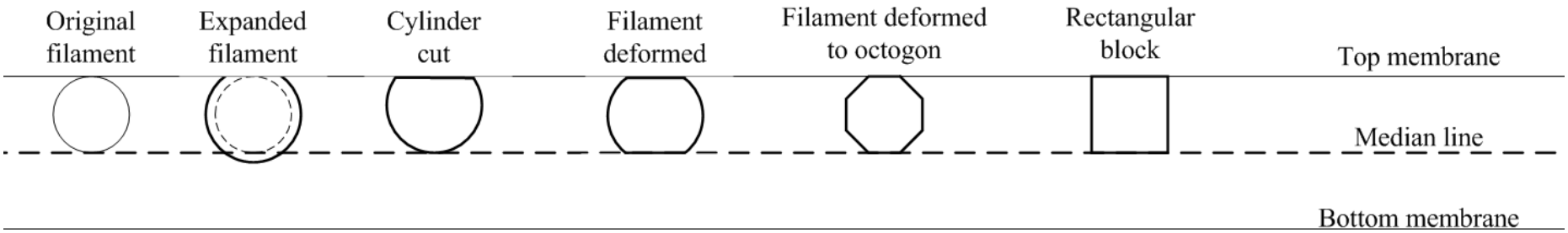

4.2 Simulation approach

4.2.1 Geometries studied

In the current work, five spacer geometries have been studied as shown in Figure 4-2. Selection of these geometries was based on their widespread use and the availability of data from previous studies, which made it possible to compare the results. For each geometry, only a representative portion of the fluid flow domain is shown in Figure 4-2. The Ladder-type geometry (Figure 4-2 a) consists of a layer of straight latitudinal filaments positioned on top of a layer of straight longitudinal filaments to form a square pattern. The Triple geometry (Figure 4-2 b) is a Ladder-type arrangement with a third layer of straight latitudinal filaments added below in the *z* direction. In the Wavy geometry (Figure 4-2 c), straight latitudinal filaments are

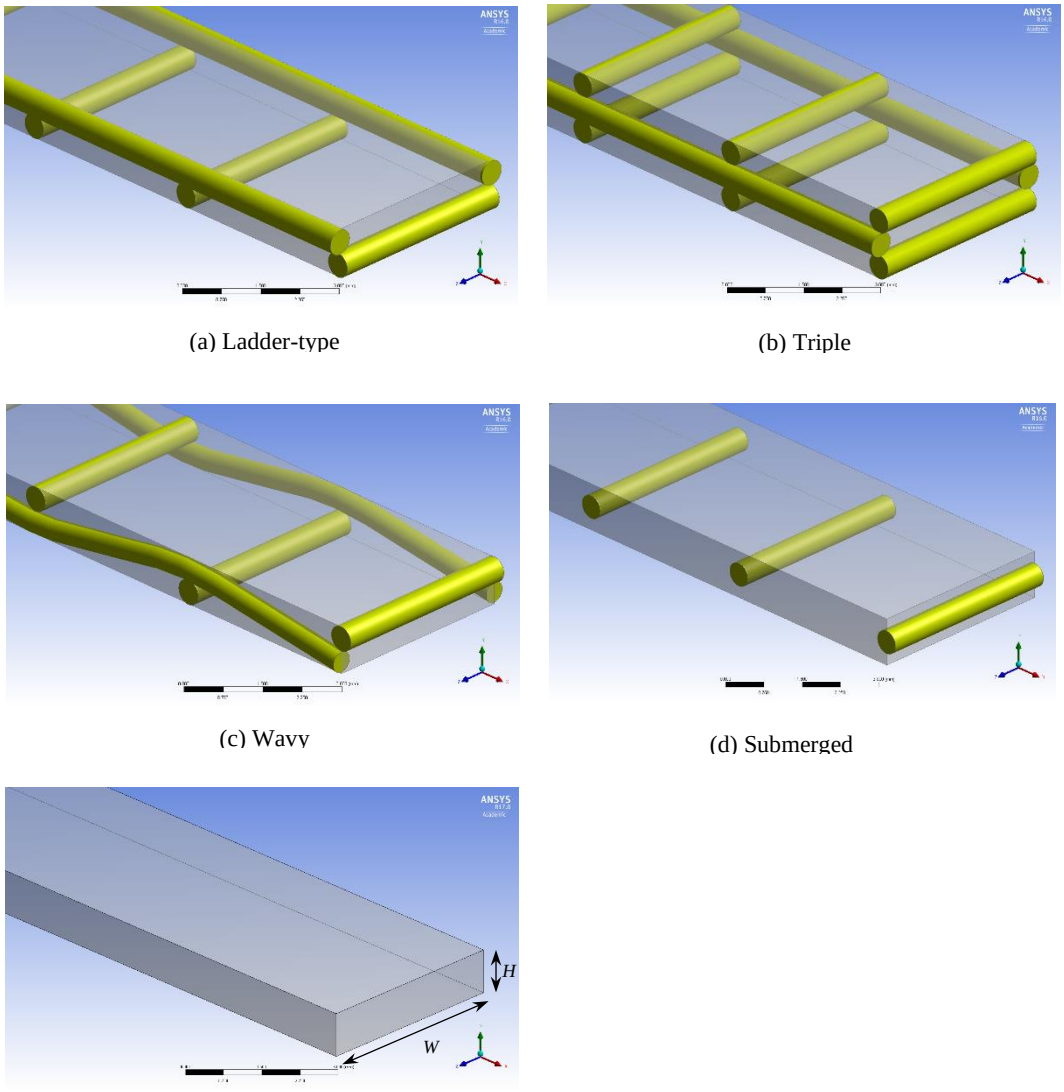

(a) Ladder-type (b) Triple

(c) Wavy (d) Submerged

(e) Plain

Figure 4-2. Schematic diagram of feed spacer geometries considered in the present study.

located alternatively adjacent to the top and bottom membranes with sinusoidal longitudinal filaments weaving between them. The Submerged geometry (Figure 4-2 d) has latitudinal filaments only, positioned midway between the top and bottom membranes. Finally, the Plain geometry (Figure 4-2 e) represents an unobstructed channel between two parallel membrane surfaces; that is, no spacer filaments are present in this geometry. All filaments are assumed to have a circular cross-section which, while not exactly true for commercial spacers, is a reasonable assumption (36). Biplanar feed spacer geometries are most the most widely used type for RO modules (37), which means both Plain and Triple are not common choices for membrane systems, but they are included for comparison purposes with the other more conventional configurations.

4.2.2 Parameters considered for simulation

Hydraulic diameter (D_h)

The hydraulic diameter, D_h, is defined as

$$D_h = \frac{4 \times volume\ occupied\ by\ fluid}{surface\ area\ of\ wetted\ walls} \tag{4-1}$$

For flow in membrane channels with spacer filaments, this becomes (15)

$$D_h = \frac{4 \times (channel\ volume - filament\ volume)}{membrane\ surface\ area + filament\ surface\ area} \tag{4-2}$$

Due to necessary approximations in the filament geometry, which will be discussed in Section 2.5, the volumes and surface areas in this study were carefully extracted from the CFD software used.

Effective velocity (u_{eff})

The effective velocity, u_{eff}, is defined (15) as the volumetric flowrate, $\dot{V}$, divided by the effective area for flow:

$$u_{eff} = \frac{\dot{V}}{A_{eff}} \tag{4-3}$$

The effective area, A_{eff}, is equal to the cross-sectional area of the channel in the flow direction, assuming no filaments are present, multiplied by the porosity of the channel system:

$$A_{eff} = WH\epsilon \tag{4-4}$$

where W is the channel width, H is the channel height, and the porosity is

$$\epsilon = 1 - \frac{filament\ volume}{unobstructed\ channel\ volume} \tag{4-5}$$

The effective velocity characterizes the 'sweeping velocity' or 'bulk average velocity' of fluid in the channel.

Hydraulic Reynolds number (Re)

In the present study, the hydraulic Reynolds number has been used to represent different flowrates through the membrane system. This definition was also used in previous studies (4, 15, 29). All cases considered in the present study were in the laminar flow regime, with Re varying between 50 and 200. The notation Re is used throughout this paper to mean the hydraulic Reynolds number:

$$\mathrm{Re} = \frac{\rho u_{eff} D_h}{\mu} \tag{4-6}$$

It should be noted that other definitions of the Reynolds number also appear in the literature. They differ in the velocity and characteristic length used. For example, the filament diameter and average velocity gives the cylinder Reynolds number ($\mathrm{Re_{cyl}}$) while the channel height and average velocity leads to the channel Reynolds number ($\mathrm{Re_{ch}}$). The different definitions and their characteristics have been discussed elsewhere (4).

Specific Power Consumption (SPC)

SPC represents the mechanical energy required to overcome the fluid's pressure drop per unit length of the domain (38). Storck and Hutin (39) define SPC as

$$SPC = u_{eff} \frac{\Delta P}{L} \tag{4-7}$$

where $\Delta P/L$ is the pressure drop per unit length in the main flow direction. A slight manipulation shows that $SPC = (A_{eff} u_{eff} \Delta P)/(A_{eff} L)$; that is, SPC is the power consumed per unit volume of fluid. Several authors have studied SPC and its relation with different geometries and Reynolds numbers (5, 6, 12, 14, 23-25).

Power number (Pn)

The Power number, Pn, is another term suggested in the literature to represent power consumption in a membrane module. Li et al. (23) introduced Pn after a dimensional analysis to represent the amount of power required to drive the RO operation; the use of Pn was continued in Li et al. (30), Saeed (4), and Haaksman et al. (36).

The Power number is defined as

$$\mathrm{Pn} = \mathrm{SPC}\left(\frac{\rho^2 H^4}{\mu^3}\right) = \frac{\Delta P}{L}\left(\frac{u_{eff}\rho^2 H^4}{\mu^3}\right) \tag{4-8}$$

It can be rearranged as $\mathrm{Pn} = \left(\frac{\Delta P}{\rho {u_{eff}}^2}\right)\left(\frac{u_{eff}\,\rho\, D_h}{\mu}\right)^3\left(\frac{H}{L}\right)\left(\frac{H}{D_h}\right)^3 = \mathrm{EuRe}^3\left(\frac{H}{L}\right)\left(\frac{H}{D_h}\right)^3$, where Eu is the Euler number. Considering this rearrangement, Pn can be interpreted as shown below:

$$\left(\frac{pressure\ forces}{inertial\ forces}\right) \times \left(\frac{inertial\ forces}{viscous\ forces}\right)^3 \times (geometrical\ ratios).$$

The Power number is also considered to be a modified friction factor (40).

Dimensionless pressure drop (ΔP^*)

In 1987, Schock et al. (15) introduced a dimensionless friction factor to interpret their experiments, but recently Shakaib et al. (28) and Koutsou et al. (34) used a new dimensionless pressure drop, ΔP^*, defined as

$$\Delta P^* = \frac{\Delta P}{L}\left(\frac{{D_h}^3}{\mathrm{Re}_{\mathrm{cyl}}^2 \rho {u_{eff}}^2}\right) \tag{4-9}$$

Sherwood number (Sh)

The Sherwood number is defined as

$$\mathrm{Sh} = \frac{k D_h}{\mathcal{D}} \tag{4-10}$$

where k is the average mass transfer coefficient, the hydraulic diameter is used as the characteristic length and $\mathcal{D}$ is the molecular diffusivity of the solute (NaCl) in water.

The result is an average Sh that accounts for mass transfer through both top and bottom membranes. The value of k calculated using a logarithmic mean driving force was negligibly

different from that calculated using the arithmetic mean over the range of conditions explored in this study.

Spacer Configuration Efficacy (SCE)

Saeed (4) recently defined a new dimensionless number, SCE, for use in membrane spacer investigations that combines both mass transfer and pressure drop phenomena:

$$\mathrm{SCE} = \frac{\mathrm{Sh}}{\mathrm{Pn}} \tag{4-11}$$

SCE aims to represent the amount of mass transfer for a given amount of consumed energy. Higher SCE is caused by higher mass transfer or lower energy requirements, which indicates a more effective spacer. This approach was used in our earlier efforts (4, 12).

4.2.3 Governing equations, modelling software and solution options

The Navier-Stokes equations were used to describe conservation and transport processes as shown below. The fluid was assumed to be Newtonian, while the flow was assumed to be steady state and laminar.

$$\frac{\partial u}{\partial x} + \frac{\partial v}{\partial y} + \frac{\partial w}{\partial z} = 0 \tag{4-12}$$

$$u\frac{\partial u}{\partial x} + v\frac{\partial u}{\partial y} + w\frac{\partial u}{\partial z} = -\frac{1}{\rho}\frac{\partial P}{\partial x} + \frac{\mu}{\rho}\left[\frac{\partial^2 u}{\partial x^2} + \frac{\partial^2 u}{\partial y^2} + \frac{\partial^2 u}{\partial z^2}\right] \tag{4-13}$$

$$u\frac{\partial v}{\partial x} + v\frac{\partial v}{\partial y} + w\frac{\partial v}{\partial z} = -\frac{1}{\rho}\frac{\partial P}{\partial y} + \frac{\mu}{\rho}\left[\frac{\partial^2 v}{\partial x^2} + \frac{\partial^2 v}{\partial y^2} + \frac{\partial^2 v}{\partial z^2}\right] \tag{4-14}$$

$$u\frac{\partial w}{\partial x} + v\frac{\partial w}{\partial y} + w\frac{\partial w}{\partial z} = -\frac{1}{\rho}\frac{\partial P}{\partial z} + \frac{\mu}{\rho}\left[\frac{\partial^2 w}{\partial x^2} + \frac{\partial^2 w}{\partial y^2} + \frac{\partial^2 w}{\partial z^2}\right] \tag{4-15}$$

$$u\frac{\partial C}{\partial x} + v\frac{\partial C}{\partial y} + w\frac{\partial C}{\partial z} = \mathcal{D}\left[\frac{\partial^2 C}{\partial x^2} + \frac{\partial^2 C}{\partial y^2} + \frac{\partial^2 C}{\partial z^2}\right] \tag{4-16}$$

Inlet boundary conditions:

$$C|_{inlet} = C_i \tag{4-17}$$

$$u = \frac{\dot{m}}{\rho A_i} \tag{4-18}$$

$$v = w = 0 \tag{4-19}$$

Membrane boundary conditions:

$$C|_{membrane} = C_m \tag{4-20}$$

$$u = v = w = 0 \tag{4-21}$$

Filament boundary conditions:

$$\frac{\partial C}{\partial n} = 0 \tag{4-22}$$

$$u = v = w = 0 \tag{4-23}$$

Symmetry face boundary conditions:

$$\frac{\partial C}{\partial z} = 0 \tag{4-24}$$

$$\frac{\partial u}{\partial z} = \frac{\partial v}{\partial z} = \frac{\partial w}{\partial z} = 0 \tag{4-25}$$

Outlet boundary condition:

$$P|_{outlet} = P_O \tag{4-26}$$

In the present study, different ANSYS 15.0 and 16.0 modules were used to simulate the flow through the membrane feed channels: ANSYS Geometry, ANSYS Meshing, ANSYS Fluent and ANSYS Workbench. The models were run on a PC equipped with an E5-1650v2 Intel Xeon CPU with 6 HT cores 3.5 GHz, 1×NVIDIA Quadro K2000 and 80 GB of ECC Registered DDR3 memory running at 1866 MHz. All parameter values used in this study are given in Sections 4.2.4–4.2.6.

For the Fluent solver, the Coupled Scheme was chosen as it offers steady convergence and a minimum of fluctuation through the iterations. For spatial discretization, the Green-Gauss Node Base method was used for Gradient, Second Order for pressure and Third Order MUSCL for momentum and salinity calculations. The maximum accepted error was set to 10^{-5}.

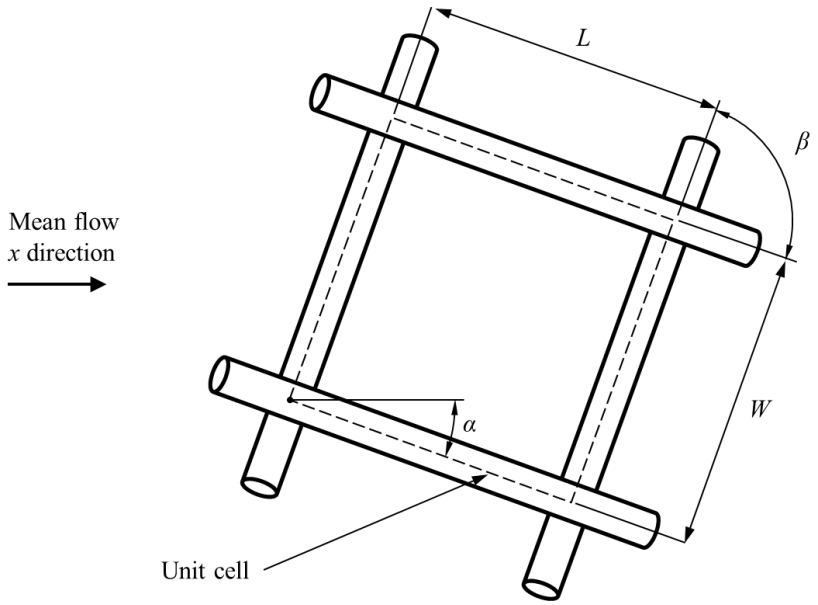

Figure 4-3. Plan view of a unit cell for a typical spacer geometry showing the flow angle of attack (α), spacer geometry angle (β), spacing between longitudinal filaments or channel width (W), and spacing between latitudinal filaments or channel length (L).

4.2.4 Domain

The unit cell is the rectilinear region on the feed side of a membrane system bounded above and below by the membrane surfaces and aligned with the filament centrelines such that it contains fluid and portions of adjacent spacer filaments that could be repeated to reconstruct the entire feed side geometry. Figure 4-3 shows a typical unit cell. In the present study, the domain of the simulated fluid channel was nine unit cells long and one unit cell wide (Figure 4-4). Flow enters the domain through the inlet face in the *x* direction, continues through the channel and leaves the domain at the outlet face. The recent literature reveals that the fluid flow will be fully developed after three or four unit cells (4). If it is assumed conservatively that outlet affects the flow similarly then, in the present study, the fifth unit cell will be most representative of fully developed conditions. It should be noted that other studies assume that one unit cell only is affected by the outlet, but they do so without any proof or justification (4).

4.2.5 Mesh generation

The interface between the cylindrical filaments and the flat membrane is impossible to mesh and model perfectly. No clear explanations or discussions are found in the literature about this specific meshing problem and its possible solutions, but from published figures it can be deduced that two approaches have been taken: (I) using a deformed filament (4, 11, 12) wherein the circular filament is approximated by a polygon or the major segment of a circle, and (II) slightly increasing the filament diameter allowing the filament and membrane to overlap partially (20, 41). In the present study, both methods have been used. Filament extension was used for the Zigzag and Triple geometries and the deformed filament method was used for the Wavy geometry. Preliminary investigations revealed that a 1% extension or cutting based on the filament diameter is the minimum amount of deformation that results in acceptable mesh quality and solution convergence. The available processing power (as detailed in Section 4.2.3) limits the meshing quality. In other words, using a larger amount of deformation results in more relaxed meshing and a lower number of cells, but it decreases simulation accuracy.

Hexahedral meshes have been used in many previous studies (3-5, 11, 12, 17, 19-21, 26-28, 42). However, in the current study, tetrahedral meshes showed lower skewness values and led to quicker and more stable convergence than hexahedral meshes. Hence, tetrahedral cells were used for meshing all models in this work.

In the present study, mesh independence was investigated for the Ladder-type geometry and then the same sizing rules were used for the Submerged and Plain geometries. More detailed meshing was needed for the Wavy and Triple geometries to achieve convergence. As it is important to make the mesh finer close to the filaments and membrane while keeping the total number of elements as low as possible, two local meshing rules were defined in those regions.

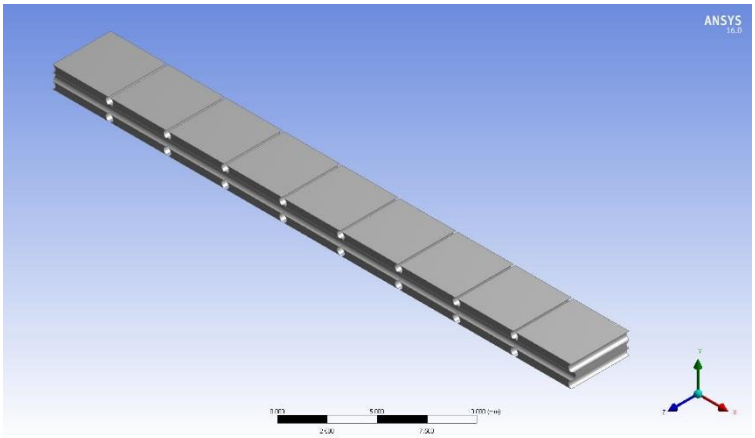

Figure 4-4. Example of the simulation domain for the Triple spacer geometry: 9 unit cells long by 1 unit cell wide.

To ensure mesh independence, the number of cells was increased until the change in key results, such as the total pressure drop and outlet salt mass flowrate, became less than 2%. Table 4-2 reports the final mesh size settings, as defined for ANSYS Meshing. The curvature angle and growth rate shown in the table are, respectively, a measure of the maximum allowed deviation from a flat plane for curved mesh faces and the maximum allowed ratio of the cell sizes of neighbouring cells. To the best of our knowledge, no other studies have reported this detailed meshing information; thus, no comparison is possible for the meshing part of this study.

Table 4-2. ANSYS Meshing mesh size settings used in this study.

Parameter	Default value	Body	Membrane	Filament
Curvature normal angle (°)	18	18	18	6
Minimum size (m)	Based on geometry	1×10^{-7}	1×10^{-7}	1×10^{-7}
Growth rate	1.15	1.15	1.03	1.08

Figure 4-5 is an example of meshing for the Ladder-type geometry, which shows one of the corners of the domain, including both longitudinal and latitudinal filaments.

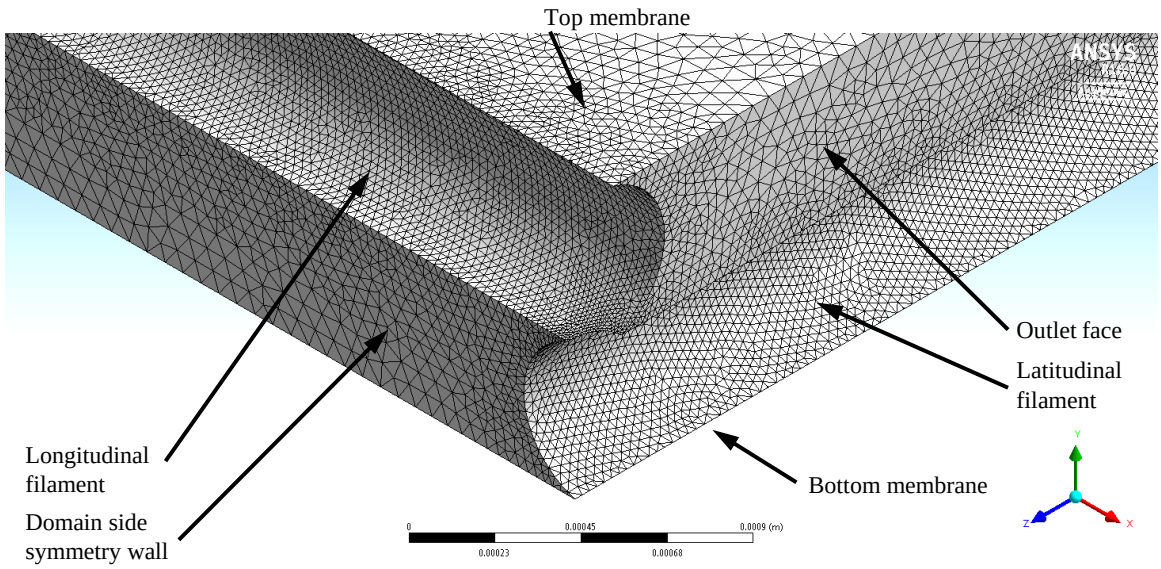

Figure 4-5. Typical example of meshing for the Ladder-type spacer geometry.

4.2.6 Simulation parameters

In the present study, the filament diameter is fixed at d = 0.5 mm. The channel height, H, is set to 2d for all geometries, except for the Triple where it is 3d, and the channel width is W = 4.1×2d in all cases (Figure 4-4), which was suggested as the most efficient size in (13). In all cases, the cells are square, meaning the longitudinal and latitudinal filament spacing is the same, L = W, and the geometry angle β = 90°. The domain is nine unit cells long, as discussed in Section 2.4.

The physical properties of the fluid are constant and assumed to be those of pure water, except for density, which was calculated as a weighted average based on the concentration. Capobianchi et al. (43) showed that NaCl diffusivity in water can be assumed to be constant, regardless of solute concentration.

The feed fluid enters the domain in the x direction, normal to the vertical inlet face. It consists of saline water with a concentration C_i = 5% w/w NaCl. The inlet mass flowrate was varied to provide the required hydraulic Reynolds numbers.

The outlet face at the far end of the channel is parallel to the inlet face and is defined as a pressure outlet. All the fluid entering the domain flows out through this face.

Both membrane planes and all filament surfaces were defined as no-slip, stationary walls. The membranes were assumed to be non-porous and impermeable, and with a fixed concentration boundary condition of C_m = 35% w/w NaCl to represent saturated conditions (44) at the membrane surface. Various recent studies (4, 5, 11, 12) have used a similar fixed concentration boundary condition at the membrane surface, but they assumed 100% w/w NaCl concentration, which possibly represents the presence of a worst-case fouling layer. As it is preferable to keep the membrane free from fouling in practice, the saturated value was used for the concentration boundary condition at the membrane surface in the current study.

In all the geometries considered in this study, the spacer was aligned with the mean flow direction (corresponding to $\alpha = 0°$ in Figure 4-4). Consequently, symmetry wall boundary conditions were used for the side boundaries of the channel not occupied by filament (Figure 4-5). All filaments were defined as solid surfaces, allowing no water or salt to pass through.

The parameter values used in the simulations are summarised in Table 4-3.

Table 4-3. Modelling input parameters used in the present study.

Parameter	Value
Geometrical parameters	
d	0.0005 m
H	0.0015 m (Triple geometry) 0.001 m (other geometries)
$W = L$	0.0041 m
α	0°
β	90°
Physical properties	
ρ	998.2 kg/m^3 (45)
μ	0.001 Pa.s (46)
$\mathcal{D}$	1.52×10^{-9} m^2/s (43)
Operating conditions	
Re	50, 100, 150, 200
C_i	5% w/w NaCl
C_m	35% w/w NaCl

4.3 Results and Discussion

Simulation runs covering 20 different cases were performed. The calculated performance measures, such as SPC, Pn and ΔP^* are based on the weighted average values extracted from ANSYS Fluent.

4.3.1 Effect of Reynolds number

The main goal of this study is to investigate the effectiveness of different feed spacers for different production rates. Previous studies occasionally used the mass flowrate or velocity to identify different cases, but due to differences in channel height and configuration, most studies choose the Reynolds number to facilitate the comparison of results.

Table 4-4 presents power law equations that approximate the CFD results. These equations are helpful for both interpreting and summarising the results. The parameters of the power law equations were obtained using MATLAB that maximized the coefficient of determination, R^2. All equations have R^2 of 0.995 or higher, except for the Sh-Re and Sh-Pn equations for the Ladder-type and Triple geometries, where it was as low as 0.97. In Figures 6–11, the symbols depict the CFD results, while the lines show the predictions of the power law correlations reported in Table 4-4.

It should be noted that each correlation was based on the four values of Re considered in the current work. High values of R^2 for pressure drop, SPC, Pn and SCE represent better predictability for these parameters.

Table 4-4 Geometrical parameters of the spacers and correlations for key variables derived from the CFD simulations.

Configuration	Ladder-type	Triple	Wavy	Submerged	Plain	Min. R^2
D_h (mm)	1.31	1.72	1.29	1.60	2.00	
A_{eff} (mm^2)	3.71	5.56	3.71	3.90	4.10	
ϵ	0.904	0.904	0.904	0.952	1.00	
$\Delta P/L$ (Pa/m)	$4.16\,Re^{1.49}$	$2.85\,Re^{1.55}$	$6.17\,Re^{1.37}$	$9.97\,Re^{1.29}$	$5.58\,Re^{1.06}$	0.9994
SPC (W/m^3)×10^3	$2.69\,Re^{2.52}$	$1.42\,Re^{2.45}$	$4.20\,Re^{2.40}$	$5.32\,Re^{2.32}$	$2.66\,Re^{2.07}$	0.9999
Pn	$4.37\,Re^{2.42}$	$11.6\,Re^{2.48}$	$5.86\,Re^{2.33}$	$7.92\,Re^{2.24}$	$2.92\,Re^{2.05}$	0.9999
ΔP^*	$3.08\,Re^{-0.596}$	$4.78\,Re^{-0.533}$	$3.99\,Re^{-0.680}$	$6.86\,Re^{-0.774}$	$2.97\,Re^{-0.955}$	0.9946
Sh	$10.1\,Re^{0.341}$	$8.43\,Re^{0.425}$	$3.62\,Re^{0.549}$	$5.85\,Re^{0.382}$	$8.94\,Re^{0.257}$	0.9743
	$8.96\,Pn^{0.140}$	$5.67\,Pn^{0.169}$	$2.44\,Pn^{0.234}$	$4.17\,Pn^{0.169}$	$7.83\,Pn^{0.125}$	0.9690
SCE	$1.48\,Re^{-1.96}$	$0.419\,Re^{-1.93}$	$0.530\,Re^{-1.75}$	$0.640\,Re^{-1.83}$	$2.89\,Re^{-1.78}$	0.9996

Pressure drop

Figure 4-6 shows that for all geometries the pressure drop per unit length increases with the Reynolds number. As expected, the Plain channel has by far the lowest pressure drop, approximately 20% that of the other types, because there are no filaments to obstruct the fluid flow. In addition, the pressure drop for the Plain channel increases essentially linearly with Re (as can be seen in Table 4-4), while for the other geometries the dependence is proportional to $Re^{1.3–1.5}$. A closer examination of the geometries with filaments in Figure 4-6 and Table 4-4 shows the Triple and Wavy geometries have the lowest pressure drop at low Re, and Triple increases most quickly with Re ($\propto Re^{1.55}$) while Wavy increases more slowly ($\propto Re^{1.37}$). This results in the Wavy geometry having the lowest pressure drop of the spacer types considered for Re > 80. Shakaib et al. (28) report a pressure drop of 3500 Pa/m for a Ladder-type spacer with $W = L = 4H$ at Re = 100, which differs by about 10% from the results reported in Figure 4-6, where $W = L = 4.1H$.

In terms of pressure drop, the Wavy configuration seems to be the best choice among the configurations tested. It is thought that this behaviour is a result of the sinusoidal longitudinal filaments (Figure 4-2 c) helping guide the flow around the latitudinal filaments with less

resistance and smoothing the eddy flows downstream of the latitudinal filaments, which are responsible for part of the energy loss.

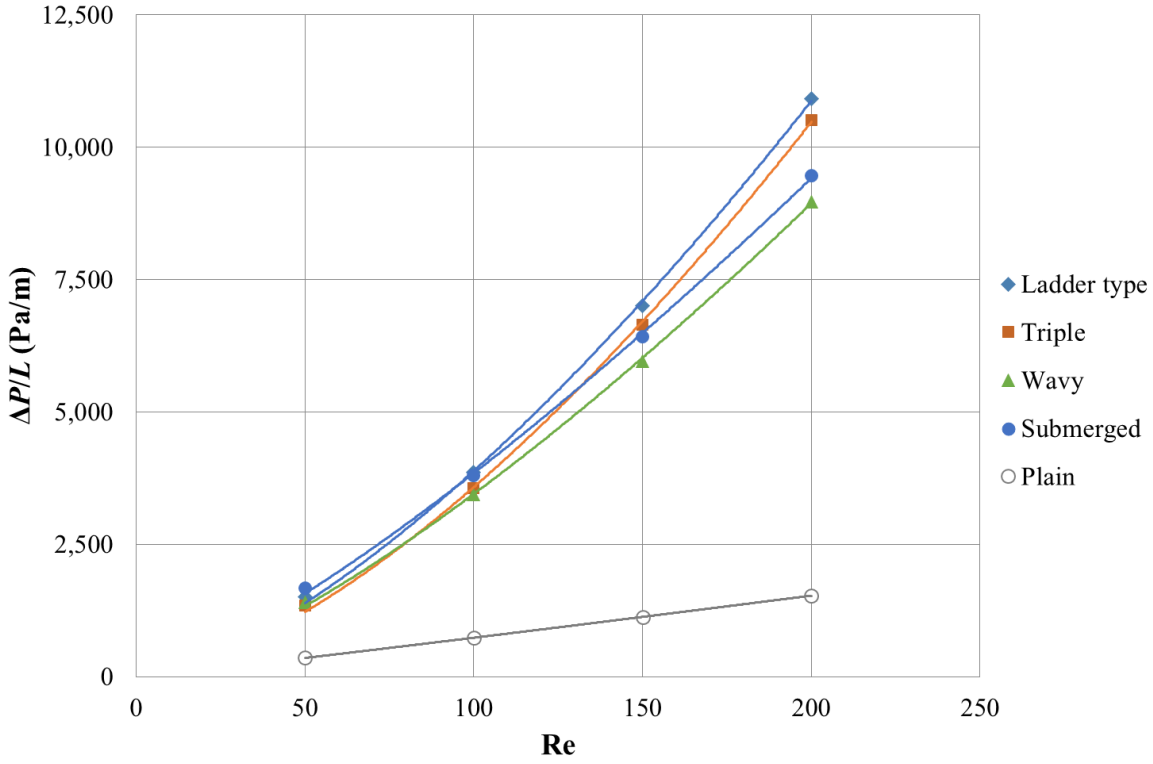

Figure 4-6. Predicted pressure drop per unit length as a function of Re for the five spacer geometries.

Power consumption

Figure 4-8 indicates that SPC increases rapidly as the flowrate increases. The Plain channel has the lowest SPC, which, as before, is a result of the lack of obstructions in the flow domain. Of the other geometries, the Ladder-type has the highest SPC while Triple and Submerged have the lowest. The highest rate of increase of SPC is for the Ladder-type geometry, which has SPC $\propto Re^{2.5}$, while the lowest is for Submerged, where SPC $\propto Re^{2.3}$ (Table 4-4).

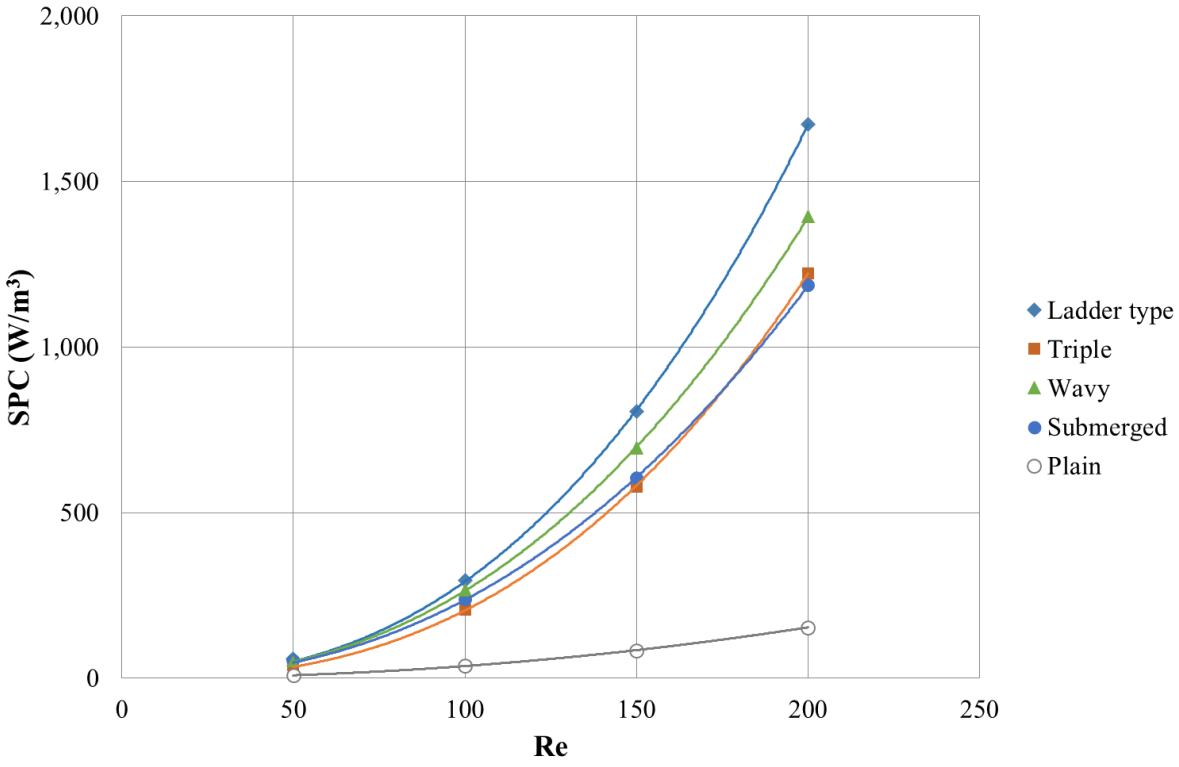

Figure 4-7. Predicted Specific Power Consumption as a function of Re for the five spacer geometries.

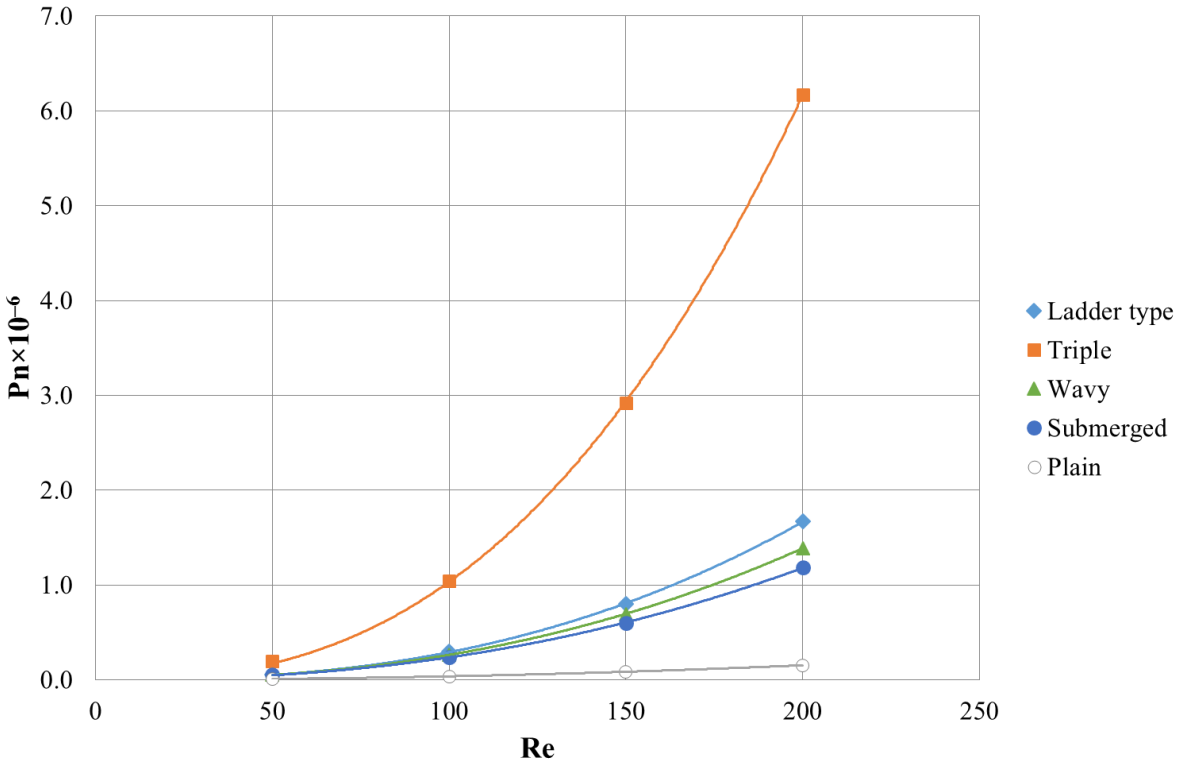

Figure 4-8. Predicted Power number as a function of Re for the five spacer geometries.

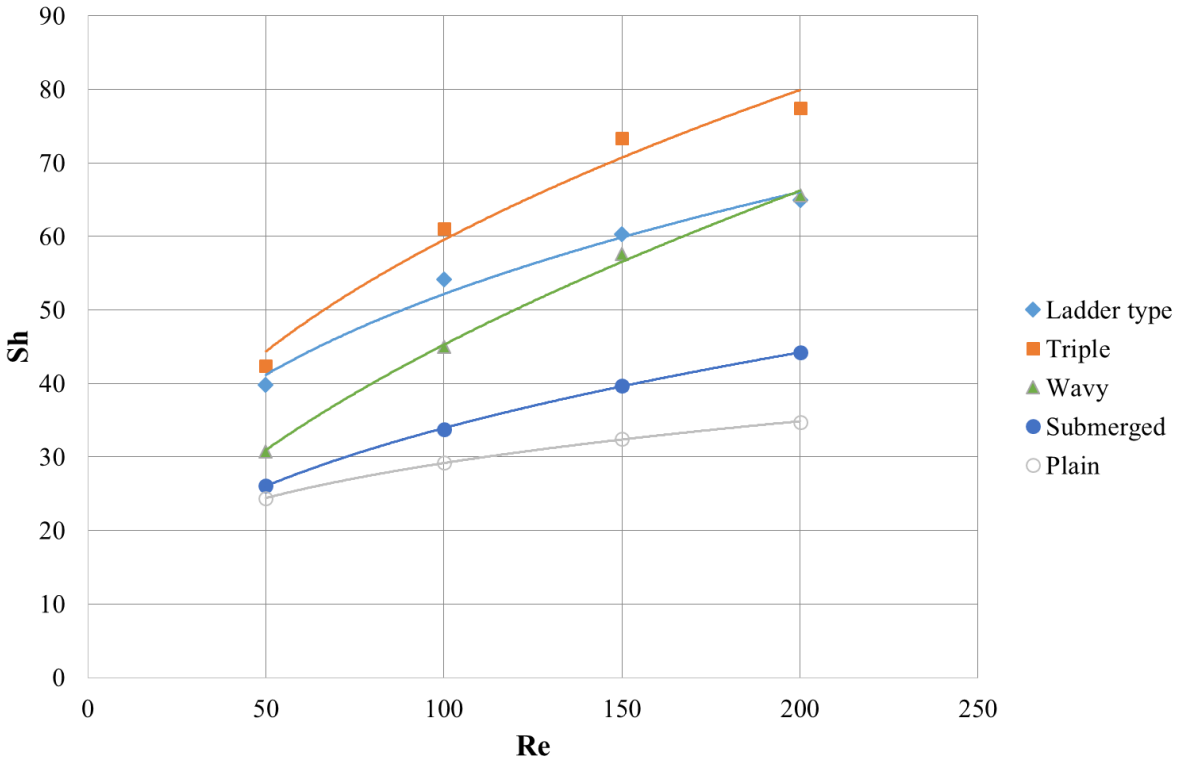

Figure 4-9. Predicted Sherwood number as a function of Re for the five spacer geometries.

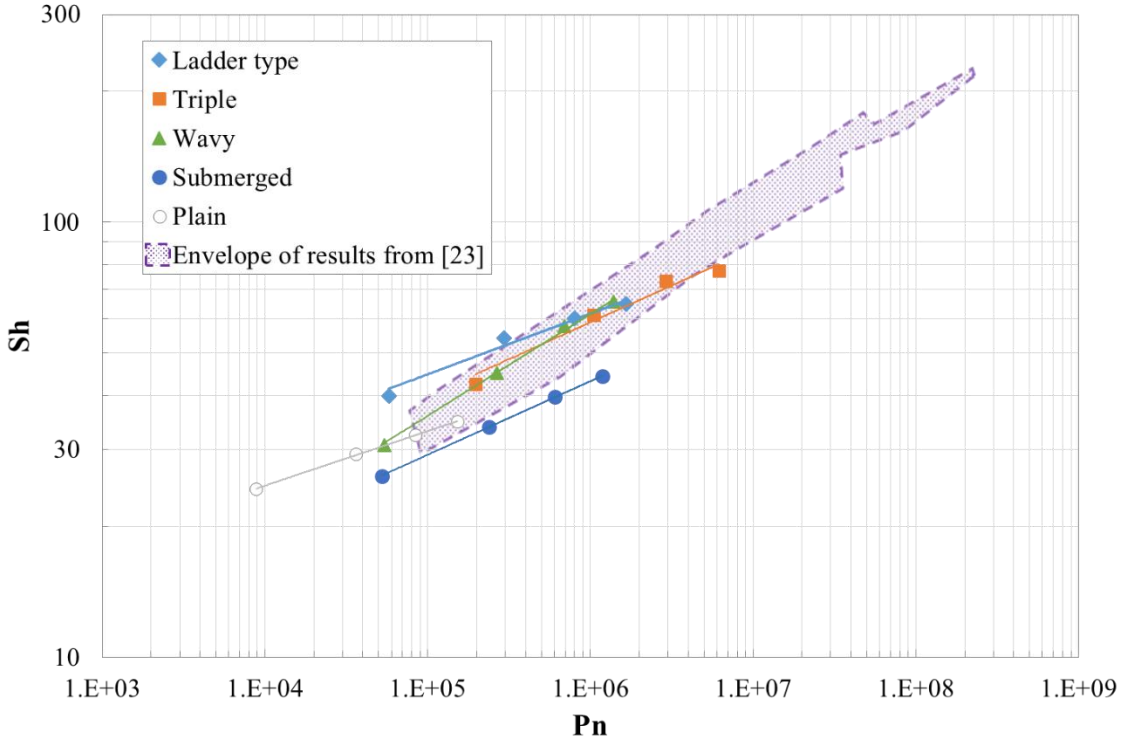

Figure 4-10. Trade-off between production capacity and energy consumption: predicted Sherwood number as a function of Power number for the five spacer geometries and the results reported by [23].

Since Pn is proportional to SPC×H^4 (Equation (4-8)) and the fluid properties are constant, the trends of Pn with Re mirror those for SPC for the spacers with the same channel height, H (Figure 4-7). The exception is the Triple geometry, which has $H = 3d$ compared to $H = 2d$ for the other geometries, resulting in Pn that is around 4 times higher than for the other geometries with filaments. It should be noted that, excluding the Plain geometry, the exponents of Re in the power law correlations for Pn reported in Table 4-4, and shown in Figure 4-7, (2.24–2.48) are in good agreement with the range of Re exponents (2.25–2.83) reported in Haaksman et al. (36) for a selection of commercial spacers.

Mass transfer

Figure 4-9 shows the relationship between Sh and Re. In all cases, the Sherwood number increases with increasing Reynolds number. The Triple geometry has the highest Sh while the Plain channel has the lowest Sh of all those studied.

Sherwood number is plotted against Power number in Figure 4-10 to show the spacer with the best trade-off between production capacity and energy consumption. In previous work, the Sh-Pn relationship has been studied using simulation and experimental data (22, 23) for a Ladder-type geometry with $L = 4d$, $\alpha = 0°$ and $\beta = 90°$. Also, the overall trend and form of equations provided by other researchers (14, 16, 40) is in accordance with our results in Figure 4-9 and Figure 4-10.

Spacer Configuration Efficacy

As defined in Equation (4-12), SCE is the ratio of Sherwood number to Power number, which represents both the mass transfer and energy consumption of SWMs. High SCE values are desirable for spacer configurations. As Figure 4-11 shows, the Plain (empty channel) geometry has the maximum SCE due to its very low pressure drop, but it is an uncommon configuration to choose due to the absence of recirculation zones, which results in a high probability of deposit build-up on the membrane surface. Setting aside the Plain channel, the Ladder-type geometry has the highest SCE for low Reynolds numbers (Re < 120), while for Re > 120, the Wavy's SCE is slightly higher. The Triple geometry has the lowest SCE due to its high Pn.

4.3.2 Comparison of local velocities and concentrations

Figure 4-12 shows contour plots for the Wavy spacer configuration for fluid velocity (a and b) and salt concentration (c and d) at the outlet face (a and c) and on a longitudinal plane parallel

to side walls positioned at z = 1 mm (b and d). The longitudinal plots show behaviour around the fifth unit cell (Figure 4-3), which is far enough from both inlet and outlet faces to be reflective of fully developed fluid flow (4) for Re = 50. Figure 4-13 shows the equivalent contour plots for Re = 200.

As evident from Figure 4-12 (b), the presence of the latitudinal filament creates a high velocity zone opposite the filament, decreasing the extent of the concentration polarization layer (Figure 4-12 d), which in turn enhances mass transfer. Figure 4-12 (b) shows the development of dead zones just before and just after the filament; the recirculating flow after the filament appears to help the solute to move away from the membrane wall into the bulk.

By increasing the flowrate fourfold, both high velocity and low velocity zones become more distinctly elongated (Figure 4-13 b). As a result, the recirculating flows become more effective in moving solute away from the membrane (Figure 4-13 d). It should also be noted from Figure 4-13 (d) that the recirculating flow appears before the latitudinal filament moving the concentrated zone away from the membrane.

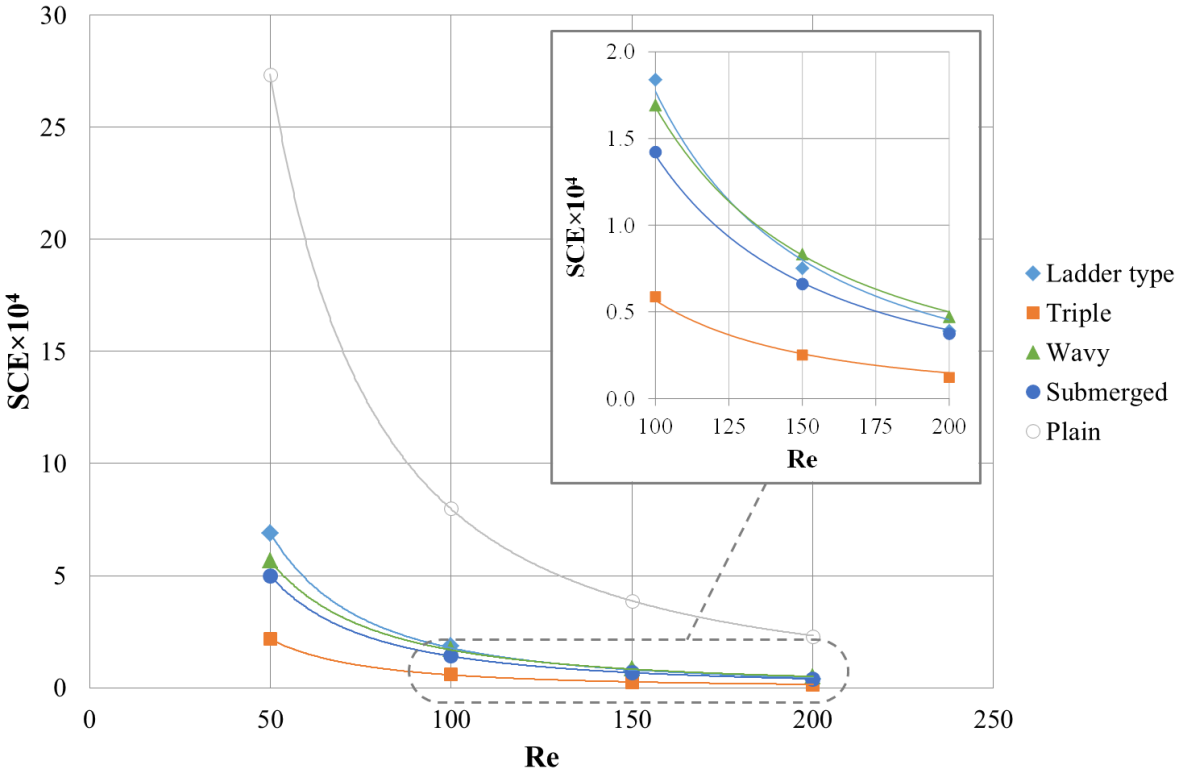

Figure 4-11. Another perspective on the production capacity and energy consumption trade-off: predicted Spacer Configuration Efficacy as a function of Re.

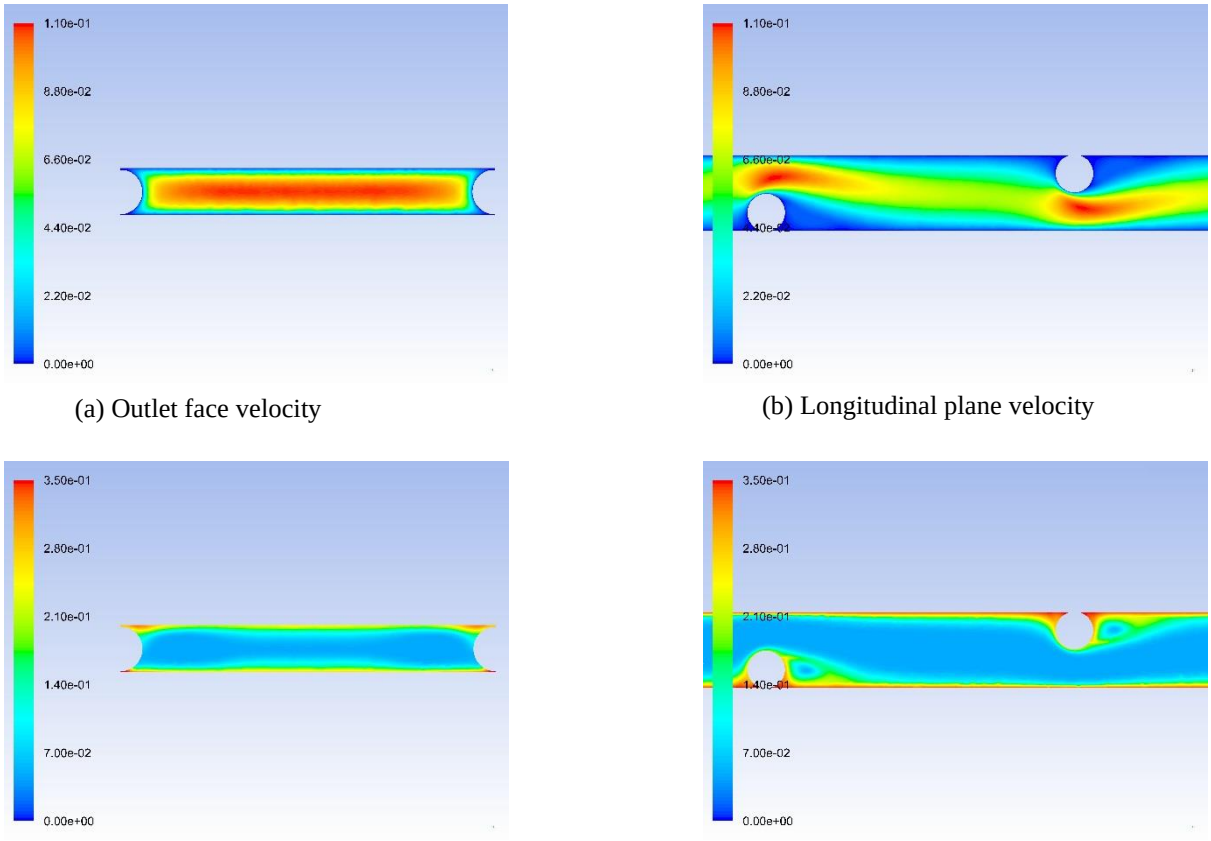

(a) Outlet face velocity

(b) Longitudinal plane velocity

(c) Outlet face concentration

(d) Longitudinal plane concentration

Figure 4-12. Contour plots for the Wavy configuration for Re = 50.

On the other hand, the outlet velocity contour plots (Figure 4-12 a and Figure 4-13 a) show similar flow patterns for Re = 50 and 200, while the concentration contour plots (Figure 4-12 c and Figure 4-13 c) reveal significant differences in the recirculating flows caused by the longitudinal filaments. For Re = 50, the recirculating flows spread over most of the channel width (Figure 4-12 c) whereas for Re = 200, they are confined to the vicinity of the longitudinal filaments (Figure 4-13 c). It should be noted that Saeed (4) reported a similar pattern for longitudinal and latitudinal recirculating zones.

4.3.3 Consistency of rankings obtained from alternative measures of spacer performance

Table 4-5 and Table 4-6 report the rankings (from best performing to worst performing) of four of the feed spacers considered in this study based on five performance measures ($\Delta P/L$, SPC, Pn, Sh and SCE) and for low and high Reynolds numbers. The tables can be interpreted in three ways. Firstly, tracing along a row reveals the differences in ranking for a given feed spacer according to the different performance measures. Secondly, looking down a column shows the ranking of the spacers according to a given performance measure. Thirdly,

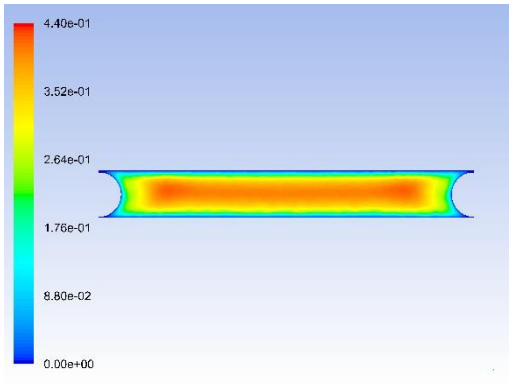

(a) Outlet face velocity

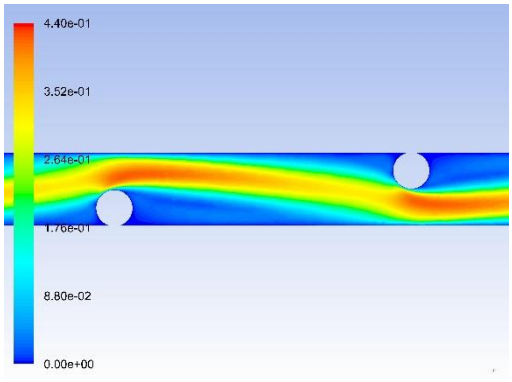

(b) Longitudinal plane velocity

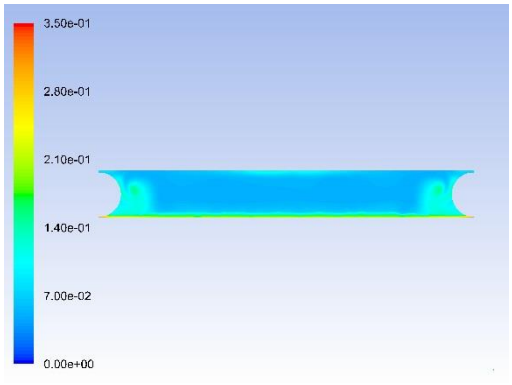

(c) Outlet face concentration

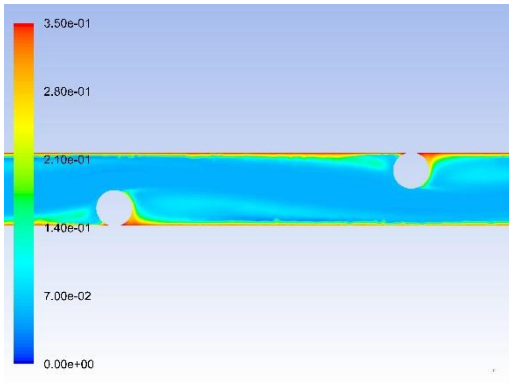

(d) Longitudinal plane concentration

Figure 4-13. Contour plots for the Wavy configuration for Re = 200.

comparing the same column in Table 4-5 and Table 4-6 indicated the ranking's sensitivity to flowrate.

Table 4-5 shows that the common measures currently being used in the literature to assess spacer performance led to different rankings for Re = 50 for the four feed spacer configurations studied. Even $\Delta P/L$, SPC and Pn, all of which focus on energy consumption, are not in agreement on the spacer ranking. On the other hand, comparing the data from Table 4-5 and Table 4-6 reveals that the $\Delta P/L$ ranking varies with Reynolds number significantly, while SPC, Sh and SCE have one minor change – one swap between neighbours – and Pn has the same ranking for Re values of 50 and 200. Returning different results for different flowrates might be thought of as useful sensitivity or as unwelcome inconsistency. To the best of the authors' knowledge, this aspect is neither discussed nor addressed in previous studies in the literature including the merits and demerits of changes in ranking with flowrate.

The observed changes in spacer ranking (as reported in Table 4-5 and Table 4-6), due to both the selection of the performance measure used and the changing flowrate, makes it critical to choose the performance measure carefully. Because the rankings SCE produced varied only

a little with flowrate and it is the only measure considered that combines mass transfer and energy consumption, it is thought that it is the best performance measure to use of those considered here, as defined in Equation (4-12) or with some modification. The authors found no previous study comparing different performance measures by relating them to more applied measures like the product unit cost, which might be the most interesting parameter for both membrane manufacturers and operators of membrane systems. Further investigations aimed at linking the various performance measures to capital and operating costs would prove to be more valuable in deciding which approach is most useful for assessing the performance of spacers.

Table 4-5. Comparison of spacer ranking using different performance measures at Re = 50.

*Key: **** indicates the most preferred spacer geometry (highest ranked), while * indicates the least preferred.*

Configuration	$\Delta P/L$	SPC	Pn	Sh	SCE
Ladder	**	*	**	***	****
Triple	****	****	*	****	*
Wavy	***	**	***	**	***
Submerged	*	***	****	*	**
Min./max.	0.80	0.67	0.27	0.61	0.31

Table 4-6. Comparison of spacer ranking using different performance measures at Re = 200.

*Key: **** indicates the most preferred spacer geometry (highest ranked), while * indicates the least preferred.*

Configuration	$\Delta P/L$	SPC	Pn	Sh	SCE
Ladder	*	*	**	**	***
Triple	**	***	*	****	*
Wavy	****	**	***	***	****
Submerged	***	****	****	*	**
Min./max.	0.82	0.71	0.19	0.57	0.26

4.3.4 Validation

In Table 4-7, the approach used in the present study is compared with some previous studies (5, 22, 28), which all used Ladder-type spacers, but of slightly different sizes as noted in the table. It is evident that the top and bottom shear stresses are 8% and 15% different from the average values reported by (5, 28), respectively. The lower pressure drop and dimensionless pressure drop observed in comparison with previous studies is thought to be acceptable given that the channel height is 23% larger in the present study. The Power number is proportional to $\Delta P \times H^4$ as shown in Equation (4-8)(4-12). The effect of 40% lower ΔP and 23% higher H will lead to a 17% difference in Pn results.

Table 4-7. Comparison of hydraulic results obtained using the approach developed in the present study with literature results for Re = 100 with a Ladder-type spacer.

Parameter	(28) [a]	(22) [b]	(5) [c]	Present study [d]
Average shear stress on top wall (N/m^2)	1	-	1.15	0.915
Average shear stress on bottom wall (N/m^2)	0.16	-	0.20	0.165
Pressure drop, $\Delta P/L$ (kPa/m)	5	-	6.29	3.859
Power number, Pn × 10^{-5}	-	1.7	1.80	2.946
Dimensionless pressure drop, ΔP^*	-	-	0.32	0.192

a. Value interpolated from plot of filament spacing vs average shear stress on walls and linear pressure drop by (5).

b. Value reported for $L = 4d$.

c. Value reported for $L = 4.1d$ and $H = 0.772$ mm.

d. Value reported for $L = 4.1d$ and $H = 1$ mm.

Mass transfer results are compared with the previous study of Saeed et al. (12) as shown in Table 4-8. Unlike the hydraulic behaviour, there is a significant difference between the current and previous results. As mentioned in their study (12), the concentration boundary condition on the membrane surface was assumed to be a salt mass fraction of 1. On the other hand, in the present study, the salt mass fraction on the membrane surface was assumed to be the saturation value, 0.35 w/w.

Furthermore, the Sherwood number is related to the mass transfer coefficient, which is inversely proportional to the salt concentration difference. As clarified earlier, the present study considers a boundary concentration much lower than used in previous studies. Thus, the lower concentration difference in the present study would result in lower mass transfer, but a higher mass transfer coefficient. Simulations show that reducing the concentration to one third will nearly double the mass transfer coefficient, leading to a nearly twofold increase in the Sherwood number and SCE (Table 4-8).

The above issue is significant because Sherwood number is commonly correlated as a function of Reynolds number, Schmidt number and geometry, which makes Sh independent of the solute concentration, assuming a negligible influence of concentration on physical properties. To the best of our knowledge, however, no published studies have investigated the change in Sh resulting from a constant surface concentration boundary condition compared to other types of boundary conditions at the membrane.

Another validation was done to ensure the current model produced a similar pattern of results to that established in previous work. The model was run in the Ladder-type geometry with the same boundary conditions as used by the previous study (12) and the results were found to be similar. The maximum difference was in the Power number, which was about 11%

different from the previously reported value, while Sh and SCE were in closer agreement (Table 4-8). The different results observed might be due to several factors, including a different meshing method and accuracy in the vicinity of the cylinder-plane contact point, which was addressed in Section 4.2.5.

Table 4-8. Comparison of mass transfer results obtained using the approach developed in the present study with literature results for Re = 100 with a Ladder-type spacer.

Study and comparison details	Dimensionless spacer size [a]		Property			
	Channel length, L/H	Channel width, W/H	Average mass transfer coefficient, $k \times 10^5$ (m/s)	Sherwood number, Sh	Power number, Pn $\times 10^{-3}$	Spacer Configuration Efficacy, SCE $\times 10^4$
Saeed et al. (12)	3.5	3.5	3.74	29	473.1	0.66
	3.5	4.5	3.75	31	329.7	0.94
	4.5	3.5	3.55	29	348.9	0.84
	4.5	4.5	3.64	31	259.1	1.21
Linearly interpolated from (12)	4.1	4.1	3.66	30	331.8	0.97
Current study	4.1	4.1	6.38	54.2	294.6	1.84
Current study with same boundary conditions as (12)	4.1	4.1	3.25	27.6	296.8	0.93
Difference between current study and linear interpolation of (12) for same boundary conditions	–	–	11.1%	8.5%	10.6%	4.0%

a. The study (12) used different definitions of channel size compared to the current study (Figure 4-4). To facilitate comparison, the L/H and W/H values from (12) reported here have been adjusted to make them consistent with the current study.

As reported in Table 4-4, the present study has developed equations for Sh as a function of Re for various spacer geometries, which is similar to work conducted by In Seok et al. (14). The present study reports values of 0.34 and 0.55 as the exponents of Re for Ladder-type and Wavy geometries, respectively, while In Seok et al. (14) report 0.294 and 0.475 for Cavity and Zigzag configurations, respectively, as shown in Table 4-1. In terms of configuration, Cavity and Ladder-type are similar, and Zigzag and Wavy are similar, with the main difference in both cases being the presence of longitudinal filaments in the Ladder-type and Wavy geometries. The introduction of longitudinal filaments leads to Re exponents that are about 20% higher in both cases. On the other hand, it should be noted that the highest exponent in the present study, 0.55 for the Wavy configuration, is smaller than the value of 0.875 reported by Schock et al. (15) for commercial spacers, as seen in Table 4-1. The difference might be attributed to two main factors: better performance of the tested commercial spacer, as well as lower inlet salinity, 0.03%, compared to 5% in the present work.

4.4 Conclusions

Computational fluid dynamics was used to study the effect of changing flowrate on four different feed spacer configurations, along with an empty channel, for spiral wound modules used in reverse osmosis systems. Both flow and overall mass transfer phenomena were investigated by calculating various performance measures (such as Power number, Sherwood number and a relatively recent measure, the Spacer Configuration Efficacy) from the CFD results. Simulations were performed using the new saturated boundary condition. The results were validated against the previous literature.

The following conclusions are drawn from this study:

- The new (35%) saturated concentration boundary condition employed at the membrane surface resulted in nearly doubling of the predicted mass transfer coefficient compared to previous studies that used a pure (100%) solute boundary condition. This finding shows the importance feed side membrane boundary conditions in RO simulations.
- Tetrahedral meshing of the fluid domain resulted in faster and more stable convergence than hexahedral meshing used in many previous studies.
- The performance measures were strongly affected by the Reynolds number of the flow in the range $50 \leq Re \leq 200$ and the spacer geometry.
- The simple power law correlations of the various performance measures with Re for each feed spacer that were developed allow rapid evaluation of spacer performance for planning purposes and facilitate comparison with other studies.
- Different performance measures led to different rankings of the feed spacers and the ranking may change with Reynolds number. This situation is not entirely satisfactory and further work should be devoted to relating the current performance measures to more industrially relevant measures, such as ones based on capital and operating costs.
- The SCE concept, which had previously only been applied to Ladder-type configurations (5, 13), was used on other configurations, and found to be a good measure to use for selecting the best spacer configuration as it considers both flow and mass transfer performance, and it did not vary as much with Re as pressure drop alone.

- According to SCE values for the four obstructed spacer geometries considered, the Ladder-type shows best results at Re values below 120, while Wavy is the best choice for Re values greater than 120; the benefits of using Wavy become greater with increasing Re.

Nomenclature

A_{eff}	Effective area (m^2)
A_i	Area of inlet face (m^2)
C_i	Inlet salt concentration (w/w)
C_m	Membrane salt concentration (w/w)
$\mathcal{D}$	Mass diffusivity (m^2/s)
d	Filament diameter (m)
D_h	Hydraulic diameter (m)
Eu	Euler number
H	Channel height (m)
k	Average mass transfer coefficient (m/s)
L	Channel length (m)
n	Distance in direction normal to the filament (m)
P_0	Ambient pressure (Pa)
ΔP	Pressure drop (Pa)
ΔP^*	Dimensionless pressure drop
Pn	Power number
Re_{ch}	Channel Reynolds number
Re_{cyl}	Cylinder Reynolds number
Re_h	Hydraulic Reynolds number
SCE	Spacer Configuration Efficacy
Sh	Sherwood number

SPC	Specific Power Consumption (W/m^3)
u_{eff}	Effective velocity (m/s)
u	Velocity in x direction (m/s)
$\dot{V}$	Volumetric flowrate (m^3/s)
v	Velocity in y direction (m/s)
W	Channel width (m)
w	Velocity in z direction (m/s)

Greek symbols

α	Flow angle of attack (°)
β	Spacer geometry angle (°)
ϵ	Porosity
μ	Dynamic viscosity (Pa.s)
ρ	Density (kg/m^3)

References

1. UNESCO. Encyclopedia of desalination and water resources: Energy requirements of desalination processes. [webpage]. Available from: http://www.desware.net/Energy-Requirements-Desalination-Processes.aspx.

2. Belfort G. Membrane modules: Comparison of different configurations using fluid-mechanics. Journal of Membrane Science. 1988; 35(3):245-270.

3. Shakaib M, Hasani SMF, Ahmed I, Yunus RM. A CFD study on the effect of spacer orientation on temperature polarization in membrane distillation modules. Desalination. 2012; 284:332-340.

4. Saeed A. Effect of feed channel spacer geometry on hydrodynamics and mass transport in membrane modules [Ph.D Thesis]. Perth, Australia: Curtin University; 2012.

5. Saeed A, Vuthaluru R, Yang YW, Vuthaluru HB. Effect of feed spacer arrangement on flow dynamics through spacer filled membranes. Desalination. 2012; 285:163-169.

6. Li YL, Lin PJ, Tung KL. CFD analysis of fluid flow through a spacer-filled disk-type membrane module. Desalination. 2011; 283:140-147.

7. Al-Sharif S, Albeirutty M, Cipollina A, Micale G. Modelling flow and heat transfer in spacer-filled membrane distillation channels using open source CFD code. Desalination. 2013; 311:103-112.

8. Sousa P, Soares A, Monteiro E, Rouboa A. A CFD study of the hydrodynamics in a desalination membrane filled with spacers. Desalination. 2014; 349:22-30.

9. Kostoglou M, Karabelas AJ. Comprehensive simulation of flat-sheet membrane element performance in steady state desalination. Desalination. 2013; 316:91-102.

10. Li YL, Tung KL, Chen YS, Hwang KJ. CFD analysis of the initial stages of particle deposition in spiral-wound membrane modules. Desalination. 2012; 287:200-208.

11. Saeed A, Vuthaluru R, Vuthaluru H. Concept of spacer configuration efficacy (sce) applied to optimize ladder type feed spacer filament spacing in narrow channels. International Conference On Water Desalination, Treatment and Management & Indian Desalination Association Annual Congress 2013. Jaipur, India: The Malaviya National Institute of Technology.

12. Saeed A, Vuthaluru R, Vuthaluru HB. Investigations into the effects of mass transport and flow dynamics of spacer filled membrane modules using CFD. Chemical Engineering Research & Design. 2015; 93:79-99.

13. Saeed A, Vuthaluru R, Vuthaluru HB. Impact of feed spacer filament spacing on mass transport and fouling propensities of ro membrane surfaces. Chemical Engineering Communications. 2015; 202(5):634-646.

14. In Seok K, Ho Nam C. The effect of turbulence promoters on mass transfer – numerical analysis and flow visualization. International Journal of Heat and Mass Transfer. 1982; 25(8):1167-1181.

15. Schock G, Miquel A. Mass-transfer and pressure loss in spiral wound modules. Desalination. 1987; 64(C):339-352.

16. DaCosta AR, Fane AG, Wiley DE. Spacer characterization and pressure drop modelling in spacer-filled channels for ultrafiltration. Journal of Membrane Science. 1994; 87(1-2):79-98.

17. Karode SK, Kumar A. Flow visualization through spacer filled channels by computational fluid dynamics i. Pressure drop and shear rate calculations for flat sheet geometry. Journal of Membrane Science. 2001; 193(1):69-84.

18. Cao Z, Wiley DE, Fane AG. CFD simulations of net-type turbulence promoters in a narrow channel. Journal of Membrane Science. 2001; 185(2):157-176.

19. Schwinge J, Wiley DE, Fletcher DF. A CFD study of unsteady flow in narrow spacer-filled channels for spiral-wound membrane modules. Desalination. 2002; 146(1-3):195-201.

20. Schwinge J, Wiley DE, Fletcher DF. Simulation of the flow around spacer filaments between narrow channel walls. 1. Hydrodynamics. Industrial & Engineering Chemistry Research. 2002; 41(12):2977-2987.

21. Schwinge J, Wiley DE, Fletcher DF. Simulation of the flow around spacer filaments between channel walls. 2. Mass-transfer enhancement. Industrial & Engineering Chemistry Research. 2002; 41(19):4879-4888.

22. Li F, Meindersma W, de Haan AB, Reith T. Experimental validation of CFD mass transfer simulations in flat channels with non-woven net spacers. Journal of Membrane Science. 2004; 232(1-2):19-30.

23. Li F, Meindersma W, de Haan AB, Reith T. Optimization of commercial net spacers in spiral wound membrane modules. Journal of Membrane Science. 2002; 208(1-2):289-302.

24. Li F, Meindersma GW, de Haan AB, Reith T. Optimization of non-woven spacers by CFD and validation by experiments. Desalination. 2002; 146(1-3):209-212.

25. Koutsou CP, Yiantsios SG, Karabelas AJ. Numerical simulation of the flow in a plane-channel containing a periodic array of cylindrical turbulence promoters. Journal of Membrane Science. 2004; 231(1-2):81-90.

26. Ranade VV, Kumar A. Fluid dynamics of spacer filled rectangular and curvilinear channels. Journal of Membrane Science. 2006; 271(1-2):1-15.

27. Santos JLC, Geraldes V, Velizarov S, Crespo JG. Investigation of flow patterns and mass transfer in membrane module channels filled with flow-aligned spacers using computational fluid dynamics (CFD). Journal of Membrane Science. 2007; 305(1-2):103-117.

28. Shakaib M, Hasani SMF, Mahmood M. Study on the effects of spacer geometry in membrane feed channels using three-dimensional computational flow modeling. Journal of Membrane Science. 2007; 297(1-2):74-89.

29. Fimbres-Weihs GA, Wiley DE. Numerical study of mass transfer in three-dimensional spacer-filled narrow channels with steady flow. Journal of Membrane Science. 2007; 306(1-2):228-243.

30. Li YL, Tung KL. CFD simulation of fluid. Flow through spacer-filled membrane module: Selecting suitable cell types for periodic boundary conditions. Desalination. 2008; 233(1-3):351-358.

31. Cipollina A, Micale G, Rizzuti L. Membrane distillation heat transfer enhancement by CFD analysis of internal module geometry. Desalination and Water Treatment. 2011; 25(1-3):195-209.

32. Cipollina A, Di Miceli A, Koschikowski J, Micale G, Rizzuti L. CFD simulation of a membrane distillation module channel. Desalination and Water Treatment. 2009; 6(1-3):177-183.

33. Qureshi M, Shakaib M. CFD study for temperature and concentration profiles in membrane channels. International conference on Energy and Sustainability 2013. Karachi, Pakistan: NED University of Engineering & Technology.

34. Koutsou CP, Yiantsios SG, Karabelas AJ. Direct numerical simulation of flow in spacer-filled channels: Effect of spacer geometrical characteristics. Journal of Membrane Science. 2007; 291(1-2):53-69.

35. Mojab SM, Pollard A, Pharoah JG, Beale SB, Hanff ES. Unsteady laminar to turbulent flow in a spacer-filled channel. Flow Turbulence and Combustion. 2014; 92(1-2):563-577.

36. Haaksman VA, Siddiqui A, Schellenberg C, Kidwell J, Vrouwenvelder JS, Picioreanu C. Characterization of feed channel spacer performance using geometries obtained by x-ray computed tomography. Journal of Membrane Science. 2017; 522:124-139.

37. Johnson J, Busch M. Engineering aspects of reverse osmosis module design. Desalination and Water Treatment. 2010; 15(1-3):236-248.

38. Lau KK, Abu Bakar MZ, Ahmad AL, Murugesan T. Feed spacer mesh angle: 3d modeling, simulation and optimization based on unsteady hydrodynamic in spiral wound membrane channel. Journal of Membrane Science. 2009; 343(1-2):16-33.

39. Storck A, Hutin D. Energetic aspects of turbulence promotion applied to electrolysis processes. Canadian Journal of Chemical Engineering. 1980; 58(1):92-102.

40. Isaacson MS, Sonin AA. Sherwood number and friction factor correlations for electrodialysis systems, with application to process optimization. Industrial & Engineering Chemistry Process Design and Development. 1976; 15(2):313-321.

41. Karabelas AJ, Kostoglou M, Koutsou CP. Modeling of spiral wound membrane desalination modules and plants: Review and research priorities. Desalination. 2015; 356:165-186.

42. Li YL, Tung KL. The effect of curvature of a spacer-filled channel on fluid flow in spiral-wound membrane modules. Journal of Membrane Science. 2008; 319(1-2):286-297.

43. Capobianchi M, Irvine TF, Tutu NK, Greene GA. A new technique for measuring the fickian diffusion coefficient in binary liquid solutions. Experimental Thermal and Fluid Science. 1998; 18(1):33-47.

44. Burgess J. Metal ions in solution. Chichester: Ellis Horwood; 1978.

45. CRC handbook of chemistry and physics. 91st ed. Boca Raton, FL: CRC Press LLC; 2010.

46. Serway RA. Physics for scientists & engineers. 3rd ed. Philadelphia: Saunders College Pub.; 1992.

Chapter 5. Studies into the mass transfer and energy consumption of commercial feed spacers for RO membrane modules using CFD: Effectiveness of performance measures[6]

Abstract

Different approaches have been reported in the literature that aim to improve the performance of reverse osmosis (RO) desalination plant operations, attempting to make the desalination process more efficient.

This study investigates the performance of four commercial feed spacers for spiral wound reverse osmosis modules by considering energy consumption and production capacity, as well as their combination, through a previously proven approach to computational fluid dynamics (CFD) modelling.

Among the performance measures studied, Spacer Configuration Efficacy (SCE), Specific Power Consumption (SPC) and Power number (Pn) showed a high level of predictability ($R^2 \geq 0.998$, 0.994 and 0.994, respectively) through power law correlations of Reynolds number(Re) with two spacer-dependent parameters. Of the four commercial spacers investigated, the DelStar Technologies Naltex N05013_90HDPE-NAT ("90 HDPE") spacer was ranked as the best or second best based on multiple performance measures over the flow range Re = 50–100. Furthermore, the very weak response to flowrate changes observed for 90 HDPE, based on pressure loss, SPC, Pn, Sherwood number (Sh) and SCE measures, indicates that there are prospects for energy savings. SPMP′, a modified definition of Spacer Performance Ratio (SPMP), showed no consistent response to flow variations for the spacers studied.

[6] The content of this chapter has been published in Chemical Engineering Research and Design 141 (2019), Q1, IF = 4.119

5.1 Introduction

Reverse osmosis (RO) operations consume less energy per unit product than other desalination processes such as multi-stage flash, multi-effect distillation and mechanical vapour compression (2). However, RO operations still consume about three times the minimum theoretical required energy (4), which provides opportunities for optimization in this area. This optimization could be achieved by refinement of the design and manufacturing of the membrane or through optimization of feed spacer configurations leading to enhanced mass transfer and lower energy consumption.

Market studies have shown that since the 1990s, Spiral Wound Modules (SWMs) have become the major membrane configuration used in RO operations. Most plants that used Hollow Fine Fibre Modules, the other major technology at that time, now use SWMs instead, which has resulted in significant cost savings (5).

Over the two decades leading to 2008, SWM technology has benefited from both spacer and membrane improvements. For example, the capacity of 20 cm (8 inch) commercial SWMs has doubled while their salt passage has reduced to about one third. The development of 40 cm (16 inch) modules and an increase in the operating pressure from 6.9 MPa (1000 psi) to 8.3 MPa (1200 psi) has further enhanced SWMs (5).

In SWMs, every feed layer neighbours two permeate layers and every permeate layer is surrounded by two feed layers. In most configurations, spacers are used on both feed and permeate sides, but they fulfil different roles during operation. Because of the higher pressure on the feed side, permeate spacers ensure that the membranes are not squeezed together and that the permeate flow pathway is kept open. On the other hand, feed spacers are meant to break down the concentration polarization layers on the feed side. Providing better mixing on the feed side reduces the concentration at the membrane surface, thus minimizing the static osmotic pressure at the membrane.

There is a well-recognized relationship between mass transfer and pressure drop in RO modules (1, 3, 6-18), which results in a trade-off between production rate and production costs. Over the last two decades, no significant benefits have been realised from the optimization of commercial spacers, despite all efforts to enhance their performance (19). This could be attributed to several factors, including lack of computational resources, low accuracy of models as a result of simplified or unrealistic assumptions, emphasis on either mass transfer or energy consumption instead of considering both, lack of a consistent method for quantifying the effect

of recirculation and dead zones on performance and maintenance costs, and/or there being simply no room for further improvement in feed spacer designs.

Since the 1970s, different methods have been used to characterize the performance of RO units. Some of them focussed on pressure drop, while the others addressed production rate. In 2002, the Spacer Performance Ratio (SPMP) was introduced (20). Significantly, it combined both aspects of performance, but it did not receive any further attention. No new combined approach was reported until 2012, when the Spacer Configuration Efficacy (SCE) concept was proposed (7) and applied to the optimization of Ladder-type spacers (8, 9). Both SPMP and SCE aim to address the disadvantages of older approaches. However, no further studies have been carried out either to investigate or compare their effectiveness in predicting the performance of spacers until our recent work (3) in which we studied four conventional spacer geometries. Apart from these studies, there was no attempt from researchers to investigate the accuracy and improve the quality of spacer performance measures.

SWM manufacturers generally do not provide practical, detailed information about their product performance. The module datasheets usually include penetration rate, minimum salt rejection rate, maximum applied pressure and maximum pressure drop. However, it is usually not clear whether all these parameters are linked to a single operational case or different cases, or even if they reflect practical conditions or design limits. No further information is available in typical datasheets to provide indications for the estimation of the performance of spacers in different operational conditions.

In the current study, SCE, SPMP′ and other performance measures are used to compare four commercially available feed spacers. In addition, the SCE and SPMP′ concepts are analysed using different methods to gain further insights into the effectiveness of commercial spacers. Reducing energy requirements while maintaining production capacity are longstanding research themes, but no previous study has explored the effectiveness of commercial spacers using performance measures, like SCE and SPMP′, that combine energy consumption and production capacity in a single measure. The results reported on the effectiveness of commercial spacers are new and of practical relevance to the design of membrane modules and the operation of RO systems.

5.2 Simulation approach

5.2.1 Geometries studied

In the present work, four different commercial spacers provided by DelStar Technologies are studied. The spacers are from the Naltex family and are denoted N05013_90HDPE–NAT (90 HDPE), N06006/06_45PP–NAT (45 PP), N06407_90PP–NAT (90 PP) and N08006_60PP–NAT (60 PP). Figure 5-1 shows a part of the fluid flow domain and the geometries of the different spacers. The specifications supplied by the manufacturer include the number of filaments per inch, spacer heights and angle of attack, but provide no information about the filament shape or dimensions.

In this study, all the spacer dimensions were measured with appropriate tools from feed spacer samples. The filament cross-sectional shapes for 90 HDPE and 90 PP were assumed to be circular, while 60 PP and 45 PP had discorectangle-shaped filaments with the straight length equal to the diameter. All filaments were straight in the longitudinal direction. Details of the geometrical parameters of the spacers are given in Table 5-1.

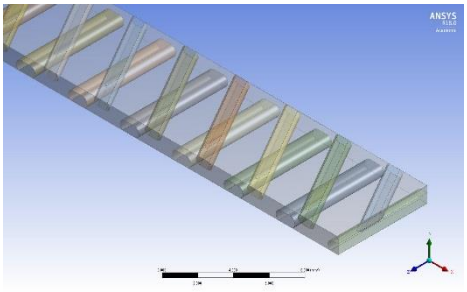

(a) 60 PP

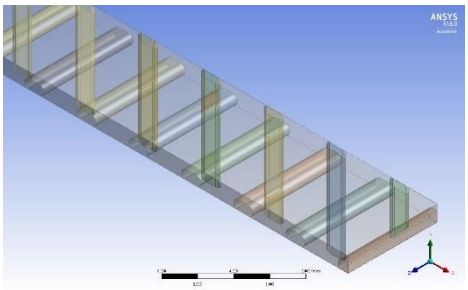

(b) 45 PP

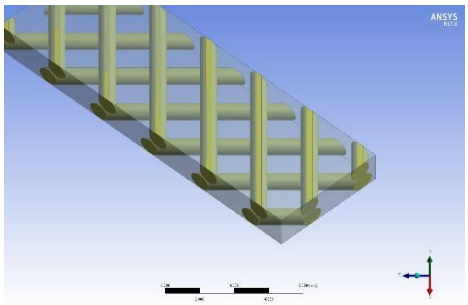

(c) 90 PP

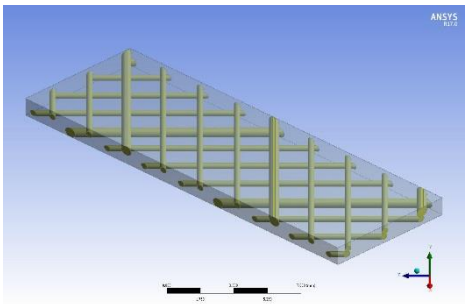

(d) 90 HDPE

Figure 5-1. Schematic diagrams of the feed spacer geometries considered in the present study.

Table 5-1. Geometrical parameters of the spacers and CFD mesh size.

Configuration	90 PP	45 PP	90 HDPE	60 PP
Filament cross section shape	Circle	Discorectangl[a] $a = h = 2r$	Circle	Discorectangl[a] $a = h = 2r$
D_h (mm)	1.74	1.25	1.14	1.24
A_{eff} (mm^2)	11.31	5.84	6.81	7.42
ε	0.772	0.681	0.883	0.865
Mesh size (number of elements)	16.2M	19.7M	10.7M	10.9M

[a.] Discorectangle shape and parameters

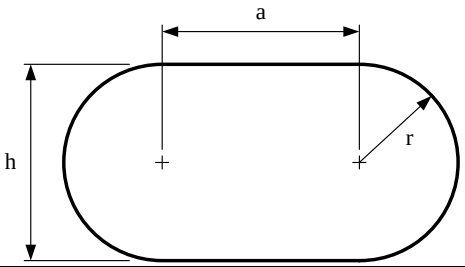

5.2.2 Parameters considered for simulation

Spacer Performance Ratio (SPMP), defined below, characterizes the ratio of 'mass transfer enhancement caused by spacer' over 'pressure drop increase caused by spacer' (20).

$$SPMP = \frac{\frac{\Delta C_{Spacer}}{\Delta C_{Slit}}}{\frac{\Delta P_{Spacer}}{\Delta P_{Slit}}} \tag{5-1}$$

As clarified in recent communications with the authors [D. Fletcher, personal communication, 2017], the same Re_{ch} was used in the original work when simulating concentration and pressure changes with a spacer and without (denoted by 'Slit' in the definition above). To eliminate the effect of the channel porosity and to make it more general, it has been decided in the current work to use the same feed mass flowrate for both empty channel and spacer cases, rather than using the same Re. Therefore, the difference between spacer and slit scenarios is the presence or absence of the spacer, with all other parameters being the same. This modified performance measure is denoted SPMP′.

All other parameters used in this study, including hydraulic diameter (D_h), effective velocity (u_{eff}), effective area (A_{eff}), porosity (ε), Reynolds number (Re), specific power consumption (SPC), power number (Pn), Sherwood number (Sh) and spacer configuration efficacy (SCE) have been defined and discussed in Section 2.3.

5.2.3 Governing equations, modelling software and solution options

The Navier-Stokes equations are used to describe the conservation and transport processes occurring in the feed side membrane channel. The fluid was assumed to be Newtonian and incompressible, while the flow was assumed to be steady-state, laminar, no slip and isothermal. Fixed values were used for the solute mass fraction at the inlet and at the membrane surface, a no flux boundary condition was employed for the filament and symmetry surfaces, and the solute mass diffusivity was taken to be constant. The governing continuity, momentum, and species conservation equations, along with hardware and software parameters, are clarified in Section 3.4.1.

In the present study, different ANSYS 15.0, 16.0 and 17.0 modules were used to model flow through the feed channels, including ANSYS Geometry, ANSYS Meshing, ANSYS Fluent and ANSYS Workbench.

The Coupled Scheme was chosen in the ANSYS Fluent solver as it offers steady convergence with minimal fluctuations through the iterations. For spatial discretization, the Green-Gauss Node Base method was used for Gradient, Second Order for pressure, Third Order MUSCL for momentum and Power Law for salinity calculations. The maximum accepted error was set to 10^{-5}.

5.2.4 Domain, mesh generation and simulation parameters

Domain definition, geometrical approximations of filaments near the membrane and other filaments, mesh generation procedures and different parameters used in the simulation are all described Section 4.2. The mesh sizes used for the four spacers are presented in Table 5-1.

5.3 Results and discussion

Simulation runs, covering 16 cases, were performed using ANSYS Fluent. All calculated performance measures, such as SPC, Pn and SPMP′, are based on the weighted average values extracted from the software. Parametric effects on the performance of the commercial spacers are reported below.

5.3.1 Effect of Reynolds number

The current work aims to evaluate and compare the effectiveness of different spacers over a range of feed rates. Different approaches to characterize the feed flowrate are used in the literature, including mass flowrate, average velocity, and Reynolds number. Hydraulic

Reynolds number was chosen to make it possible to compare the results with other commercial spacers, which have different channel heights and porosities. All models were run at Re values of 50, 100, 150 and 200, except for 60 PP for which the flow becomes turbulent at lower-than-usual Re, making it unsuitable for modelling with laminar flow equations in steady-state mode. To keep the results comparable, 60 PP was studied for Re values of 50, 75, 100 and 125, where the flow remains laminar.

Table 5-2 presents a summary of the simulation results in the form of power law equations and provides a clear comparison of the different configurations. A custom-written MATLAB® program was used to optimize the power law parameters to yield the maximum coefficient of determination (R^2) for every data set. Together with the equations, Table 5-2 also presents the lowest value of R^2 for each correlation for the four spacers. Comparison of the power law equations and the CFD results is shown in Figure 5-2 to Figure 5-6 and Figure 5-8, with symbols representing the CFD results and lines representing the power law correlations. To facilitate comparison of the new results in Table 5-2 with our previous work, selected results from Section 4.3 are reproduced in Table 5-3.

Table 5-2. Correlations for key variables derived from the current CFD simulations.

Configuration	90 PP	45 PP	90 HDPE	60 PP	Minimum R^2
$\Delta P/L$ (Pa/m)	0.640 $Re^{2.02}$	11.1 $Re^{1.68}$	13.5 $Re^{1.39}$	17.6 $Re^{1.64}$	0.983
SPC (W/m^3)	1.63E–03 $Re^{2.85}$	8.23E–03 $Re^{2.70}$	1.23E–02 $Re^{2.42}$	1.69E–02 $Re^{2.66}$	0.994
Pn	21.3 $Re^{2.84}$	20.2 $Re^{2.68}$	24.9 $Re^{2.43}$	36.5 $Re^{2.66}$	0.994
Sh	32.2 $Re^{0.208}$	11.4 $Re^{0.323}$	54.2 $Re^{0.134}$	50.5 $Re^{0.189}$	0.977
	29.0 $Pn^{0.0665}$	7.75 $Pn^{0.122}$	44.1 $Pn^{0.0567}$	38.4 $Pn^{0.0720}$	0.973
SPMP′	7.08 $Re^{-1.84}$	7.85E–4 $Re^{0.878}$	0.806 $Re^{-0.300}$	2.93 $Re^{1.11}$	0.944
SCE	0.980 $Re^{-2.47}$	0.503 $Re^{-2.33}$	1.11 $Re^{-2.16}$	0.930 $Re^{-2.38}$	0.998

Table 5-3. Correlations for selected key variables reported in Section 4.3.

Configuration	Ladder-type	Triple	Wavy	Submerged	Minimum R^2
$\Delta P/L$ (Pa/m)	4.16 $Re^{1.49}$	2.85 $Re^{1.55}$	6.17 $Re^{1.37}$	9.97 $Re^{1.29}$	0.9994
SPC (W/m^3)	2.69E–3 $Re^{2.52}$	1.42 E–3 $Re^{2.45}$	4.20 E–3 $Re^{2.40}$	5.32 E–3 $Re^{2.32}$	0.9999
Pn	4.37 $Re^{2.42}$	11.6 $Re^{2.48}$	5.86 $Re^{2.33}$	7.92 $Re^{2.24}$	0.9999
Sh	10.1 $Re^{0.341}$	8.43 $Re^{0.425}$	3.62 $Re^{0.549}$	5.85 $Re^{0.382}$	0.9743
	8.96 $Pn^{0.140}$	5.67 $Pn^{0.169}$	2.44 $Pn^{0.234}$	4.17 $Pn^{0.169}$	0.9690
SCE	1.48 $Re^{-1.96}$	0.419 $Re^{-1.93}$	0.530 $Re^{-1.75}$	0.640 $Re^{-1.83}$	0.9996

Pressure drop

In agreement with other studies (1, 6-18), Figure 5-2 indicates that for all geometries, the pressure drop per unit length increases with Re.

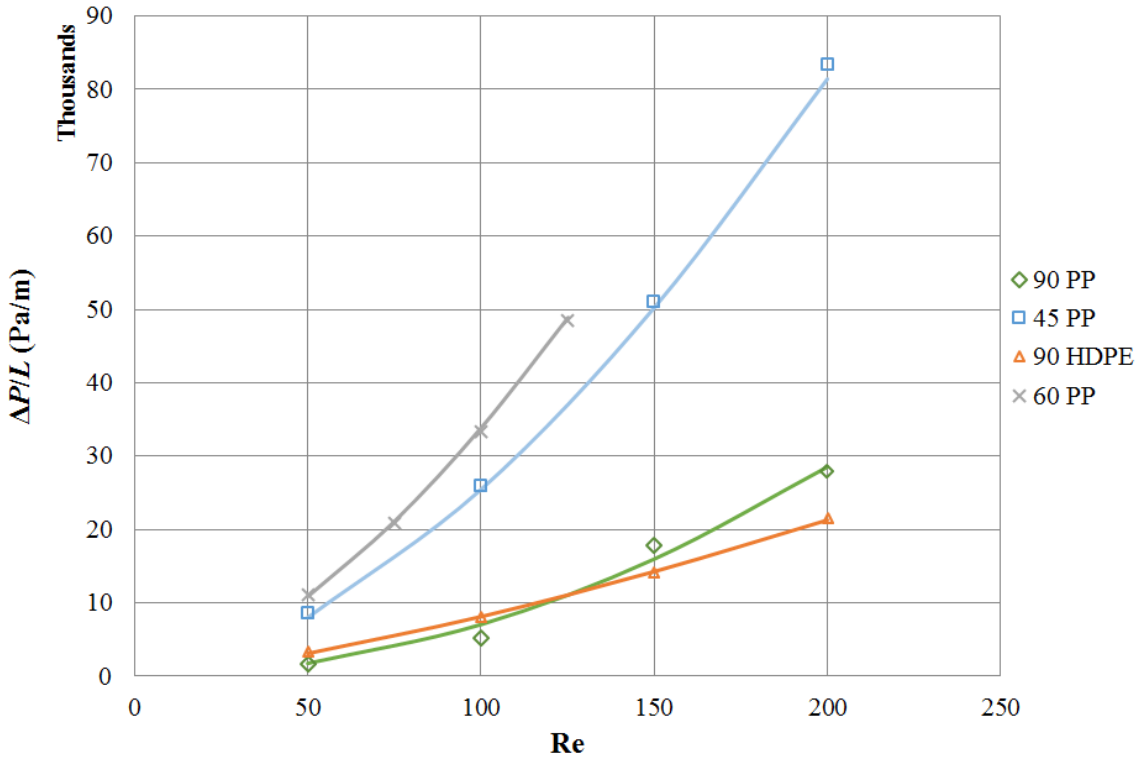

Figure 5-2. Predicted pressure drop per unit length as a function of Re for the four spacers.

Table 5-2 shows that the pressure drop is proportional to $Re^{1.4–2.0}$ depending on the spacer geometry. The power law exponent is in the expected range but is slightly higher than reported previously in Table 5-3 for more simple geometries ($Re^{1.29–1.55}$). This means that the commercial spacers are more responsive to flow changes and will experience larger relative increase in pressure drop with flowrate, compared to the simpler geometries. The commercial spacers would provide more benefit from being used in the lower range of Re values, with respect to change in pressure drop.

As shown in Figure 5-2, 90 PP has the lowest pressure drop for low flowrates (Re < 120) but, owing to its strong relation with Re ($\propto Re^{2.02}$), for higher flowrates, it loses this position, with 90 HDPE showing the lowest pressure drop according to its weaker relation to Re ($\propto Re^{1.39}$).

On the other hand, comparing the values of pressure drop for different spacers, including the four simple geometries studied in previous chapter reveals that for Re = 200, spacers show comparable values when categorized into three groups: simple spacers (Ladder-type, Triple,

Wavy and Submerged, termed the "base group"), commercial spacers (90 PP, 45 PP, 90 HDPE and 60 PP) and a plain open channel.

- Simple spacers have a pressure drop in the range 9–11 kPa/m;
- Commercial spacers have 2–10 times greater pressure drop compared to the base group;
- The plain channel has 15% of the base group pressure drop.

In addition, it is notable that the 90 HDPE spacer has the lowest power law exponent among the four, which could be a result of having three small filaments ($d = 0.3H$) after every normal-sized filament ($d = 0.5H$) as seen in Figure 5-1 (d). This will increase the porosity of the channel and provide a higher cross-sectional area for fluid passage. These small filaments cause the flow to act differently at low and high flowrates. This matter is discussed in more detail in Section 5.3.2.

Power consumption

Similar to our previous work and other studies, Figure 5-3 shows that SPC increases significantly with increasing flowrate. The 90 PP spacer has the lowest SPC for Reynolds numbers less than 110, while for Re > 110, 90 HDPE has the lowest SPC. On the other hand, 60 PP has the highest SPC over the Re range studied. The highest rate of increase in SPC is for

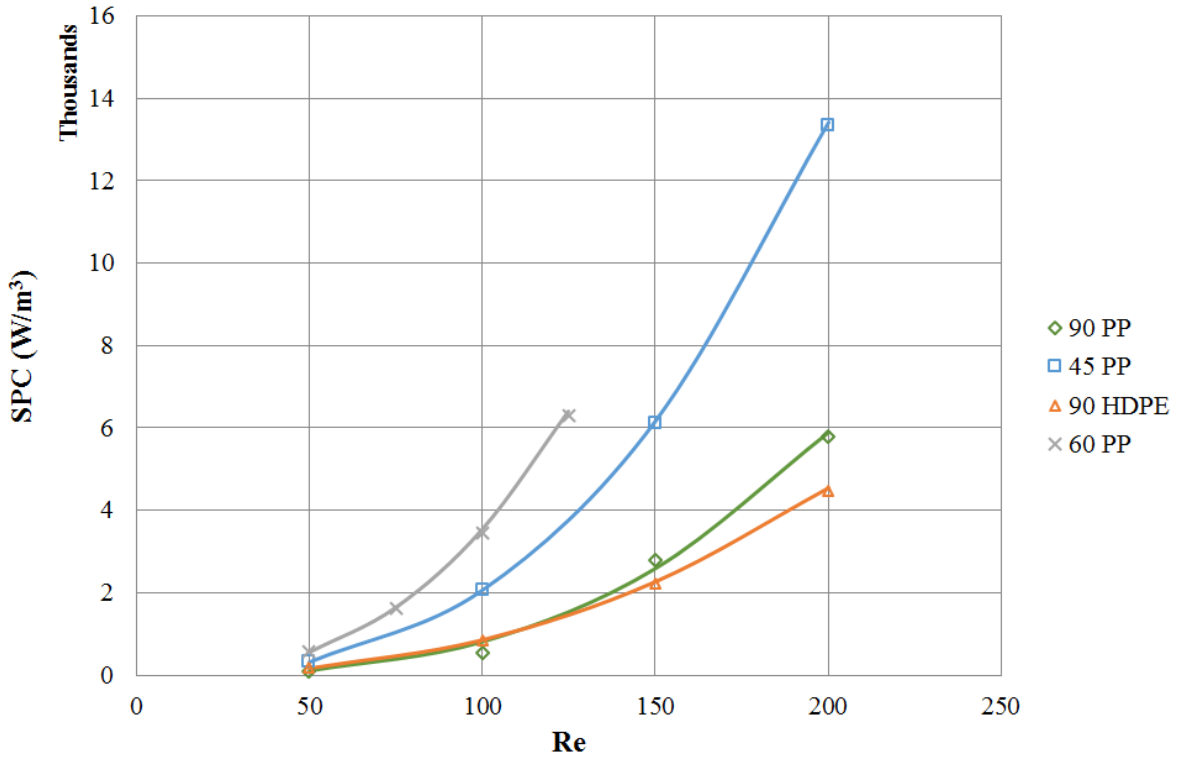

Figure 5-3. Predicted Specific Power Consumption as a function of Re for the four spacers.

the 90 PP geometry, which has SPC $\propto$ $Re^{2.85}$, while the lowest is for 90 HDPE, which has SPC $\propto$ $Re^{2.42}$ (Table 5-2).

Including the results from the previous chapter (Table 5-3), it is notable that the power law exponent for SPC varies in a narrower range than for pressure drop (2.32–2.85 for SCE compared to 1.29–2.02 for pressure drop) among all eight spacer-filled channels investigated.

The relationship between Pn and Re is shown in Figure 5-4 and is consistent with the SPC results for the 90 HDPE, 45 PP and 60 PP spacers. Because Pn $\propto$ SPC$\times H^4$, it is very sensitive to channel height. The channel height of 90 PP is greater than for the other spacers, which explains why its Pn results are higher than those of the other spacers.

In addition, similar to pressure drop, the three categories of spacers display different Pn ranges. The Pn values of commercial spacers are an order of magnitude greater than those of the simple spacers, which in turn are an order of magnitude greater than the Pn of a plain channel.

Mass transfer

Figure 5-5 shows Sh results for different flowrates and spacers. Previous studies revealed that mass transfer and Sherwood number increase with Re (1, 3, 6-15, 20-22). Some of these

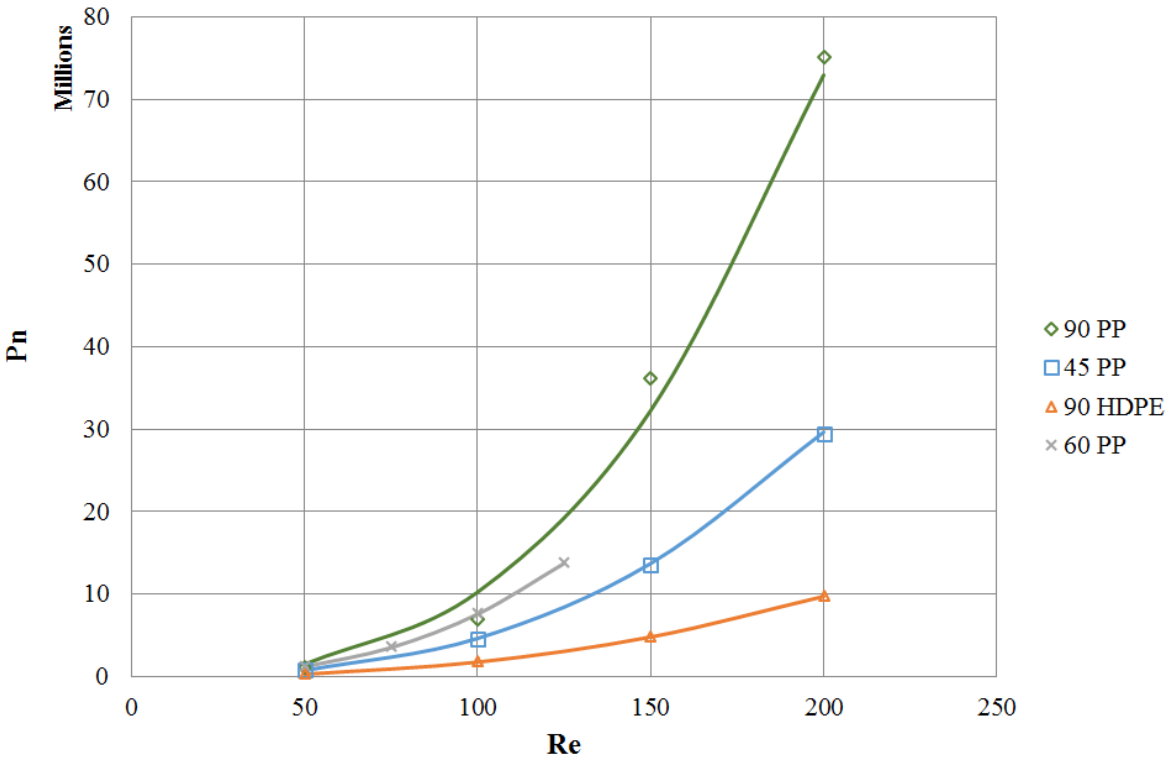

Figure 5-4. Predicted Power number as a function of Re for the four spacers.

studies attempt to quantify that relationship and reported equations linking Sh and Re for different geometries (3, 11, 12, 21).

In all cases, the recommended equations are in the form of a power law in which the exponent is positive and less than one. Of the four geometries studied in this work, 60 PP has the highest Sh value while 45 PP has the lowest over the Re range studied. Further, 45 PP has the strongest relationship with Re ($Sh \propto Re^{0.323}$) while 90 HDPE shows weakest relationship ($Sh \propto Re^{0.134}$). Our results vary from those reported in previous works: Schock et al. (12) reported 0.875 and DaCosta et al. (21) reported 0.5 for the Re exponent for other commercial spacers, but this could be the result of different spacer geometries.

It appears that most geometries have been optimized to maximize the exponent, which means that the spacer will get the greatest benefit from flow increases. On the other hand, as a result of the weak relation to flowrate, both 60 PP and 90 HDPE will lose a minimum of their performance from a reduction in flowrate. Overall, comparing the three spacer categories shows that Sh values for all of them are of the same order of magnitude.

Figure 5-6 plots Sh against Pn, thereby combining mass transfer and energy consumption results, and including previously reported data in Section 4.3 and Li et al. (1). It serves to highlight the trade-off between production rate and energy costs. It should be noted that the rate of increase of Sh with Pn for the four commercial geometries studied herein is slower than reported by the literature performance envelopes. Figure 5-6 also shows that 60 PP and 90

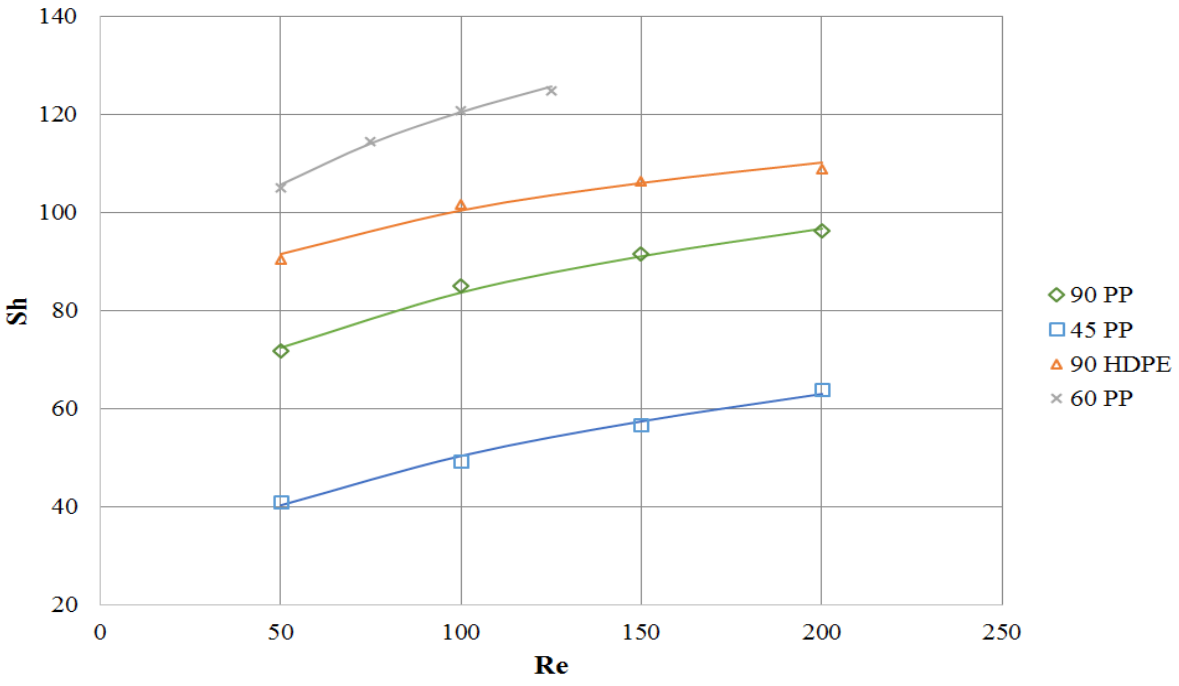

Figure 5-5. Predicted Sherwood number as a function of Re for the four spacers.

HDPE have significantly higher mass transfer performance for Pn below around 5×10^6, compared to any of the other geometries studied. Based on Figure 5-6, 90 HDPE would be the best choice of spacer, as it delivers high Sh with a relatively low energy requirement. While the Sh value of 60 PP is around 10% higher than that of 90 HDPE at the same Pn, its corresponding Re value is around 60% lower, meaning that 60 PP's production capacity is substantially lower.

Examination of the detailed CFD results could explain the behaviour of the 90 HDPE spacer. An explanation for the high mass transfer coefficient of the spacer for low flowrates, as well as its weak relationship with Re, is given in Section 5.3.2.

Spacer Performance Ratio (SPMP)

Schwinge et al. (20) defined and calculated SPMP for three filament configurations and three d/H values, but while the flowrate or Re is not clear, it is probable that they were generated for $Re_{ch} = 200$. On the other hand, there is no mention of a relationship between SPMP and Re by the authors. Table 5-4 shows the SPMP values reported by (20) alongside the SPMP′ values calculated in present work.

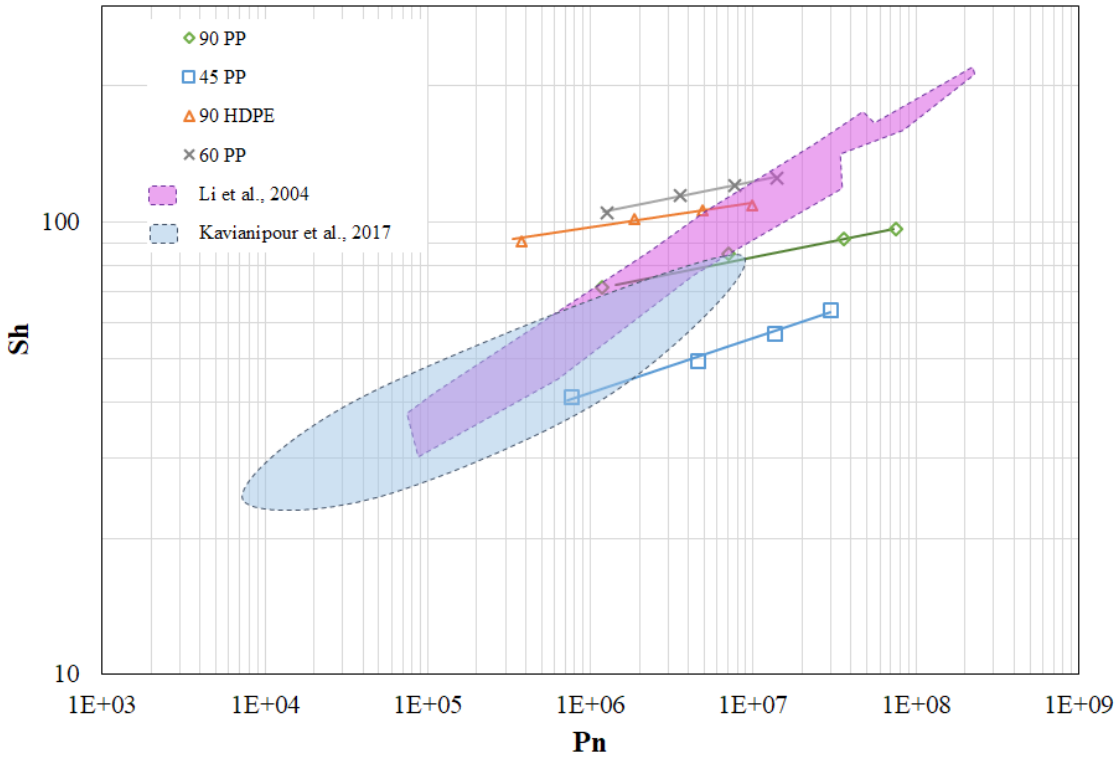

Figure 5-6. Trade-off between production capacity and energy consumption: Sherwood number as a function of Power number for the four commercial spacers and the results reported by (1) and (3).

Table 5-4. Comparison of SPMP and SPMP′ results.

	SPMP′ based on (3)			SPMP′ from the current work				SPMP reported by (20)			
Re	Ladder-type	Wavy	Submerged	90 PP	45 PP	90 HDPE	60 PP	Spacer / *d*/*H*	Zigzag	Cavity	Submerged
50	0.5768	0.4908	0.2846	0.0053	0.0242	0.2501	0.0258				
100	0.5282	0.5019	0.2771	0.0017	0.0433	0.2008	0.0355	0.3	3.45	2.80	1.11
150	0.4500	0.5128	0.2673	0.0006	0.0664	0.1801	0.0437	0.5	1.33	0.92	0.59
200	0.3967	0.4936	0.2567	0.0003	0.0808	0.1652	0.0663	0.7	0.89	0.54	0.28

The study for different *d*/*H* values reveals that the Zigzag configuration is the best of the three geometries for all filament diameters. On the other hand, smaller filaments lead to better SPMP values in all cases (20). The difference between Zigzag / Cavity and Wavy / Ladder-type geometries is that the latter pair has longitudinal filaments that are absent in the former, while all the geometries have latitudinal filaments. The difference in values observed between Schwinge et al. (20) and our studies can be explained by the difference in bulk and wall solute concentration values (mass fractions of 0 and 1 in (20) compared to 0.05 and 0.35 in present work, respectively) as well as our use of constant feed mass flowrate compared to constant Re. This issue has been already clarified in previous chapter, Section 4.3.4.

Our study indicates that SPMP′ does not vary in a consistent way with Re as shown in Figure 5-7 for seven different spacers. For different spacers, SPMP′ might increase, decrease, or do both with increasing Re. All the commercial spacers studied had very low values for SPMP′. All values presented in the current work are less than one and are in accordance with our previous results. This means that the Plain configuration, that is, a feed channel without any spacer, would be the best performing one among the spacers studied according to SPMP′.

Spacer Configuration Efficacy (SCE)

As defined by Saeed (6), SCE is the ratio of Sh to Pn, and it thus includes both the mass transfer and energy requirement characteristics of a spacer. As indicated in Figure 5-8, 90 HDPE has the highest SCE values over the Re range studied for the commercial spacers. In addition, it suffers a lower negative impact from increased flowrate as well (Table 5-2). Both behaviours can be explained by examining the detailed flow path and concentration polarization layer results around the filaments (Section 5.3.2).

The 45 PP and 90 PP spacers show the lowest SCE because of their high demand for energy and low mass transfer performance.

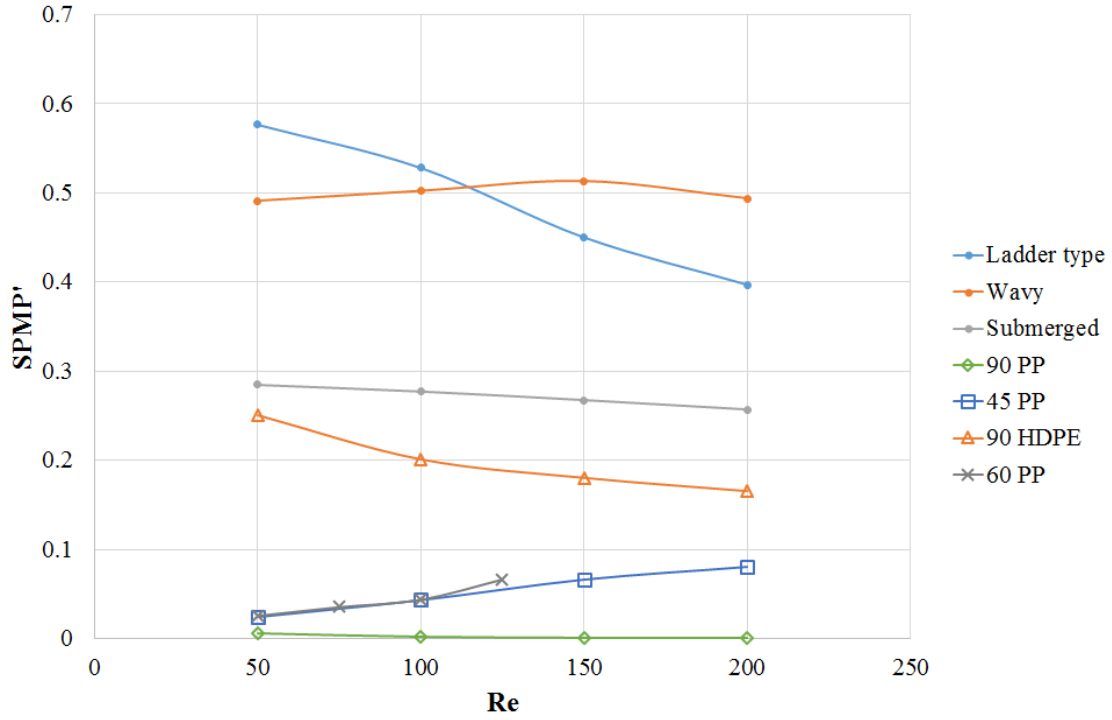

Figure 5-7. Predicted SPMP' as a function of Re for the four commercial spacers and three conventional spacer geometries studied in [19].

5.3.2 An insight into 90 HDPE

The 90 HDPE spacer would be best or second choice among commercial spacers, according to six different performance measures at both low and high flowrates (Section 5.3.3). In addition, Table 5-2 shows that the effect of flowrate on pressure drop and Sh is weaker than

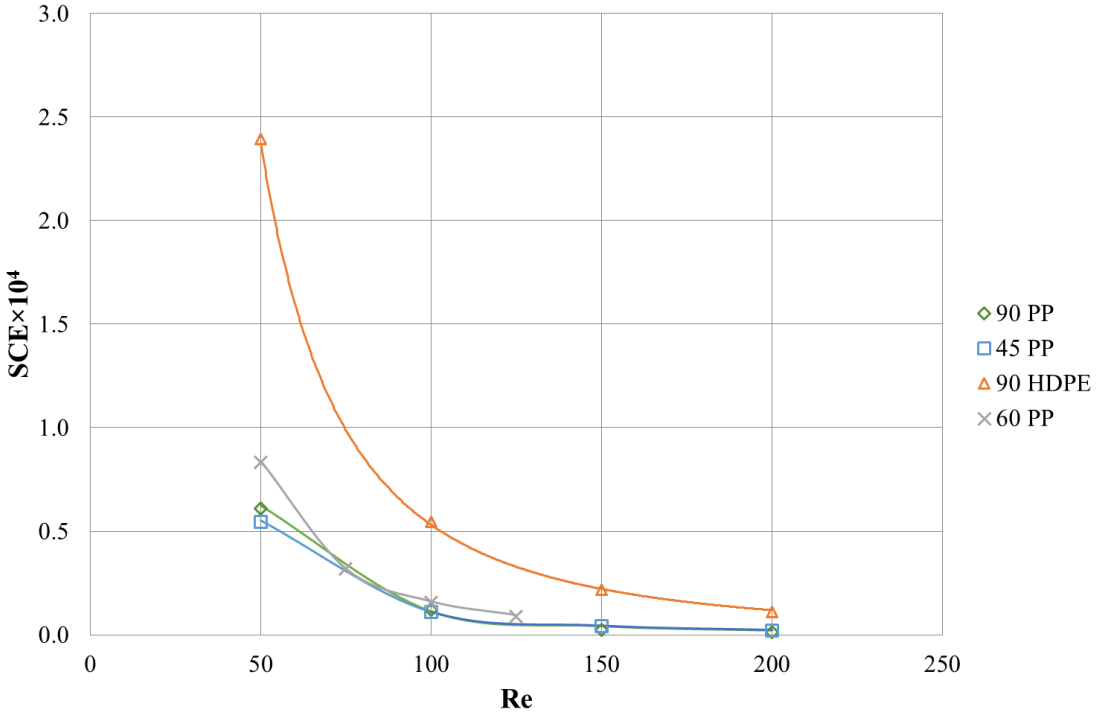

Figure 5-8. Predicted SCE as a function of Re for the four spacers.

for the other configurations studied. Both phenomena can be explained by the physical configuration of 90 HDPE. Figure 5-10 shows velocity and concentration contour plots for Re values of 50 and 200 for 90 HDPE. The velocity scales for the two Re plots were chosen to make the low and high flowrate plots visually comparable (Figure 5-9(a)). That is, the velocity scale for Re = 200 is four times higher than that for Re = 50, which is the same as the mass flowrate ratio, making the same colours represent the same ratio to the average velocity. On the other hand, for the concentration contour plots (Figure 5-9(b)), the maximum scale concentration was set to a value 1.5 times the weighted average outlet concentration. Logarithmic concentration scales were used to emphasise differences in the lower concentration ranges in both plots.

Examination of the circled area in Figure 5-9 (a) shows different behaviour at low and high Re values. At low flow, most of the fluid goes through the wider gap and a low velocity zone is observed after the filament in the lower part of the channel. In contrast, at high flow, both wide and narrow gaps are almost equally used. The wider gap offers greater clearance, but a longer path, while the narrower gap has a shorter path, but with a smaller clearance. As visible in Figure 5-9 (b), the concentration layer after the filament in the lower section of the channel for Re = 50 has been washed away at Re = 200, as indicated by the magnified region. The concentration plots also show that the small filaments are effective in depressing the concentration layers when they appear. Comparing the width and strength of the concentration layers around the thin and thick filaments indicates how effectively these small filaments can wash away rejected salts, reducing the osmotic pressure increase at the membrane surface and potentially also the deposition of scale.

Further investigation and possibly optimization in terms of L/H and d/H for thin and thick filaments and the number of thin filaments between thick filaments might lead to a better configuration.

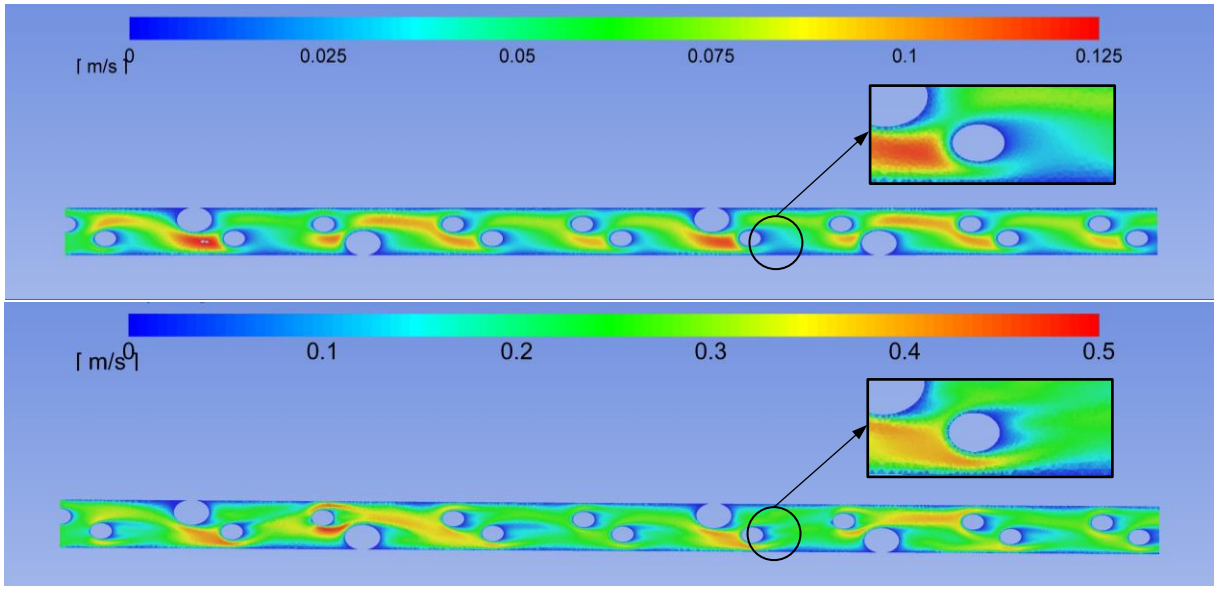

(a) Velocity magnitude for Re = 50 (top) and Re = 200 (bottom).

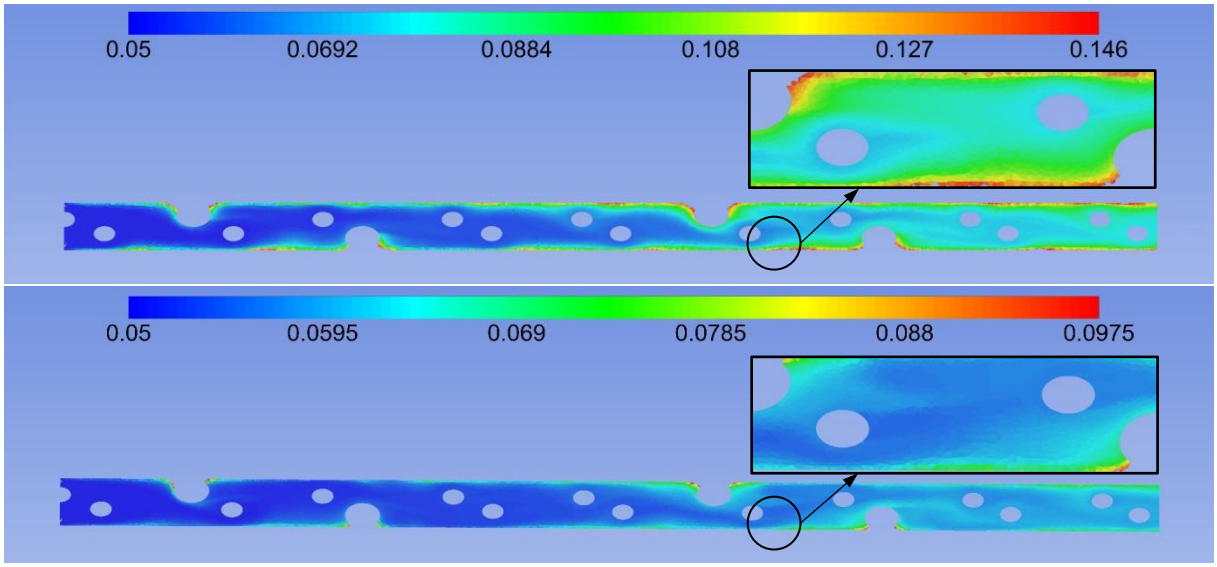

(b) Solute mass fraction for Re = 50 (top) and Re = 200 (bottom). Note that solute mass fractions higher than the upper limit of the colour scale are not shown in the solute contour plot.

Figure 5-9. Contour plots for the 90 HDPE spacer.

5.3.3 Consistency of rankings obtained from alternative measures of spacer performance

The rankings of the commercial spacers, from best to poorest performing, based on the various performance measures ($\Delta P/L$, SPC, Pn, Sh, SPMP′ and SCE), are shown in Figure 10 for low and high flowrates. For Re = 50, the pressure gradient and SPC are in full agreement. However, when it comes to Pn, 90 PP falls from first to third ranking. On the other hand, the

three mass transfer measures are in partial agreement: 45 PP and 90 PP are ranked as the worst choices, while 60 PP and 90 HDPE are the best.

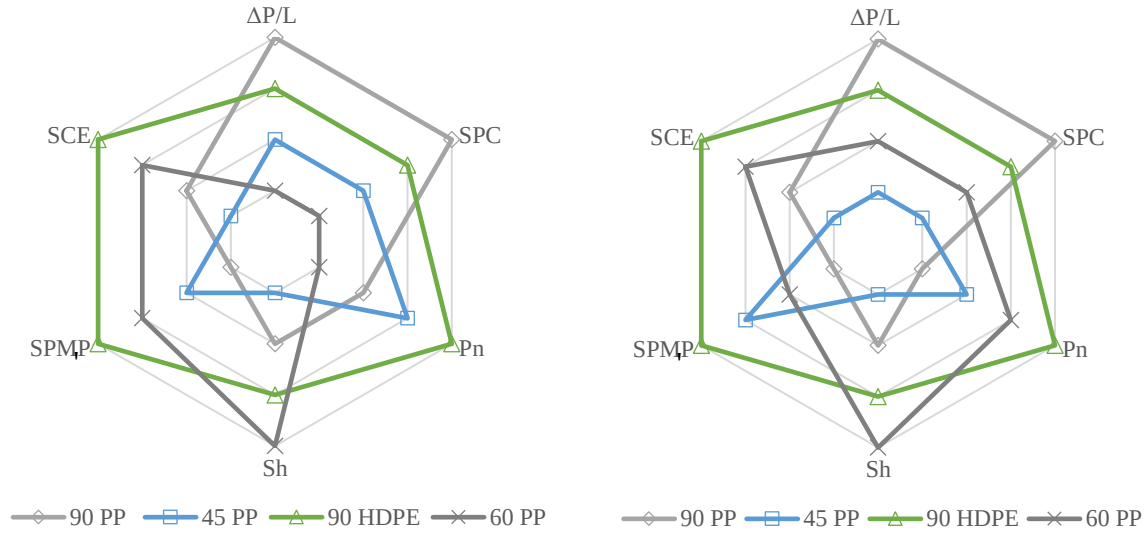

Figure 5-10. Spacer ranking using different performance measures (the outermost zone represents the best performance and the innermost zone the poorest performance).

A similar result is observed for Re = 100 (Figure 5-10). There is agreement in the rankings for pressure gradient and SPC, as well as the same change in Pn observed for 90 PP, as explained above. The same partial agreement between SCE and Sh is displayed; 45 PP improves from being the worst choice according to SCE and Sh to being the second best by SPMP′.

Table 5-5 shows the range of variation in the various performance measures among the different spacers at Re = 50 and 100 by presenting the ratio of the minimum to the maximum value. For example, at Re = 50, in terms of pressure drop, the best spacer has only 16% of the $\Delta P/L$ of the worst spacer. The reported values of $\Delta P/L$, SPC, Pn, Sh and SCE are all in the same order of magnitude, while for SPMP′ the variation can be up to three orders of magnitude. Comparison of the performance measure ratios at Re = 50 and 100 also reveals that (except for SPMP′) they will not change abruptly with flowrate, being only doubled, or halved at most, as a result of a two-fold increase in the flowrate. For SPMP′, however, the difference is as high as one order of magnitude.

Table 5-5. Ratio of the minimum to maximum values of the indicated spacer performance measure at Re = 50 and 100.

Re	$\Delta P/L$	SPC	Pn	Sh	SPMP′	SCE
50	0.16	0.16	0.30	0.39	0.021	0.23
100	0.26	0.33	0.13	0.51	0.0017	0.12

To the best of the authors' knowledge, no other study has discussed the potential advantages and disadvantages, in terms of either consistency or sensitivity, of the results for different performance measures for feed spacers.

5.4 Conclusions

In the current work, CFD investigations have been carried out to predict the effect of changes in flowrate on four commercial feed spacer configurations used in spiral wound modules in RO systems. Energy consumption and mass transfer of solute on the feed side are investigated through multiple performance measures including pressure drop, Specific Power Consumption, Power number, Sherwood number, modified Spacer Performance Ratio (SPMP′) and Spacer Configuration Efficacy. The modelling approach validated in our previous work was used again in this study.

Based on the simulations, the following conclusions are drawn:

- Most of the performance measures were strongly affected by the Reynolds number, except for SPMP′.
- SPMP′ did not vary in a consistent way with Reynolds number for the different spacers. Further attention is needed to define a flow-independent performance measure based on the SPMP concept.
- Regression of the CFD results yielded good power law correlations for SCE, SPC and Pn as functions of Re. The correlations are very quick to apply and are in agreement with previous works (3, 11, 12, 21).
- Different performance measures result in different spacer rankings for different Re values.
- SCE appears to be the preferred choice for the performance measure because it considers both mass transfer and energy consumption, and has predictable behaviour with Re, in contrast to the current definition of SPMP′.
- One of the four commercial spacers studied, the Naltex N05013_90HDPE-NAT (90 HDPE) from DelStar Technologies, which ranked best or second best with respect to all measures, shows a surprisingly weak response to changes in flowrate, indicating the prospect of large energy savings with a small loss in mass transfer performance at low flowrates. Further studies are required to provide optimum spacer design parameters.

Nomenclature

a	Discorectangle filament side length (m)
A_{eff}	Effective area (m^2)
ΔC_{Spacer}	Difference in average concentration at inlet and outlet in spacer-filled channel (w/w)
ΔC_{Slit}	Difference in average concentration at inlet and outlet in open channel (w/w)
d	Filament diameter (m)
D_h	Hydraulic diameter (m)
h	Discorectangle filament height (m)
H	Channel height (m)
L	Channel length (m)
$\Delta P/L$	Pressure drop per unit length (Pa/m)
ΔP_{Spacer}	Difference in average pressure at inlet and outlet in spacer-filled channel (Pa)
ΔP_{Slit}	Difference in average pressure at inlet and outlet in open channel (Pa)
Pn	Power number
r	Discorectangle filament radius (m)
Re_{ch}	Channel Reynolds number
Re_h	Hydraulic Reynolds number
SCE	Spacer Configuration Efficacy
Sh	Sherwood number
SPC	Specific Power Consumption (W/m^3)
SPMP	Spacer Performance Ratio introduced by (20)
SPMP′	Spacer Performance Ratio based on constant feed mass flowrate
u_{eff}	Effective velocity (m/s)

Greek symbols

ε	Porosity

References

1. Li F, Meindersma W, de Haan AB, Reith T. Experimental validation of CFD mass transfer simulations in flat channels with non-woven net spacers. Journal of Membrane Science. 2004; 232(1-2):19-30.

2. UNESCO. Encyclopedia of desalination and water resources: Energy requirements of desalination processes. [webpage]. Available from: http://www.desware.net/Energy-Requirements-Desalination-Processes.aspx.

3. Kavianipour O, Ingram GD, Vuthaluru HB. Investigation into the effectiveness of feed spacer configurations for reverse osmosis membrane modules using computational fluid dynamics. Journal of Membrane Science. 2017; 526:156-171.

4. Dashtpour R, Al-Zubaidy S. Energy efficient reverse osmosis desalination process. International Journal of Environmental Science and Development. 2012; 3(4):339-345.

5. Johnson J, Busch M. Engineering aspects of reverse osmosis module design. Desalination and Water Treatment. 2010; 15(1-3):236-248.

6. Saeed A. Effect of feed channel spacer geometry on hydrodynamics and mass transport in membrane modules [Ph.D Thesis]. Perth, Australia: Curtin University; 2012.

7. Saeed A, Vuthaluru R, Yang YW, Vuthaluru HB. Effect of feed spacer arrangement on flow dynamics through spacer filled membranes. Desalination. 2012; 285:163-169.

8. Saeed A, Vuthaluru R, Vuthaluru H. Concept of spacer configuration efficacy (sce) applied to optimize ladder type feed spacer filament spacing in narrow channels. International Conference On Water Desalination, Treatment and Management & Indian Desalination Association Annual Congress, 2013. Jaipur, India: The Malaviya National Institute of Technology.

9. Saeed A, Vuthaluru R, Vuthaluru HB. Investigations into the effects of mass transport and flow dynamics of spacer filled membrane modules using CFD. Chemical Engineering Research & Design. 2015; 93:79-99.

10. Saeed A, Vuthaluru R, Vuthaluru HB. Impact of feed spacer filament spacing on mass transport and fouling propensities of RO membrane surfaces. Chemical Engineering Communications. 2015; 202(5):634-646.

11. In Seok K, Ho Nam C. The effect of turbulence promoters on mass transfer – numerical analysis and flow visualization. International Journal of Heat and Mass Transfer. 1982; 25(8):1167-1181.

12. Schock G, Miquel A. Mass-transfer and pressure loss in spiral wound modules. Desalination. 1987; 64(C):339-352.

13. Li F, Meindersma W, de Haan AB, Reith T. Optimization of commercial net spacers in spiral wound membrane modules. Journal of Membrane Science. 2002; 208(1-2):289-302.

14. Li F, Meindersma GW, de Haan AB, Reith T. Optimization of non-woven spacers by CFD and validation by experiments. Desalination. 2002; 146(1-3):209-212.

15. Fimbres-Weihs GA, Wiley DE. Numerical study of mass transfer in three-dimensional spacer-filled narrow channels with steady flow. Journal of Membrane Science. 2007; 306(1-2):228-243.

16. Cipollina A, Micale G, Rizzuti L. Membrane distillation heat transfer enhancement by CFD analysis of internal module geometry. Desalination and Water Treatment. 2011; 25(1-3):195-209.

17. Cipollina A, Di Miceli A, Koschikowski J, Micale G, Rizzuti L. CFD simulation of a membrane distillation module channel. Desalination and Water Treatment. 2009; 6(1-3):177-183.

18. Qureshi M, Shakaib M. CFD study for temperature and concentration profiles in membrane channels. International conference on Energy and Sustainability, 2013. Karachi, Pakistan: NED University of Engineering & Technology.

19. Jon Johnson MB. Engineering aspects of reverse osmosis module design. http://www.lenntech.com/Data-sheets/Filmtec-System-Design-L.pdf: Lenntech; 2009.

20. Schwinge J, Wiley DE, Fletcher DF. Simulation of the flow around spacer filaments between channel walls. 2. Mass-transfer enhancement. Industrial & Engineering Chemistry Research. 2002; 41(19):4879-4888.

21. DaCosta AR, Fane AG, Wiley DE. Spacer characterization and pressure drop modelling in spacer-filled channels for ultrafiltration. Journal of Membrane Science. 1994; 87(1-2):79-98.

22. Santos JLC, Geraldes V, Velizarov S, Crespo JG. Investigation of flow patterns and mass transfer in membrane module channels filled with flow-aligned spacers using computational fluid dynamics (CFD). Journal of Membrane Science. 2007; 305(1-2):103-117.

Chapter 6. A detailed approach for the analysis and prediction of SWM feed spacer performance based on CFD results[7]

Abstract

In reverse osmosis applications, feed spacers are used in spiral wound membranes to separate the membrane surfaces and enhance mass transfer while incurring a reasonable level of pressure drop. In this study, an attempt has been made to understand the effect of spacer characteristics, such as arrangement and size, on mass transfer and pressure drop.

Power-law equations were successfully developed to describe different spacer performance measures as a function of Reynolds number (Re), where both the multiplier of the Re term and the Re exponent vary for each spacer arrangement. Although at the macro level, it was not possible to adequately correlate the equation parameters with the spacers' geometrical parameters (such as porosity), examining the post-processed CFD results at the micro-level led to explanations for the observed concentration profiles, trends in spacer performance and changes in the equation parameters. A key observation was the importance of lateral flow recirculation, which was termed side-washing.

Overall, this study found that based on the Spacer Configuration Efficacy performance measure and by assessing the trade-off between Sherwood number and pressure drop, the Woven configuration shows the best performance among the spacer arrangements and range of flowrates studied.

6.1 Introduction

Performance measures are critical to assessing the efficacy of feed spacers used in spiral wound membranes (SWM) for reverse osmosis (RO) operations, such as desalination. In general, the efficacy is assessed through dimensionless parameters characterising mass transfer and energy consumption that are largely dependent on the geometrical features of the spacers.

The effect of flowrate on various RO feed spacer performance measures has been extensively studied in the literature, and many studies have suggested various equations to link performance measures with Reynolds number (1-7). Some works considered the relationship

[7] This chapter has been submitted to the journal Chemical Engineering Science and currently is under review for publication.

between mass transfer and pressure drop (1, 2, 6-18). However, investigation of the general problem of linking mass transfer and heat transfer rates with flowrate and pressure drop started more than a century ago.

Attempts to find a correlation for predicting heat/mass transfer coefficient(s) between a solid body and a fluid in forced convection started in the late 1800s and early 1900s. As summarised by Drew et al. (19), in 1883 Graetz proposed an approach for predicting the heat conduction for fluids in laminar flow, based on the Fourier-Poisson equation, with coefficients adjusted by Nusselt in 1910, as

$$\frac{t_{out} - t_{in}}{T_{wall} - t_{in}} = \frac{\text{actual temperature rise}}{\text{initial temperature difference}} = 1 - 8 \times P_2 \tag{6-1}$$

where

$$P_2 = 0.10238e^{-14.6272\alpha} + 0.01220e^{-89.22\alpha} + 0.00237e^{-212\alpha} + \cdots \tag{6-2}$$

and $\alpha = \left(\frac{D}{L}\,\mathrm{Re}\,\mathrm{Pr}\right)^{-1}$ for Reynolds number, Re, and Prandtl number, Pr. Meanwhile, according to Nusselt (20) in 1910, based on dimensional analysis and similarity theory, the following relation was suggested for turbulent flow,

$$\frac{hD}{k} = a\,\mathrm{Re}^n\,\mathrm{Pr}^m \tag{6-3}$$

wherein *a*, *m*, and *n* are dependent on the shape of the body, and the group hD/k came to be known as the Nusselt number, Nu.

These equations provided the foundation for further research work that reported values for the parameters or introduced correction factors. Table 6-1 summarises some of the most important historical studies and their main outcomes, excluding the corrections for physical property changes, to highlight the steps and the trends related to the advancement of the art.

Apart from chronicling the historical progression of the equations, improvements in their accuracy and expanded applicability, Table 6-1 provides some other relevant outcomes. First, while dimensional analysis indicates Nu that should be a function of Re and Pr, there is no adequate theoretical method available to determine that function across all flow regimes. Also, the studies are based on empiricism using the author's original experiments or other researchers' data. In addition, it is clear that different functions were used for laminar and

turbulent flows. Second, in early studies, the exponents of Re and Pr were not necessarily chosen to optimise accuracy, but for convenience. For example, in 1915, Nusselt clarified that using the same exponent for Re and Pr was for simplicity (21), which was followed by Gröber in 1921 and Nusselt again in 1925. This, along with the complex nature of forced convection heat transfer, explains the limited accuracy of these equations, which is well known and discussed in the literature (22-25). Third, aside from Re and Pr, several other terms were introduced into these correlations, including the ratio D/L_{total} or its reciprocal, a friction factor and the Grashof number when natural convection may be important in laminar flow; sometimes Re, Pr and D/L_{total} were combined to form the Graetz number Gz = Re Pr (D/L_{total}) or the group wc_p/kL_{total}. Fourth, it should be acknowledged that analysing similar datasets could result in different conclusions, since it relies on researchers to interpret the data.

All equations presented in Table 6-1 were developed for fluids flowing inside a circular pipe. For other shapes, the equation types and their parameters might change (20, 24-26).

Focusing on RO feed spacers, this study aims to develop equations to predict feed spacer performance measures as simple functions of well-known dimensionless groups, and the correlation of those equations' parameters with geometrical characteristics of the spacers. While several other researchers have addressed the first goal, only a few recent articles investigated the effect of the spacer characteristics on the equation parameters (4, 27). In the present study, the simple functions for the performance measures are derived by post-processing detailed computational fluid dynamics results obtained using ANSYS Fluent. A further aim of this study is to explain the macro-level performance of the spacers through detailed observation of the micro-level fluid flow.

Development of the simple correlating equations would benefit RO desalination plant staff by assisting them to optimise their operating conditions. It may be possible to optimise the plant further in the face of ongoing changes in the operating conditions by using real time optimisation, rather than using a setup optimised for design conditions. In addition, knowing the effect of spacer characteristics on the micro-level fluid flow behaviour could allow spacer designers and manufacturers to improve current spacers more efficiently. It could also help plant operators choose the best spacer for their particular constraints and priorities.

Table 6-1. Summary of historical developments to equation (6-1)

Year	Author(s)	Equation for $\frac{hD}{k}$	Re range	Comments	Reference
1910	Nusselt	$a\ \mathrm{Re}^{0.786}\ \mathrm{Pr}^{0.85}$	Turbulent		(20)
1913	Nusselt	$a\ \mathrm{Re}^{0.786}\ \mathrm{Pr}^{0.786}\ \left(\frac{D}{L_{\mathrm{total}}}\right)^{0.054}$	Turbulent	Nusselt assumed that the Pr exponent is equal to the Re exponent for simplicity.	(28)
1921	Gröber	$a\ \mathrm{Re}^{0.79}\ \mathrm{Pr}^{0.79}\ \frac{1}{r^{0.05}}$	Turbulent	Used pipe radius (r) only, not the length.	(29)
1924	McAdams & Frost	$15.4\ (1+\frac{50D}{L_{\mathrm{total}}})\ \mathrm{Re}^{0.8}$	10,000–750,000	Focussed on water only, they omitted Pr from the equation. Used D/L_{total} in the form of an additive term instead of a multiplier.	(29)
1924	Rice	$\frac{1}{63}\ \mathrm{Re}^{5/6}\ \mathrm{Pr}^{1/2}$	5000–25,0000	Assumed a constant Pr. Noted poor correlation quality.	(22)
1925	Nusselt	$a\ \mathrm{Re}^{0.786}\ \mathrm{Pr}^{0.786}\ \left(\frac{D}{L_{\mathrm{total}}}\right)^{0.2}$	Turbulent	Compared to his earlier work in 1913, the same exponents for Re and Pr were used, but the suggested exponent for D/L_{total} was increased.	(28)
1925	Merkel	$a\ \mathrm{Re}^{0.87}\ \mathrm{Pr}^{0.435}$	Turbulent		(20)
1925	Nusselt	$a\ \mathrm{Re}^{n}\ \mathrm{Pr}^{m}$	Turbulent	Suggested the general format, with no D/L_{total} term. Depending on experimental conditions, $0.72 < m < 0.91$ and $0.35 < n < 0.5$.	(20)
1928	Morris & Whitman	$a\ \mathrm{Re}^{0.83}\ \mathrm{Pr}^{0.37}$	5000–313,000	Assumptions were the same as McAdams & Frost (29).	(30)
1928	Cox	$\frac{1}{52.1}\ \mathrm{Re}^{5/6}\ \mathrm{Pr}^{1/3}$	Turbulent	Assumptions were the same as Rice (22).	(31)
1929	Rice	$\frac{1}{60}\ \mathrm{Re}^{5/6}\ \mathrm{Pr}^{1/2}$	Very turbulent	Assumptions were the same as Rice's earlier work (22).	(26)
1930	Stender	$C_1\ (\mathrm{Re\ Pr})^{0.75} + C_2\ \mathrm{Re\ Pr}\ \left(\frac{D}{L_{\mathrm{total}}}\right)$	Turbulent	Noted that heat transfer coefficient given by equations that includes D/L_{total} as a multiplier, e.g., Nusselt (1913) and Nusselt (1925) would approach zero for very long pipes. He recommended separating the terms for flow entry and for developed flow	(28)
1930	Dittus & Boelter	$0.024\ \mathrm{Re}^{0.8}\ \mathrm{Pr}^{n}$	Re > 10,000	For cooling, $n = 0.3$ and for heating, $n = 0.4$.	(32)
1930	Eagle & Ferguson	$\frac{6}{11}\ \mathrm{Re}\frac{f_D}{2}\frac{L_{\mathrm{total}}}{D}$	Laminar	Separate correlations for laminar and turbulent flow. The variable f_D is the Darcy friction factor. Investigated and stated no correlation between Nu and D/L_{total}.	(33)
		$\frac{\mathrm{Re\ Pr}}{(A+B(\mathrm{Pr}-1)-C(\mathrm{Pr}-1)^2)}$	Turbulent		

Year	Author(s)	Equation for $\frac{hD}{k}$	Re range	Comments	Reference
1931	Drew, Hogan & McAdams	$1.75\left(\frac{wc_p}{kL_{\text{total}}}\right)^{1/3}$	Re < 2100	The term wc_p/kL_{total} is simply $\pi/4$ times the Graetz number, which appears in several other correlations in this table. Applicable for Gz > 12.	(19)
1931	Lawrence & Sherwood	$0.056\ \text{Re}^{0.73}\ \text{Pr}^{0.49}$	680–18,400	Investigated and stated no correlation between Nu and D/L_{total}, for L_{total}/D between 59 and 224.	(28)
1931	Nusselt	$\frac{1}{47.3}\ \text{Re}^{0.819}\ \text{Pr}^{0.365}$ $\frac{1}{11.7}\ \text{Re}^{0.764}\ \text{Pr}^{0.355}\left(\frac{D}{L_{\text{total}}}\right)^{0.0552}$	Turbulent	Nusselt analysed the experimental data gathered by other researchers (33, 34) and developed these equations. The top equation is based on the data from (33) and the bottom equation is based on the results of (34).	(35)
1932	Sherwood & Petrie	$0.024\ \text{Re}^{0.8}\ \text{Pr}^{0.4}$	2800–37,600		(36)
1933	Colburn	$1.75\left(\frac{wc_p}{kL_{\text{total}}}\right)^{1/3}(1+0.015\text{Gr}^{1/3})$ $0.023\ \text{Re}^{0.8}\ \text{Pr}^{1/3}$	Laminar Turbulent	While Colburn incorrectly reported the constant 1.65 (23), McAdams suggested 1.75 in the original work (19) and emphasised on this value later (24, 25). The correction factor involving Gr represents the occurrence of free convection inside the tube. Colburn concluded that in laminar flow, L_{total}/D should not be used as a term in the equation. He recommended using a figure to predict heat/mass transfer and provided different curves based on L_{total}/D in the laminar region. He recommended correlations for both laminar and turbulent flow.	(23)
1936	Sieder & Tate	$1.86\ \text{Gz}^{1/3}\ (1+0.015\text{Gr}^{1/3})$	10–2000		(37)
1942	Martinelli & Boelter	$1.75F_1\left(\frac{wc_p}{kL_{\text{total}}}+0.0722F_2\left(\text{Gr Pr}\ \frac{D}{L_{\text{total}}}\right)^{0.75}\right)^{1/3}$	Laminar	F_1 uses the arithmetic average temperature difference instead of the log-mean; F_2 addresses changes in the fluid bulk temperature.	(25)
1943	Kern	$1.86\ \text{Gz}^{1/3}\ \frac{2.25(1+0.010\text{Gr}^{1/3})}{\ln(\text{Re})}$	Laminar		(38)
1951	Eubank & Proctor	$1.8\left(\frac{wc_p}{kL_{\text{total}}}+12.6\left(\text{Gr Pr}\ \frac{D}{L_{\text{total}}}\right)^{0.4}\right)^{1/3}$	Laminar	Mainly based on the equation format suggested by Martinelli & Boelter (39). Applicable for $\frac{wc_p}{kL_{\text{total}}} > 20$ and ½" < D < 2½".	(40)
1962	Oliver	$1.75\left(\frac{wc_p}{kL_{\text{total}}}+0.00056\left(\text{Gr Pr}\ \frac{L_{\text{total}}}{D}\right)^{0.7}\right)^{1/3}$	Laminar	Applicable for $\frac{wc_p}{kL_{\text{total}}} > 13$. Inconsistent results with (Gr Pr D/L_{total}) as a term in the equation. Improved results with (Gr Pr) only. Better agreement with (Gr Pr L_{total}/D); power of L_{total}/D is provisional.	(41)

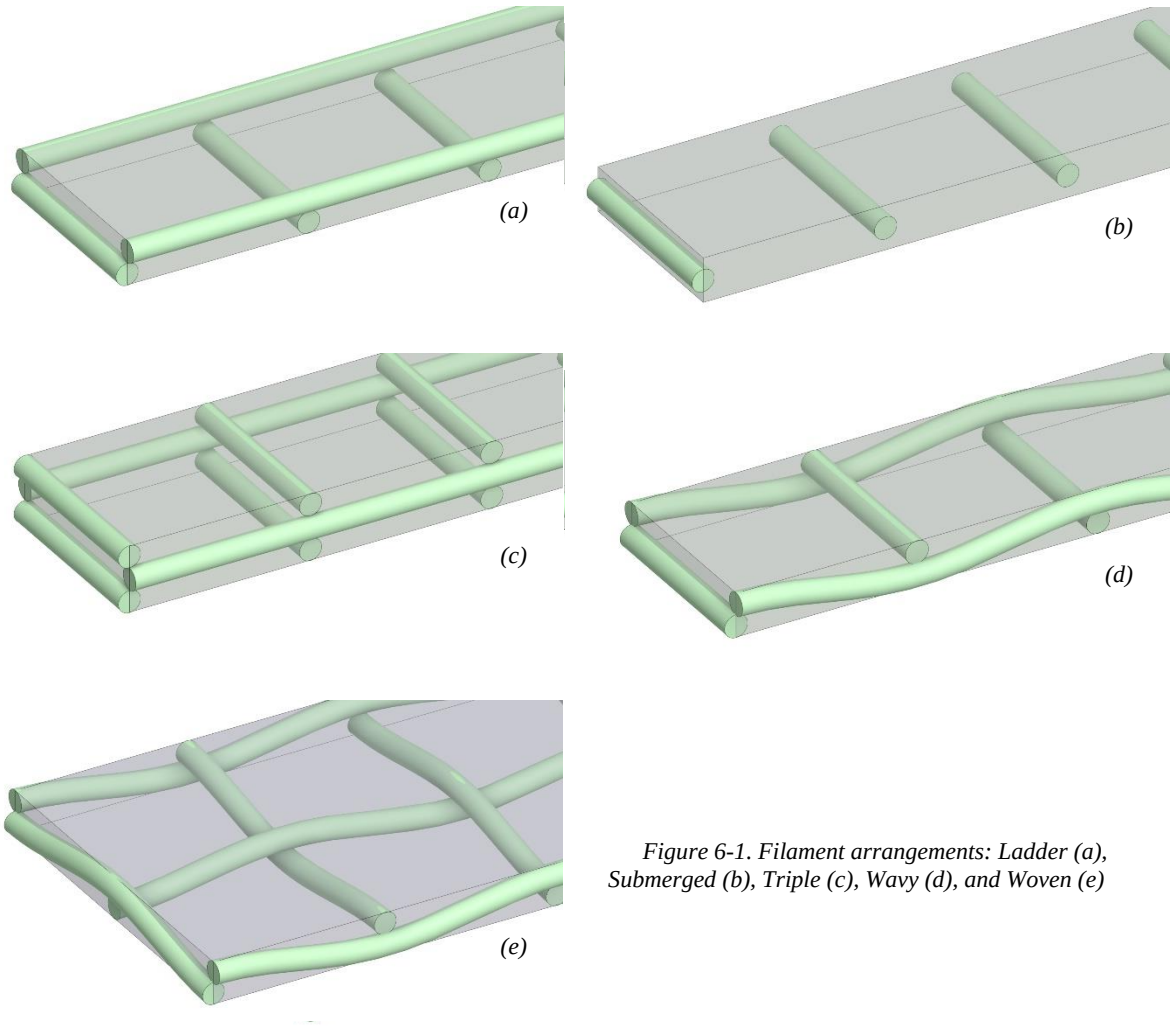

Figure 6-1. Filament arrangements: Ladder (a), Submerged (b), Triple (c), Wavy (d), and Woven (e)

6.2 Simulation approach

6.2.1 Geometries studied

The present work investigates four commercial feed spacers, termed PP45, PP60, PP90 and HDPE90, along with five simple geometries, namely Ladder, Triple, Wavy, Submerged, and Woven. All of these geometries, aside from Woven, were described in our previous works (6, 7).

The Woven arrangement is similar to Wavy in regard to the dimensions and the sinusoidal longitudinal filaments. Wavy's straight latitudinal filaments have been replaced by sinusoidal filaments in the Woven configuration and alternate longitudinal filaments have been flipped vertically to accommodate the new shape of the latitudinal filaments. Figure 6-1 shows the Wavy and Woven spacers with the other simple geometries.

Compared to our previous studies (6, 7), the current work also includes study of the effect of changing the spacer cell length and width for all five simple geometries (3.6 mm and 4.6

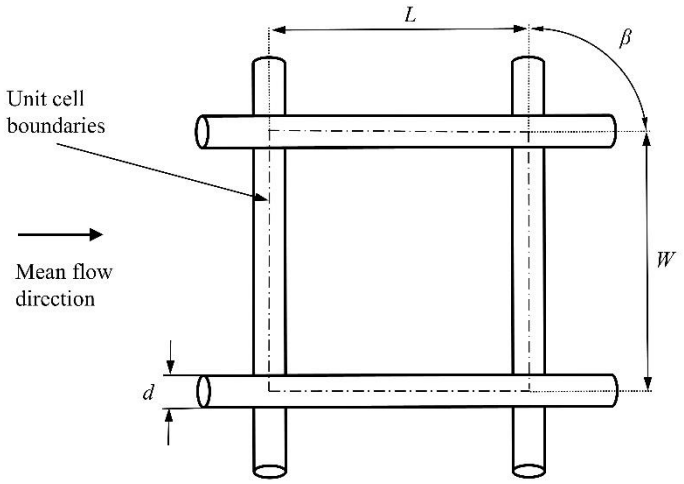

Figure 6-3. Definition of spacer geometrical parameters β, d, L, and W

mm spacings were investigated along with the original 4.1 mm spacing), as well as extending the flowrate range considered (Re values of 25 and 75 were included on top of the previous Re values of 50, 100, 150 and 200).

6.2.2 Parameters

Some geometrical characteristics, namely spacer geometry angle (β), filament diameter (d), cell length (L), cell height (H), and cell width (W), have been defined in Figure 6-3.

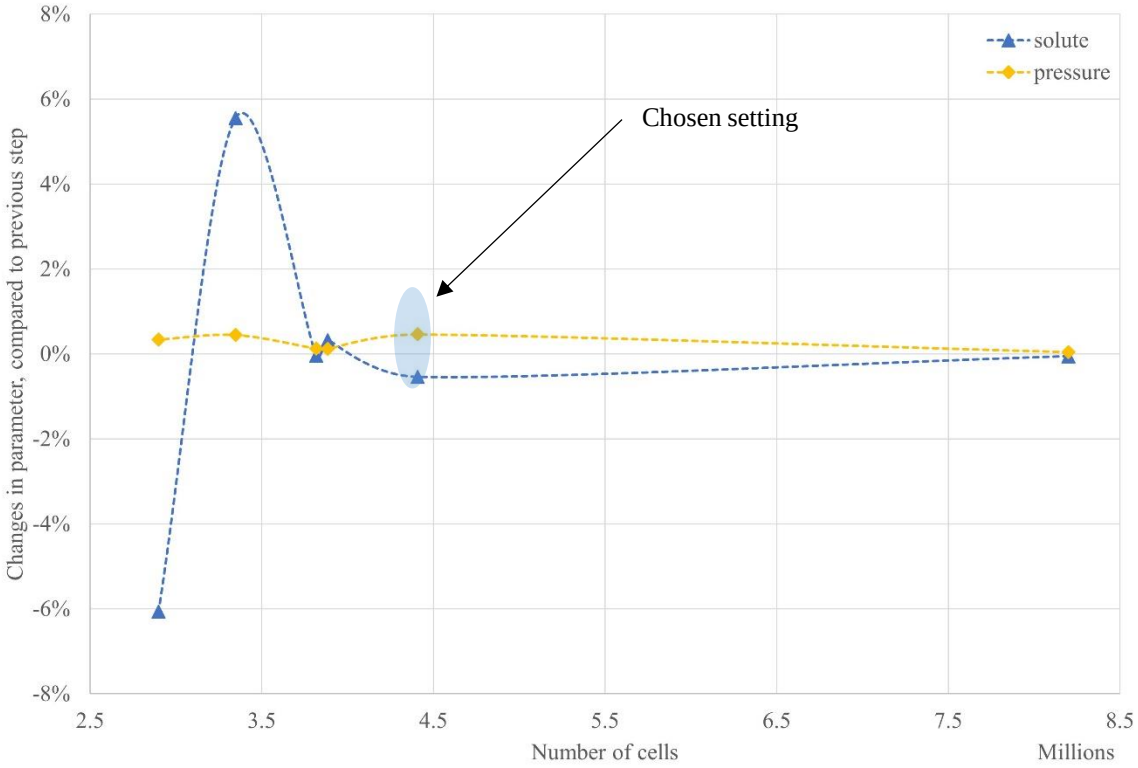

Figure 6-2. Mesh independence tests and results

Other parameters and the performance measures used in the present work have been defined earlier in Section 2.3. These are the parameters: hydraulic diameter (D_h); porosity (ε); effective area (A_{eff}); effective velocity (u_{eff}); pressure drop (ΔP); and hydraulic Reynolds number (Re) and the performance measures: pressure drop per length (dP); specific power consumption (SPC); power number (Pn); Sherwood number (Sh); and Spacer Configuration Efficacy (SCE). It should be noted that while L is the cell length, the variable L_{total} is the overall length of the domain that participates in heat/mass transfer; for the CFD results, L_{total} is the distance between the inlet and outlet.

6.2.3 Mesh generation

Because of instability issues with the ANSYS Fluent mesh engine V201 (also known as 2020R1), V195 (2019R3) was used for meshing the spacer geometries using the polygonal-hexahedral approach. To ensure the consistency of the generated meshes, a meshing script was used. Body of interest (BOI) zones around the filaments, and inflation layers around the filaments and the top/bottom membranes, were used to improve the model's ability to capture the fluid movement.

A mesh independence study confirmed the efficiency of the mesh size and its accuracy. Figure 6-2 demonstrates the changes in key simulation results compared to the number of cells, which is related to mesh size. The chosen setting shows about 0.5% deviation, gained from a 14% increase in cell number compared to the previous step. A further increase in cell number did not yield much further change in the results. Details of the meshing parameters used in the current work are reported in Table 6-2.

Table 6-2. Meshing parameters used in the present work

Parameter	General	BOI
Minimum size (mm)	0.01	
Maximum size (mm)	0.1	0.025
Growth rate	1.25	1.2
Curvature normal angle (°)	12	
Cells per gap	5	
Inflation layers	5	
First aspect ratio	20	
Inflation layer growth rate	1.4	
Last aspect ratio	5.2	

Different geometries led to meshes with 2–7M cells and 5–17M nodes. As an example, part of a mesh is shown in Figure 6-4.

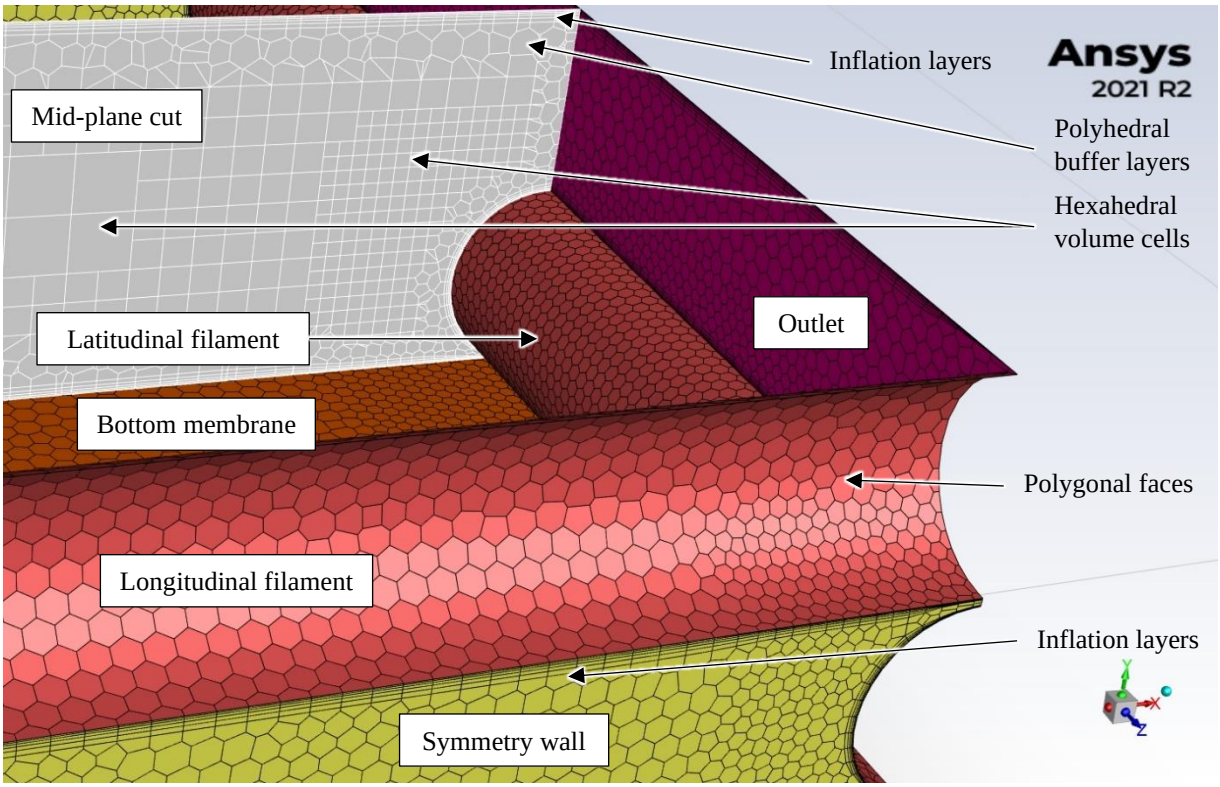

Figure 6-4. Typical meshing example for the Ladder spacer at the domain outlet

6.2.4 CFD model

The governing equations, boundary conditions, solver parameters and modelling assumptions have been described in Section 2.3.

To solve the model, ANSYS Fluent V201 was run on eight parallel Magnus nodes at the Pawsey Supercomputing Centre, each equipped with two Intel Xeon E5-2690 v3 (Haswell) 12-core CPUs and 64 GB DDR4 memory, with Cray's Aries interconnect for inter-node communications and a Cray Sonexion 1600 Lustre filesystem connected through InfiniBand for storage. Overall, each case ran on 192 physical cores, with hyperthreading disabled.

6.2.5 Validation

The model has been adequately validated using the available CFD and experimental results. The validation process and accuracy of the results, including the comparison of shear stress on top and bottom membranes, *dP*, Pn, Sh and SCE, have been discussed in Section 3.4.5

6.2.6 Parametric matrix

The present work considers five simple filament configurations, with three different gap sizes between the filaments. The filament diameter remains the same in all arrangements. The change in the gap size is applied to both longitudinal and latitudinal filaments; hence, all the

arrangements have a square-shaped cell with *L*=*W* (Figure 2). The four commercial spacers of fixed geometry plus the five simple geometries with three gap sizes leads to the nineteen arrangements that are considered in the present work. In terms of flowrate variations, six Re values for each arrangement have been simulated, leading to 114 cases in total (Table 3). Results, including salt concentrations and pressure drop, have been extracted from the CFD simulations and prepared for post-processing. Pressure drop is defined as the difference in the area-weighted average static pressure at the inlet and outlet, while the change in the salt concentration was calculated by the difference in the mass-weighted average of the salt concentrations at the inlet and outlet.

Table 6-3. Parameters considered, including their ranges, in the current CFD study

Parameter	Values and comment
Filament configurations	PP45, PP60, PP90, and HDPE90 (commercial spacers) Submerged, Ladder, Triple, Wavy, and Woven (non-commercial spacers)
Filament gap, *L*=*W* (mm)	3.6, 4.1, and 4.6, applied to non-commercial spacers only. The arrangement names used throughout the paper combine the filament configuration and the gap size; e.g., Ladder36 is the Ladder configuration with a gap of *L*=*W*=3.6 mm.
Hydraulic Reynolds number, Re	25, 50, 75, 100, 150, and 200

6.2.7 Post-processing of CFD results

In the present work, five performance measures, namely the pressure drop per unit length, power number, specific power consumption, Sherwood number, and spacer configuration efficacy, were post-processed using MATLAB version 9.9.0.1592791 (R2020b) Update 5. The post-processing occurred in two steps.

In the first step, prospects for possible correlations between the performance measures (dependent variables) and Re (independent variable) were investigated. For the mass transfer performance measures, additional parameters *dP*, Pn, and SPC were added to the list of independent variables. The equations were generated by using the MATLAB *'fit'* function with the fitting type being limited to power-law ($y = ax^b$) and exponential ($y = ae^{bx}$) forms. For the power-law equation, the 'non-linear least square' method and 'Levenberg-Marquardt' algorithm were employed with tolerances of 10^{-10}, maximum change in coefficients was set to 10^{-3}, and the maximum number of iterations was set to 10^3. For the exponential equation, to avoid not-a-number (NaN) values, it was necessary to define a limit for the exponent. As the 'Levenberg-Marquardt' algorithm does not accept limits, the 'non-linear least square' method and 'Trust-Region' algorithm were used for the exponential equation, with the software's

default fit options. To assure repeatability of the fit results, the default random initial values for *a* and *b* were replaced with a starting point of (0,0) for all fits.

In the second step of post-processing, in an attempt to generalise the results, the possible correlation of the parameters *a* and *b* from the first step with various geometrical characteristics of the spacers, such as the porosity, was investigated. The same methods were employed for obtaining the fitting parameters that were used for the first stage.

In addition to the numerical post-processing, the CFD results, including concentration contour plots and velocity vector plots, were examined qualitatively to explore how the non-commercial spacer geometries affect the micro-scale fluid flow behaviour and, if possible, the correlations found in the first step of post-processing.

6.3 Results and Discussion

The results from the CFD simulations covering the 114 cases described in Table 6-3 makes it possible to investigate the effect of Reynolds number, gap size, porosity, and D_h/L_{total} on different performance measures. Among the two equation types investigated, power-law equations showed notably better fitting quality for all the performance measures covered in the present study.

Table 6-4 summarises the equations for predicting the various performance measures for the different spacer arrangements as described in Section 6.2.7. For each equation, the lowest R^2 value among all the geometries was calculated and used as the measure of the quality of fit. For all performance measures and equations shown in Table 6-4 except Sh, the minimum R^2 values are above 0.9991. For Sh, the minimum R^2 values are at least 0.9918 when Re, Pn and SPC are the independent parameters, and 0.9894 when *dP* is the independent parameter.

6.3.1 Effect of Reynolds number

As expected, and as reported extensively in the literature, increasing Re will increase both pressure drop and Sh, but at different rates.

For each set of equations, the exponent *b* varies over a small range and coefficient *a* is almost within the same order of magnitude. It is also notable that among the cases studied, the power measures (*dP*, Pn and SPC) increase remarkably quicker with Re than Sh does. Approximately, the exponents *b* for all of *dP*-Re equations are 0.9–1.4 times larger than the *b* values in the matching Sh-Re equation. This trend is reflected in the other forms as well; e.g., the exponent for the Sh-*dP* equations is smaller than one and is negative for all the SCE equations.

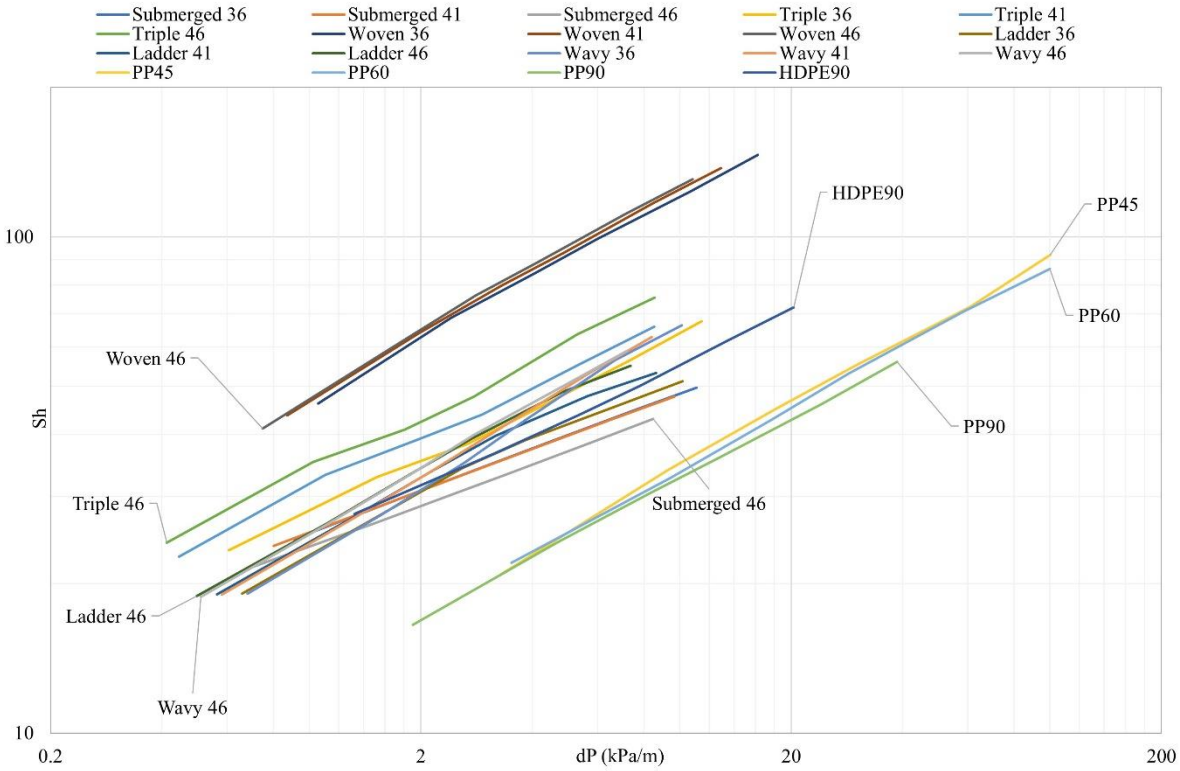

Figure 6-5. Predicted Sh vs. dP for different configurations and Re (Re increases from left to right along each line)

In Figure 6-5, the ordinate shows the Sherwood number, and the abscissa shows the pressure drop per unit length. Better mass transfer means enhanced mixing and lower concentration on the membrane's feed side, which would increase the driving force for permeate to flow through it, while a lower pressure drop means less power consumption and thus less ongoing energy costs.

By combining mass transfer and energy consumption in Figure 6-5, the trade-off between energy costs and production rate is highlighted. The figure can be interpreted as follows: the closer a datapoint is to the top-left corner of the graph, the better is the combination of *low energy demand* and *high production rate* in terms of operational performance. In addition, the performance of an arrangement with a higher slope in this figure would have relatively higher increases in mass transfer performance with flowrate for the same increase in pressure drop or energy costs, compared to the arrangements with a lower slope. It should be noted that the slopes of all lines in Figure 6-5 are less than one, which highlights that the mass transfer benefit from a higher flowrate will always be less than the increase in energy consumption, in all of the studied spacer arrangements.

Based on the results in Figure 6-5, the Woven configuration shows the best combination of mass transfer and energy consumption, which can also be concluded by comparing the coefficients and exponents of the Sh-*dP* equations reported in Table 6-4.

Table 6-4. Power-law correlations for selected performance measures and spacers derived from CFD simulations

Arrangement	dP (Pa/m)	Pn	SPC	Sh				SCE			
PP45	$10.4\ Re^{1.730}$	$20.5\ Re^{2.729}$	$9.28E{-}3\ Re^{2.729}$	$2.01\ Re^{0.719}$	$0.702\ dP^{0.423}$	$0.868\ Pn^{0.266}$	$6.74\ SPC^{0.266}$	$0.0568\ Re^{-1.885}$	$1.96\ dP^{-1.188}$	$0.808\ Pn^{-0.729}$	$2.96E{-}3\ SPC^{-0.729}$
PP60	$8.01\ Re^{1.779}$	$10.9\ Re^{2.828}$	$4.96E{-}3\ Re^{2.828}$	$2.26\ Re^{0.687}$	$0.805\ dP^{0.407}$	$1.02\ Pn^{0.255}$	$7.30\ SPC^{0.255}$	$0.0642\ Re^{-1.898}$	$3.81\ dP^{-1.249}$	$1.15\ Pn^{-0.753}$	$3.49E{-}3\ SPC^{-0.753}$
PP90	$9.51\ Re^{1.567}$	$107\ Re^{2.603}$	$8.21E{-}3\ Re^{2.603}$	$2.30\ Re^{0.600}$	$0.821\ dP^{0.400}$	$0.664\ Pn^{0.240}$	$6.44\ SPC^{0.240}$	$8.86E{-}3\ Re^{-1.813}$	$0.534\ dP^{-1.316}$	$0.689\ Pn^{-0.762}$	$5.04E{-}4\ SPC^{-0.762}$
HDPE90	$14.7\ Re^{1.364}$	$11.3\ Re^{2.390}$	$0.0114\ Re^{2.390}$	$5.63\ Re^{0.479}$	$2.01\ dP^{0.360}$	$3.21\ Pn^{0.206}$	$13.3\ SPC^{0.206}$	$0.368\ Re^{-1.852}$	$29.9\ dP^{-1.442}$	$3.93\ Pn^{-0.810}$	$0.0146\ SPC^{-0.810}$
Submerged36	$11.5\ Re^{1.297}$	$6.02\ Re^{2.336}$	$6.04E{-}3\ Re^{2.336}$	$7.96\ Re^{0.344}$	$3.68\ dP^{0.280}$	$5.56\ Pn^{0.154}$	$16.1\ SPC^{0.154}$	$0.590\ Re^{-1.820}$	$86.6\ dP^{-1.593}$	$5.78\ Pn^{-0.849}$	$0.0165\ SPC^{-0.849}$
Submerged41	$10.4\ Re^{1.289}$	$5.27\ Re^{2.329}$	$5.29E{-}3\ Re^{2.329}$	$7.82\ Re^{0.340}$	$3.74\ dP^{0.277}$	$5.59\ Pn^{0.153}$	$16.1\ SPC^{0.153}$	$0.670\ Re^{-1.820}$	$84.2\ dP^{-1.600}$	$5.86\ Pn^{-0.851}$	$0.0164\ SPC^{-0.851}$
Submerged46	$9.52\ Re^{1.280}$	$4.74\ Re^{2.320}$	$4.76E{-}3\ Re^{2.320}$	$7.11\ Re^{0.337}$	$3.49\ dP^{0.277}$	$5.18\ Pn^{0.152}$	$14.8\ SPC^{0.152}$	$0.715\ Re^{-1.826}$	$77.5\ dP^{-1.610}$	$5.64\ Pn^{-0.855}$	$0.0154\ SPC^{-0.855}$
Triple36	$4.12\ Re^{1.495}$	$10.0\ Re^{2.539}$	$1.98E{-}3\ Re^{2.539}$	$4.05\ Re^{0.527}$	$2.17\ dP^{0.367}$	$2.20\ Pn^{0.216}$	$13.9\ SPC^{0.216}$	$0.221\ Re^{-1.887}$	$3.51\ dP^{-1.380}$	$2.65\ Pn^{-0.797}$	$2.96E{-}3\ SPC^{-0.797}$
Triple41	$2.68\ Re^{1.521}$	$5.85\ Re^{2.568}$	$1.16E{-}3\ Re^{2.568}$	$4.30\ Re^{0.512}$	$2.70\ dP^{0.352}$	$2.63\ Pn^{0.209}$	$15.6\ SPC^{0.209}$	$0.294\ Re^{-1.860}$	$2.99\ dP^{-1.363}$	$2.50\ Pn^{-0.787}$	$3.06E{-}3\ SPC^{-0.787}$
Triple46	$1.87\ Re^{1.590}$	$4.17\ Re^{2.628}$	$8.26E{-}4\ Re^{2.628}$	$3.59\ Re^{0.572}$	$2.45\ dP^{0.378}$	$2.27\ Pn^{0.228}$	$15.8\ SPC^{0.228}$	$0.353\ Re^{-1.867}$	$2.91\ dP^{-1.349}$	$2.62\ Pn^{-0.783}$	$3.31E{-}3\ SPC^{-0.783}$
Ladder36	$6.54\ Re^{1.387}$	$4.66\ Re^{2.399}$	$4.68E{-}3\ Re^{2.399}$	$4.66\ Re^{0.455}$	$2.33\ dP^{0.337}$	$3.30\ Pn^{0.194}$	$12.6\ SPC^{0.194}$	$0.449\ Re^{-1.765}$	$12.7\ dP^{-1.391}$	$2.35\ Pn^{-0.778}$	$0.0109\ SPC^{-0.778}$
Ladder41	$4.93\ Re^{1.409}$	$3.02\ Re^{2.441}$	$3.03E{-}3\ Re^{2.441}$	$4.08\ Re^{0.488}$	$2.09\ dP^{0.360}$	$2.97\ Pn^{0.207}$	$12.4\ SPC^{0.207}$	$0.507\ Re^{-1.740}$	$12.3\ dP^{-1.389}$	$2.32\ Pn^{-0.772}$	$0.0113\ SPC^{-0.772}$
Ladder46	$4.55\ Re^{1.393}$	$2.62\ Re^{2.431}$	$2.63E{-}3\ Re^{2.431}$	$3.53\ Re^{0.521}$	$1.77\ dP^{0.389}$	$2.57\ Pn^{0.223}$	$11.9\ SPC^{0.223}$	$0.559\ Re^{-1.722}$	$12.4\ dP^{-1.393}$	$2.35\ Pn^{-0.770}$	$0.0115\ SPC^{-0.770}$
Wavy36	$6.84\ Re^{1.377}$	$4.51\ Re^{2.408}$	$4.53E{-}3\ Re^{2.408}$	$2.39\ Re^{0.628}$	$0.889\ dP^{0.469}$	$1.45\ Pn^{0.268}$	$9.27\ SPC^{0.268}$	$0.320\ Re^{-1.677}$	$9.22\ dP^{-1.343}$	$1.71\ Pn^{-0.746}$	$9.92E{-}3\ SPC^{-0.746}$
Wavy41	$6.24\ Re^{1.359}$	$4.01\ Re^{2.386}$	$4.02E{-}3\ Re^{2.386}$	$2.63\ Re^{0.598}$	$1.06\ dP^{0.452}$	$1.70\ Pn^{0.257}$	$10.0\ SPC^{0.257}$	$0.407\ Re^{-1.688}$	$10.5\ dP^{-1.365}$	$1.95\ Pn^{-0.755}$	$0.0106\ SPC^{-0.755}$
Wavy46	$5.66\ Re^{1.349}$	$3.51\ Re^{2.375}$	$3.52E{-}3\ Re^{2.375}$	$3.00\ Re^{0.562}$	$1.31\ dP^{0.429}$	$2.04\ Pn^{0.243}$	$10.9\ SPC^{0.243}$	$0.485\ Re^{-1.693}$	$11.4\ dP^{-1.381}$	$2.12\ Pn^{-0.760}$	$0.0111\ SPC^{-0.760}$
Woven36	$9.18\ Re^{1.411}$	$6.11\ Re^{2.444}$	$6.13E{-}3\ Re^{2.444}$	$7.86\ Re^{0.551}$	$2.88\ dP^{0.405}$	$4.65\ Pn^{0.234}$	$23.3\ SPC^{0.234}$	$0.526\ Re^{-1.699}$	$27.4\ dP^{-1.354}$	$3.97\ Pn^{-0.753}$	$0.0219\ SPC^{-0.753}$
Woven41	$8.27\ Re^{1.387}$	$5.22\ Re^{2.421}$	$5.23E{-}3\ Re^{2.421}$	$7.31\ Re^{0.554}$	$2.76\ dP^{0.414}$	$4.47\ Pn^{0.237}$	$22.9\ SPC^{0.237}$	$0.622\ Re^{-1.692}$	$27.6\ dP^{-1.365}$	$4.08\ Pn^{-0.755}$	$0.0222\ SPC^{-0.755}$
Woven46	$7.54\ Re^{1.371}$	$4.58\ Re^{2.404}$	$4.60E{-}3\ Re^{2.404}$	$6.86\ Re^{0.556}$	$2.67\ dP^{0.420}$	$4.33\ Pn^{0.239}$	$22.6\ SPC^{0.239}$	$0.672\ Re^{-1.675}$	$24.9\ dP^{-1.361}$	$3.85\ Pn^{-0.751}$	$0.0216\ SPC^{-0.751}$
Min R^2	0.9991	0.9999	0.9999	0.9919	0.9894	0.9918	0.9918	0.9995	0.9997	0.9998	0.9998

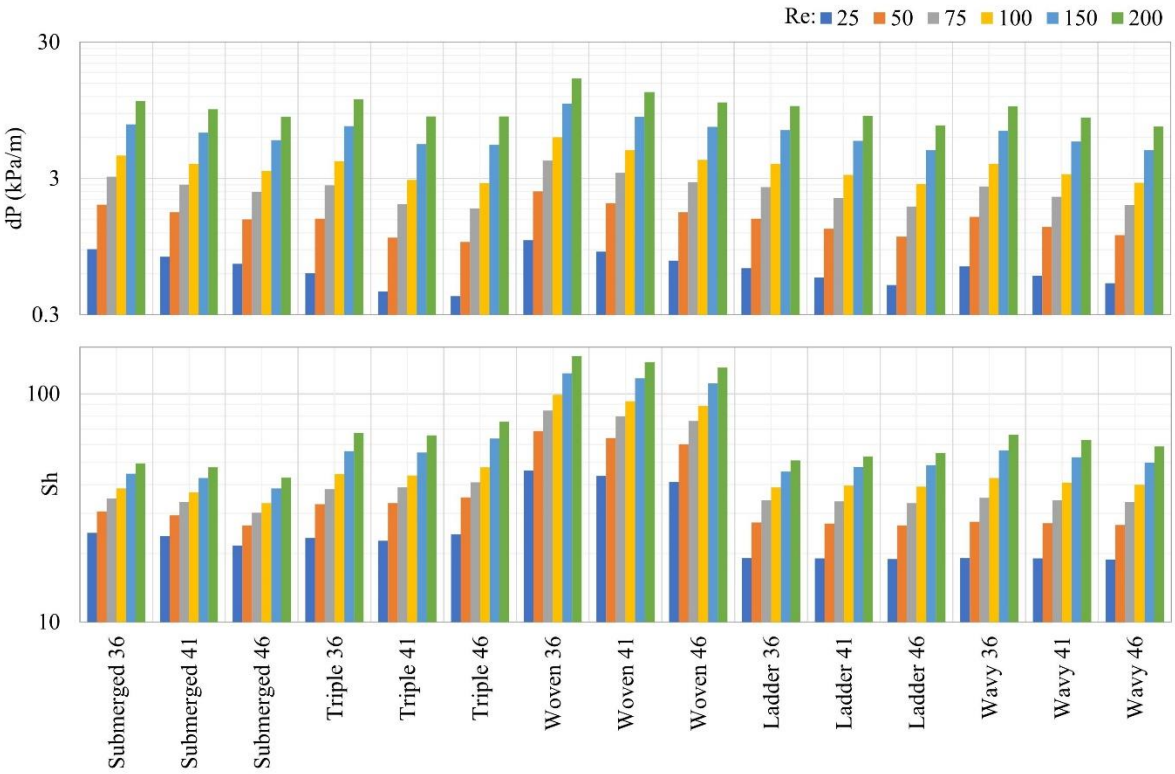

Figure 6-6. Predicted dP (top) -lower is better- and Sh (bottom) -higher is better- for different configurations and Re

6.3.2 Effect of the gap between filaments for non-commercial spacers

As expected, increasing the gap between the filaments affects the power-related performance measures and reduces energy consumption, but it is not consistent for all cases. The top part of Figure 6-6 shows that while for Wavy, Woven, and Ladder and Submerged, *dP* reduces consistently with increasing gap size, for Triple, the response to changes in the gap is different. The variations observed between gaps of 3.6 mm and 4.1 mm are larger compared to changing the gap from 4.1 mm to 4.6 mm.

The consistency and proportionality of the spacers' response of Sh and pressure drop per unit length to changing the gap size and Re can be seen in Figure 6-6. Similar patterns can be observed for Pn and SPC as for *dP*, because Pn and SPC are directly related to *dP*.

In contrast to the power measures, the mass transfer measures show a less consistent response to gap changes, which depends on both filament configuration and flowrate. For example, in Figure 6-6 (bottom), the Ladder spacer shows a minor reduction in Sh as the gap increases in the low Re range, while in the high Re range, Sh increases slightly with increasing gap size. However, for Wavy, Sh steadily decreases with increasing gap size, and this decrease is larger for higher flowrates. For Triple, the response to the gap changing from 3.6 mm to 4.1 mm is a small decrease, while increasing the gap to 4.6 mm gives higher Sh values compared

to other two gaps, and the increase is larger for high Re. The Submerged response to increasing the gap size is similar to the Ladder configuration: a reduction for low Re, which switches to an increase for high Re. Lastly, the Woven spacer demonstrates a consistent decrease in Sh over the entire Re range when increasing the gap between the spacer filaments.

The mass transfer performance data can be visualised in a different way to bring out the response of the Sherwood number to changing the gap size through the range of flowrates studied. Figure 6-7 plots the ratio of (Sh for spacers with gaps of 3.6 and 4.6 mm) to (Sh for the same spacer with a gap of 4.1 mm) as evaluated at the same Reynolds number, for the five spacer configurations and six flowrates. That is, the responses of the spacers with small and large gaps are normalised with respect to their performance for the middle-sized gap. The left side of Figure 6-7 compares the Sh changes for 3.6 mm gaps compared to 4.1 mm gaps, while the right side shows the changes for 4.6 mm gaps compared to 4.1 mm gaps. Each dataset of six bars represents the effect of the flowrate for that arrangement. The horizontal dividing line at 100% represents Sh for a gap of 4.1 mm.

Table 6-5 presents a summary of the observations arising from Figure 6-7.

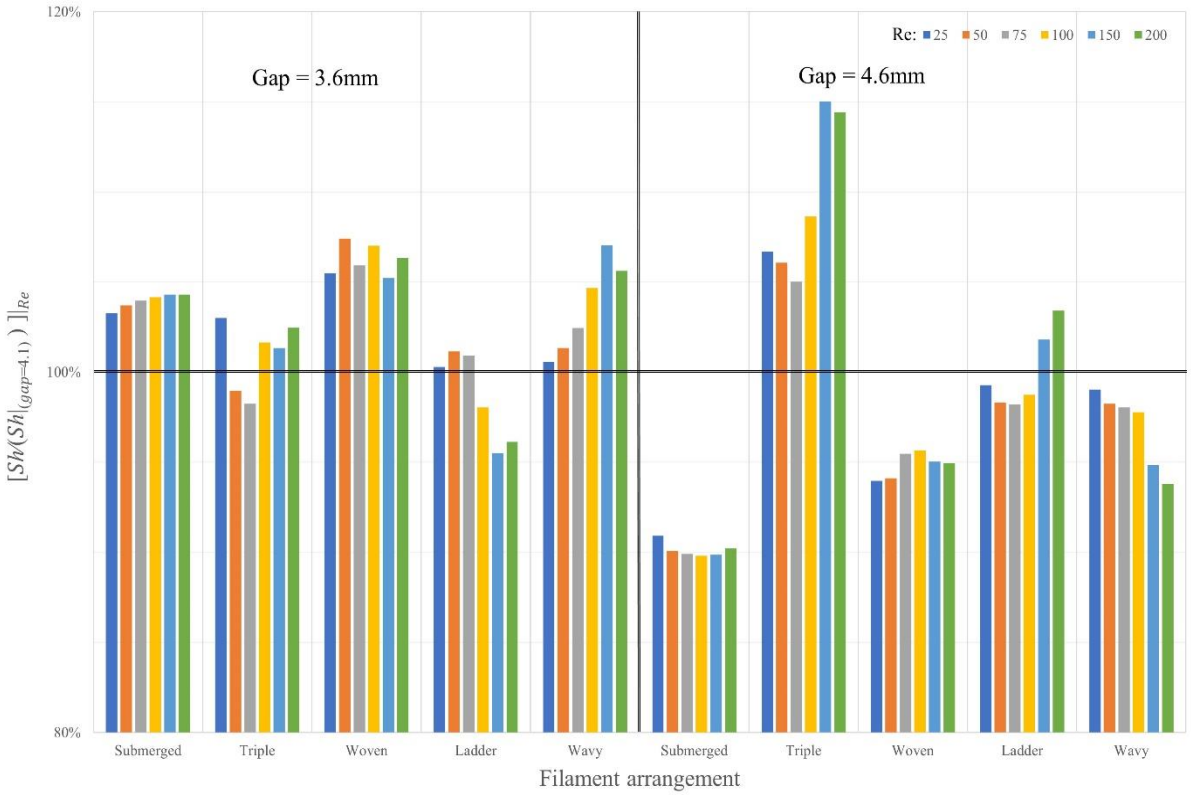

Figure 6-7. Ratio of predicted Sh at the specified gap, to Sh with a gap of 4.1 mm at the same Re, for different configurations and Re

Table 6-5. Response of Sh to changes in the gap size and Re

Configuration change	Gap reduced from 4.1 to 3.6 mm	Gap increased from 4.1 to 4.6 mm
Submerged	Approx. 4% gain in average Sh for smaller gap Slight Sh gain with increasing Re	Approx. 10% reduction in average Sh for larger gap Slight Sh gain at low and high Re
Triple	Negligible change in average Sh for smaller gap Effect of Re is inconsistent	Approx. 10% gain in average Sh for larger gap Generally ~5% gain at low Re and ~15% gain at high Re
Woven	Approx. 6% gain in average Sh for smaller gap Effect of Re is inconsistent	Approx. 5% reduction in average Sh for larger gap Slight Sh gain for mid-range Re
Ladder	Negligible change in Sh for smaller gap at low Re Approx. 3% reduction in Sh for smaller gap at high Re	Approx. 2% reduction in Sh for larger gap at low Re Approx. 2% gain in Sh for larger gap at high Re
Wavy	Gain in Sh for smaller gap varies from approx. 0% at low Re to approx. 5% at high Re	Reduction in Sh for larger gap varies from approx. 1% at low Re to approx. 6% at high Re

6.3.3 Effect of porosity on performance measures

In the current work, an attempt was made to investigate the correlation between the performance measures and porosity. The reason for attempting this correlation was to check whether it is possible to generalise the results in Table 6-4, to avoid using different coefficient *a* and exponent *b* values for each spacer and gap. However, for both the power and mass transfer performance measures, no adequate general correlation with porosity could be found. However, for each spacer configuration separately, some correlation with porosity is evident. The trend can be increasing, decreasing, or having an extremum in the middle, depending on the spacer. As examples, Figure 6-8 presents how *dP* and Sh vary with porosity for a common value of Re.

In the second stage of post-processing, correlations between the power-law equation coefficient *a* and exponent *b* values from Table 6-4 and the spacer's geometrical parameters have been investigated in four possible formats, namely linear, exponential, logarithmic and power-law equations. Table 6-6 summarises the correlation coefficients (r) of the relationship between the equation coefficients *a* and exponents *b* and the porosity or D_h/L as geometrical parameters. Correlation coefficients stronger than 0.8 are highlighted.

Table 6-6. Pearson correlation coefficients (r) for equation parameters and spacer characteristics, with correlations stronger than 0.8 highlighted.

Equation coefficient a									
Equation variables		Porosity correlations for a				D_h/L_{total} correlations for a			
Dependent	Independent	$a'\varepsilon + b'$	$a'e^{b'\varepsilon}$	$a'\log(\varepsilon) + b'$	$a'\varepsilon^{b'}$	$a' D_h/L + b'$	$a'e^{b'(D_h/L)}$	$a'\log(D_h/L) + b'$	$a'(D_h/L)^{b'}$
dP	Re	−0.191*	−0.207	−0.201	−0.218	0.073	−0.105	0.034	−0.130
Pn	Re	−0.781	−0.865	−0.810	−0.878	0.146	0.157	0.134	0.104
SPC	Re	−0.439	−0.350	−0.442	−0.357	0.004	−0.188	−0.050	−0.216
Sh	Re	0.584	0.658	0.566	0.642	0.279	0.352	0.310	0.385
Sh	dP	0.677	0.747	0.657	0.731	0.405	0.448	0.441	0.487
Sh	Pn	0.689	0.840	0.669	0.829	0.235	0.278	0.276	0.322
Sh	SPC	0.613	0.746	0.608	0.741	0.168	0.267	0.207	0.309
SCE	Re	0.852	0.973	0.834	0.977	0.014	0.074	0.081	0.123
SCE	dP	0.482	0.758	0.454	0.748	0.217	0.072	0.240	0.109
SCE	Pn	0.684	0.852	0.662	0.840	0.349	0.374	0.378	0.410
SCE	SPC	0.618	0.790	0.608	0.795	−0.087	−0.132	−0.040	−0.091
Equation exponent b									
Equation variables		Porosity correlations for b				D_h/L correlations for b			
Dependent	Independent	$a'\varepsilon + b'$	$a'e^{b'\varepsilon}$	$a'\log(\varepsilon) + b'$	$a\varepsilon^{b'}$	$a' D_h/L + b'$	$a'e^{b'(D_h/L)}$	$a'\log(D_h/L) + b'$	$a'(D_h/L)^{b'}$
dP	Re	−0.783*	−0.780	−0.758	−0.755	−0.307	−0.289	−0.373	−0.354
Pn	Re	−0.769	−0.768	−0.745	−0.744	−0.277	−0.267	−0.341	−0.330
SPC	Re	−0.769	−0.768	−0.745	−0.744	−0.277	−0.267	−0.341	−0.330
Sh	Re	−0.636	−0.593	−0.607	−0.563	−0.513	−0.464	−0.552	−0.498
Sh	dP	−0.333	−0.350	−0.310	−0.327	−0.471	−0.453	−0.475	−0.460
Sh	Pn	−0.487	−0.476	−0.461	−0.449	−0.497	−0.463	−0.518	−0.484
Sh	SPC	−0.487	−0.476	−0.461	−0.449	−0.497	−0.463	−0.518	−0.484
SCE	Re	−0.393	−0.390	−0.385	−0.383	0.329	0.335	0.252	0.258
SCE	dP	0.645	0.666	0.613	0.634	0.467	0.487	0.508	0.530
SCE	Pn	0.455	0.458	0.428	0.432	0.591	0.603	0.600	0.612
SCE	SPC	0.455	0.458	0.428	0.432	0.591	0.603	0.600	0.612

* To clarify: for these marked entries, the equation $dP = a\mathrm{Re}^b$ is explored; the linear correlation of coefficient $a = a'\varepsilon + b'$ has $r = -0.191$ while the linear correlation of exponent $b = a'\varepsilon + b'$ has r = –0.783.

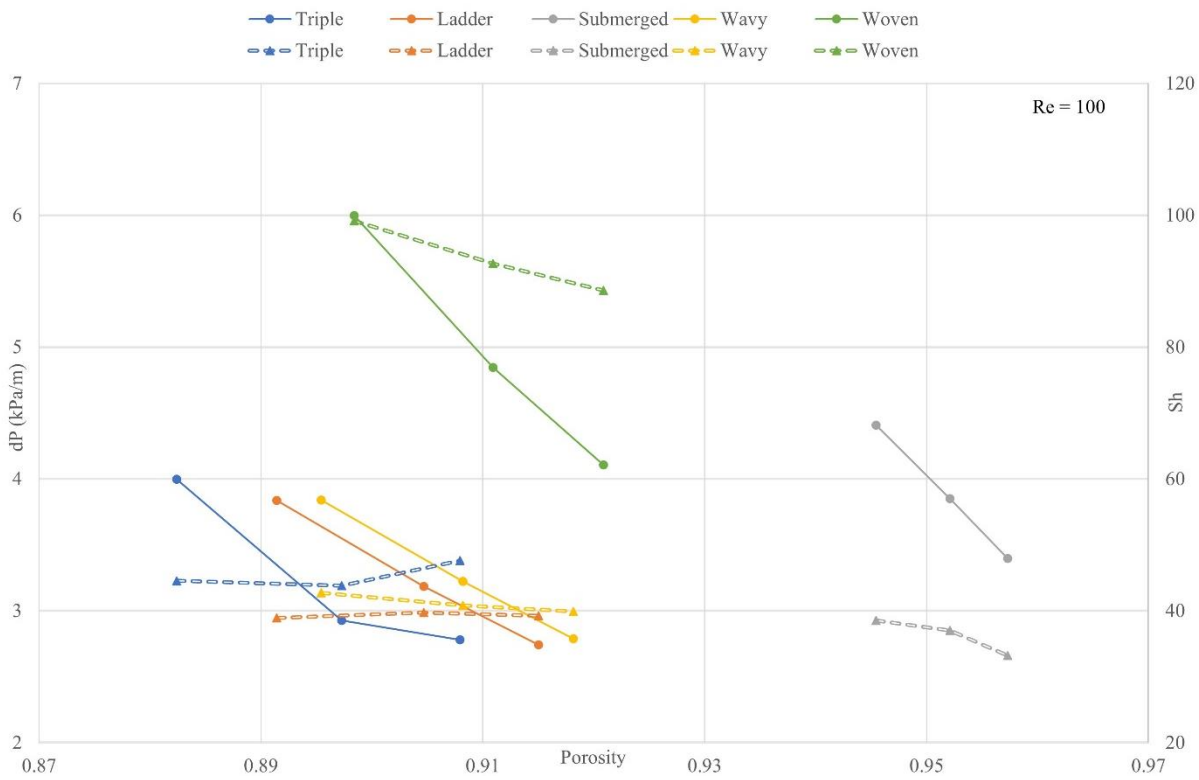

Figure 6-8. Predicted dP -lower is better- (solid lines, left side axis) and Sh -higher is better- (dashed lines, right side axis) vs. porosity for Re = 100

Table 6-6 shows that the strongest correlation (r = 0.977) is observed between coefficient a and porosity in a power-law correlation for the SCE-Re equation (SCE = $a\mathrm{Re}^b$). This case is

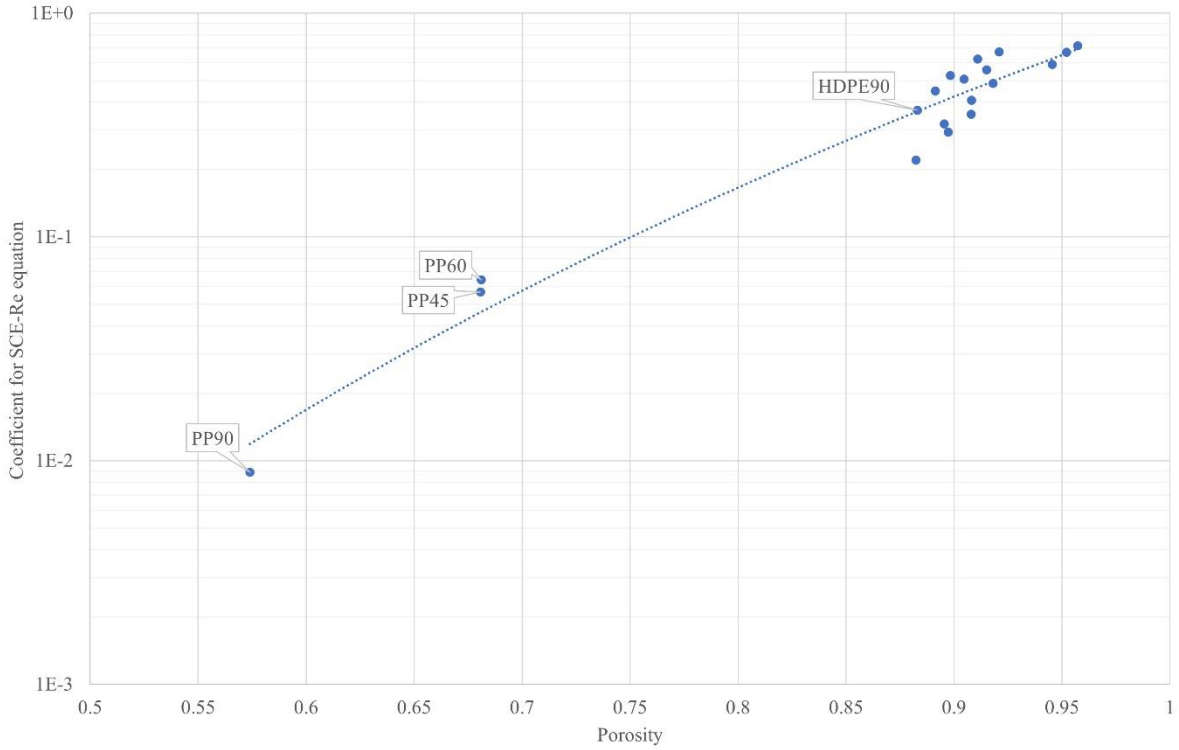

Figure 6-9. SCE-Re equation coefficient (a) vs. porosity with a power-law trendline

taken as an example for detailed discussion.

Figure 6-9 presents the coefficient *a* value for the SCE-Re equation as a function of porosity. The coefficient of determination (R^2) of this relationship is 0.83 for the power-law correlation (trend line) indicated. By replacing the calculated coefficients with the trend line indicated, and leaving the exponent as before, the original equation of $\mathrm{SCE} = a\mathrm{Re}^b$ is transformed into $\mathrm{SCE} = (a'\varepsilon^c)\mathrm{Re}^b$. This approach passes on the inaccuracy of the a-ε correlation to the calculated SCE and reduces the RMS and minimum R^2 values, from 0.99989 and 0.99970 to 0.85 and 0.61, respectively, which is a much poorer fit. Alternatively, refitting the datapoints in a one-step fit ($\mathrm{SCE} = a''\mathrm{Re}^{b''}\varepsilon^{c''}$), instead of two-step fitting as previously explained would result in the quality of fit (RMS and minimum values of R^2) being the same as for $\mathrm{SCE} = a\mathrm{Re}^b$. But a detailed inspection of the equation parameters led to another conclusion. Table 6-7 presents the calculated value for c″ that varies between −1E−5 and −0.01, resulting in $\varepsilon^{c''}$ being between 1 and 1.0012. In other words, from the details in Table 6-7 and Figure 6-9, it seems that using the $SCE = a''\,Re^{b''}\varepsilon^{c''}$ equation format would provide an extra numeric adjustment point to the MATLAB fitting engine, rather than reflecting an actual correlation between SCE and porosity.

Table 6-7. Predicted porosity exponent (c"), in equation that defines SCE as a function of Re and porosity.

Configuration	L = 3.6 mm	L = 4.1 mm	L = 4.6 mm
Submerged	−7.36E−03	−8.51E−03	−8.88E−03
Triple	−2.46E−03	−3.34E−03	−4.23E−03
Woven	−1.06E−02	−1.34E−02	−1.42E−02
Ladder	−7.84E−03	−9.18E−03	−1.08E−02
Wavy	−4.84E−03	−6.83E−03	−8.26E−03
PP45		−4.20E−04	
PP60		−6.23E−04	
PP90		−1.44E−05	
HDPE90		−7.67E−03	

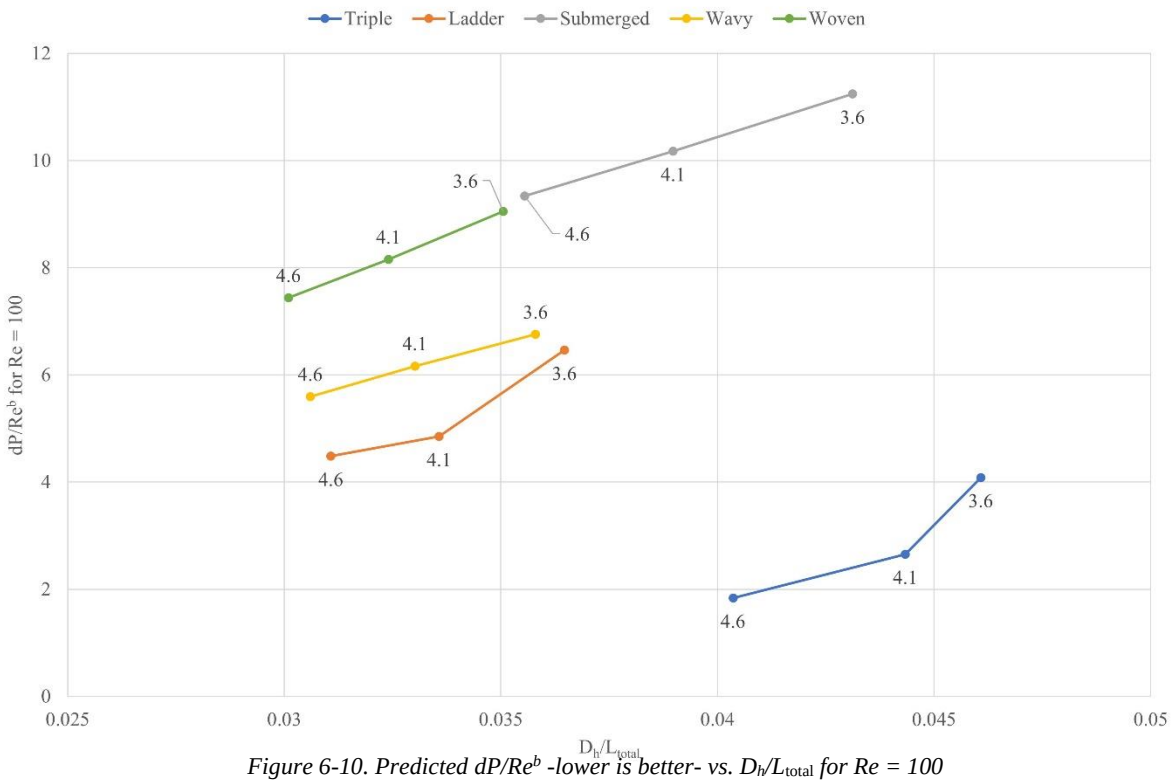

Figure 6-10. Predicted dP/Re^b -lower is better- vs. D_h/L_{total} for Re = 100

6.3.4 Effect of D_h/L_{total} on performance measures

Figure 6-10 provides some insight into the connection between power measures and D_h/L_{total}.

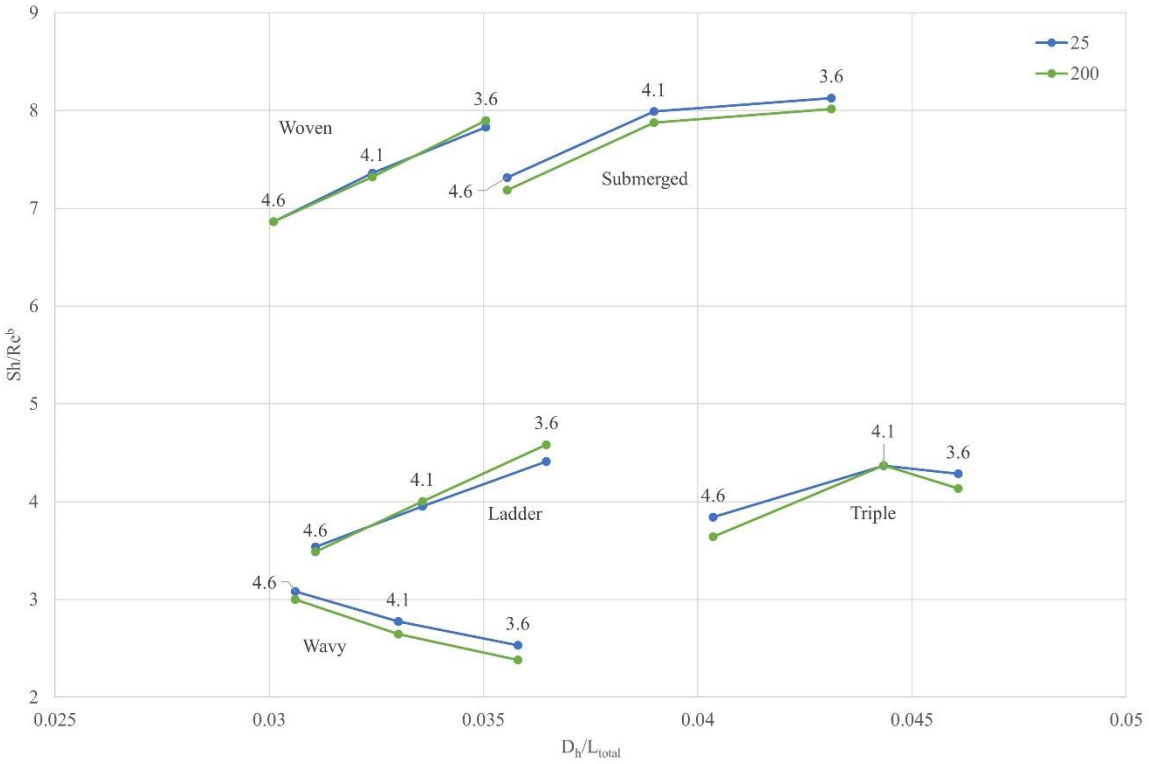

Figure 6-11. Predicted Sh/Reb -higher is better- vs. Dh/Ltotal for Re = 25 and 200

Despite that some similarity can be observed in the trend and slope of the line for each spacer configuration, the datapoints are scattered and no general connection can be seen between dP/Re^b and D_h/L_{total}. Similar behaviour is observed for Pn and SPC.

Considering mass transfer, Figure 6-11 visualises $\mathrm{Sh}/\mathrm{Re}^b$ as a function of D_h/L_{total}, where b for each arrangement can be found in Table 6-4. Similar to the power measures, this study found no general correlation between mass transfer and D_h/L_{total}.

The authors noted a curious feature in the data: using the reciprocal of the Re exponent ($1/b$) as the ordinate and comparing it with $\mathrm{Sh}/\mathrm{Re}^b$, as presented in Figure 6-12, indicates that except for the Submerged configuration, the pattern of changes observed in mass transfer closely matches the pattern of $1/b$; we have not pursued this further.

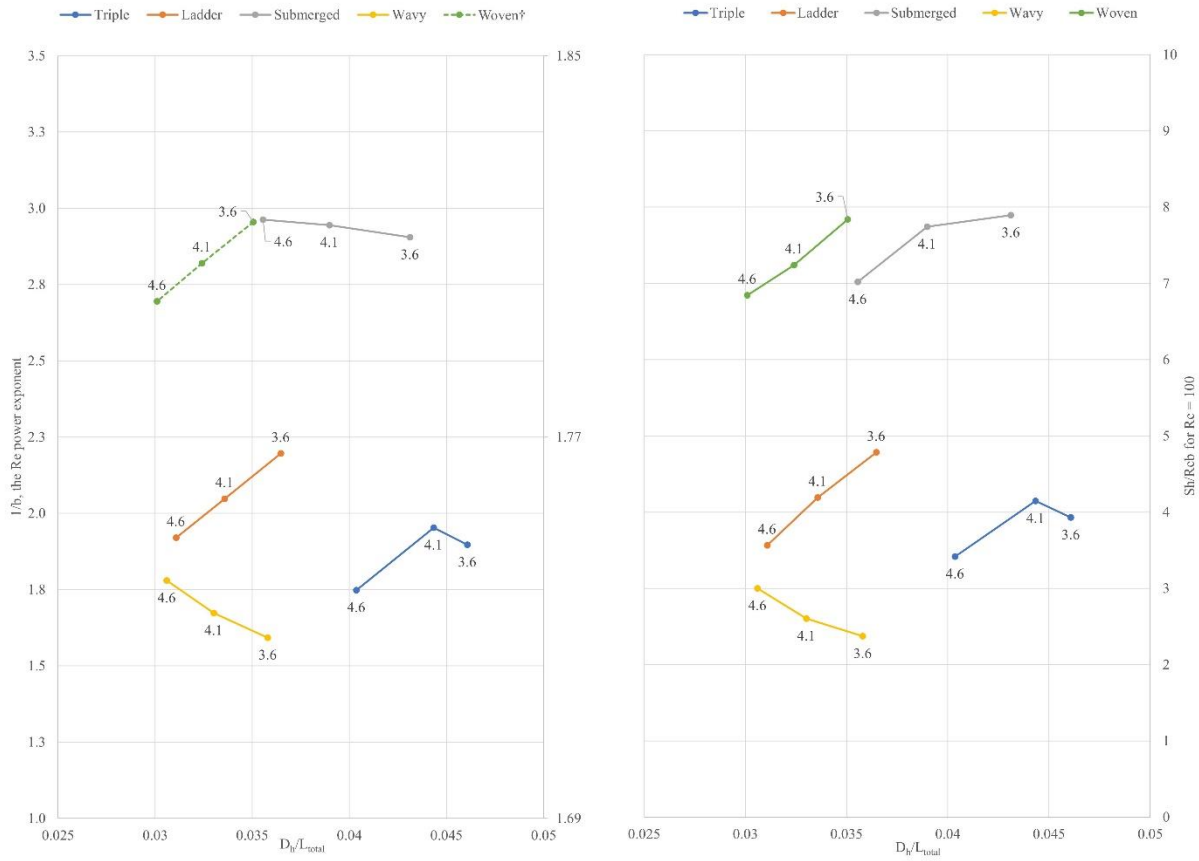

Figure 6-12. Predicted 1/b (left) and $\mathrm{Sh}/\mathrm{Re}^b$ (right) vs. D_h/L_{total}, for Re = 100.
† 1/b values for Woven are displayed on the right side axis.

6.3.5 Estimation of mass transfer from literature equations

The analogy between equations describing heat transfer and mass transfer (namely, the ability to substitute Nu with Sh, and Pr with Sc) is well known and discussed in the literature, for both laminar and turbulent regions. For example, Lienhard IV and Lienhard V (42)

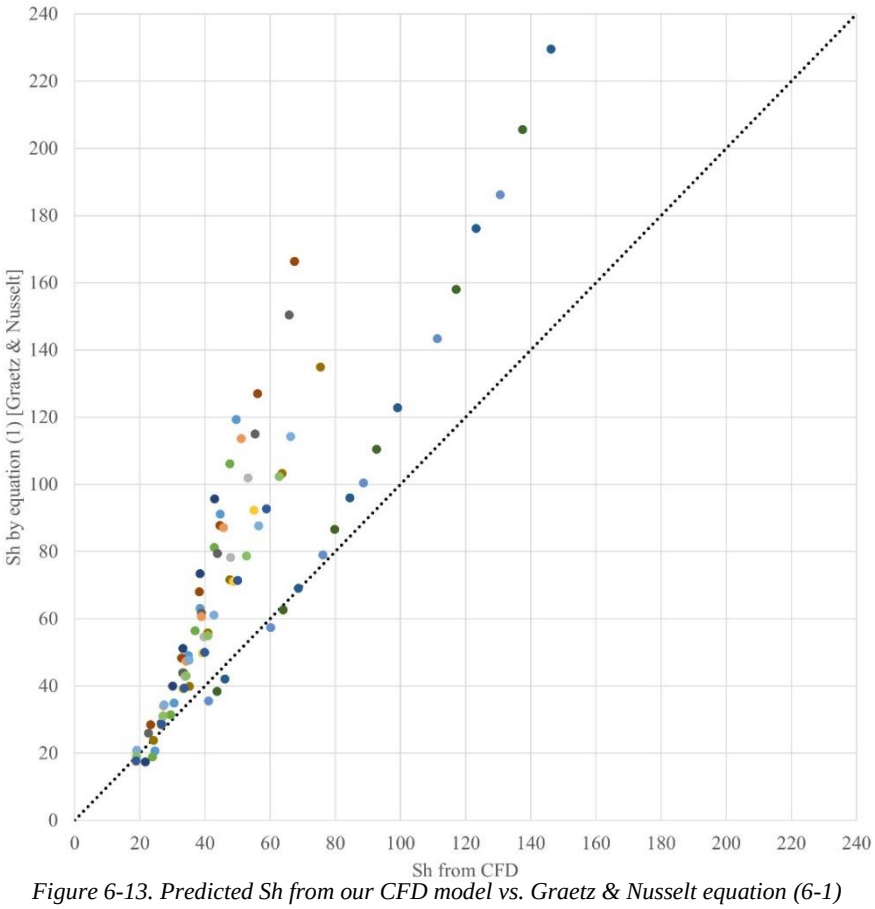

Figure 6-13. Predicted Sh from our CFD model vs. Graetz & Nusselt equation (6-1)

discussed the comparability of these phenomena in detail, and in another standard work, Holman (43) wrote:

> The similarities between the governing equations for heat, mass, and momentum transfer suggest that empirical correlations for the mass-transfer coefficient would be similar to those for the heat-transfer coefficient.

As presented previously, Table 6-1 summarised some of the important empirical equations suggested in the literature to estimate heat transfer in both laminar and turbulent flow.

The Graetz & Nusselt equation (6-1) was used to predict the outlet salt concentration and then the corresponding Sh value was calculated. Figure 6-13 shows that their equation gives closer results to our CFD studies at lower flowrates, namely from −15% to +30% deviation from our CFD results at Re = 25, which increases notably at higher flows; that is, from +45% to +150% deviation at Re = 200. This could be a result of turbulence, as well as terminating the series for calculating P2 at the third term in equation (6-2).

The other equation from Table 6-1 investigated was the Sieder-Tate equation (37), which is still widely used (44). As is clear in Figure 6-14 (left) and noted by other studies (24, 25), the

Sieder-Tate equation underestimates Sh, where, in the worst case, it could be as low as 25% of our CFD model results.

Lastly, an equation suggested in the literature that specifically focusses on mass transfer in spacer-filled channels was investigated. DaCosta (27) summarised several previous approaches for predicting Sh and concluded that a modified version of the Gröber equation (45) of the form

$$\mathrm{Sh} = 1.0982 \left(\frac{H}{d}\right)^{0.039} \varepsilon^{0.75} \left(sin\left(\frac{\beta}{2}\right)\right)^{0.086} \mathrm{Re}^{0.5}\mathrm{Sc}^{0.33} \left(\frac{2D_h}{L}\right)^{m} \quad (6\text{-}4)$$

would result in the best predictions. It should be noted that the equation proposed by DaCosta (27) used the cell length (L) instead of channel length (L_{total}), and that all physical properties are evaluated at the membrane concentration. The authors suggested m = 0.33 for empty channels and m = 0 for all spacer-filled arrangements covered in their work (3). In other words, although they included the D_h/L term in their equation, they did not observe any correlation between Sh and D_h/L when spacers were present.

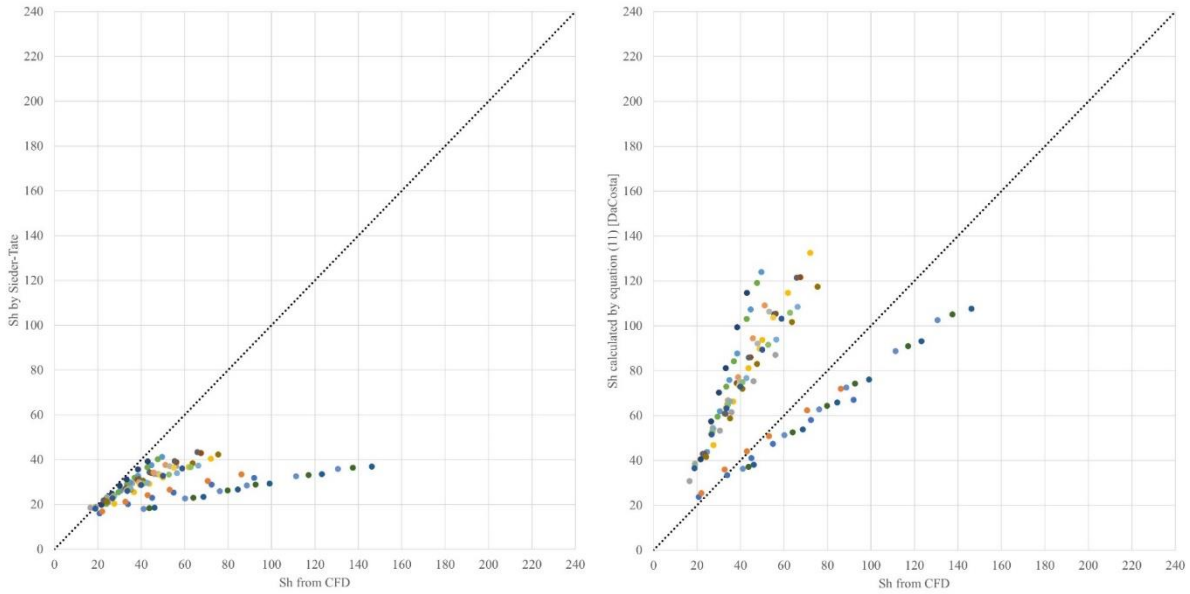

Figure 6-14. Parity plots for Sh from our CFD model vs. Sieder-Tate equation (left) and DaCosta equation (6-4) (right)

Figure 6-14 (right) compares the values for Sh calculated by the DaCosta equation (6-4) and our CFD results. The DaCosta equation underestimates Sh in most cases for PP60, PP45 and all Woven configurations, while for all other arrangements, Sh is overestimated compared to our CFD results. The deviations ranged from −27% to +170%, with an average of 31%, and average absolute deviation of 65%, which shows a general tendency of overestimation

compared to our CFD model results. The deviation between equation (6-4) and our CFD results seems more dependent on the spacer arrangement than on the Re value.

Considering the three attempts above, general equations should be used cautiously for predicting Sh. Further work is needed before they can be used with confidence for RO spacers.

6.3.6 An insight into mass transfer in non-commercial spacers

In this section, the predicted concentration, velocity, and shear stress plots of the non-commercial spacers for the three gap sizes are examined in detail. Most plots view the domain from the side: perpendicular to the membranes and aligned with the main flow direction and are presented at selected locations across the width of the domain to bring out specific features of the flow (e.g., at 25% of the cell width, with 0% representing the location of the centreline of a longitudinal filament if one exists for the geometry). The main flow direction is from left to right in these plots. An effort has been made to explain the micro-scale variations in concentration based on the spacer geometry and velocity field, to identify phenomena such as lateral flow recirculation, and to relate them to spacer performance, including changes in the equation parameters reported in previous sections, where possible.

Submerged

The Submerged spacer (Figure 6-1b) has straight lateral filaments in the middle of the domain equidistant from the top and bottom membranes; there are no longitudinal filaments. High salinity zones are present at both top and bottom membranes, with a maximum size of about 10% of the channel height for all three gap sizes. The thickness of the high salinity zone at both membranes was reduced in the vicinity of the filaments (highlighted in Figure 6-15a, Figure 6-16a, and Figure 6-17a). The salinity gradient remains uniform through the domain width because of the absence of longitudinal filaments.

The latitudinal filaments push the fluid towards the membranes and produce high velocity zones between the filament and membrane (circled in Figure 6-15b, Figure 6-16b, and Figure 6-17b). This increases the shear stress on both top and bottom membranes (shown in Figure 6-15c, Figure 6-16c, and Figure 6-17c), which improves the convective mass transfer.

The effect of gap size on spacer performance can be seen by comparing Figure 6-15, Figure 6-16, and Figure 6-17. It is clear that increasing the gap between filaments does not significantly affect the area of the membrane subject to high shear stress, but it does increase

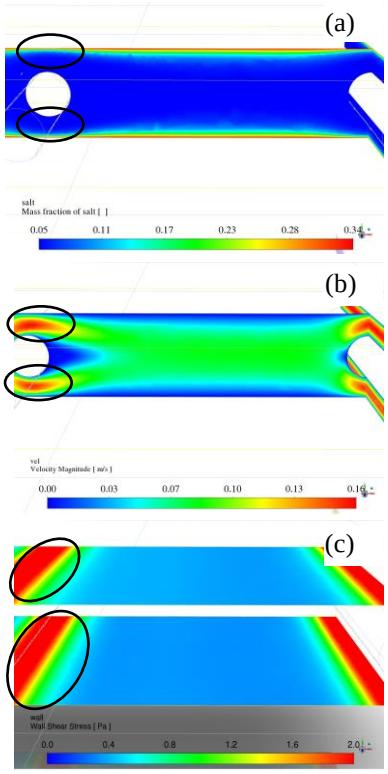

Figure 6-15. Concentration (a), velocity (b), and shear stress on the membrane (c) for Submerged36

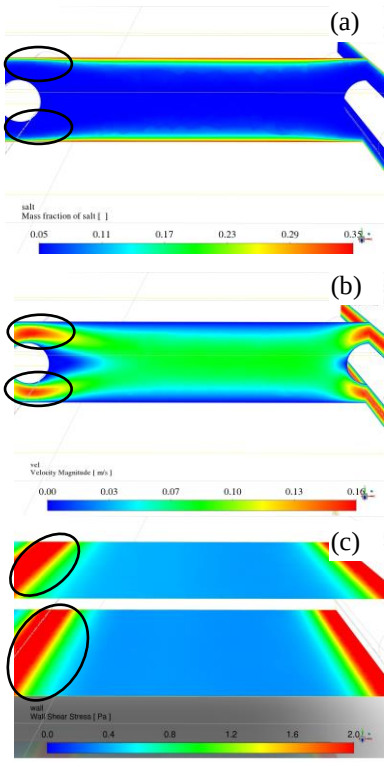

Figure 6-16. Concentration (a), velocity (b), and shear stress on the membrane (c) for Submerged41

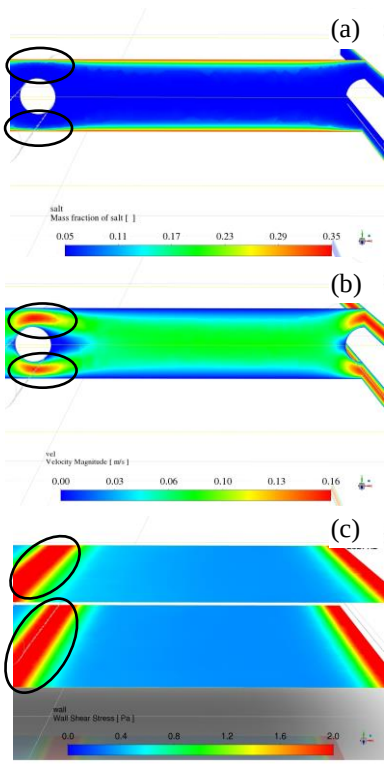

Figure 6-17. Concentration (a), velocity (b), and shear stress on the membrane (c) for Submerged46

the membrane area that experiences low shear stress, which explains the reduction in mass transfer performance for spacers with bigger gaps, as reported also in Figure 6-8.

Triple

The Triple spacer (Figure 6-1c) has straight latitudinal filaments located in pairs touching the top and bottom membranes with a straight longitudinal filament separating them. Comparing the concentration plots for Submerged and Triple configurations shows that, unlike for the Submerged spacer, the salinity gradient for the Triple spacer changes through the domain width, which is in response to the presence of the longitudinal filaments.

Close to the longitudinal filaments, for example, 15% of the cell width (Figure 6-18a), high salinity is only observed very close to the membranes, but further away from the longitudinal filament, e.g., 25% of the cell width (Figure 6-18b), larger high salinity zones form downstream of the latitudinal filaments. The local velocity vectors (Figure 6-18c) indicate that the salt is moving towards the main flow stream (Figure 6-18d) not by diffusion, but by the fluid's bulk movement. The backwashing streams (where the fluid next to the membrane, downstream of the latitudinal filaments, is flowing in the opposite direction to the bulk flow, or towards the

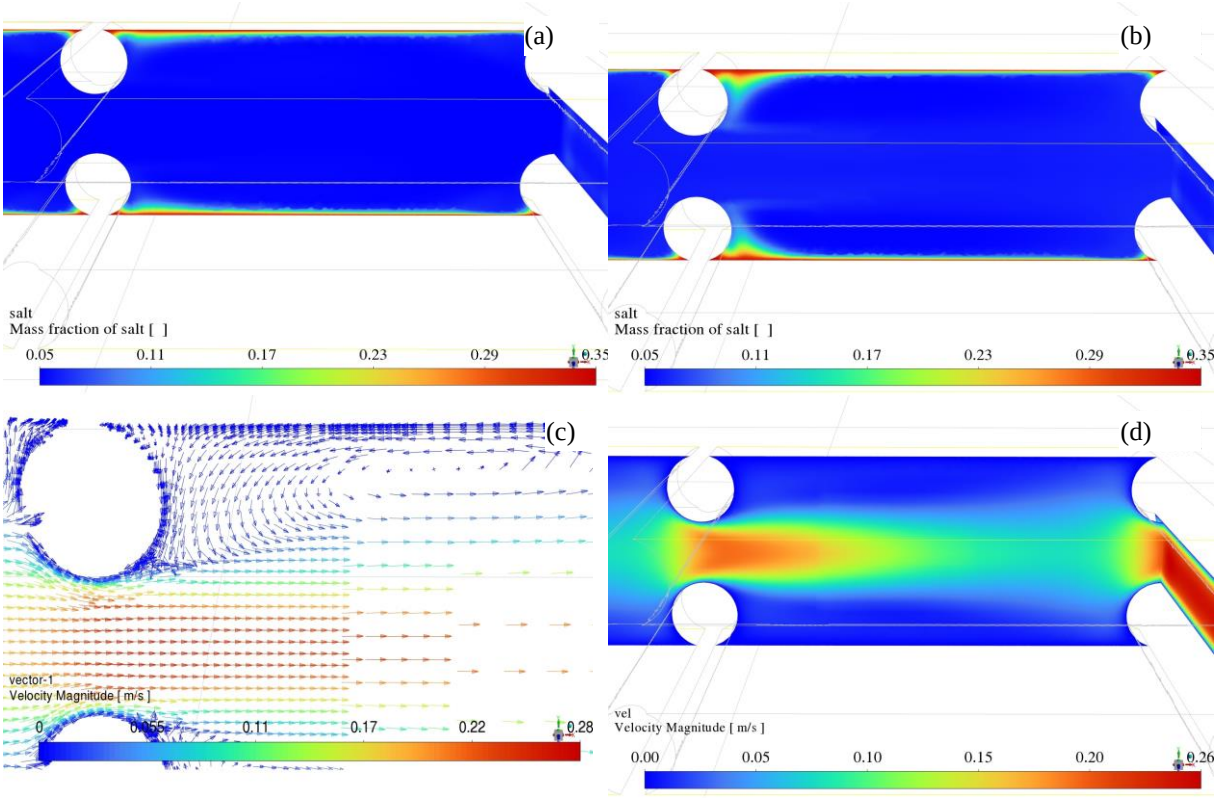

Figure 6-18. Concentration at 15% of the cell width (a) and concentration (b), velocity (c), and velocity vectors (d) at 25% of the cell width for Triple36

inlet) remaining effective through the middle of the domain width and gradually disappearing near the next longitudinal filament.

The velocity contour plot (Figure 6-18d) shows that latitudinal filaments direct most of the fluid's movement to the middle part of the domain and this causes low-velocity zones of significant size at the top and bottom of the domain. In addition, it appears that the latitudinal filaments are generally slowing the overall flow.

Increasing the gap from 3.6 to 4.1 mm leads to similar patterns of high salinity and backwashing. Backwash streams appear at almost the same latitudinal distance away from the longitudinal filaments as for the smaller gap, allowing a larger portion of domain width to receive the benefit of backwashing. On the other hand, the greater gap between latitudinal filaments means the benefits of latitudinal filaments will occur less frequently and the ratio of the membrane area affected by latitudinal filaments to the total membrane area is reduced. Overall, this slightly reduces the effect of Re on mass transfer (e.g., Sh), and the Re exponent slightly decreases (Table 6-4) compared to the spacer with a gap of 3.6 mm.

Increasing the gap further to 4.6 mm leads to patterns of high salinity and backwashing that are similar in shape and significance compared to the other two arrangements. However, a new

feature has appeared: a high salinity zone before every alternate top and bottom latitudinal filament (Figure 6-19a). For comparison, magnified views of the salt concentration at the second-last latitudinal filament at a position 9 mm from the centreline of the longitudinal filament are shown for Triple46 (Figure 6-19b) and Triple36 (Figure 6-19c). Comparing the velocity vector plots at the same locations (Figure 6-19d,e) reveals that where the gap between the filaments is smaller (Figure 6-19e), backwash streams have started just before the latitudinal filament (visible on the left side of the filament) and have extended all the way back to the previous filament (visible at the right side of the filament). The short gap between the

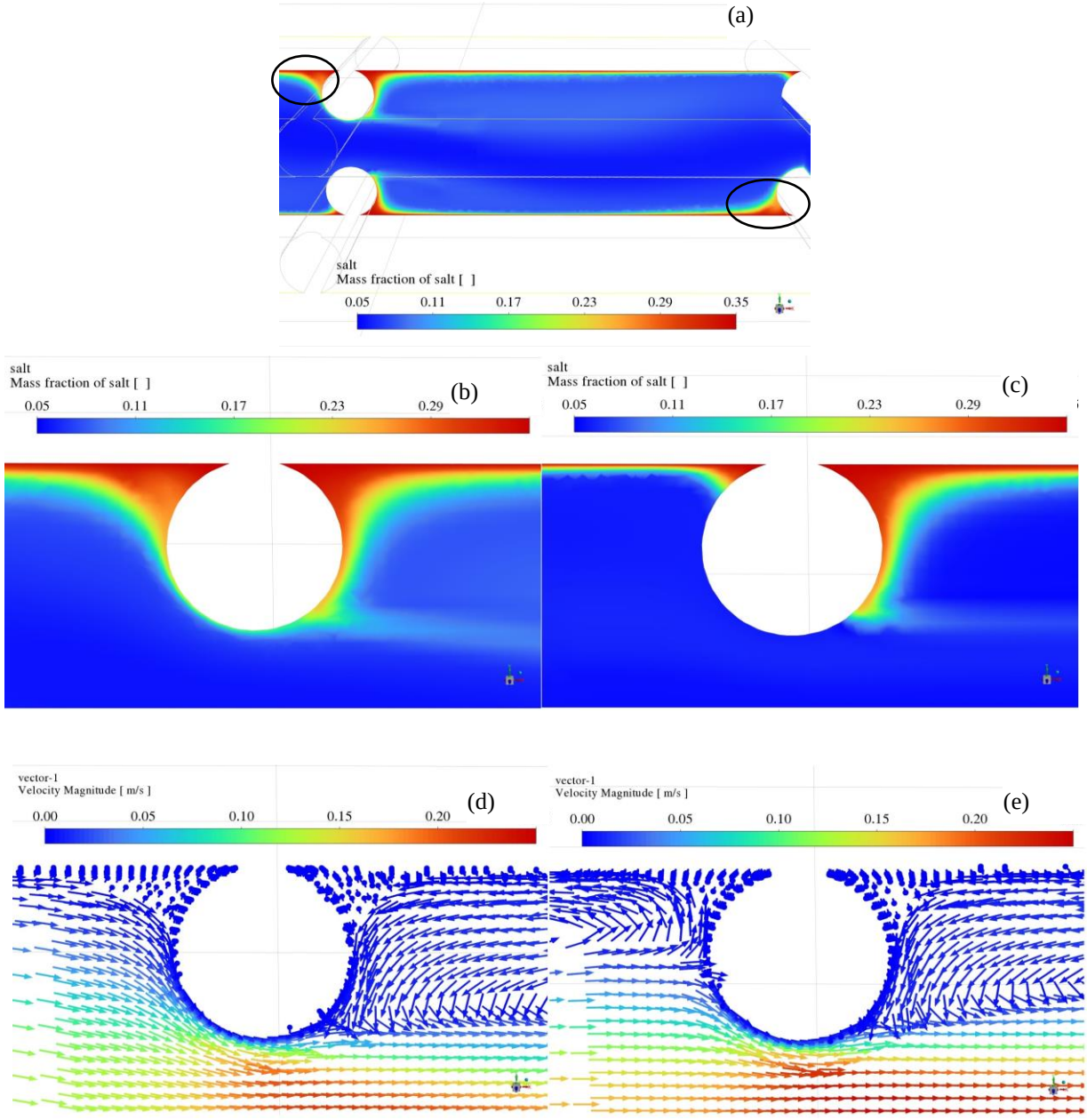

Figure 6-19. Concentration for Triple 46 (a), comparison of magnified view of concentration for Triple46 (b) and Triple36 (c), and velocity vectors for Triple46 (d) and Triple36 (e), all at 9 mm width.

latitudinal filaments prevents the main stream flow from interfering and overcoming the backwash streams. On the other hand, moving the latitudinal filaments apart provides sufficient space for the main flow to overcome the backwash streams and make the fluid move in the forward direction, which is visible on the right side of the filament (Figure 6-19d). The main difference between these patterns is that backwashing will not become significantly stronger with increasing the flowrate, while higher flowrates notably strengthen the main stream flowing in the forward direction. The additional link between flowrate and mass transfer for Triple46 can explain its higher Re exponent for Sh compared to the other Triple spacers with smaller gaps as shown in Table 6-4.

Ladder

The Ladder spacer (Figure 6-1a) has longitudinal filaments that touch the top membrane resting on latitudinal filaments that are in contact with the bottom membrane. The top half of the domain is mostly affected by the longitudinal filaments, while the bottom half of the domain is mainly influenced by the latitudinal filaments.

Near the longitudinal filaments, a high salinity zone is observable at the top membrane (Figure 6-20a), which is notably larger than the zone at the bottom membrane. Inspecting the velocity vectors (Figure 6-20c) and comparing the fluid motion at the top and bottom membranes indicates that the presence of the latitudinal filaments at the bottom membrane enhances convective mass transfer, while the top membrane mainly receives the benefits of diffusional mass transfer.

Away from the longitudinal filaments, at the cell's mid-plane (50% cell width, Figure 6-20b,d), it can be seen that both backwash and forward-wash streams (where the fluid motion close to the membrane and upstream of the latitudinal filaments is towards the outlet) are well developed and move salt away from the bottom membrane towards the main stream flow.

Comparing the velocity vectors at these two widths reveals more information about the detailed flow patterns. Closer to the longitudinal filaments (Figure 6-20c), convective mass transfer at the top membrane is impacted by two factors. First, the streamlines are repeatedly squeezed together and pushed towards the top membrane by the latitudinal filaments and then allowed to relax in the region between the latitudinal filaments. Second, the longitudinal filaments slightly reduce the sideways turbulent flow.

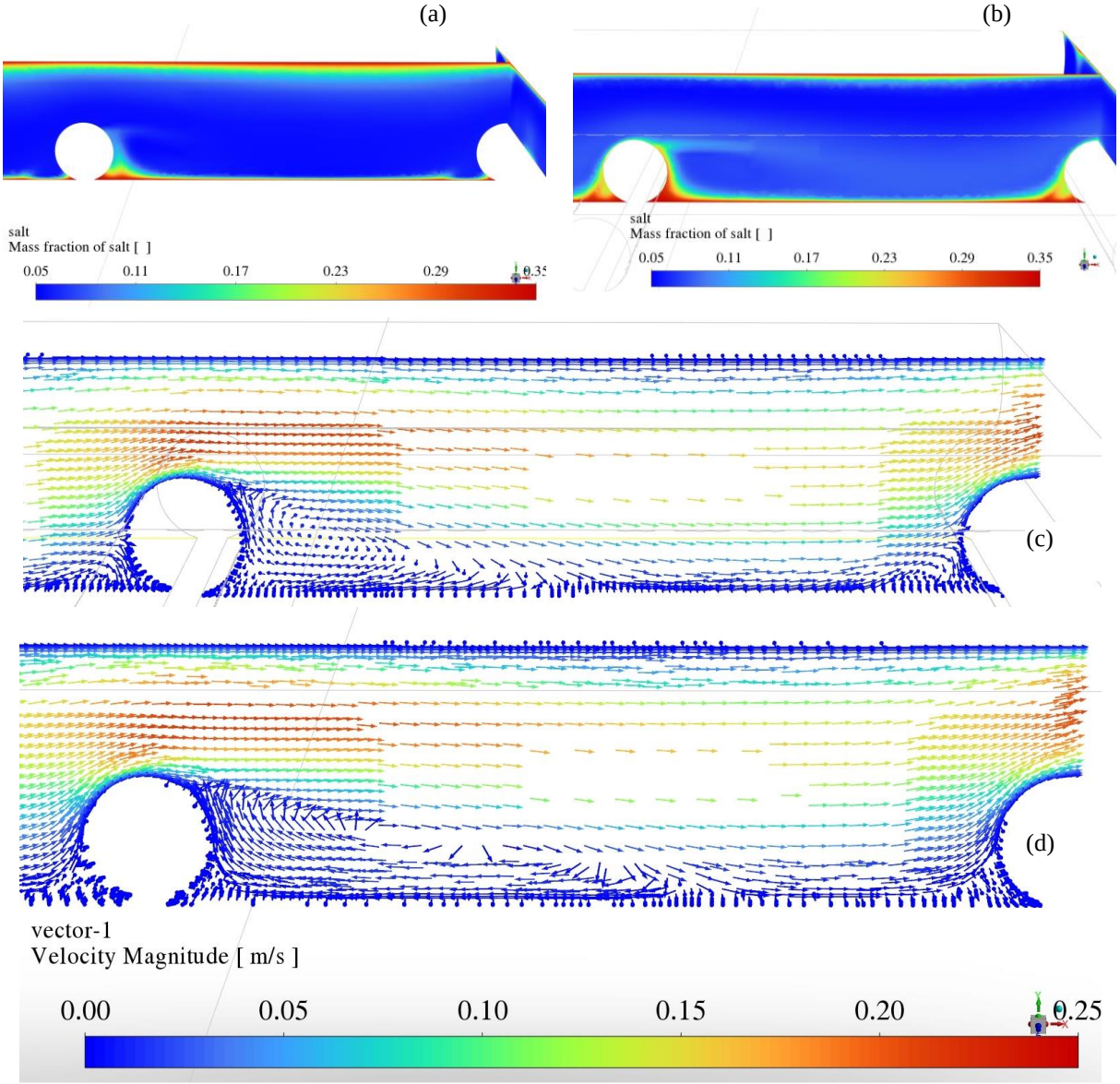

Figure 6-20. Concentration at 25% cell width (a) and mid-plane (b), and velocity vectors at 25% cell width (c) and mid-plane (d), for Ladder36.

Away from the longitudinal filaments, at the cell mid-plane (Figure 6-20d), the flow streams are little affected by the longitudinal filaments. Small sideways eddies are observable at the top and bottom membranes that increase convective mass transfer. The result is the thinner concentration layer at the top membrane and larger zones with high salinity observable before and after each latitudinal filament.

Increasing the gap between the filaments does not result in notable changes in the fluid motion or salinity patterns. The consistency of the fluid's response to latitudinal and longitudinal filaments gives the Ladder configuration predictable behaviour over the range of gap sizes investigated. Increasing the gap between filaments leads to larger areas being affected

by backwash and forward-wash streams, and the arrangement shows a stronger response to flowrate changes, which explains the change in the Re power exponent observed in Table 6-4 for this spacer.

Wavy

The Wavy spacer (Figure 6-1d) has straight latitudinal filaments that touch alternately the top and bottom membranes. Sinusoidal longitudinal filaments weave between the latitudinal filaments and the opposite membrane surface. The observations in this configuration can be divided into two parts: at the sides of the domain, which are close to and mostly affected by the sinusoidal longitudinal filaments, and in the middle of the domain, which is mainly under the influence of the alternating latitudinal filaments.

For the gap of 3.6 mm, close to the sides of the domain and the longitudinal filaments, large high salinity zones are observable upstream of the latitudinal filaments, which affect mass transfer, as clearly visible in Figure 6-22a and b. On the other hand, at the domain's mid-plane (Figure 6-22c), both backwash and forward-wash streams are well developed and move the salt away from the bottom membrane to the main stream flow.

The presence and shape of the high salinity zones close to longitudinal filaments in this configuration can be explained by the existence of side-wash streams. Side-washing refers to the presence of lateral flows located just upstream and downstream of lateral filaments; they bring fluid from the side of the domain towards the mid-plane, or push it away. Figure 6-22d shows the velocity vectors with fixed length, without binding them to be in-plane. This means that the velocity vectors that have a smaller in-plane component will appear shorter, or even as a dot if pointing normal to the viewing plane. The magnified section of Figure 6-22d shows how side-wash streams help to move the salt away from the longitudinal filament and then the backwash and forward-wash streams move it further towards the main stream flow. The contour plot of the velocity component in the direction normal to the viewing plane (Figure 6-22e,f) is consistent with the velocity vector plot, and highlights the significance of the side-wash streams.

The phenomena observed at the domain's mid-plane (Figure 6-22c) are very similar to observations for the Ladder configuration and follow the same reasoning.

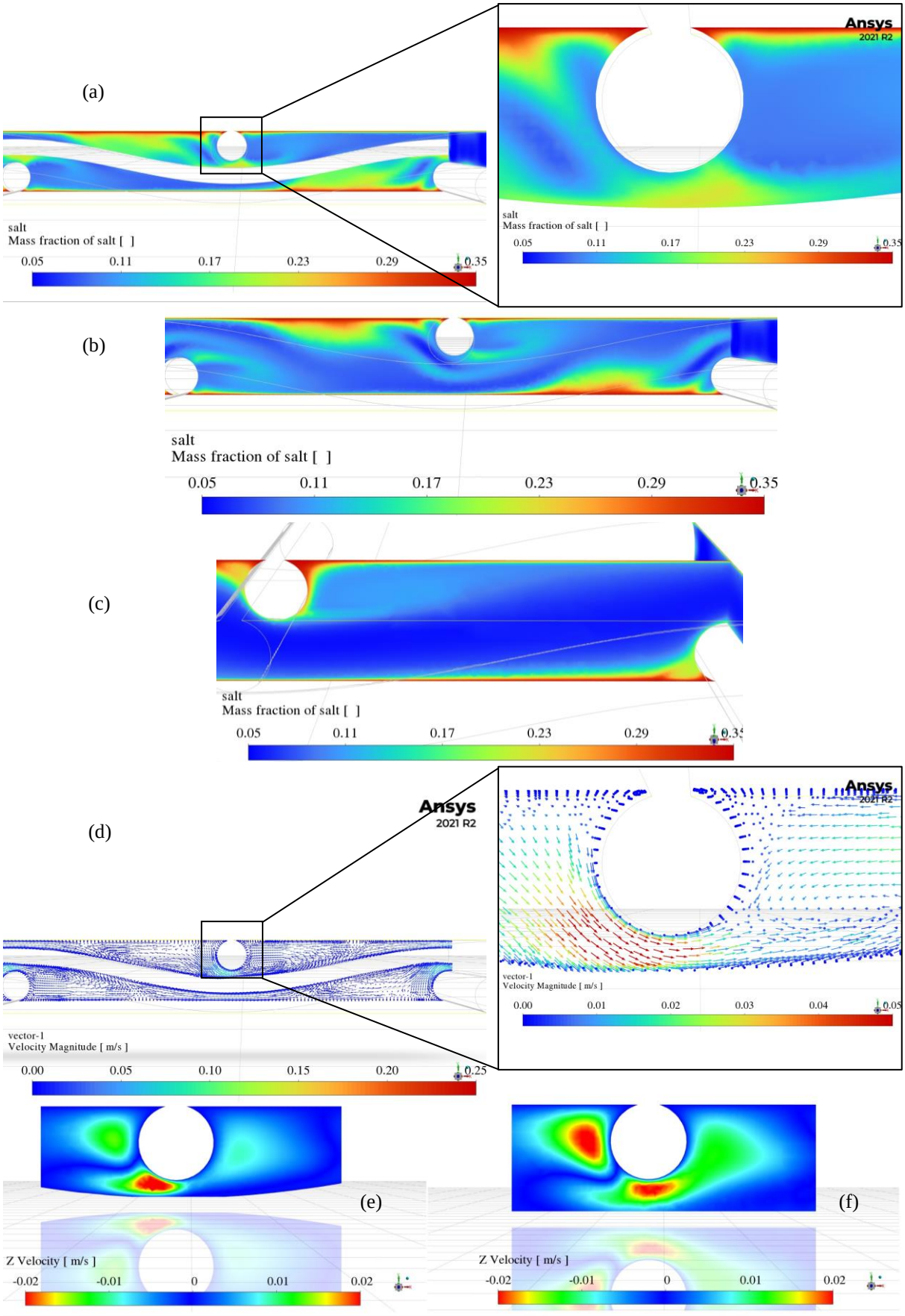

Figure 6-22. Concentration at 6% of the cell width (a), 9% of the cell width (b), and mid-plane (c), velocity vectors at 6% of the cell width (d), and z-velocity (normal to viewing plane) at 6% of the cell width (e) and 9% of the cell width (f), for Wavy36

Increasing the gap between filaments to 4.1 mm affects the sides and the centre of the domain differently. The effect of longitudinal filaments is less significant and disappears sooner in Wavy41 (Figure 6-21a,b), compared to Wavy36, while at the domain's mid-plane (Figure 6-21c), both arrangements perform in a similar manner.

Comparing the contour plots of the z-direction velocity component (direction normal to the viewing plane) at 6% (Figure 6-21d) and 9% of the domain's width (Figure 6-21e), shows that the side streams sweeping fluid away from the longitudinal filament have become stronger, which can explain why the high salinity zones are smaller and disappear sooner in Wavy41 compared to Wavy36. A comparable pattern of changes resulting from increasing the gap size was also observed for Wavy46.

In addition, at the mid-plane of the domain, increasing the gap between the filaments does not notably affect the backwash pattern, but it does extend the size of the forward-wash region (Figure 6-22c, Figure 6-21c). This does not result in a proportional improvement in mass transfer and thus, in accordance with the Re exponents for Sh reported in Table 6-4, the Wavy arrangement with a larger gap receives less benefit from a flowrate increase.

Woven

The Woven arrangement (Figure 6-1e) is similar to the Wavy spacer, except that both the longitudinal and latitudinal filaments are sinusoidal. Because of the complexity of the Woven arrangement, various types of fluid motion in different regions combine to determine the mass transfer behaviour. Starting with the sides of the domain, the longitudinal filaments cause high salinity zones at 6% (Figure 6-23a) and 9% of the cell width (Figure 6-23b) that are comparable to the Wavy configuration in their general shape, but with slightly smaller size and higher concentration. A comparison between the concentration and velocity vector plots for Wavy36 and Woven36 can provide a better understanding of the impact of having sinusoidal-shaped latitudinal filaments. Unlike straight filaments, which are always in contact with the membrane, the sinusoidal shape provides an opening between the filament and the membrane that varies from zero to one filament diameter. Inspecting the velocity vectors at 6% (Figure 6-23c) and 9% of the cell width (Figure 6-23d) emphasises that the low concentration zone after the filament that is identifiable in the magnified view of the contour plots at 6% (Figure 6-23a) and 9% of the cell width (Figure 6-23b) is a result of fluid flow through the opening between the latitudinal filament and the membrane. It also highlights that clearing the channel and moving

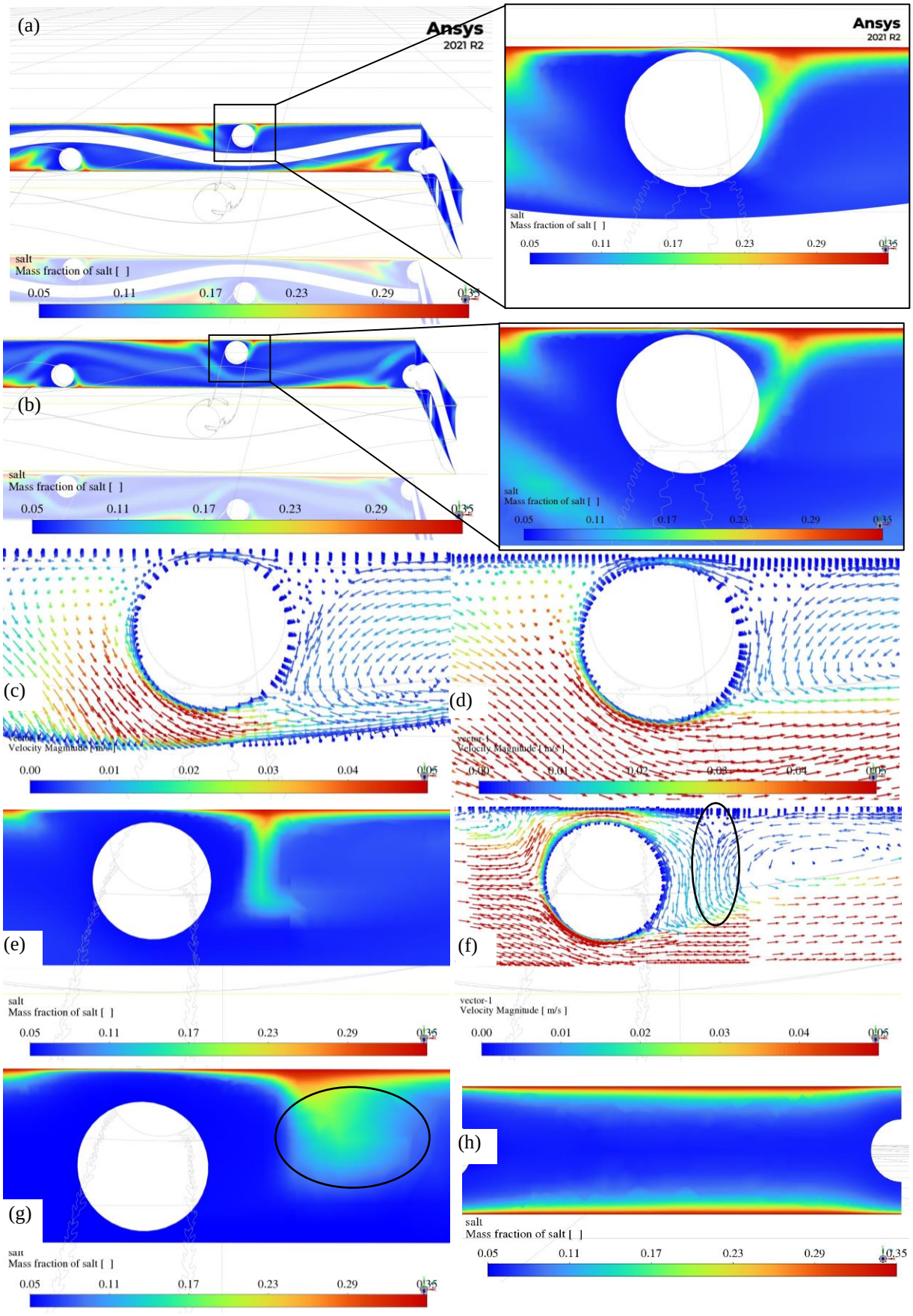

Figure 6-23. Concentration at 6% of the cell width (a) and 9% of the cell width (b), velocity vectors at 6% of the cell width (c) and 9% of the cell width (d), concentration (e) and velocity vectors (f) at 19% of the cell width, and concentration at 30% of the cell width (g) and 50% of the cell width (mid-plane) (h), for Woven36

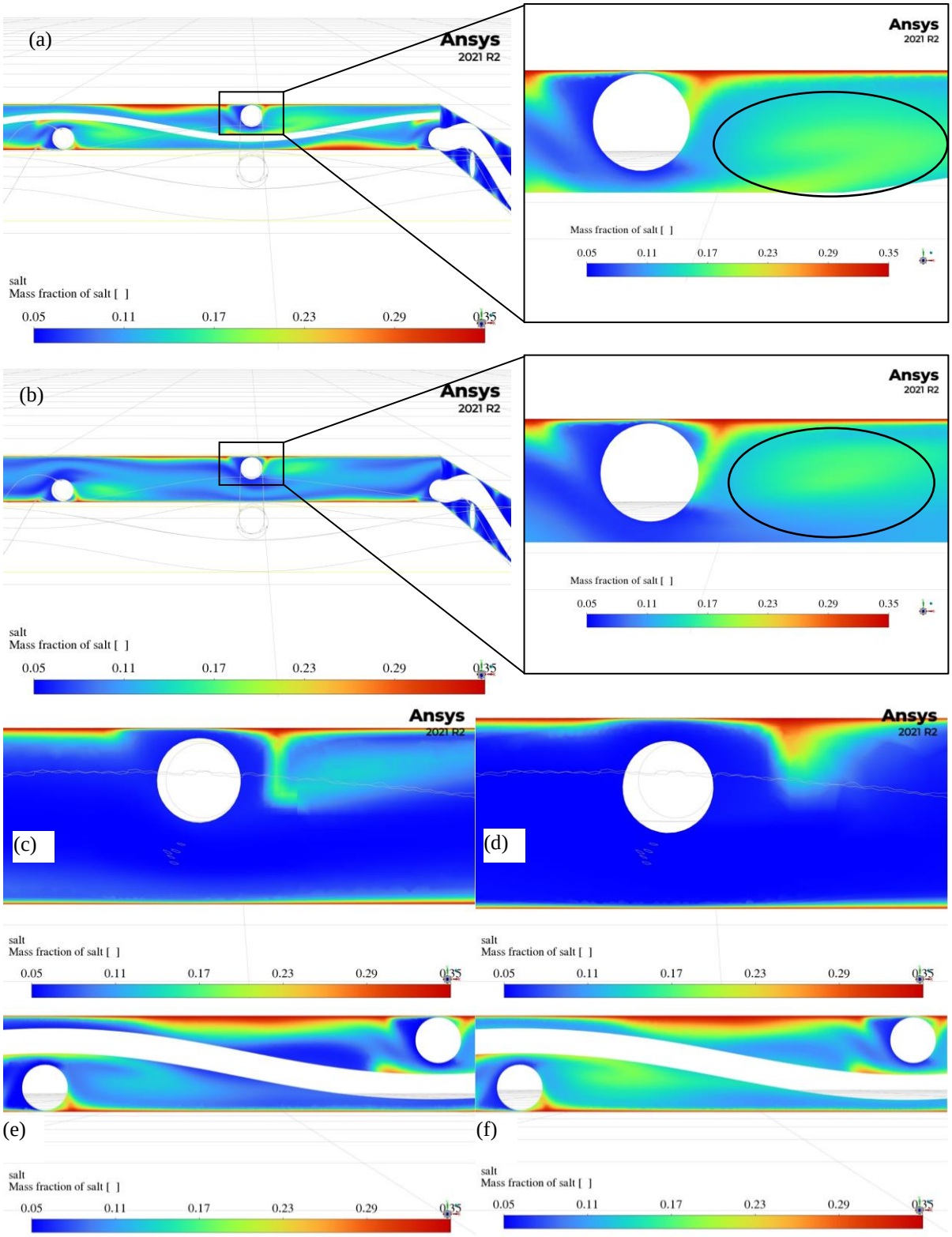

Figure 6-24. Concentration at 6% (a), 9% (b), 19% (c), and 30% (d) of the cell width, as well as 0.2 mm from the symmetry wall, in 3rd cell (e) and 9th cell (f), for Woven41

on mass transfer.

The impact of the sinusoidal shape of the latitudinal filament grows as it separates from the membrane and leaves a bigger opening for the fluid to pass through. At 19% of the cell width

(Figure 6-23e), the flow stream through the opening is strong enough to efficiently wash away the concentrated layer and completely separate it from the filament. Based on the velocity vector plot at the same plane (Figure 6-23f), it seems that the stream passing through the gap and the backwash stream cancel out each other's x-velocity in the highlighted area, and hence, the fluid flows directly downward.

At 30% of the cell width (Figure 6-23g), the flow stream through the opening overcomes the backwash stream and forces the backwashed salt to move slightly towards the membrane again. This effect grows in magnitude until the mid-plane of the cell, where the backwash stream disappears and the concentration contour plot (Figure 6-23h) is comparable with the Submerged configuration (e.g., Figure 6-15a).

By increasing the gap between the filaments from 3.6 mm to 4.1 mm, the salt concentration close to the symmetry walls is observed to be similar to Woven36, before and around the latitudinal filament, but substantially different after the latitudinal filament, as highlighted in the magnified views of Figure 6-24a and b. It seems that this phenomenon of concentration build-up near a longitudinal filament, results from a combination of factors. Figure 6-24 also shows the concentration contours at 0.2 mm from the symmetry wall for the third (Figure 6-24e) and ninth (Figure 6-24f) cells in the main flow direction, highlighting that the concentrated zone's shape remains the same, while the magnitude of the concentration increases through the domain.

Focusing on the 0.2 mm cut plane, the fluid flow in Woven41, which has a larger gap between the latitudinal filaments, would experience less turbulence normal to the plane, compared to Woven36. Quantitatively, the mass-weighted averages of the *magnitude* of the velocity component normal to the plane (z-velocity) are $\overline{|u_z|}$ = 12.3 mm/s and $\overline{|u_z|}$ = 9.6 mm/s for Woven36 and Woven41, respectively. On the other hand, the mass-weighted average z-velocities on the same plane are $\overline{u_z}$ = 0.4 mm/s and $\overline{u_z}$ = 3.6 mm/s, respectively, for Woven36 and Woven41. This difference is the key to understanding the different behaviour of these arrangements. Woven36 experiences larger sideways flows (higher $\overline{|u_z|}$) that act in an almost symmetric manner (lower $\overline{u_z}$), bringing in fresh fluid from the mid-channel and washing away the salt, while Woven41 has weaker sideways flows (lower $\overline{|u_z|}$) that are not acting in a symmetric manner (higher $\overline{u_z}$), but have a higher tendency to move away from the sides, without bringing in the same amount of fresh fluid from the mid-channel. Lack of mixing might be observed in another way: by comparing the average salt concentration at the domain outlet

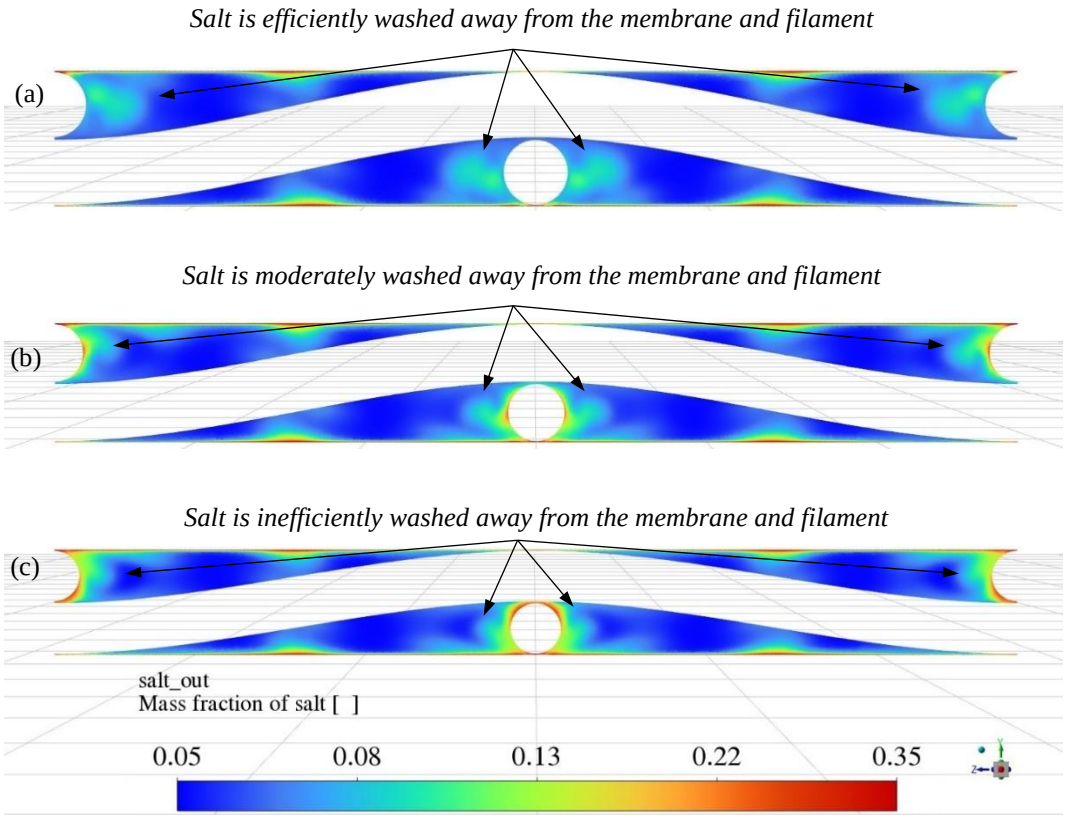

Figure 6-25. Concentration at the domain outlet for Woven36 (a), Woven41 (b), and Woven46 (c)

and on the 0.2 mm plane. For Woven36, mass-weighted salt concentration is 6.80% at the outlet and 8.50% on the 0.2 mm plane, while for Woven41, the values are 6.88% and 11.7%, respectively. While there is a very small difference in the outlet concentrations, there is a 37% concentration difference on the 0.2 mm cut plane, which shows the overall mass transfer performance is comparable, but Woven36 performs notably better on the sides of the domain.

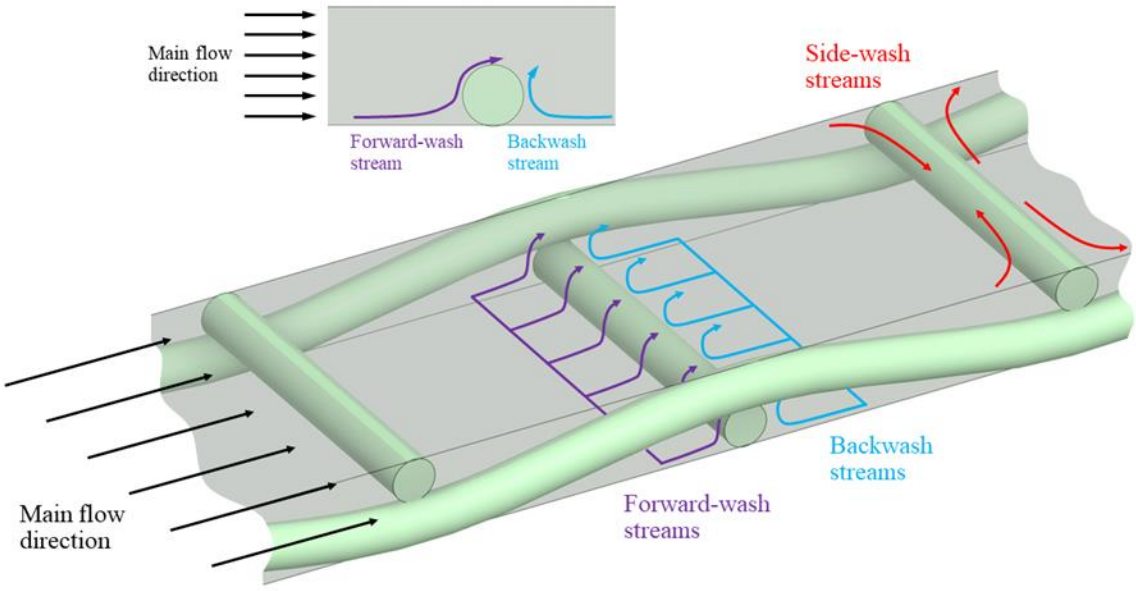

Figure 6-26. Schematic illustration of backwashing, forward-washing, and side-washing flows

Comparing Woven46 (not shown in figures) with Woven41 reveals that the poor mixing on the domain sides is slightly worse in Woven 46, which has a 12% lower average z-velocity magnitude and a 12% higher average z-velocity, and 1.6% higher outlet concentration and 7% higher concentration on the 0.2 mm cut plane. Figure 6-25 compares the outlet concentrations for the three different Woven gap sizes and shows the impact of lateral recirculation (or side-washing) on the mass transfer.

Away from the domain's sides and close to the middle of the channel, a wider opening between the Woven latitudinal filament and the membrane causes the fluid that passes through the opening to play a stronger role and override the effect of the side-wash streams. In other words, increasing the gap between filaments weakens the side-wash streams, while it enhances the forward-washing effect. Interestingly, among the three studied gap sizes, it seems that gain from one effect is balanced by the loss from the other, so that the performance of Woven46 and Woven41 are comparable with Woven36 at 19% (Figure 6-24c) and 30% (Figure 6-24d) of the cell width.

Summary of mass transfer observations

This analysis of the micro-scale velocity and concentration results has helped provide a better understanding of the reasons for the observed fluid movement patterns and the macro-scale performance for spacers on the feed side of spiral wound membrane modules. The insights of the importance of the small gap between a latitudinal filament and the membrane, and the presence of lateral recirculation (side-washing) flows, are considered the main findings for this section. The three key flows (backwashing, forward-washing, and side-washing) that help to reduce concentration layers at the membrane are illustrated in Figure 6-26. These results may assist designers working towards more efficient feed spacer arrangements to improve the overall performance of desalination plants.

6.4 Conclusion

Computational Fluid Dynamics was used to study the effect of changes in the flowrate and the gap between filaments for different feed spacer arrangements for Spiral Wound Modules used in reverse osmosis applications. The modelling approach has been validated in our previous study (6).

Both energy consumption and mass transfer on the feed side were studied by comparing different performance measures, e.g., pressure drop per unit length, power number, specific

power consumption, Sherwood number and spacer configuration efficacy. Based on these results, the key conclusions are:

- The spacer performance measures are strongly affected by the flowrate and the spacer geometry.
- Power law equations can be used to describe the correlation between performance measures and flowrate as expressed by the Reynolds number. The regression quality for pressure drop, power number, specific power consumption and spacer configuration efficacy is particularly good, and for Sherwood number is acceptable. The correlation form and parameter values are in agreement with previous studies (1, 2, 4, 6, 7, 27).
- Changing the selected performance measure and flowrate results in different rankings of spacer performance.
- While pressure drop, Pn and SCE show some level of correlation with porosity and D_h/L, Sh shows no consistent correlation with porosity or D_h/L.
- Despite the coefficients of the Pn-Re and SCE-Re correlations showing some correlation with porosity, it is not possible to accurately describe the equation parameters as a function of geometrical properties.
- Flow recirculation, both in the lateral direction (side-washing) and longitudinal direction (backwashing and forward-washing), plays a significant role in mass transfer.
- According to SCE, for the nineteen different spacer arrangements studied, Woven46 shows best results through the Re range studied.

Overall, the performance analysis and prediction of SWM feed spacers carried out in the current work using CFD indicates that valuable insights can be gained into spacer arrangements. Detailed examination of the micro-scale concentration and velocity profiles provides more transparent explanations for macro-level phenomena, including changes in the equation parameters, illustrating the importance of lateral flow recirculation. Observations based on CFD results as reported in the current work may prove valuable for designers working towards more efficient feed spacer arrangements employed in desalination plants.

Acknowledgement

This work was supported by resources provided by the Pawsey Supercomputing Centre with funding from the Australian Government and the Government of Western Australia.

Nomenclature

c_p	Specific heat capacity (J/kg °C)
D	Tube diameter (m)
D_h	Hydraulic diameter (m)
d	Filament diameter (m)
dP	Pressure drop per unit length (Pa/m)
f_D	Darcy friction factor
Gr	Grashof number
Gz	Graetz number
H	Channel height (m)
h	Convective heat transfer coefficient (W/m^2 °C)
k	Thermal conductivity (W/m °C)
L	Cell length (m)
L_{total}	Total channel length (m)
Nu	Nusselt number
ΔP	Pressure drop (Pa)
Pn	Power number
Pr	Prandtl number
R^2	Coefficient of determination
Re	Hydraulic Reynolds number
r	Pearson correlation coefficient
Sc	Schmidt number
SCE	Spacer Configuration Efficacy
Sh	Sherwood number
SPC	Specific Power Consumption (W/m^3)
u_{eff}	Effective velocity (m/s)

u_z	Velocity component in the z-direction (m/s or mm/s)
W	Cell width (m)
w	Mass flowrate (kg/s)

Greek symbols

β	Spacer geometry angle (°)
ϵ	Porosity

References

1. In Seok K, Ho Nam C. The effect of turbulence promoters on mass transfer – numerical analysis and flow visualization. International Journal of Heat and Mass Transfer. 1982; 25(8):1167-1181.

2. Schock G, Miquel A. Mass-transfer and pressure loss in spiral wound modules. Desalination. 1987; 64(C):339-352.

3. DaCosta AR, Fane AG, Fell CJD, Franken ACM. Optimal channel spacer design for ultrafiltration. Journal of Membrane Science. 1991; 62(3):275-291.

4. DaCosta AR, Fane AG, Wiley DE. Spacer characterization and pressure drop modelling in spacer-filled channels for ultrafiltration. Journal of Membrane Science. 1994; 87(1-2):79-98.

5. Karode SK, Kumar A. Flow visualization through spacer filled channels by computational fluid dynamics 1. Pressure drop and shear rate calculations for flat sheet geometry. Journal of Membrane Science. 2001; 193(1):69-84.

6. Kavianipour O, Ingram GD, Vuthaluru HB. Investigation into the effectiveness of feed spacer configurations for reverse osmosis membrane modules using computational fluid dynamics. Journal of Membrane Science. 2017; 526:156-171.

7. Kavianipour O, Ingram GD, Vuthaluru HB. Studies into the mass transfer and energy consumption of commercial feed spacers for RO membrane modules using CFD: Effectiveness of performance measures. Chemical Engineering Research and Design. 2019; 141:328-338.

8. Li F, Meindersma GW, de Haan AB, Reith T. Optimization of non-woven spacers by CFD and validation by experiments. Desalination. 2002; 146(1-3):209-212.

9. Li F, Meindersma W, de Haan AB, Reith T. Optimization of commercial net spacers in spiral wound membrane modules. Journal of Membrane Science. 2002; 208(1-2):289-302.

10. Li F, Meindersma W, de Haan AB, Reith T. Experimental validation of CFD mass transfer simulations in flat channels with non-woven net spacers. Journal of Membrane Science. 2004; 232(1-2):19-30.

11. Fimbres-Weihs GA, Wiley DE. Numerical study of mass transfer in three-dimensional spacer-filled narrow channels with steady flow. Journal of Membrane Science. 2007; 306(1-2):228-243.

12. Cipollina A, Di Miceli A, Koschikowski J, Micale G, Rizzuti L. CFD simulation of a membrane distillation module channel. Desalination and Water Treatment. 2009; 6(1-3):177-183.

13. Cipollina A, Micale G, Rizzuti L. Membrane distillation heat transfer enhancement by CFD analysis of internal module geometry. Desalination and Water Treatment. 2011; 25(1-3):195-209.

14. Saeed A. Effect of feed channel spacer geometry on hydrodynamics and mass transport in membrane modules [Ph.D Thesis]. Perth, Australia: Curtin University; 2012.

15. Qureshi M, Shakaib M. CFD study for temperature and concentration profiles in membrane channels. International conference on Energy and Sustainability, 2013. Karachi, Pakistan: NED University of Engineering & Technology.

16. Saeed A, Vuthaluru R, Vuthaluru H. Concept of spacer configuration efficacy (sce) applied to optimize ladder type feed spacer filament spacing in narrow channels. International

Conference On Water Desalination, Treatment and Management & Indian Desalination Association Annual Congress, 2013. Jaipur, India: The Malaviya National Institute of Technology.

17. Saeed A, Vuthaluru R, Vuthaluru HB. Investigations into the effects of mass transport and flow dynamics of spacer filled membrane modules using CFD. Chemical Engineering Research & Design. 2015; 93:79-99.

18. Saeed A, Vuthaluru R, Vuthaluru HB. Impact of feed spacer filament spacing on mass transport and fouling propensities of RO membrane surfaces. Chemical Engineering Communications. 2015; 202(5):634-646.

19. Drew TB, Hogan JJ, McAdams WH. Heat transfer in stream-line flow. Industrial & Engineering Chemistry. 1931; 23(8):936-945.

20. Nusselt W. Heat transfer, diffusion, and evaporation. Washington: National Advisory Committee for Aeronautics; 1954.

21. Nusselt W. Das grundgesetz des wärmeüberganges. Gesundheits-Ingenieur. 1915; 38(42): 477–482. 490–496.

22. Rice CW. Forced convection of heat in gases and liquids – II. Industrial & Engineering Chemistry. 1924; 16(5):460-467.

23. Colburn AP. A method of correlating forced convection heat transfer data and a comparison with fluid friction. Transactions of the American Institute of Chemical Engineers. 1933; 29.

24. McAdams WH. Heat transmission. 2nd ed. New York and London: McGraw-Hill; 1942.

25. McAdams WH. Heat transmission. 3rd ed. Malabar: R.E. Krieger Pub. Co.; 1954.

26. Rice CW. International critical tables of numerical data, physics, chemistry and technology. 1929. p.234-236.

27. DaCosta AR. Fluid flow and mass transfer in spacer-filled channels for ultrafiltration [Ph.D thesis]. Sydney, Australia: University of New South Wales; 1993.

28. Lawrence AE, Sherwood TK. Heat transmission to water flowing in pipes. Industrial & Engineering Chemistry. 1931; 23(3):301-309.

29. McAdams WH, Frost TH. Heat transfer for water flowing inside pipes. Refrigrating Engineering. 1924; 10(9):323-334.

30. Morris FH, Whitman WH. Heat transfer for oils and water in pipes. Industrial & Engineering Chemistry. 1928; 20(3):7.

31. Cox ER. General heat transfer formulas for conduction and convection. Transactions of the American Institute of Chemical Engineers. 1928; 49-50.

32. Dittus FW, Boelter LMK. Heat transfer in automobile radiators of the tubular type. University of California publications in engineering. 1930; 2(13).

33. Eagle A, Ferguson RM. On the coefficient of heat transfer from the internal surface of tube walls. Proceedings of the Royal Society of London. Series A, Containing Papers of a Mathematical and Physical Character. 1930; 127(806):540-566.

34. Burbach T, Hermann R. Flow resistance and heat transfer in pipes. ZAMM. 1930; 10(5).

35. Nusselt W. Der wärmeaustausch zwischen wand und wasser im rohr. Forschung auf dem Gebiet des Ingenieurwesens A. 1931; 2(9):309-313.

36. Sherwood TK, Petrie JM. Heat transmission to liquids flowing in pipes. Industrial & Engineering Chemistry. 1932; 24(7):736-745.

37. Sieder EN, Tate GE. Heat transfer and pressure drop of liquids in tubes. Industrial & Engineering Chemistry. 1936; 28(12):1429-1435.

38. Kern DQ, Othmer DF. Effect of free convection on viscous heat transfer in horizontal tubes. Transactions of the American Institute of Chemical Engineers. 1943; 39(4):39.

39. Martinelli RC, Boelter LMK. The analytical prediction of superposed free and forced viscous convection in a vertical pipe. University of California publications in engineering. 1942; 5(2):35.

40. Eubank OC, Proctor WS. Effect of natural convection on heat transfer with laminar flow in tubes: Massachusetts Institute of Technology; 1951.

41. Oliver DR. The effect of natural convection on viscous-flow heat transfer in horizontal tubes. Chemical Engineering Science. 1962; 17(5):335-350.

42. Lienhard IV JH, Lienhard V JH. A heat transfer textbook. 5th ed. Mineola, NY: Dover Publications; 2020.

43. Holman JP. Heat transfer. 10th ed. Boston: McGraw Hill Higher Education; 2010.

44. Serth RW, Lestina TG. Process heat transfer: Principles and applications. 2nd ed: Oxford, UK, and Waltham, MA: Academic Press; 2014.

45. Gröber H, Erk S, Grigull U. Fundamentals of heat transfer. New York: McGraw-Hill; 1961.

Chapter 7. Conclusions and recommendations

7.1 Conclusions

In the present thesis, different ANSYS modules were used to build a CFD model that was used to investigate the impact of feed spacer filament arrangements on the performance of SWM RO systems over a range of flowrates in the laminar region. The spacer configurations studied were a combination of four commercial spacers, plus five simple geometries with three gap sizes each. Post-processing of the CFD results was categorised into two types, numerical and visual. The former approach was used to discover the correlation between design/operating parameters and performance, and the latter was used to identify the logic behind the observed patterns. The conclusions from the thesis can be summarised as follows:

- Tetrahedral meshing of the fluid domain resulted in faster and more stable convergence, comparing to hexahedral meshing, while a polyhedral-hexahedral approach can make the convergence achievable with minimum required iterations and computational power, compared the other two approaches (Chapter 4 and Chapter 6).
- In the range of flowrates studied ($25 \leq Re \leq 200$), all performance measures were strongly affected by Reynolds number (Re) and the spacer arrangement (Chapter 4, Chapter 5, and Chapter 6).
- Spacer performance ratio (SPMP) did not vary in a consistent way with Reynolds number for the different spacers (Chapter 5).
- The Spacer Configuration Efficacy (SCE) appears to be the best choice for the performance measure because it considers both mass transfer and energy consumption, and has predictable behaviour with Re, in contrast to the current definition of SPMP′ (Chapter 5).
- Power law equations can be used to describe the correlation between performance measures and flowrate as expressed by the Reynolds number. The regression quality for pressure drop, power number, specific power consumption and spacer configuration efficacy is particularly good ($R^2 > 0.999$), and for Sherwood number is acceptable ($R^2 > 0.99$). The correlation form and parameter values are in agreement with previous studies (Chapter 4, Chapter 5, and Chapter 6).

- Different performance measures led to different rankings of the feed spacers and the ranking may change with Reynolds number (Chapter 4, Chapter 5, and Chapter 6). For example, comparing the Ladder41 and Wavy41 spacers based on SCE values, Ladder41 shows better performance at Re values below 120, while Wavy performs better for Re values greater than 120, with the benefits of using Wavy growing with increasing Re (Chapter 4).
- While pressure drop, Pn and SCE show some level of correlation with porosity and D_h/L, Sh shows no consistent correlation with porosity or D_h/L (Chapter 6).
- Despite the coefficients of the Pn-Re and SCE-Re equations showing some correlation with porosity, it was not possible to describe accurately the equation parameters as a function of geometrical properties (Chapter 6).
- Close observation of fluid flow vectors and concentration profiles in the neighbourhood of both latitudinal and longitudinal filaments at the micro-level in the post-processing stage can be a valuable tool to explain the patterns and trends of changes found at the macro-level, and the patterns of changes in the correlation parameters (Chapter 6).
- Flow recirculation, both in the lateral direction (side-washing) and longitudinal direction (backwashing and forward-washing), plays a significant role in mass transfer (Chapter 6).
- According to the measure of SCE, for the nineteen different spacer arrangements studied, Woven46 (closely followed by Woven41 and Woven36) showed the best results through the Re range studied (Chapter 6).
- Overall, the performance analysis and prediction of SWM feed spacers carried out in the current work using CFD indicates that valuable insights can be gained into spacer arrangements with this technique (Chapter 4, Chapter 5, and Chapter 6).
- The following table summarises the relative performance of the studied spacers based on four selected performance measures for Re = 100:

Spacer	ΔP/L	Pn	Sh	SCE
PP45	Low	Low	Moderate	Low
PP60	Low	Low	Moderate	Low
PP90	Low	Low	Low	Low
HDPE90	Low	Low	Moderate	Low
Ladder36	Good	Moderate	Low	Low
Ladder41	Very good	Good	Low	Moderate
Ladder46	Very good	Very good	Low	Moderate
Wavy36	Good	Moderate	Low	Low
Wavy41	Very good	Good	Low	Moderate
Wavy46	Very good	Very good	Low	Moderate
Submerged36	Moderate	Moderate	Low	Low
Submerged41	Good	Good	Low	Moderate
Submerged46	Good	Very good	Low	Moderate
Triple36	Moderate	Low	Low	Low
Triple41	Very good	Low	Low	Low
Triple46	Very good	Low	Low	Low
Woven36	Low	Low	Very good	Moderate
Woven41	Moderate	Moderate	Very good	Very good
Woven46	Moderate	Moderate	Very good	Very good

Performance of spacer, relative to best-performing spacer for the given performance measure.

85% ≤ Very good ≤ 100%
70% ≤ Good < 85%
50% ≤ Moderate < 70%
0% ≤ Low < 50%

Evaluating the equations used to predict RO units' performance may be a step towards implementation of Real-Time Optimisation (RTO) and optimised RO desalination plants' economics. This could involve analysis of the impact of various extra parameters, such as seasonal or daily changes in feed salinity and variations in electrical grid conditions (including real-time fluctuations in energy prices, and peak shaving strategies), base-load management and aiming to optimise the unit economics, while meeting the production goals.

Observations based on CFD results as reported in the current work can prove valuable for designers working towards more efficient feed spacer arrangements employed in desalination plants.

7.2 Recommendations for future research

Based on the findings of this thesis, the following recommendations are proposed for further research:

- In this thesis, a limited number of filament arrangements for two-layer spacers with circular cross-section filaments were studied. Expanding the range of study to

include more filament shapes, arrangements, filament sizes, and variations in the gaps between the filaments is suggested, in order to improve the performance of spacers.

- Further investigation into developing new filament arrangements, emphasising the lessons learnt from HDPE90, Woven and Submerged arrangements with a focus on possible alterations in the gaps between the filaments and the membranes is recommended to investigate the possible impact of enhanced forward-washing streams on the unit's performance.
- Further investigation into defining a performance measure based on the SPMP concept that can show more consistency with changes in flowrate, which could include being independent of flowrate.
- Further investigation into the correlation between porosity and performance measures, based on a wider range of datapoints is suggested to investigate possible correlations that describe the performance measures as a function of Re and ε.
- Further investigation into possible RTO implications and the extent of their benefits, with a focus on productivity, energy consumption, operation and maintenance costs, and a plant's carbon footprint, could benefit the whole desalination industry.

  Notwithstanding the extensive efforts that have been reported in the literature to provide a simplified techno-economic model, SWM purchasing decisions are complicated by a lack of consistency in the outcomes of economic modelling. This arises because the modelled financial outcomes are highly dependent on the simplifying assumptions embedded in the range of models currently in use. On the other hand, the magnitude of changes in the product's unit price reported by present techno-economic models are so small that they can be easily masked by the impact of the model's simplifying assumptions. In other words, variations between the assumptions embedded in the models can lead to contradictory and misleading outcomes. This situation is not entirely satisfactory and further work is recommended to enhance the accuracy of these models, by either evaluating the validity and uniformity of current assumptions or developing a more robust model that can offer higher levels of reliability. This is an essential step for switching from theoretically based performance measures to economic performance measures that will enable the evaluation of feed spacers with more confidence.

Appendices

Appendix I. Attribution tables

A. Kavianipour O, Ingram GD, Vuthaluru HB. *Investigation into the effectiveness of feed spacer configurations for reverse osmosis membrane modules using Computational Fluid Dynamics*. Journal of Membrane Science. 2017; 526:156-71. https://doi.org/10.1016/j.memsci.2016.12.034.

Co-authors: Gordon Ingram, Hari Vuthaluru

	Conception and Design	Acquisition of Data and Method	Data Conditioning and Manipulation	Analysis and Statistical Method	Interpretation and Discussion	Academic and editorial advice	Final approval
Co-Author 1: **Hari Vuthaluru**						☑	☑
Co-Author 1 Acknowledgment: I acknowledge that these represent my contribution to the above research output, and I have approved the final version. Signed:							
Co-Author 2: **Gordon Ingram**						☑	☑
Co-Author 2 Acknowledgment: I acknowledge that these represent my contribution to the above research output, and I have approved the final version. Signed:							

B. Kavianipour O, Ingram GD, Vuthaluru HB. *Investigation into the effectiveness of feed spacer configurations for reverse osmosis membrane modules using Computational Fluid Dynamics*. Journal of Membrane Science. 2017; 526:156-71. https://doi.org/10.1016/j.memsci.2016.12.034.

Co-authors: Gordon Ingram, Hari Vuthaluru

	Conception and Design	Acquisition of Data and Method	Data Conditioning and Manipulation	Analysis and Statistical Method	Interpretation and Discussion	Academic and editorial advice	Final approval
Co-Author 1: **Hari Vuthaluru**						☑	☑
Co-Author 1 Acknowledgment: I acknowledge that these represent my contribution to the above research output, and I have approved the final version. Signed:							
Co-Author 2: **Gordon Ingram**						☑	☑
Co-Author 2 Acknowledgment: I acknowledge that these represent my contribution to the above research output, and I have approved the final version. Signed:							

C. Kavianipour O, Ingram GD, Vuthaluru HB. *Chapter 6.A detailed approach for the analysis and prediction of SWM feed spacer performance based on CFD results*. Submitted to Desalination, currently under reiew for publication.

Co-authors: Gordon Ingram, Hari Vuthaluru

	Conception and Design	Acquisition of Data and Method	Data Conditioning and Manipulation	Analysis and Statistical Method	Interpretation and Discussion	Academic and editorial advice	Final approval
Co-Author 1: **Hari Vuthaluru**						☑	☑
Co-Author 1 Acknowledgment: I acknowledge that these represent my contribution to the above research output, and I have approved the final version. Signed:							
Co-Author 2: **Gordon Ingram**						☑	☑
Co-Author 2 Acknowledgment: I acknowledge that these represent my contribution to the above research output, and I have approved the final version. Signed:							

Appendix II. Copyright permission statements

A. Figure 1-1. Configuration of a typical SWM is obtained from:

> Johnson J, Busch M. *Engineering aspects of reverse osmosis module design*. Desalination and Water Treatment. 2010;15(1-3):236-48; https://doi.org/10.5004/dwt.2010.1756. ©copyright [2010]

The figure is reprinted by permission of Informa UK Limited, trading as Taylor & Taylor & Francis Group, http://www.tandfonline.com

B. Chapter 4 is a reprint of:

> Kavianipour O, Ingram GD, Vuthaluru HB. *Investigation into the effectiveness of feed spacer configurations for reverse osmosis membrane modules using Computational Fluid Dynamics*. Journal of Membrane Science. 2017; 526:156-71. https://doi.org/10.1016/j.memsci.2016.12.034.

As the author of this Elsevier article, https://www.elsevier.com/about/policies/copyright#Author-rights implies that I have the right to include it in a thesis, with no permission required.

C. Chapter 5 is a reprint of:

> Kavianipour O, Ingram GD, Vuthaluru HB. *Studies into the mass transfer and energy consumption of commercial feed spacers for RO membrane modules using CFD: Effectiveness of performance measures.* Chemical Engineering Research and Design. 2019;141:328-38. https://doi.org/10.1016/j.memsci.2016.12.034.

As the author of this Elsevier article, https://www.elsevier.com/about/policies/copyright#Author-rights implies that I have the right to include it in a thesis, with no permission required.

D. Figure 1-1 is reprinted by permission of Informa UK Limited, trading as T aylor & Taylor & Francis Group, as below:

Omid Kavianipour

From: Taylor & Francis Journal Permissions Support <taylorandfrancissupport@tandf.co.uk>
Sent: Saturday, 31 December 2022 1:11 PM
To: Omid Kavianipour
Subject: tdwt20:Engineering Aspects of Reverse Osmosis Module Design

Categories: Thesis permission

Taylor & Francis Group
an informa business

Our Ref: tdwt/02851928

12/31/2022

Dear Requester,

Thank you for your correspondence requesting permission to reproduce content from a Taylor & Francis Group journal content in your thesis to be posted on your university's repository.

We will be pleased to grant free permission on the condition that your acknowledgement must be included showing article title, author, full Journal title, and **© copyright # [year]**, reprinted by permission of Informa UK Limited, trading as Taylor & Taylor & Francis Group, http://www.tandfonline.com

This permission does not cover any third party copyrighted work which may appear in the article by permission. Please ensure you have checked all original source details for the rights holder and if need apply for permission from the original rightsholder.

Please note that this license **does not allow you to post our content on any other third-party websites.**

Please note permission does not provide access to our article, if you are affiliated to an institution and your institution holds a subscription to the content you are requesting you will be able to view the article free of charge, if your institution does not hold a subscription or you are not affiliated to an institution that has a subscription then you will need to purchase this for your own personal use as we do not provide our articles free of charge for research.

Thank you for your interest in our Journal.

With best wishes,

Taylor & Francis Journal Permissions
Web: www.tandfonline.com
4 Park Square, Milton Park, Abingdon, OX14 4RN
(+44 (0)20 8052 0600

1

Appendix III. An example of the ANSYS Fluent's meshing script

This script is taking the domain geometry with SpaceClaim file format –*geometry.scdoc*– as input file and produces a 3-D mesh file that is suitable for Fluent Solver with msh file format –*mesh-output.msh*– that uses polyhedral method on its surfaces and transition layers, and structured hexahedral method for meshing the bulk volume of the domain. Except for the input geometry and output mesh file names, all other parameters were remained unchanged for different geometries.

/file import cad yes "geometry.scdoc" no yes mm

(define global-min 0.02)

(define global-max 1)

(define global-growth-rate 1.25)

(define min-face-size-curv 0.02)

(define max-face-size-curv 1)

(define norm-angle 12)

(define min-prox-size 0.02)

(define max-prox-size 1)

(define prox-gap-cell 5)

(define boi-size 0.04)

(define boi-growth-rate 1.2)

/size-functions set-global-controls global-min global-max global-growth-rate

/scoped-sizing create Curv curvature object-faces-and-edges yes yes body min-face-size-curv max-face-size-curv global-growth-rate norm-angle

/scoped-sizing create Prox proximity object-faces-and-edges yes yes body min-prox-size max-prox-size global-growth-rate prox-gap-cell both no yes

/scoped-sizing create boi boi face-zone y y boi boi-size boi-growth-rate*

/scoped-sizing compute

/file write-size-field "size-field.sf" ok

/file import cad-options tessellation cfd-surface-mesh yes " size-field.sf"

/file import cad yes "geometry.scdoc" no yes 40 yes mm ok

/objects volumetric-regions compute body no

/objects volumetric-regions change-type body (*) fluid

/diagnostics quality general-improve objects (*) skewness 0.9 30 8 y

/diagnostics quality general-improve objects (*) skewness 0.8 30 8 y

/diagnostics quality general-improve objects (*) skewness 0.7 30 8 y

/diagnostics quality general-improve objects (*) skewness 0.6 30 8 y

/diagnostics quality general-improve objects (*) skewness 0.5 30 8 y

/mesh scoped-prisms create control-1 aspect-ratio 20 5 1.4 body fluid-regions selected-labels "top-wall bot-wall"

/parallel auto-partition yes

/mesh auto-mesh body no scoped no poly-h yes yes

/mesh modify auto-node-move (*) (*) 0.90 10 120 yes 3

/mesh modify auto-node-move (*) (*) 0.80 10 120 yes 3

/mesh modify auto-node-move (*) (*) 0.75 10 120 yes 3

/mesh modify auto-node-move (*) (*) 0.70 10 120 yes 3

/mesh modify auto-node-move (*) (*) 0.65 10 120 yes 3

/mesh modify auto-node-move (*) (*) 0.60 10 120 yes 3

/file write-mesh "mesh-output.msh"

/exit

Appendix IV. An example of the ANSYS Fluent's running script

This script loads the Fluent's basic case –*base-case.cas.h5*– as the basis of the model, replaces its mesh with mesh of the desired geometry –*Wavy-3_6.msh*–, defines the inlet mass flowrate to meet the desired Reynolds number and solves the model to the state of convergence. The output files are Fluent's solution and a text file that contains the values for pressure drop and mass transfer.

/file read-case "base-case.cas.h5" ok

/file replace-mesh "Wavy-3_6.msh" ok

/define boundary-conditions mass-flow-inlet inlet yes yes no 6.25314180995313E-05 no 0 no yes no no yes 5 10 no no 0.05

/define boundary-conditions wall bot-wall no no no no 0 n 0.5 no yes no 0.35

/define boundary-conditions wall top-wall no no no no 0 n 0.5 no yes no 0.35

/solve initialize hyb-initialization yes

/solve iterate 2000

/report surface-integrals mass-weighted-avg inlet outlet () salt y Wavy-3.6.txt y

/report surface-integrals area-weighted-avg inlet () pressure y Wavy-3.6.txt y

/file write-case-data "Wavy_3.6_25_0.05_0.35" ok

/exit

Appendix V. CFD model extracted data

Geometry	Re	*L* *(mm)*	Inlet salinity *(w/w)*	Wall concentration *(w/w)*	Outlet salinity *(w/w)*	Pressure drop *(Pa)*	dP/m *(Pa/m)*	Average velocity *(m/s)*	SPC *(W/m^3)*	Pn	Sh	SCE	Q *(m^3/s)*
Plain	25	N/A	0.05	0.35	0.078965	5.933218	144.7126	0.012523	1.81217	1805.6519	19.86244	0.011	5.13424E-08
Plain	25	N/A	0.05	1	0.172051	5.740925	140.0226	0.012523	1.753438	1747.1316	26.88053	0.015386	5.13424E-08
Plain	25	N/A	0	0.35	0.033735	6.089383	148.5215	0.012523	1.859867	1853.1776	19.82685	0.010699	5.13424E-08
Plain	25	N/A	0	1	0.128103	5.894129	143.7592	0.012523	1.800231	1793.7559	26.79737	0.014939	5.13424E-08
Plain	50	N/A	0.05	0.35	0.068294	12.17063	296.8446	0.025045	7.434498	7407.7578	24.62918	0.003325	1.02685E-07
Plain	50	N/A	0.05	1	0.127521	11.90172	290.2859	0.025045	7.270234	7244.0847	33.3119	0.004598	1.02685E-07
Plain	50	N/A	0	0.35	0.02153	12.49509	304.7582	0.025045	7.632694	7605.2408	24.85194	0.003268	1.02685E-07
Plain	50	N/A	0	1	0.082112	12.21901	298.0247	0.025045	7.464053	7437.2066	33.52958	0.004508	1.02685E-07
Plain	75	N/A	0.05	0.35	0.064087	18.64622	454.7859	0.037568	17.08523	17023.774	28.24422	0.001659	1.54027E-07
Plain	75	N/A	0.05	1	0.109762	18.30736	446.5209	0.037568	16.77473	16714.393	38.1494	0.002282	1.54027E-07
Plain	75	N/A	0	0.35	0.016706	19.14585	466.972	0.037568	17.54303	17479.929	28.72067	0.001643	1.54027E-07
Plain	75	N/A	0	1	0.063708	18.79599	458.4388	0.037568	17.22245	17160.51	38.65081	0.002252	1.54027E-07
Plain	100	N/A	0.05	0.35	0.061715	25.33266	617.8697	0.05009	30.94919	30837.875	31.19089	0.001011	2.0537E-07
Plain	100	N/A	0.05	1	0.099705	24.92652	607.964	0.05009	30.45301	30343.482	42.07585	0.001387	2.0537E-07
Plain	100	N/A	0	0.35	0.013964	26.01358	634.4775	0.05009	31.78108	31666.774	31.88165	0.001007	2.0537E-07
Plain	100	N/A	0	1	0.053239	25.59295	624.2182	0.05009	31.26719	31154.733	42.83384	0.001375	2.0537E-07
Plain	150	N/A	0.05	0.35	0.059043	39.25429	957.4216	0.075135	71.9361	71677.367	35.95239	0.000502	3.08054E-07
Plain	150	N/A	0.05	1	0.088371	38.71604	944.2936	0.075135	70.94973	70694.541	48.42538	0.000685	3.08054E-07
Plain	150	N/A	0	0.35	0.010909	40.31267	983.2359	0.075135	73.87567	73609.958	37.19439	0.000505	3.08054E-07
Plain	150	N/A	0	1	0.041514	39.75256	969.5747	0.075135	72.84923	72587.212	49.80134	0.000686	3.08054E-07
Plain	200	N/A	0.05	0.35	0.057517	53.80196	1312.243	0.10018	131.4609	130988.1	39.74339	0.000303	4.10739E-07
Plain	200	N/A	0.05	1	0.081902	53.1336	1295.941	0.10018	129.8278	129360.87	53.49678	0.000414	4.10739E-07
Plain	200	N/A	0	0.35	0.009153	55.25466	1347.675	0.10018	135.0105	134524.88	41.50205	0.000309	4.10739E-07
Plain	200	N/A	0	1	0.034789	54.55552	1330.622	0.10018	133.3022	132822.73	55.45514	0.000418	4.10739E-07
45-PP	25	N/A	0.05	0.35	0.092106	158.108	3274.813	0.022027	72.13313	159224.25	20.84261	0.000131	1.28562E-07
45-PP	25	N/A	0.05	1	0.225674	151.3131	3134.074	0.022027	69.03312	152381.4	28.13536	0.000185	1.28562E-07
45-PP	25	N/A	0	0.35	0.04904	162.1953	3359.471	0.022027	73.99787	163340.43	20.8046	0.000127	1.28562E-07
45-PP	25	N/A	0	1	0.184422	155.3091	3216.841	0.022027	70.8562	156405.6	28.05188	0.000179	1.28562E-07
45-PP	50	N/A	0.05	0.35	0.084699	449.5063	9310.403	0.044053	410.1539	905359.91	33.90237	3.74E-05	2.57125E-07
45-PP	50	N/A	0.05	1	0.195379	434.845	9006.731	0.044053	396.7761	875830.28	45.76295	5.23E-05	2.57125E-07
45-PP	50	N/A	0	0.35	0.040386	461.333	9555.365	0.044053	420.9452	929180.41	33.81666	3.64E-05	2.57125E-07
45-PP	50	N/A	0	1	0.152503	446.4782	9247.684	0.044053	407.3909	899260.95	45.59219	5.07E-05	2.57125E-07
45-PP	75	N/A	0.05	0.35	0.080908	877.7213	18179.81	0.06608	1201.321	2651755.1	44.996	1.7E-05	3.85687E-07
45-PP	75	N/A	0.05	1	0.179702	852.6784	17661.11	0.06608	1167.045	2576095.9	60.69982	2.36E-05	3.85687E-07

Geometry	Re	*L* *(mm)*	Inlet salinity *(w/w)*	Wall concentration *(w/w)*	Outlet salinity *(w/w)*	Pressure drop *(Pa)*	dP/m *(Pa/m)*	Average velocity *(m/s)*	SPC *(W/m^3)*	Pn	Sh	SCE	Q *(m^3/s)*
45-PP	75	N/A	0	0.35	0.035969	900.969	18661.33	0.06608	1233.139	2721990.4	44.87659	1.65E-05	3.85687E-07
45-PP	75	N/A	0	1	0.136028	875.601	18135.9	0.06608	1198.419	2645349.4	60.46089	2.29E-05	3.85687E-07
45-PP	100	N/A	0.05	0.35	0.078448	1438.101	29786.68	0.088107	2624.402	5793017	54.98133	9.49E-06	5.14249E-07
45-PP	100	N/A	0.05	1	0.169435	1401.536	29029.34	0.088107	2557.675	5645726.7	74.09627	1.31E-05	5.14249E-07
45-PP	100	N/A	0	0.35	0.033104	1476.377	30579.47	0.088107	2694.252	5947201.9	54.8341	9.22E-06	5.14249E-07
45-PP	100	N/A	0	1	0.125241	1439.317	29811.87	0.088107	2626.622	5797916.9	73.79478	1.27E-05	5.14249E-07
45-PP	150	N/A	0.05	0.35	0.075108	2949.708	61095.85	0.13216	8074.419	17823201	72.36632	4.06E-06	7.71374E-07
45-PP	150	N/A	0.05	1	0.155829	2879.723	59646.3	0.13216	7882.847	17400332	97.73617	5.62E-06	7.71374E-07
45-PP	150	N/A	0	0.35	0.029437	3024.458	62644.11	0.13216	8279.037	18274870	72.74038	3.98E-06	7.71374E-07
45-PP	150	N/A	0	1	0.110255	2987.897	61886.85	0.13216	8178.958	18053958	96.6738	5.35E-06	7.71374E-07
45-PP	200	N/A	0.05	0.35	0.073989	4828.703	100014.6	0.176213	17623.88	38902363	92.01163	2.37E-06	1.0285E-06
45-PP	200	N/A	0.05	1	0.147049	4685.08	97039.76	0.176213	17099.68	37745264	118.9212	3.15E-06	1.0285E-06
45-PP	200	N/A	0	0.35	0.027554	4956.162	102654.5	0.176213	18089.08	39929232	90.52921	2.27E-06	1.0285E-06
45-PP	200	N/A	0	1	0.103739	4824.507	99927.65	0.176213	17608.57	38868560	120.8638	3.11E-06	1.0285E-06
60-PP	25	N/A	0.05	0.35	0.094352	169.5089	3510.954	0.019999	70.21583	154992.07	22.05536	0.000142	1.16791E-07
60-PP	25	N/A	0.05	1	0.235809	161.7059	3349.335	0.019999	66.9836	147857.37	29.95054	0.000203	1.16791E-07
60-PP	25	N/A	0	0.35	0.051923	173.8525	3600.922	0.019999	72.0151	158963.73	22.13765	0.000139	1.16791E-07
60-PP	25	N/A	0	1	0.195721	165.9078	3436.366	0.019999	68.72414	151699.37	29.97312	0.000198	1.16791E-07
60-PP	50	N/A	0.05	0.35	0.083536	457.2202	9470.177	0.039998	378.7896	836127.43	32.71682	3.91E-05	2.33581E-07
60-PP	50	N/A	0.05	1	0.191761	441.8679	9152.193	0.039998	366.0708	808052.41	44.55612	5.51E-05	2.33581E-07
60-PP	50	N/A	0	0.35	0.039451	469.1856	9718.012	0.039998	388.7025	858008.9	33.00494	3.85E-05	2.33581E-07
60-PP	50	N/A	0	1	0.149262	453.5427	9394.007	0.039998	375.7429	829402.35	44.569	5.37E-05	2.33581E-07
60-PP	75	N/A	0.05	0.35	0.079555	862.2521	17859.41	0.059997	1071.515	2365225.8	42.94705	1.82E-05	3.50372E-07
60-PP	75	N/A	0.05	1	0.175185	836.8585	17333.44	0.059997	1039.958	2295569.1	58.46793	2.55E-05	3.50372E-07
60-PP	75	N/A	0	0.35	0.034631	884.9702	18329.95	0.059997	1099.746	2427543.4	43.14421	1.78E-05	3.50372E-07
60-PP	75	N/A	0	1	0.131881	859.0447	17792.97	0.059997	1067.529	2356427.6	58.51909	2.48E-05	3.50372E-07
60-PP	100	N/A	0.05	0.35	0.077494	1385.032	28687.48	0.079996	2294.893	5065669	53.0771	1.05E-05	4.67163E-07
60-PP	100	N/A	0.05	1	0.166195	1347.167	27903.21	0.079996	2232.153	4927180.8	71.99437	1.46E-05	4.67163E-07
60-PP	100	N/A	0	0.35	0.032217	1421.63	29445.53	0.079996	2355.533	5199525	53.32166	1.03E-05	4.67163E-07
60-PP	100	N/A	0	1	0.122478	1382.954	28644.44	0.079996	2291.449	5058068.1	72.09935	1.43E-05	4.67163E-07
60-PP	150	N/A	0.05	0.35	0.07451	2807.247	58145.13	0.119994	6977.093	15401003	70.6067	4.58E-06	7.00744E-07
60-PP	150	N/A	0.05	1	0.154459	2739.43	56740.47	0.119994	6808.542	15028948	96.44972	6.42E-06	7.00744E-07
60-PP	150	N/A	0	0.35	0.028667	2881.539	59683.9	0.119994	7161.737	15808579	70.79365	4.48E-06	7.00744E-07
60-PP	150	N/A	0	1	0.108993	2817.089	58348.98	0.119994	7001.553	15454995	95.55502	6.18E-06	7.00744E-07
60-PP	200	N/A	0.05	0.35	0.072507	4818.813	99809.71	0.159993	15968.82	35249028	86.14989	2.44E-06	9.34326E-07
60-PP	200	N/A	0.05	1	0.143612	4696.737	97281.21	0.159993	15564.27	34356058	114.5536	3.33E-06	9.34326E-07
60-PP	200	N/A	0	0.35	0.026316	4913.012	101760.8	0.159993	16280.98	35938084	86.34757	2.4E-06	9.34326E-07

Geometry	Re	*L* *(mm)*	Inlet salinity *(w/w)*	Wall concentration *(w/w)*	Outlet salinity *(w/w)*	Pressure drop *(Pa)*	dP/m *(Pa/m)*	Average velocity *(m/s)*	SPC *(W/m^3)*	Pn	Sh	SCE	Q *(m^3/s)*
60-PP	200	N/A	0	1	0.097342	4790.727	99227.99	0.159993	15875.74	35043587	113.0907	3.23E-06	9.34326E-07
90-PP	25	N/A	0.05	0.35	0.063343	44.83348	1902.949	0.025941	49.36471	641011.93	16.54009	2.58E-05	2.1351E-07
90-PP	25	N/A	0.05	1	0.10664	44.2147	1876.685	0.025941	48.68339	632164.87	22.34599	3.53E-05	2.1351E-07
90-PP	25	N/A	0	0.35	0.015603	46.04739	1954.473	0.025941	50.70131	658367.98	16.57971	2.52E-05	2.1351E-07
90-PP	25	N/A	0	1	0.0597	45.41615	1927.68	0.025941	50.00627	649342.71	22.37618	3.45E-05	2.1351E-07
90-PP	50	N/A	0.05	0.35	0.059845	110.7441	4700.515	0.051882	243.8737	3166754.7	24.26284	7.66E-06	4.27019E-07
90-PP	50	N/A	0.05	1	0.091842	109.6027	4652.065	0.051882	241.3599	3134113.5	32.75214	1.05E-05	4.27019E-07
90-PP	50	N/A	0	0.35	0.01157	113.7575	4828.415	0.051882	250.5094	3252921	24.44511	7.51E-06	4.27019E-07
90-PP	50	N/A	0	1	0.04427	112.5865	4778.715	0.051882	247.9308	3219438.3	32.92422	1.02E-05	4.27019E-07
90-PP	75	N/A	0.05	0.35	0.058274	196.7391	8350.555	0.077823	649.8693	8438700.3	30.50788	3.62E-06	6.40529E-07
90-PP	75	N/A	0.05	1	0.085161	194.9928	8276.433	0.077823	644.1009	8363796.1	41.13596	4.92E-06	6.40529E-07
90-PP	75	N/A	0	0.35	0.009771	202.1026	8578.208	0.077823	667.5861	8668756.5	30.88593	3.56E-06	6.40529E-07
90-PP	75	N/A	0	1	0.037339	200.3055	8501.93	0.077823	661.6499	8591673.4	41.50654	4.83E-06	6.40529E-07
90-PP	100	N/A	0.05	0.35	0.057311	301.288	12788.12	0.103765	1326.954	17230804	35.88533	2.08E-06	8.54039E-07
90-PP	100	N/A	0.05	1	0.081069	298.8884	12686.26	0.103765	1316.386	17093567	48.35884	2.83E-06	8.54039E-07
90-PP	100	N/A	0	0.35	0.008665	309.5115	13137.16	0.103765	1363.173	17701109	36.46179	2.06E-06	8.54039E-07
90-PP	100	N/A	0	1	0.033129	307.0336	13031.99	0.103765	1352.259	17559395	48.99783	2.79E-06	8.54039E-07
90-PP	150	N/A	0.05	0.35	0.05626	568.3918	24125.29	0.155647	3755.028	48759892	46.00611	9.44E-07	1.28106E-06
90-PP	150	N/A	0.05	1	0.076565	564.4339	23957.29	0.155647	3728.88	48420357	61.87456	1.28E-06	1.28106E-06
90-PP	150	N/A	0	0.35	0.007437	583.9317	24784.88	0.155647	3857.691	50092995	46.85393	9.35E-07	1.28106E-06
90-PP	150	N/A	0	1	0.028373	579.841	24611.25	0.155647	3830.666	49742065	62.79305	1.26E-06	1.28106E-06
90-PP	200	N/A	0.05	0.35	0.055718	909.9577	38622.99	0.207529	8015.402	104081811	55.98385	5.38E-07	1.70808E-06
90-PP	200	N/A	0.05	1	0.074235	904.4069	38387.39	0.207529	7966.508	103446910	75.16992	7.27E-07	1.70808E-06
90-PP	200	N/A	0	0.35	0.006789	934.8976	39681.56	0.207529	8235.087	106934467	56.97564	5.33E-07	1.70808E-06
90-PP	200	N/A	0	1	0.025945	929.1111	39435.95	0.207529	8184.116	106272598	76.46555	7.2E-07	1.70808E-06
90-HDPE	25	N/A	0.05	0.35	0.075888	30.58699	1322.052	0.022114	29.23586	29130.71	27.63114	0.000949	1.506E-07
90-HDPE	25	N/A	0.05	1	0.158661	29.70774	1284.048	0.022114	28.39546	28293.326	37.17038	0.001314	1.506E-07
90-HDPE	25	N/A	0	0.35	0.030206	31.39571	1357.007	0.022114	30.00886	29900.922	27.63413	0.000924	1.506E-07
90-HDPE	25	N/A	0	1	0.114303	30.5014	1318.352	0.022114	29.15405	29049.191	37.14375	0.001279	1.506E-07
90-HDPE	50	N/A	0.05	0.35	0.067421	73.16875	3162.55	0.044228	139.8733	139370.21	36.64853	0.000263	3.01201E-07
90-HDPE	50	N/A	0.05	1	0.123424	71.71581	3099.75	0.044228	137.0958	136602.68	49.26407	0.000361	3.01201E-07
90-HDPE	50	N/A	0	0.35	0.020355	75.13077	3247.353	0.044228	143.624	143107.42	36.70447	0.000256	3.01201E-07
90-HDPE	50	N/A	0	1	0.077385	73.64825	3183.275	0.044228	140.7899	140283.55	49.32822	0.000352	3.01201E-07
90-HDPE	75	N/A	0.05	0.35	0.063951	123.8178	5351.738	0.066342	355.0452	353768.16	43.76217	0.000124	4.51801E-07
90-HDPE	75	N/A	0.05	1	0.108935	121.8503	5266.697	0.066342	349.4034	348146.65	58.84751	0.000169	4.51801E-07
90-HDPE	75	N/A	0	0.35	0.016344	127.1575	5496.09	0.066342	364.6217	363310.27	43.9475	0.000121	4.51801E-07
90-HDPE	75	N/A	0	1	0.062298	125.143	5409.015	0.066342	358.845	357554.3	59.10304	0.000165	4.51801E-07

Geometry	Re	*L* *(mm)*	Inlet salinity *(w/w)*	Wall concentration *(w/w)*	Outlet salinity *(w/w)*	Pressure drop *(Pa)*	dP/m *(Pa/m)*	Average velocity *(m/s)*	SPC *(W/m^3)*	Pn	Sh	SCE	Q *(m^3/s)*
90-HDPE	100	N/A	0.05	0.35	0.062011	180.5078	7802.029	0.088456	690.1366	687654.32	50.06757	7.28E-05	6.02401E-07
90-HDPE	100	N/A	0.05	1	0.100784	178.0349	7695.147	0.088456	680.6822	678233.98	67.31281	9.92E-05	6.02401E-07
90-HDPE	100	N/A	0	0.35	0.014123	185.3908	8013.087	0.088456	708.8059	706256.53	50.46959	7.15E-05	6.02401E-07
90-HDPE	100	N/A	0	1	0.05376	182.8545	7903.461	0.088456	699.1088	696594.32	67.70515	9.72E-05	6.02401E-07
90-HDPE	150	N/A	0.05	0.35	0.059922	312.5742	13510.29	0.132684	1792.601	1786153.1	61.82243	3.46E-05	9.03602E-07
90-HDPE	150	N/A	0.05	1	0.091959	308.9193	13352.32	0.132684	1771.64	1765267.8	83.02741	4.7E-05	9.03602E-07
90-HDPE	150	N/A	0	0.35	0.011703	321.054	13876.82	0.132684	1841.232	1834609.9	62.51535	3.41E-05	9.03602E-07
90-HDPE	150	N/A	0	1	0.044532	317.2954	13714.36	0.132684	1819.677	1813131.7	83.72855	4.62E-05	9.03602E-07
90-HDPE	200	N/A	0.05	0.35	0.058698	470.7592	20347.47	0.176912	3599.714	3586766.6	72.11163	2.01E-05	1.2048E-06
90-HDPE	200	N/A	0.05	1	0.086779	465.7746	20132.03	0.176912	3561.599	3548788.6	96.76566	2.73E-05	1.2048E-06
90-HDPE	200	N/A	0	0.35	0.010314	483.5475	20900.22	0.176912	3697.501	3684202.2	73.3089	1.99E-05	1.2048E-06
90-HDPE	200	N/A	0	1	0.039184	478.409	20678.12	0.176912	3658.209	3645051.3	97.96335	2.69E-05	1.2048E-06
Submerged	25	3.6	0.05	0.35	0.083095	32.75289	909.8024	0.016135	14.67925	14626.448	24.6144	0.001683	5.49163E-08
Submerged	25	3.6	0.05	1	0.188568	31.59921	877.7557	0.016135	14.16219	14111.248	33.16909	0.002351	5.49163E-08
Submerged	25	3.6	0	0.35	0.038535	33.61088	933.6356	0.016135	15.06378	15009.601	24.56328	0.001637	5.49163E-08
Submerged	25	3.6	0	1	0.145356	32.44203	901.1675	0.016135	14.53992	14487.628	33.04523	0.002281	5.49163E-08
Submerged	50	3.6	0.05	0.35	0.070943	69.46846	1929.68	0.032269	62.26899	62045.022	30.4997	0.000492	1.09833E-07
Submerged	50	3.6	0.05	1	0.137987	67.81209	1883.669	0.032269	60.78428	60565.654	40.94747	0.000676	1.09833E-07
Submerged	50	3.6	0	0.35	0.024392	71.32202	1981.167	0.032269	63.93045	63700.503	30.44488	0.000478	1.09833E-07
Submerged	50	3.6	0	1	0.092316	69.6425	1934.514	0.032269	62.42499	62200.461	40.80742	0.000656	1.09833E-07
Submerged	75	3.6	0.05	0.35	0.066085	111.276	3090.999	0.048404	149.6155	149077.4	34.84447	0.000234	1.64749E-07
Submerged	75	3.6	0.05	1	0.117688	109.094	3030.39	0.048404	146.6818	146154.27	46.72716	0.00032	1.64749E-07
Submerged	75	3.6	0	0.35	0.018734	114.2651	3174.031	0.048404	153.6346	153082.04	34.78305	0.000227	1.64749E-07
Submerged	75	3.6	0	1	0.071016	112.0516	3112.544	0.048404	150.6584	150116.51	46.56785	0.00031	1.64749E-07
Submerged	100	3.6	0.05	0.35	0.063399	158.6448	4406.801	0.064538	284.4069	283383.92	38.5233	0.000136	2.19665E-07
Submerged	100	3.6	0.05	1	0.106441	155.9016	4330.6	0.064538	279.489	278483.74	51.63392	0.000185	2.19665E-07
Submerged	100	3.6	0	0.35	0.015604	162.9222	4525.618	0.064538	292.0751	291024.55	38.4538	0.000132	2.19665E-07
Submerged	100	3.6	0	1	0.059211	160.1385	4448.291	0.064538	287.0845	286051.96	51.45459	0.00018	2.19665E-07
Submerged	150	3.6	0.05	0.35	0.060407	269.653	7490.361	0.096807	725.1213	722513.19	44.65327	6.18E-05	3.29498E-07
Submerged	150	3.6	0.05	1	0.093889	265.739	7381.638	0.096807	714.596	712025.79	59.81903	8.4E-05	3.29498E-07
Submerged	150	3.6	0	0.35	0.012122	276.9548	7693.189	0.096807	744.7564	742077.71	44.58021	6.01E-05	3.29498E-07
Submerged	150	3.6	0	1	0.046052	272.9796	7582.765	0.096807	734.0666	731426.38	59.62429	8.15E-05	3.29498E-07
Submerged	200	3.6	0.05	0.35	0.058705	400.2249	11117.36	0.129076	1434.988	1429826.5	49.6572	3.47E-05	4.39331E-07
Submerged	200	3.6	0.05	1	0.086741	395.1086	10975.24	0.129076	1416.643	1411548.1	66.51324	4.71E-05	4.39331E-07
Submerged	200	3.6	0	0.35	0.010143	411.0907	11419.19	0.129076	1473.947	1468645.3	49.59308	3.38E-05	4.39331E-07
Submerged	200	3.6	0	1	0.038562	405.891	11274.75	0.129076	1455.303	1450068.9	66.31572	4.57E-05	4.39331E-07
Submerged	25	4.1	0.05	0.35	0.086051	32.82623	800.6397	0.015672	12.54754	12502.411	23.83316	0.001906	6.11776E-08

Geometry	Re	*L* *(mm)*	Inlet salinity *(w/w)*	Wall concentration *(w/w)*	Outlet salinity *(w/w)*	Pressure drop *(Pa)*	dP/m *(Pa/m)*	Average velocity *(m/s)*	SPC *(W/m^3)*	Pn	Sh	SCE	Q *(m^3/s)*
Submerged	25	4.1	0.05	1	0.200771	31.57524	770.1279	0.015672	12.06936	12025.953	32.13457	0.002672	6.11776E-08
Submerged	25	4.1	0	0.35	0.041979	33.68191	821.5101	0.015672	12.87462	12828.313	23.78471	0.001854	6.11776E-08
Submerged	25	4.1	0	1	0.158168	32.41417	790.5896	0.015672	12.39004	12345.473	32.0161	0.002593	6.11776E-08
Submerged	50	4.1	0.05	0.35	0.072768	69.4684	1694.351	0.031344	53.10739	52916.378	29.41033	0.000556	1.22355E-07
Submerged	50	4.1	0.05	1	0.145593	67.68707	1650.904	0.031344	51.74559	51559.474	39.50246	0.000766	1.22355E-07
Submerged	50	4.1	0	0.35	0.02652	71.3164	1739.424	0.031344	54.52015	54324.055	29.36169	0.00054	1.22355E-07
Submerged	50	4.1	0	1	0.100303	69.50985	1695.362	0.031344	53.13908	52947.947	39.36943	0.000744	1.22355E-07
Submerged	75	4.1	0.05	0.35	0.067455	110.9786	2706.796	0.047016	127.2619	126804.13	33.51293	0.000264	1.83533E-07
Submerged	75	4.1	0.05	1	0.123415	108.6483	2649.96	0.047016	124.5897	124141.55	44.95399	0.000362	1.83533E-07
Submerged	75	4.1	0	0.35	0.020334	113.953	2779.341	0.047016	130.6726	130202.61	33.46103	0.000257	1.83533E-07
Submerged	75	4.1	0	1	0.077035	111.5885	2721.672	0.047016	127.9613	127501.02	44.80622	0.000351	1.83533E-07
Submerged	100	4.1	0.05	0.35	0.064521	157.841	3849.78	0.062688	241.3334	240465.41	36.98619	0.000154	2.4471E-07
Submerged	100	4.1	0.05	1	0.111134	154.9267	3778.7	0.062688	236.8776	236025.59	49.57835	0.00021	2.4471E-07
Submerged	100	4.1	0	0.35	0.016914	162.0886	3953.38	0.062688	247.8279	246936.48	36.92494	0.00015	2.4471E-07
Submerged	100	4.1	0	1	0.064143	159.1309	3881.242	0.062688	243.3057	242430.59	49.41243	0.000204	2.4471E-07
Submerged	150	4.1	0.05	0.35	0.061267	267.3886	6521.673	0.094031	613.2419	611036.19	42.80873	7.01E-05	3.67066E-07
Submerged	150	4.1	0.05	1	0.097488	263.2493	6420.715	0.094031	603.7486	601577.09	57.3418	9.53E-05	3.67066E-07
Submerged	150	4.1	0	0.35	0.013124	274.6179	6697.998	0.094031	629.8219	627556.58	42.74183	6.81E-05	3.67066E-07
Submerged	150	4.1	0	1	0.049832	270.4138	6595.459	0.094031	620.1801	617949.45	57.15934	9.25E-05	3.67066E-07
Submerged	200	4.1	0.05	0.35	0.059427	396.1818	9662.97	0.125375	1211.496	1207138.9	47.60914	3.94E-05	4.89421E-07
Submerged	200	4.1	0.05	1	0.089765	390.7858	9531.36	0.125375	1194.996	1190697.8	63.7566	5.35E-05	4.89421E-07
Submerged	200	4.1	0	0.35	0.010986	406.9233	9924.959	0.125375	1244.343	1239867.8	47.55401	3.84E-05	4.89421E-07
Submerged	200	4.1	0	1	0.041743	401.4387	9791.187	0.125375	1227.572	1223156.4	63.57718	5.2E-05	4.89421E-07
Submerged	25	4.6	0.05	0.35	0.086545	32.64942	709.7701	0.015314	10.86964	10830.544	21.67038	0.002001	6.74389E-08
Submerged	25	4.6	0.05	1	0.202643	31.37952	682.1634	0.015314	10.44686	10409.288	29.18704	0.002804	6.74389E-08
Submerged	25	4.6	0	0.35	0.042492	33.49982	728.2569	0.015314	11.15275	11112.638	21.59239	0.001943	6.74389E-08
Submerged	25	4.6	0	1	0.159942	32.21349	700.2932	0.015314	10.72451	10685.935	29.042	0.002718	6.74389E-08
Submerged	50	4.6	0.05	0.35	0.072878	69.04919	1501.069	0.030629	45.97568	45810.318	26.48994	0.000578	1.34878E-07
Submerged	50	4.6	0.05	1	0.146022	67.24266	1461.797	0.030629	44.77283	44611.79	35.56847	0.000797	1.34878E-07
Submerged	50	4.6	0	0.35	0.026624	70.88485	1540.975	0.030629	47.19794	47028.177	26.42008	0.000562	1.34878E-07
Submerged	50	4.6	0	1	0.100709	69.05193	1501.129	0.030629	45.97751	45812.136	35.43256	0.000773	1.34878E-07
Submerged	75	4.6	0.05	0.35	0.06751	110.1272	2394.07	0.045943	109.9906	109594.98	30.13056	0.000275	2.02317E-07
Submerged	75	4.6	0.05	1	0.123684	107.7568	2342.54	0.045943	107.6232	107236.06	40.44031	0.000377	2.02317E-07
Submerged	75	4.6	0	0.35	0.020423	113.0748	2458.147	0.045943	112.9345	112528.27	30.12281	0.000268	2.02317E-07
Submerged	75	4.6	0	1	0.077419	110.664	2405.739	0.045943	110.5267	110129.15	40.36235	0.000367	2.02317E-07
Submerged	100	4.6	0.05	0.35	0.06455	156.281	3397.414	0.061257	208.1162	207367.66	33.21363	0.00016	2.69755E-07
Submerged	100	4.6	0.05	1	0.111338	153.305	3332.716	0.061257	204.153	203418.72	44.58458	0.000219	2.69755E-07

Geometry	Re	*L* *(mm)*	Inlet salinity *(w/w)*	Wall concentration *(w/w)*	Outlet salinity *(w/w)*	Pressure drop *(Pa)*	dP/m *(Pa/m)*	Average velocity *(m/s)*	SPC *(W/m^3)*	Pn	Sh	SCE	Q *(m^3/s)*
Submerged	100	4.6	0	0.35	0.016953	160.4827	3488.754	0.061257	213.7115	212942.8	33.16947	0.000156	2.69755E-07
Submerged	100	4.6	0	1	0.064384	157.4599	3423.041	0.061257	209.686	208931.85	44.45397	0.000213	2.69755E-07
Submerged	150	4.6	0.05	0.35	0.061297	263.7002	5732.613	0.091886	526.7461	524851.47	38.46815	7.33E-05	4.04633E-07
Submerged	150	4.6	0.05	1	0.097711	259.4303	5639.789	0.091886	518.2169	516353	51.6366	0.0001	4.04633E-07
Submerged	150	4.6	0	0.35	0.013169	270.8216	5887.426	0.091886	540.9712	539025.44	38.4375	7.13E-05	4.04633E-07
Submerged	150	4.6	0	1	0.050105	266.4826	5793.1	0.091886	532.304	530389.46	51.51335	9.71E-05	4.04633E-07
Submerged	200	4.6	0.05	0.35	0.059488	389.7699	8473.26	0.122514	1038.097	1034363.2	42.94909	4.15E-05	5.39511E-07
Submerged	200	4.6	0.05	1	0.090124	384.146	8351.001	0.122514	1023.119	1019438.6	57.66349	5.66E-05	5.39511E-07
Submerged	200	4.6	0	0.35	0.011065	400.3251	8702.718	0.122514	1066.209	1062374.2	42.92829	4.04E-05	5.39511E-07
Submerged	200	4.6	0	1	0.042144	394.6098	8578.475	0.122514	1050.987	1047207.3	57.53543	5.49E-05	5.39511E-07
Triple	25	3.6	0.05	0.35	0.072856	21.82994	606.3871	0.015098	9.155116	46181.071	23.37634	0.000506	7.19408E-08
Triple	25	3.6	0.05	1	0.145378	21.22063	589.4618	0.015098	8.899581	44892.082	31.19716	0.000695	7.19408E-08
Triple	25	3.6	0	0.35	0.026639	22.40826	622.4516	0.015098	9.397655	47404.509	23.35191	0.000493	7.19408E-08
Triple	25	3.6	0	1	0.100203	21.79038	605.2882	0.015098	9.138525	46097.382	31.13363	0.000675	7.19408E-08
Triple	50	3.6	0.05	0.35	0.066225	54.87227	1524.23	0.030196	46.02505	232163.78	32.8117	0.000141	1.43882E-07
Triple	50	3.6	0.05	1	0.118533	53.82162	1495.045	0.030196	45.14381	227718.51	44.17608	0.000194	1.43882E-07
Triple	50	3.6	0	0.35	0.018893	56.34761	1565.211	0.030196	47.26252	238405.93	32.74766	0.000137	1.43882E-07
Triple	50	3.6	0	1	0.071941	55.28281	1535.634	0.030196	46.3694	233900.76	44.04916	0.000188	1.43882E-07
Triple	75	3.6	0.05	0.35	0.062687	96.23608	2673.224	0.045293	121.0795	610760.2	38.25222	6.26E-05	2.15822E-07
Triple	75	3.6	0.05	1	0.103848	94.84505	2634.585	0.045293	119.3294	601932.05	51.65121	8.58E-05	2.15822E-07
Triple	75	3.6	0	0.35	0.01477	98.84252	2745.626	0.045293	124.3588	627301.92	38.17039	6.08E-05	2.15822E-07
Triple	75	3.6	0	1	0.056517	97.43121	2706.422	0.045293	122.5831	618345.06	51.49571	8.33E-05	2.15822E-07
Triple	100	3.6	0.05	0.35	0.061108	143.9543	3998.732	0.060391	241.4883	1218137.5	44.53811	3.66E-05	2.87763E-07
Triple	100	3.6	0.05	1	0.097223	142.1279	3947.998	0.060391	238.4245	1202682.5	60.17871	5E-05	2.87763E-07
Triple	100	3.6	0	0.35	0.012931	147.8631	4107.309	0.060391	248.0455	1251213.6	44.43788	3.55E-05	2.87763E-07
Triple	100	3.6	0	1	0.049552	146.0082	4055.782	0.060391	244.9337	1235516.9	59.98454	4.86E-05	2.87763E-07
Triple	150	3.6	0.05	0.35	0.059357	260.6033	7238.979	0.090587	655.7563	3307826	56.10561	1.7E-05	4.31645E-07
Triple	150	3.6	0.05	1	0.089824	257.3349	7148.192	0.090587	647.5321	3266340.8	75.82238	2.32E-05	4.31645E-07
Triple	150	3.6	0	0.35	0.010896	267.6148	7433.744	0.090587	673.3994	3396823	55.99752	1.65E-05	4.31645E-07
Triple	150	3.6	0	1	0.041785	264.1813	7338.371	0.090587	664.7599	3353242.4	75.57329	2.25E-05	4.31645E-07
Triple	200	3.6	0.05	0.35	0.058459	412.2614	11451.7	0.120782	1383.165	6977087.6	67.52719	9.68E-06	5.75526E-07
Triple	200	3.6	0.05	1	0.086058	408.4689	11346.36	0.120782	1370.441	6912904.1	91.35078	1.32E-05	5.75526E-07
Triple	200	3.6	0	0.35	0.009851	423.5299	11764.72	0.120782	1420.972	7167795.4	67.402	9.4E-06	5.75526E-07
Triple	200	3.6	0	1	0.037838	419.6981	11658.28	0.120782	1408.116	7102946.4	91.0627	1.28E-05	5.75526E-07
Triple	25	4.1	0.05	0.35	0.074516	18.24432	444.9834	0.013777	6.130748	30925.278	22.69519	0.000734	7.68538E-08
Triple	25	4.1	0.05	1	0.152308	17.66238	430.7897	0.013777	5.935194	29938.847	30.31927	0.001013	7.68538E-08
Triple	25	4.1	0	0.35	0.028586	18.72434	456.6912	0.013777	6.292052	31738.944	22.68272	0.000715	7.68538E-08

Geometry	Re	*L* *(mm)*	Inlet salinity *(w/w)*	Wall concentration *(w/w)*	Outlet salinity *(w/w)*	Pressure drop *(Pa)*	dP/m *(Pa/m)*	Average velocity *(m/s)*	SPC *(W/m^3)*	Pn	Sh	SCE	Q *(m^3/s)*
Triple	25	4.1	0	1	0.107508	18.13408	442.2947	0.013777	6.093704	30738.417	30.26457	0.000985	7.68538E-08
Triple	50	4.1	0.05	0.35	0.068105	45.33271	1105.676	0.027555	30.46684	153683.63	33.15117	0.000216	1.53708E-07
Triple	50	4.1	0.05	1	0.126277	44.26031	1079.52	0.027555	29.74611	150048.04	44.56471	0.000297	1.53708E-07
Triple	50	4.1	0	0.35	0.021088	46.54273	1135.188	0.027555	31.28006	157785.74	33.09656	0.00021	1.53708E-07
Triple	50	4.1	0	1	0.080085	45.45587	1108.68	0.027555	30.54962	154101.17	44.44531	0.000288	1.53708E-07
Triple	75	4.1	0.05	0.35	0.064268	79.76361	1945.454	0.041332	80.41033	405613.13	38.93143	9.6E-05	2.30561E-07
Triple	75	4.1	0.05	1	0.110444	78.39134	1911.984	0.041332	79.02693	398634.87	52.51563	0.000132	2.30561E-07
Triple	75	4.1	0	0.35	0.016614	81.91462	1997.918	0.041332	82.57878	416551.41	38.85507	9.33E-05	2.30561E-07
Triple	75	4.1	0	1	0.063433	80.52367	1963.992	0.041332	81.17655	409478.17	52.35125	0.000128	2.30561E-07
Triple	100	4.1	0.05	0.35	0.062089	120.0293	2927.544	0.05511	161.3366	813829.05	43.81822	5.38E-05	3.07415E-07
Triple	100	4.1	0.05	1	0.101341	118.3675	2887.012	0.05511	159.1029	802561.56	59.18271	7.37E-05	3.07415E-07
Triple	100	4.1	0	0.35	0.014072	123.2828	3006.899	0.05511	165.7099	835888.88	43.7188	5.23E-05	3.07415E-07
Triple	100	4.1	0	1	0.053872	121.5962	2965.76	0.05511	163.4428	824452.9	58.9903	7.16E-05	3.07415E-07
Triple	150	4.1	0.05	0.35	0.060215	219.589	5355.829	0.082665	442.7387	2233303.2	55.3608	2.48E-05	4.61123E-07
Triple	150	4.1	0.05	1	0.093542	217.3066	5300.161	0.082665	438.137	2210090.9	74.97225	3.39E-05	4.61123E-07
Triple	150	4.1	0	0.35	0.011891	225.564	5501.562	0.082665	454.7858	2294072	55.23727	2.41E-05	4.61123E-07
Triple	150	4.1	0	1	0.04568	223.2148	5444.263	0.082665	450.0492	2270179.3	74.71437	3.29E-05	4.61123E-07
Triple	200	4.1	0.05	0.35	0.059136	350.4118	8546.63	0.11022	942.0078	4751761.6	65.90087	1.39E-05	6.1483E-07
Triple	200	4.1	0.05	1	0.08904	348.0196	8488.284	0.11022	935.5769	4719322.6	89.41005	1.89E-05	6.1483E-07
Triple	200	4.1	0	0.35	0.010639	359.9153	8778.422	0.11022	967.5558	4880633.6	65.77811	1.35E-05	6.1483E-07
Triple	200	4.1	0	1	0.040894	356.8342	8703.274	0.11022	959.273	4838852.8	88.96396	1.84E-05	6.1483E-07
Triple	25	4.6	0.05	0.35	0.079081	18.95323	412.0268	0.01349	5.558127	28036.813	24.21251	0.000864	8.45124E-08
Triple	25	4.6	0.05	1	0.170736	18.29129	397.6368	0.01349	5.364011	27057.633	32.25483	0.001192	8.45124E-08
Triple	25	4.6	0	0.35	0.033892	19.44952	422.8156	0.01349	5.703666	28770.951	24.18563	0.000841	8.45124E-08
Triple	25	4.6	0	1	0.126826	18.7785	408.2282	0.01349	5.506885	27778.334	32.18326	0.001159	8.45124E-08
Triple	50	4.6	0.05	0.35	0.071402	47.13716	1024.721	0.026979	27.6464	139456.51	35.16465	0.000252	1.69025E-07
Triple	50	4.6	0.05	1	0.139958	45.90721	997.9828	0.026979	26.92502	135817.67	47.24781	0.000348	1.69025E-07
Triple	50	4.6	0	0.35	0.024921	48.3906	1051.969	0.026979	28.38155	143164.83	35.09411	0.000245	1.69025E-07
Triple	50	4.6	0	1	0.094428	47.14445	1024.879	0.026979	27.65068	139478.07	47.10919	0.000338	1.69025E-07
Triple	75	4.6	0.05	0.35	0.066725	83.18744	1808.423	0.040469	73.18536	369168.28	40.88894	0.000111	2.53537E-07
Triple	75	4.6	0.05	1	0.120722	81.54333	1772.681	0.040469	71.73893	361872.07	55.13127	0.000152	2.53537E-07
Triple	75	4.6	0	0.35	0.019468	85.42211	1857.002	0.040469	75.15135	379085.3	40.79296	0.000108	2.53537E-07
Triple	75	4.6	0	1	0.074212	83.75602	1820.783	0.040469	73.68557	371691.51	54.95205	0.000148	2.53537E-07
Triple	100	4.6	0.05	0.35	0.064657	127.8217	2778.733	0.053959	149.9373	756327.61	47.60831	6.29E-05	3.38049E-07
Triple	100	4.6	0.05	1	0.112253	125.7154	2732.943	0.053959	147.4666	743864.4	64.40737	8.66E-05	3.38049E-07
Triple	100	4.6	0	0.35	0.017067	131.2738	2853.778	0.053959	153.9867	776753.68	47.51593	6.12E-05	3.38049E-07
Triple	100	4.6	0	1	0.065348	129.1376	2807.338	0.053959	151.4809	764113.56	64.22266	8.4E-05	3.38049E-07

Geometry	Re	*L* *(mm)*	Inlet salinity *(w/w)*	Wall concentration *(w/w)*	Outlet salinity *(w/w)*	Pressure drop *(Pa)*	dP/m *(Pa/m)*	Average velocity *(m/s)*	SPC *(W/m^3)*	Pn	Sh	SCE	Q *(m^3/s)*
Triple	150	4.6	0.05	0.35	0.063104	243.9033	5302.245	0.080938	429.1549	2164782.6	63.67633	2.94E-05	5.07074E-07
Triple	150	4.6	0.05	1	0.105698	240.3532	5225.069	0.080938	422.9084	2133273.1	86.12994	4.04E-05	5.07074E-07
Triple	150	4.6	0	0.35	0.015249	250.5071	5445.806	0.080938	440.7745	2223395.1	63.51113	2.86E-05	5.07074E-07
Triple	150	4.6	0	1	0.058414	246.902	5367.434	0.080938	434.4312	2191397.5	85.80453	3.92E-05	5.07074E-07
Triple	200	4.6	0.05	0.35	0.061668	393.3521	8551.132	0.107918	922.8192	4654969.1	75.4142	1.62E-05	6.76099E-07
Triple	200	4.6	0.05	1	0.0996	388.1776	8438.644	0.107918	910.6798	4593734.2	101.9314	2.22E-05	6.76099E-07
Triple	200	4.6	0	0.35	0.013578	404.0201	8783.045	0.107918	947.8468	4781215.5	75.2175	1.57E-05	6.76099E-07
Triple	200	4.6	0	1	0.052438	398.6504	8666.313	0.107918	935.2493	4717670.1	102.3865	2.17E-05	6.76099E-07
Woven	25	3.6	0.05	0.35	0.082668	38.05254	1057.015	0.019845	20.97692	20901.473	46.12686	0.002207	1.28334E-07
Woven	25	3.6	0.05	1	0.186391	36.64671	1017.964	0.019845	20.20194	20129.283	61.95219	0.003078	1.28334E-07
Woven	25	3.6	0	0.35	0.038086	39.04557	1084.599	0.019845	21.52435	21446.927	46.09381	0.002149	1.28334E-07
Woven	25	3.6	0	1	0.143239	37.62038	1045.011	0.019845	20.73869	20664.098	61.79848	0.002991	1.28334E-07
Woven	50	3.6	0.05	0.35	0.074664	86.92262	2414.517	0.039691	95.8343	95489.606	68.68236	0.000719	2.56668E-07
Woven	50	3.6	0.05	1	0.154269	84.43799	2345.5	0.039691	93.09493	92760.093	93.02923	0.001003	2.56668E-07
Woven	50	3.6	0	0.35	0.028758	89.22377	2478.438	0.039691	98.37137	98017.548	68.64099	0.0007	2.56668E-07
Woven	50	3.6	0	1	0.109541	86.70249	2408.403	0.039691	95.5916	95247.779	92.83493	0.000975	2.56668E-07
Woven	75	3.6	0.05	0.35	0.070383	146.3411	4065.03	0.059536	242.0169	241146.43	84.51317	0.00035	3.85002E-07
Woven	75	3.6	0.05	1	0.136293	142.8377	3967.714	0.059536	236.2231	235373.44	114.3412	0.000486	3.85002E-07
Woven	75	3.6	0	0.35	0.023764	150.2447	4173.464	0.059536	248.4726	247578.95	84.45221	0.000341	3.85002E-07
Woven	75	3.6	0	1	0.090641	146.6901	4074.726	0.059536	242.5941	241721.57	114.0864	0.000472	3.85002E-07
Woven	100	3.6	0.05	0.35	0.068006	215.9486	5998.571	0.079382	476.1771	474464.36	99.1361	0.000209	5.13336E-07
Woven	100	3.6	0.05	1	0.126046	211.4881	5874.67	0.079382	466.3416	464664.27	133.5961	0.000288	5.13336E-07
Woven	100	3.6	0	0.35	0.020991	221.7393	6159.424	0.079382	488.9458	487187.21	99.05806	0.000203	5.13336E-07
Woven	100	3.6	0	1	0.079872	217.2161	6033.78	0.079382	478.972	477249.23	133.2908	0.000279	5.13336E-07
Woven	150	3.6	0.05	0.35	0.064995	383.1386	10642.74	0.119073	1267.259	1262700.6	123.1997	9.76E-05	7.70004E-07
Woven	150	3.6	0.05	1	0.113282	376.5613	10460.04	0.119073	1245.504	1241024.1	165.6011	0.000133	7.70004E-07
Woven	150	3.6	0	0.35	0.017473	393.4688	10929.69	0.119073	1301.427	1296745.8	123.0456	9.49E-05	7.70004E-07
Woven	150	3.6	0	1	0.066442	386.7986	10744.41	0.119073	1279.365	1274763.1	165.1626	0.00013	7.70004E-07
Woven	200	3.6	0.05	0.35	0.063388	585.7482	16270.78	0.158763	2583.207	2573915.4	146.2567	5.68E-05	1.02667E-06
Woven	200	3.6	0.05	1	0.106531	576.8057	16022.38	0.158763	2543.769	2534619.9	196.5252	7.75E-05	1.02667E-06
Woven	200	3.6	0	0.35	0.015591	601.5884	16710.79	0.158763	2653.063	2643521	145.9865	5.52E-05	1.02667E-06
Woven	200	3.6	0	1	0.059319	592.5204	16458.9	0.158763	2613.072	2603673.8	195.8855	7.52E-05	1.02667E-06
Woven	25	4.1	0.05	0.35	0.084654	35.75741	872.132	0.01885	16.43926	16380.13	43.7288	0.00267	1.40798E-07
Woven	25	4.1	0.05	1	0.203122	29.00889	707.5339	0.01885	13.33667	13288.698	62.53167	0.004706	1.40798E-07
Woven	25	4.1	0	0.35	0.042761	31.04562	757.2103	0.01885	14.27304	14221.705	46.41416	0.003264	1.40798E-07
Woven	25	4.1	0	1	0.160829	29.77553	726.2325	0.01885	13.68913	13639.89	62.38336	0.004574	1.40798E-07
Woven	50	4.1	0.05	0.35	0.07574	81.14893	1979.242	0.037699	74.61549	74347.111	63.95136	0.00086	2.81596E-07

Geometry	Re	*L* *(mm)*	Inlet salinity *(w/w)*	Wall concentration *(w/w)*	Outlet salinity *(w/w)*	Pressure drop *(Pa)*	dP/m *(Pa/m)*	Average velocity *(m/s)*	SPC *(W/m^3)*	Pn	Sh	SCE	Q *(m^3/s)*
Woven	50	4.1	0.05	1	0.16408	65.70454	1602.55	0.037699	60.41455	60197.256	91.13908	0.001514	2.81596E-07
Woven	50	4.1	0	0.35	0.031628	69.63886	1698.509	0.037699	64.03211	63801.802	67.5172	0.001058	2.81596E-07
Woven	50	4.1	0	1	0.119887	67.46019	1645.37	0.037699	62.02885	61805.743	90.9796	0.001472	2.81596E-07
Woven	75	4.1	0.05	0.35	0.071565	135.577	3306.756	0.056549	186.9922	186319.61	79.78925	0.000428	4.22394E-07
Woven	75	4.1	0.05	1	0.147044	109.2313	2664.178	0.056549	150.6553	150113.47	115.1949	0.000767	4.22394E-07
Woven	75	4.1	0	0.35	0.02679	115.2681	2811.417	0.056549	158.9815	158409.67	85.16656	0.000538	4.22394E-07
Woven	75	4.1	0	1	0.101997	112.1645	2735.719	0.056549	154.7009	154144.45	115.0101	0.000746	4.22394E-07
Woven	100	4.1	0.05	0.35	0.068867	198.6485	4845.086	0.075398	365.31	363996.04	92.64463	0.000255	5.63192E-07
Woven	100	4.1	0.05	1	0.135127	159.4111	3888.076	0.075398	293.1533	292098.9	133.8468	0.000458	5.63192E-07
Woven	100	4.1	0	0.35	0.023478	167.6833	4089.836	0.075398	308.3656	307256.5	99.02896	0.000322	5.63192E-07
Woven	100	4.1	0	1	0.089475	163.7086	3992.892	0.075398	301.0562	299973.41	133.6398	0.000446	5.63192E-07
Woven	150	4.1	0.05	0.35	0.065976	348.9132	8510.079	0.113097	962.4648	959003.04	117.0897	0.000122	8.44788E-07
Woven	150	4.1	0.05	1	0.121639	278.4376	6791.162	0.113097	768.0604	765297.84	167.7128	0.000219	8.44788E-07
Woven	150	4.1	0	0.35	0.019803	291.617	7112.609	0.113097	804.4151	801521.83	124.6138	0.000155	8.44788E-07
Woven	150	4.1	0	1	0.075275	285.9832	6975.201	0.113097	788.8746	786037.22	167.4028	0.000213	8.44788E-07
Woven	200	4.1	0.05	0.35	0.06412	530.1439	12930.34	0.150796	1949.844	1942831	137.5408	7.08E-05	1.12638E-06
Woven	200	4.1	0.05	1	0.11324	420.7261	10261.61	0.150796	1547.411	1541845.2	196.4974	0.000127	1.12638E-06
Woven	200	4.1	0	0.35	0.017465	439.6753	10723.79	0.150796	1617.105	1611288.8	146.0395	9.06E-05	1.12638E-06
Woven	200	4.1	0	1	0.066379	432.1616	10540.53	0.150796	1589.47	1583753	195.9197	0.000124	1.12638E-06
Woven	25	4.6	0.05	0.35	0.08606	34.4203	748.2674	0.018089	13.53523	13486.542	41.0918	0.003047	1.53212E-07
Woven	25	4.6	0.05	1	0.223761	24.26756	527.5557	0.018089	9.542825	9508.5016	64.68691	0.006803	1.53212E-07
Woven	25	4.6	0	0.35	0.048598	26.1038	567.4738	0.018089	10.26489	10227.973	47.94378	0.004688	1.53212E-07
Woven	25	4.6	0	1	0.182506	24.90455	541.4033	0.018089	9.793312	9758.0875	64.53111	0.006613	1.53212E-07
Woven	50	4.6	0.05	0.35	0.076837	77.77759	1690.817	0.036178	61.16955	60949.541	60.17916	0.000987	3.06423E-07
Woven	50	4.6	0.05	1	0.175	54.24105	1179.153	0.036178	42.65882	42505.388	90.51235	0.002129	3.06423E-07
Woven	50	4.6	0	0.35	0.034865	57.66959	1253.687	0.036178	45.35526	45192.127	67.3723	0.001491	3.06423E-07
Woven	50	4.6	0	1	0.131376	55.68495	1210.542	0.036178	43.7944	43636.887	90.36279	0.002071	3.06423E-07
Woven	75	4.6	0.05	0.35	0.072803	129.4234	2813.552	0.054266	152.6809	152131.79	76.1654	0.000501	4.59635E-07
Woven	75	4.6	0.05	1	0.157115	89.17014	1938.481	0.054266	105.1941	104815.78	115.1821	0.001099	4.59635E-07
Woven	75	4.6	0	0.35	0.029724	94.37387	2051.606	0.054266	111.333	110932.53	85.49377	0.000771	4.59635E-07
Woven	75	4.6	0	1	0.11262	91.55611	1990.35	0.054266	108.0089	107620.38	115.0388	0.001069	4.59635E-07
Woven	100	4.6	0.05	0.35	0.069994	188.8525	4105.488	0.072355	297.0527	295984.23	88.61117	0.000299	6.12846E-07
Woven	100	4.6	0.05	1	0.145571	128.8575	2801.25	0.072355	202.6845	201955.44	136.1478	0.000674	6.12846E-07
Woven	100	4.6	0	0.35	0.026402	135.9478	2955.387	0.072355	213.837	213067.91	100.7531	0.000473	6.12846E-07
Woven	100	4.6	0	1	0.100469	132.3183	2876.484	0.072355	208.128	207379.46	135.9595	0.000656	6.12846E-07
Woven	150	4.6	0.05	0.35	0.066829	329.5345	7163.793	0.108533	777.5045	774708.02	111.2698	0.000144	9.1927E-07
Woven	150	4.6	0.05	1	0.129353	221.7441	4820.523	0.108533	523.1835	521301.75	168.0556	0.000322	9.1927E-07

Geometry	Re	*L* *(mm)*	Inlet salinity *(w/w)*	Wall concentration *(w/w)*	Outlet salinity *(w/w)*	Pressure drop *(Pa)*	dP/m *(Pa/m)*	Average velocity *(m/s)*	SPC *(W/m^3)*	Pn	Sh	SCE	Q *(m^3/s)*
Woven	150	4.6	0	0.35	0.021956	232.8434	5061.812	0.108533	549.3713	547395.3	124.8557	0.000228	9.1927E-07
Woven	150	4.6	0	1	0.083441	227.7315	4950.685	0.108533	537.3103	535377.7	167.8705	0.000314	9.1927E-07
Woven	200	4.6	0.05	0.35	0.064865	498.295	10832.5	0.14471	1567.571	1561933.3	130.6092	8.36E-05	1.22569E-06
Woven	200	4.6	0.05	1	0.120409	331.4066	7204.491	0.14471	1042.562	1038812.2	197.8468	0.00019	1.22569E-06
Woven	200	4.6	0	0.35	0.019473	346.9982	7543.439	0.14471	1091.611	1087685	147.1111	0.000135	1.22569E-06
Woven	200	4.6	0	1	0.073975	340.3888	7399.756	0.14471	1070.819	1066967.4	197.4595	0.000185	1.22569E-06
Ladder	25	3.6	0.05	0.35	0.077496	23.7229	658.9696	0.019077	12.57115	12525.936	19.09332	0.001524	6.12214E-08
Ladder	25	3.6	0.05	1	0.165349	22.93232	637.0089	0.019077	12.15221	12108.499	25.69502	0.002122	6.12214E-08
Ladder	25	3.6	0	0.35	0.032055	24.34609	676.2803	0.019077	12.90139	12854.984	19.07862	0.001484	6.12214E-08
Ladder	25	3.6	0	1	0.121159	23.54469	654.0191	0.019077	12.47671	12431.837	25.63604	0.002062	6.12214E-08
Ladder	50	3.6	0.05	0.35	0.069914	54.88267	1524.519	0.038154	58.16643	57957.22	27.29442	0.000471	1.22443E-07
Ladder	50	3.6	0.05	1	0.133559	53.46189	1485.052	0.038154	56.66064	56456.848	36.57546	0.000648	1.22443E-07
Ladder	50	3.6	0	0.35	0.023212	56.34211	1565.059	0.038154	59.71319	59498.42	27.26964	0.000458	1.22443E-07
Ladder	50	3.6	0	1	0.087759	54.90088	1525.025	0.038154	58.18573	57976.454	36.48918	0.000629	1.22443E-07
Ladder	75	3.6	0.05	0.35	0.066718	93.21295	2589.249	0.057231	148.1852	147652.18	34.18235	0.000232	1.83664E-07
Ladder	75	3.6	0.05	1	0.120443	91.24535	2534.593	0.057231	145.0572	144535.43	45.92007	0.000318	1.83664E-07
Ladder	75	3.6	0	0.35	0.019474	95.71047	2658.624	0.057231	152.1556	151608.32	34.12877	0.000225	1.83664E-07
Ladder	75	3.6	0	1	0.073946	93.71383	2603.162	0.057231	148.9814	148445.58	45.78836	0.000308	1.83664E-07
Ladder	100	3.6	0.05	0.35	0.064342	138.1708	3838.078	0.076308	292.8758	291822.4	38.94017	0.000133	2.44886E-07
Ladder	100	3.6	0.05	1	0.110604	135.7027	3769.519	0.076308	287.6442	286609.65	52.39309	0.000183	2.44886E-07
Ladder	100	3.6	0	0.35	0.016705	141.8915	3941.432	0.076308	300.7625	299680.74	38.87655	0.00013	2.44886E-07
Ladder	100	3.6	0	1	0.063609	139.3851	3871.809	0.076308	295.4497	294387.05	52.23637	0.000177	2.44886E-07
Ladder	150	3.6	0.05	0.35	0.061277	244.8361	6801.003	0.114462	778.4558	775655.85	45.69111	5.89E-05	3.67329E-07
Ladder	150	3.6	0.05	1	0.097714	241.3803	6705.007	0.114462	767.4679	764707.47	61.44316	8.03E-05	3.67329E-07
Ladder	150	3.6	0	0.35	0.01314	251.4657	6985.159	0.114462	799.5346	796658.89	45.63124	5.73E-05	3.67329E-07
Ladder	150	3.6	0	1	0.050092	247.9483	6887.453	0.114462	788.351	785515.46	61.27575	7.8E-05	3.67329E-07
Ladder	200	3.6	0.05	0.35	0.059497	366.2737	10174.27	0.152616	1552.755	1547169.9	51.14906	3.31E-05	4.89771E-07
Ladder	200	3.6	0.05	1	0.090205	361.5729	10043.69	0.152616	1532.827	1527313.3	68.75361	4.5E-05	4.89771E-07
Ladder	200	3.6	0	0.35	0.011068	376.2088	10450.24	0.152616	1594.873	1589136.7	51.09531	3.22E-05	4.89771E-07
Ladder	200	3.6	0	1	0.042219	371.413	10317.03	0.152616	1574.542	1568878.8	68.58406	4.37E-05	4.89771E-07
Ladder	25	4.1	0.05	0.35	0.0806	23.08142	562.9615	0.018193	10.24221	10205.371	19.03749	0.001865	6.74827E-08
Ladder	25	4.1	0.05	1	0.178422	22.23606	542.343	0.018193	9.867087	9831.5971	25.67956	0.002612	6.74827E-08
Ladder	25	4.1	0	0.35	0.035683	23.68434	577.6669	0.018193	10.50975	10471.949	19.02793	0.001817	6.74827E-08
Ladder	25	4.1	0	1	0.134911	22.82714	556.7595	0.018193	10.12937	10092.941	25.62444	0.002539	6.74827E-08
Ladder	50	4.1	0.05	0.35	0.072012	52.69414	1285.223	0.036387	46.76526	46597.061	26.9827	0.000579	1.34965E-07
Ladder	50	4.1	0.05	1	0.142356	51.19368	1248.626	0.036387	45.43363	45270.213	36.19856	0.0008	1.34965E-07
Ladder	50	4.1	0	0.35	0.025664	54.08936	1319.253	0.036387	48.0035	47830.848	26.96434	0.000564	1.34965E-07

Geometry	Re	*L* *(mm)*	Inlet salinity *(w/w)*	Wall concentration *(w/w)*	Outlet salinity *(w/w)*	Pressure drop *(Pa)*	dP/m *(Pa/m)*	Average velocity *(m/s)*	SPC *(W/m^3)*	Pn	Sh	SCE	Q *(m^3/s)*
Ladder	50	4.1	0	1	0.097015	52.56749	1282.134	0.036387	46.65286	46485.061	36.11954	0.000777	1.34965E-07
Ladder	75	4.1	0.05	0.35	0.068533	88.64049	2161.963	0.05458	118.0007	117576.25	33.87241	0.000288	2.02448E-07
Ladder	75	4.1	0.05	1	0.127982	86.55517	2111.102	0.05458	115.2246	114810.2	45.48502	0.000396	2.02448E-07
Ladder	75	4.1	0	0.35	0.021596	91.0061	2219.661	0.05458	121.1498	120714.09	33.83103	0.00028	2.02448E-07
Ladder	75	4.1	0	1	0.081878	88.89021	2168.054	0.05458	118.3331	117907.5	45.36476	0.000385	2.02448E-07
Ladder	100	4.1	0.05	0.35	0.066359	130.6267	3186.018	0.072774	231.8585	231024.6	39.71742	0.000172	2.69931E-07
Ladder	100	4.1	0.05	1	0.119032	127.9672	3121.152	0.072774	227.138	226321.08	53.42416	0.000236	2.69931E-07
Ladder	100	4.1	0	0.35	0.019056	134.1302	3271.469	0.072774	238.0772	237220.88	39.6549	0.000167	2.69931E-07
Ladder	100	4.1	0	1	0.072459	131.4301	3205.612	0.072774	233.2845	232445.41	53.26681	0.000229	2.69931E-07
Ladder	150	4.1	0.05	0.35	0.063207	231.9905	5658.304	0.109161	617.6643	615442.71	47.83886	7.77E-05	4.04896E-07
Ladder	150	4.1	0.05	1	0.10586	228.2174	5566.279	0.109161	607.6187	605433.23	64.38238	0.000106	4.04896E-07
Ladder	150	4.1	0	0.35	0.01539	238.2513	5811.007	0.109161	634.3334	632051.85	47.77933	7.56E-05	4.04896E-07
Ladder	150	4.1	0	1	0.058648	234.414	5717.414	0.109161	624.1167	621871.93	64.21101	0.000103	4.04896E-07
Ladder	200	4.1	0.05	0.35	0.061057	354.0917	8636.384	0.145548	1257.005	1252483.4	53.20777	4.25E-05	5.39862E-07
Ladder	200	4.1	0.05	1	0.096806	349.2391	8518.027	0.145548	1239.778	1235318.8	71.57756	5.79E-05	5.39862E-07
Ladder	200	4.1	0	0.35	0.012883	363.6836	8870.331	0.145548	1291.055	1286411.5	53.1373	4.13E-05	5.39862E-07
Ladder	200	4.1	0	1	0.049138	358.7375	8749.694	0.145548	1273.497	1268916.2	71.38243	5.63E-05	5.39862E-07
Ladder	25	4.6	0.05	0.35	0.083522	22.8333	496.3761	0.01752	8.696416	8665.1374	18.89871	0.002181	7.3744E-08
Ladder	25	4.6	0.05	1	0.190741	21.92658	476.6648	0.01752	8.351079	8321.0419	25.54874	0.00307	7.3744E-08
Ladder	25	4.6	0	0.35	0.039097	23.42664	509.2748	0.01752	8.922399	8890.3069	18.89218	0.002125	7.3744E-08
Ladder	25	4.6	0	1	0.147862	22.50708	489.2844	0.01752	8.572171	8541.3387	25.49536	0.002985	7.3744E-08
Ladder	50	4.6	0.05	0.35	0.073926	51.60962	1121.948	0.03504	39.31265	39171.25	26.52792	0.000677	1.47488E-07
Ladder	50	4.6	0.05	1	0.15032	50.02136	1087.421	0.03504	38.10282	37965.776	35.60428	0.000938	1.47488E-07
Ladder	50	4.6	0	0.35	0.027892	52.97107	1151.545	0.03504	40.3497	40204.573	26.50601	0.000659	1.47488E-07
Ladder	50	4.6	0	1	0.105369	51.36044	1116.531	0.03504	39.12284	38982.12	35.52212	0.000911	1.47488E-07
Ladder	75	4.6	0.05	0.35	0.070131	86.14661	1872.752	0.052559	98.43081	98076.777	33.26131	0.000339	2.21232E-07
Ladder	75	4.6	0.05	1	0.134661	83.93709	1824.719	0.052559	95.90622	95561.271	44.68151	0.000468	2.21232E-07
Ladder	75	4.6	0	0.35	0.023454	88.43849	1922.576	0.052559	101.0495	100686.06	33.21454	0.00033	2.21232E-07
Ladder	75	4.6	0	1	0.088882	86.19773	1873.864	0.052559	98.48922	98134.982	44.55827	0.000454	2.21232E-07
Ladder	100	4.6	0.05	0.35	0.067873	126.143	2742.24	0.070079	192.1741	191482.9	39.22019	0.000205	2.94976E-07
Ladder	100	4.6	0.05	1	0.125297	123.3318	2681.126	0.070079	187.8913	187215.47	52.71353	0.000282	2.94976E-07
Ladder	100	4.6	0	0.35	0.020812	129.5167	2815.581	0.070079	197.3138	196604.13	39.14464	0.000199	2.94976E-07
Ladder	100	4.6	0	1	0.079014	126.6647	2753.579	0.070079	192.9688	192274.71	52.54373	0.000273	2.94976E-07
Ladder	150	4.6	0.05	0.35	0.064873	222.0049	4826.194	0.105119	507.3241	505499.33	48.7059	9.64E-05	4.42464E-07
Ladder	150	4.6	0.05	1	0.112861	217.9387	4737.797	0.105119	498.0319	496240.63	65.56439	0.000132	4.42464E-07
Ladder	150	4.6	0	0.35	0.017322	227.9784	4956.053	0.105119	520.9747	519100.9	48.61912	9.37E-05	4.42464E-07
Ladder	150	4.6	0	1	0.065968	223.8484	4866.269	0.105119	511.5367	509696.86	65.35841	0.000128	4.42464E-07

Geometry	Re	*L* *(mm)*	Inlet salinity *(w/w)*	Wall concentration *(w/w)*	Outlet salinity *(w/w)*	Pressure drop *(Pa)*	dP/m *(Pa/m)*	Average velocity *(m/s)*	SPC *(W/m^3)*	Pn	Sh	SCE	Q *(m^3/s)*
Ladder	200	4.6	0.05	0.35	0.062649	338.6537	7362.036	0.140158	1031.852	1028140.6	55.0196	5.35E-05	5.89952E-07
Ladder	200	4.6	0.05	1	0.103513	333.3575	7246.903	0.140158	1015.715	1012061.7	74.04339	7.32E-05	5.89952E-07
Ladder	200	4.6	0	0.35	0.014733	347.802	7560.913	0.140158	1059.726	1055914.6	54.92878	5.2E-05	5.89952E-07
Ladder	200	4.6	0	1	0.056166	342.4139	7443.78	0.140158	1043.309	1039556.6	73.82172	7.1E-05	5.89952E-07
Wavy	25	3.6	0.05	0.35	0.0774	24.52325	681.2013	0.019433	13.23764	13190.03	19.10866	0.001449	6.26442E-08
Wavy	25	3.6	0.05	1	0.165084	23.69463	658.1842	0.019433	12.79036	12744.352	25.74763	0.00202	6.26442E-08
Wavy	25	3.6	0	0.35	0.03197	25.16684	699.079	0.019433	13.58506	13536.193	19.11109	0.001412	6.26442E-08
Wavy	25	3.6	0	1	0.12097	24.32659	675.7385	0.019433	13.13148	13084.254	25.70889	0.001965	6.26442E-08
Wavy	50	3.6	0.05	0.35	0.069982	56.25979	1562.772	0.038866	60.73804	60519.582	27.51478	0.000455	1.25288E-07
Wavy	50	3.6	0.05	1	0.13405	54.76696	1521.305	0.038866	59.12638	58913.722	36.96593	0.000627	1.25288E-07
Wavy	50	3.6	0	0.35	0.023311	57.75402	1604.278	0.038866	62.35121	62126.95	27.51338	0.000443	1.25288E-07
Wavy	50	3.6	0	1	0.08836	56.23993	1562.22	0.038866	60.7166	60498.221	36.91613	0.00061	1.25288E-07
Wavy	75	3.6	0.05	0.35	0.067059	94.3989	2622.192	0.058298	152.8695	152319.68	35.05762	0.00023	1.87933E-07
Wavy	75	3.6	0.05	1	0.122005	92.2899	2563.608	0.058298	149.4542	148916.64	47.18995	0.000317	1.87933E-07
Wavy	75	3.6	0	0.35	0.019902	96.92317	2692.31	0.058298	156.9573	156392.76	35.05818	0.000224	1.87933E-07
Wavy	75	3.6	0	1	0.075705	94.78438	2632.899	0.058298	153.4938	152941.67	47.13161	0.000308	1.87933E-07
Wavy	100	3.6	0.05	0.35	0.065637	138.1927	3838.686	0.077731	298.3855	297312.29	42.74242	0.000144	2.50577E-07
Wavy	100	3.6	0.05	1	0.116295	135.4991	3763.865	0.077731	292.5696	291517.3	57.75012	0.000198	2.50577E-07
Wavy	100	3.6	0	0.35	0.018242	141.905	3941.806	0.077731	306.4012	305299.12	42.74157	0.00014	2.50577E-07
Wavy	100	3.6	0	1	0.069696	139.1729	3865.913	0.077731	300.5019	299421.06	57.67394	0.000193	2.50577E-07
Wavy	150	3.6	0.05	0.35	0.063812	241.3119	6703.108	0.116597	781.5606	778749.52	56.45442	7.25E-05	3.75865E-07
Wavy	150	3.6	0.05	1	0.108468	237.3018	6591.718	0.116597	768.5728	765808.43	76.07228	9.93E-05	3.75865E-07
Wavy	150	3.6	0	0.35	0.016089	247.8249	6884.024	0.116597	802.6547	799767.78	56.36765	7.05E-05	3.75865E-07
Wavy	150	3.6	0	1	0.061381	243.7575	6771.042	0.116597	789.4814	786641.84	75.86361	9.64E-05	3.75865E-07
Wavy	200	3.6	0.05	0.35	0.062206	365.2619	10146.16	0.155462	1577.346	1571672.9	66.33827	4.22E-05	5.01153E-07
Wavy	200	3.6	0.05	1	0.101644	359.8188	9994.966	0.155462	1553.841	1548251.9	89.26191	5.77E-05	5.01153E-07
Wavy	200	3.6	0	0.35	0.014213	375.1473	10420.76	0.155462	1620.035	1614208.2	66.20992	4.1E-05	5.01153E-07
Wavy	200	3.6	0	1	0.054195	369.6296	10267.49	0.155462	1596.208	1590466.5	88.97963	5.59E-05	5.01153E-07
Wavy	25	4.1	0.05	0.35	0.080431	23.79207	580.2944	0.018502	10.73649	10697.877	19.00033	0.001776	6.88939E-08
Wavy	25	4.1	0.05	1	0.177844	22.91264	558.8448	0.018502	10.33964	10302.448	25.65512	0.00249	6.88939E-08
Wavy	25	4.1	0	0.35	0.0355	24.41315	595.4427	0.018502	11.01676	10977.139	18.99873	0.001731	6.88939E-08
Wavy	25	4.1	0	1	0.134353	23.52147	573.6943	0.018502	10.61438	10576.201	25.6103	0.002422	6.88939E-08
Wavy	50	4.1	0.05	0.35	0.072061	54.13329	1320.324	0.037004	48.85676	48681.032	27.15053	0.000558	1.37788E-07
Wavy	50	4.1	0.05	1	0.142656	52.55928	1281.934	0.037004	47.43617	47265.552	36.46354	0.000771	1.37788E-07
Wavy	50	4.1	0	0.35	0.025729	55.56502	1355.244	0.037004	50.14893	49968.56	27.14026	0.000543	1.37788E-07
Wavy	50	4.1	0	1	0.097376	53.96876	1316.311	0.037004	48.70827	48533.074	36.40218	0.00075	1.37788E-07
Wavy	75	4.1	0.05	0.35	0.068648	90.46278	2206.409	0.055505	122.4676	122027.16	34.22321	0.00028	2.06682E-07

Geometry	Re	*L* *(mm)*	Inlet salinity *(w/w)*	Wall concentration *(w/w)*	Outlet salinity *(w/w)*	Pressure drop *(Pa)*	dP/m *(Pa/m)*	Average velocity *(m/s)*	SPC *(W/m^3)*	Pn	Sh	SCE	Q *(m^3/s)*
Wavy	75	4.1	0.05	1	0.128526	88.22376	2151.799	0.055505	119.4365	119006.9	45.99512	0.000386	2.06682E-07
Wavy	75	4.1	0	0.35	0.021751	92.87266	2265.187	0.055505	125.7301	125277.9	34.21417	0.000273	2.06682E-07
Wavy	75	4.1	0	1	0.082541	90.6024	2209.815	0.055505	122.6567	122215.51	45.9265	0.000376	2.06682E-07
Wavy	100	4.1	0.05	0.35	0.066742	132.0955	3221.84	0.074007	238.4394	237581.81	40.8314	0.000172	2.75576E-07
Wavy	100	4.1	0.05	1	0.12067	129.2224	3151.766	0.074007	233.2534	232414.49	54.95424	0.000236	2.75576E-07
Wavy	100	4.1	0	0.35	0.019528	135.6315	3308.086	0.074007	244.8222	243941.64	40.8229	0.000167	2.75576E-07
Wavy	100	4.1	0	1	0.074286	132.7191	3237.051	0.074007	239.5651	238703.47	54.87466	0.00023	2.75576E-07
Wavy	150	4.1	0.05	0.35	0.064472	229.5135	5597.89	0.111011	621.4264	619191.28	52.74052	8.52E-05	4.13364E-07
Wavy	150	4.1	0.05	1	0.111317	225.5067	5500.164	0.111011	610.5777	608381.64	71.15818	0.000117	4.13364E-07
Wavy	150	4.1	0	0.35	0.01687	235.6997	5748.772	0.111011	638.1759	635880.54	52.69334	8.29E-05	4.13364E-07
Wavy	150	4.1	0	1	0.064408	231.6372	5649.688	0.111011	627.1765	624920.71	71.00282	0.000114	4.13364E-07
Wavy	200	4.1	0.05	0.35	0.062961	344.4745	8401.817	0.148014	1243.59	1239117.3	62.81363	5.07E-05	5.51152E-07
Wavy	200	4.1	0.05	1	0.104858	339.1144	8271.082	0.148014	1224.24	1219836.2	84.58534	6.93E-05	5.51152E-07
Wavy	200	4.1	0	0.35	0.0151	353.7863	8628.933	0.148014	1277.207	1272612.8	62.72398	4.93E-05	5.51152E-07
Wavy	200	4.1	0	1	0.057596	348.3475	8496.281	0.148014	1257.572	1253049	84.36122	6.73E-05	5.51152E-07
Wavy	25	4.6	0.05	0.35	0.083277	23.46643	510.1398	0.017792	9.076415	9043.7689	18.8166	0.002081	7.5147E-08
Wavy	25	4.6	0.05	1	0.189826	22.53008	489.7843	0.017792	8.714248	8682.905	25.45658	0.002932	7.5147E-08
Wavy	25	4.6	0	0.35	0.038828	24.07595	523.3902	0.017792	9.312166	9278.6721	18.81931	0.002028	7.5147E-08
Wavy	25	4.6	0	1	0.146964	23.12634	502.7464	0.017792	8.944871	8912.6987	25.41536	0.002852	7.5147E-08
Wavy	50	4.6	0.05	0.35	0.073974	52.94969	1151.08	0.035584	40.96007	40812.748	26.67463	0.000654	1.50294E-07
Wavy	50	4.6	0.05	1	0.150538	51.2938	1115.083	0.035584	39.67913	39536.416	35.80845	0.000906	1.50294E-07
Wavy	50	4.6	0	0.35	0.027959	54.34514	1181.416	0.035584	42.03954	41888.333	26.6641	0.000637	1.50294E-07
Wavy	50	4.6	0	1	0.105654	52.66604	1144.914	0.035584	40.74065	40594.114	35.74569	0.000881	1.50294E-07
Wavy	75	4.6	0.05	0.35	0.070236	88.07568	1914.689	0.053376	102.1985	101830.91	33.55594	0.00033	2.25441E-07
Wavy	75	4.6	0.05	1	0.135065	85.71352	1863.337	0.053376	99.45757	99099.848	45.05883	0.000455	2.25441E-07
Wavy	75	4.6	0	0.35	0.023598	90.41415	1965.525	0.053376	104.9119	104534.6	33.53949	0.000321	2.25441E-07
Wavy	75	4.6	0	1	0.089398	88.019	1913.457	0.053376	102.1327	101765.39	44.98288	0.000442	2.25441E-07
Wavy	100	4.6	0.05	0.35	0.068121	128.2753	2788.593	0.071168	198.4587	197744.91	39.9188	0.000202	3.00588E-07
Wavy	100	4.6	0.05	1	0.126343	125.2179	2722.128	0.071168	193.7286	193031.77	53.66069	0.000278	3.00588E-07
Wavy	100	4.6	0	0.35	0.021135	131.6977	2862.994	0.071168	203.7537	203020.88	39.90743	0.000197	3.00588E-07
Wavy	100	4.6	0	1	0.080247	128.5986	2795.623	0.071168	198.959	198243.41	53.58132	0.00027	3.00588E-07
Wavy	150	4.6	0.05	0.35	0.065214	222.1997	4830.428	0.106752	515.6583	513803.59	50.02208	9.74E-05	4.50882E-07
Wavy	150	4.6	0.05	1	0.11439	217.9092	4737.157	0.106752	505.7014	503882.52	67.44616	0.000134	4.50882E-07
Wavy	150	4.6	0	0.35	0.017743	228.1713	4960.245	0.106752	529.5165	527611.93	50.00254	9.48E-05	4.50882E-07
Wavy	150	4.6	0	1	0.067671	223.8215	4865.684	0.106752	519.4219	517553.66	67.33477	0.00013	4.50882E-07
Wavy	200	4.6	0.05	0.35	0.06348	332.3241	7224.437	0.142336	1028.298	1024599.6	58.92198	5.75E-05	6.01176E-07
Wavy	200	4.6	0.05	1	0.107081	326.9422	7107.44	0.142336	1011.645	1008006.7	79.40411	7.88E-05	6.01176E-07

Geometry	Re	*L* *(mm)*	Inlet salinity *(w/w)*	Wall concentration *(w/w)*	Outlet salinity *(w/w)*	Pressure drop *(Pa)*	dP/m *(Pa/m)*	Average velocity *(m/s)*	SPC *(W/m^3)*	Pn	Sh	SCE	Q *(m^3/s)*
Wavy	200	4.6	0	0.35	0.015714	341.2969	7419.497	0.142336	1056.062	1052263.9	58.87284	5.59E-05	6.01176E-07
Wavy	200	4.6	0	1	0.059961	335.8339	7300.736	0.142336	1039.158	1035420.8	79.23557	7.65E-05	6.01176E-07

Appendix VI. MATLAB code

Main MATLAB code

This script loads the CFD results –*Input.mat*–, calculates the equation parameters, prepares the results tabels, and exports the equation parameters and the results in Excel files.

```
%% preparation
global name name1 Dep1 Dep2 InDep1 InDep11 InDep2 InDep3 Flow Type Geometry Type1
Type2 dep depen indep indep1 indep3;
load('Input.mat')
name = 'output.xlsx';
%% Power measures
for c1 = 1:size(Dep1,2)
    for i = 1
        for d = 1
            for k = 1:size(Type1,2)
                dep = [Dep1{c1}, num2str(d)];
                indep = [InDep1{i}, num2str(d)];
                typ = Type1{k};
                depen = dep;
                [general_1D.(dep).(indep).(typ)] =
                Opt10(k,eval(indep),eval(dep));
                [individual_1D.(dep).(indep)] = raw_calc_1D(eval(dep),Re1);
                for l = 1:size(InDep3,2)
                    indep3 = [InDep3{l}, num2str(d)];
                    [individual_2D.(dep).(indep).(indep3)] =
                    raw_calc_2D(eval(dep),eval(indep),eval(indep3));
                end
            end
        end
    end
end
 %% Mass transfer measures
for c1 = 1:size(Dep2,2)
```

```
    for i = 1:size(InDep2,2)
        for d = 1
            for k = 1:size(Type1,2)
                dep = [Dep2{c1}, num2str(d)];
                indep = [InDep2{i}, num2str(d)];
                typ = Type1{k};
                depen = dep;
                [general_1D.(dep).(indep).(typ)] =
                Opt10(k,eval(indep),eval(dep));
                [individual_1D.(dep).(indep)] =
                raw_calc_1D(eval(dep),eval(indep));
                for l = 1:size(InDep3,2)
                    indep3 = [InDep3{l}, num2str(d)];
                    [individual_2D.(dep).(indep).(indep3)] =
                    raw_calc_2D(eval(dep),eval(indep),eval(indep3));
                end
            end
        end
    end
end
%% Export General equations
row = 2;
c = 1;
export{1,c} = 'Dependent';
c = c+1;
export{1,c} = 'Independent';
c = c+1;
export{1,c} = 'Equation';
c = c+1;
export{1,c} = 'Ci';
c = c+1;
export{1,c} = 'Cw';
c = c+1;
export{1,c} = 'Average R2';
```

```
c = c+1;
export{1,c} = 'R2 RMS';
c = c+1;
export{1,c} = 'min R2';
c = c+1;
export{1,c} = 'b';
c = c+1;
for i = 1:size(Geometry,2)
    export{1,c} = ['R2 for ', char(Geometry(1,i))];
    c = c+1;
    export{1,c} = ['a for ', char(Geometry(1,i))];
    c = c+1;
    export{1,c} = ['c for ', char(Geometry(1,i))];
    c = c+1;
end
for c1 = 1:size(Dep1,2)
    depen = Dep1{c1};
    for i = 1
        for j = 1
            for k = 1:size(Type1,2)
                indep1 = InDep1{i};
                indep = [indep1, num2str(j)];
                dep = [depen, num2str(j)];
                typ = Type1{k};
                c = 1;
                r2_min = 1;
                r2_rms = 0;
                export{row,c} = depen;
                c = c+1;
                export{row,c} = indep1;
                c = c+1;
                export{row,c} = typ;
                c = c+1;
                export{row,c} = Ci1(j);
```

```
        c = c+1;
        export{row,c} = Cw1(j);
        c = c+1;
        export{row,c} = general_1D.(dep).(indep).(typ).r2_aver;
        c = c+3;
        export{row,c} = general_1D.(dep).(indep).(typ).b_all;
        c = c+1;
        for l = 1:size(Geometry,2)
            export{row,c} = general_1D.(dep).(indep).(typ).r2(l);
            c = c+1;
            export{row,c} = general_1D.(dep).(indep).(typ).a(l);
            c = c+1;
            parameters.(dep).(indep).(typ)(1,l) =
            general_1D.(dep).(indep).(typ).a(l);
            try
                export{row,c} =
                general_1D.(dep).(indep).(typ).c(l);
                c = c+1;
                parameters.(dep).(indep).(typ)(2,l) =
                general_1D.(dep).(indep).(typ).c(l);
            catch
                c = c + 1;
            end
            r2_min =
             min(general_1D.(dep).(indep).(typ).r2(l),r2_min);
            r2_rms = r2_rms +
            general_1D.(dep).(indep).(typ).r2(l)^2;
        end
        r2_rms = sqrt(r2_rms/size(Geometry,2));
        export{row,8} = r2_min;
        export{row,7} = r2_rms;
        row = row + 1;
    end
end
```

```
    end
end
for c1 = 1:size(Dep2,2)
    depen = Dep2{c1};
    for i = 1:size(InDep2,2)
        for j = 1
            for k = 1:size(Type1,2)
                indep1 = InDep2{i};
                indep = [indep1, num2str(j)];
                dep = [depen, num2str(j)];
                typ = Type1{k};
                c = 1;
                r2_min = 1;
                r2_rms = 0;
                export{row,c} = depen;
                c = c+1;
                export{row,c} = indep1;
                c = c+1;
                export{row,c} = typ;
                c = c+1;
                export{row,c} = Ci1(j);
                c = c+1;
                export{row,c} = Cw1(j);
                c = c+1;
                export{row,c} = general_1D.(dep).(indep).(typ).r2_aver;
                c = c+3;
                export{row,c} = general_1D.(dep).(indep).(typ).b_all;
                c = c+1;
                for l = 1:size(Geometry,2)
                    export{row,c} = general_1D.(dep).(indep).(typ).r2(l);
                    c = c+1;
                    export{row,c} = general_1D.(dep).(indep).(typ).a(l);
                    c = c+1;
                    parameters.(dep).(indep).(typ)(1,l) =
```

```
                general_1D.(dep).(indep).(typ).a(l);
                try
                    export{row,c} =
                    general_1D.(dep).(indep).(typ).c(l);
                    c = c+1;
                    parameters.(dep).(indep).(typ)(2,l) =
                    general_1D.(dep).(indep).(typ).c(l);
                catch
                    c = c + 1;
                end
                r2_min =
                min(general_1D.(dep).(indep).(typ).r2(l),r2_min);
                r2_rms = r2_rms +
                general_1D.(dep).(indep).(typ).r2(l)^2;
            end
            r2_rms = sqrt(r2_rms/size(Geometry,2));
            export{row,8} = r2_min;
            export{row,7} = r2_rms;
            row = row + 1;
        end
    end
end
end
[export1] = trim(export, 8, 0.9);
name1 = 'General.xlsx';
writecell (export, name1, 'Sheet', 'Gen. Eqs.');
writecell (export1, name1, 'Sheet', 'Gen. Eqs - trimmed');
%% Calculating second step equations, Exporting and trimming individual equations
calc_param;
[exported_param] = export_param(param);
[exported_param_t] = trim(exported_param, 10, 0.9);
writecell (exported_param, name1, 'Sheet', 'Gen. par. by independent');
writecell (exported_param_t, name1, 'Sheet', 'Gen. par. by independent trim');
[exported_param1] = export_param1(param1);
```

```
[exported_param_t1] = trim(exported_param1, 10, 0.9);
writecell (exported_param1, name1, 'Sheet', 'Ind. par. by independent');
writecell (exported_param_t1, name1, 'Sheet', 'Ind. par. by independent trim');
[raw_table_1D] = par_raw_export_1D(individual_1D);
[raw_trim_1D] = trim(raw_table_1D, 8, 0.999);
writecell (raw_table_1D, name, 'Sheet', 'individual eqs_1D');
writecell (raw_trim_1D, name, 'Sheet', 'trimmed ind eqs_1D');
[raw_table_2D] = par_raw_export_2D(individual_2D);
[raw_trim_2D] = trim(raw_table_2D, 9, 0.999);
writecell (raw_table_2D, name, 'Sheet', 'individual eqs_2D');
writecell (raw_trim_2D, name, 'Sheet', 'trimmed ind eqs_2D');
[a1] = export_a(individual_1D);
writecell (a1, name, 'Sheet', 'individual eqs_1D_a');
[b1] = export_b(individual_1D);
writecell (b1, name, 'Sheet', 'individual eqs_1D_b');
[r1] = export_r(individual_1D);
writecell (r1, name, 'Sheet', 'individual eqs_1D_r');
[a2,b2,c2,r2] = export_2D(individual_2D,individual_1D);
writecell (a2, name, 'Sheet', 'individual eqs_2D_a');
writecell (b2, name, 'Sheet', 'individual eqs_2D_b');
writecell (c2, name, 'Sheet', 'individual eqs_2D_c');
writecell (r2, name, 'Sheet', 'individual eqs_2D_r');
name1 = 'cropped data.xlsx';
writecell (raw_table_2D, name1, 'Sheet', 'individual eqs_2D');
writecell (raw_trim_2D, name1, 'Sheet', 'trimmed ind eqs_2D');
writecell (raw_table_1D, name1, 'Sheet', 'individual eqs_1D');
writecell (raw_trim_1D, name1, 'Sheet', 'trimmed ind eqs_1D');
```

Optimiser function

```
function [output] = fun10 (in)
warning off;
    global xs ys out_test typ;
    low = in;
    up = in;
    HB = Inf;
    LB = Inf;
    out_test = struct( 'type' , [] , 'rsquare' , [] , 'parameters' , [] , 'CFD', [], 'calculated', []);
    temp01 = struct( 'type' , [] , 'rsquare' , [] , 'parameters' , [] , 'CFD', [], 'calculated', []);
    s = size(ys,2);
    out_test.rsquare_average = 0;
    parfor i = 1:s
        in_x = xs(:,i);
        in_y = ys(:,i);
        [xData, yData] = prepareCurveData( in_x , in_y );
        opts = fitoptions( 'Method', 'NonlinearLeastSquares' );
        opts.Display = 'Off';
%       opts.Algorithm = 'Levenberg-Marquardt';
        if (typ == 1)
            ft = fittype( 'power1' );
            opts.Lower = [-HB low];
            opts.Upper = [HB up];
            opts.StartPoint = [0.1 0.1];
        elseif (typ == 2)
            ft = fittype( 'power2' );
            opts.Lower = [-HB low -LB];
            opts.Upper = [HB up LB];
            opts.StartPoint = [0.1 0.1 0.1];
        elseif (typ == 3)
            ft = fittype( 'exp1' );
            opts.Lower = [-LB low];
            opts.Upper = [LB up];
```

```
            opts.StartPoint = [0.001 0.00001];
        elseif (typ == 4)
            ft = fittype( 'a*exp(b*x) + c', 'independent', 'x', 'dependent', 'y' );
            opts.Lower = [-LB low -LB];
            opts.Upper = [LB up LB];
            opts.StartPoint = [0.001 0.00001 0.001];
        end
        [fitresult, gof] = fit( xData, yData, ft, opts );
        temp01(i).type = formula(fitresult);
        temp01(i).rsquare = gof.rsquare;
        temp01(i).parameters = coeffvalues(fitresult);
    end
    for i = 1:s
        out_test(i).type = temp01(i).type ;
        out_test(i).rsquare = temp01(i).rsquare ;
        out_test(i).parameters = temp01(i).parameters ;
    end
    for i = 1:s
        out_test(1).rsquare_average = out_test(1).rsquare_average +
        out_test(i).rsquare;
    end
    out_test(1).rsquare_average = out_test(1).rsquare_average / s;
    output = abs(1 - out_test(1).rsquare_average);
end
```

Function for finding parameters with common power exponent

```
function out = Opt10(varargin)
    global xs ys out_test typ;
    out = struct( 'type' , [] , 'CFD', [], 'calculated', []);
    typ = varargin{1};
    xs = varargin{2};
    ys = varargin{3};
    if (typ == 1) || (typ == 2) || (typ == 5) || (typ == 6)
        Params = 1.2;
        lim = 3.5;
    elseif (typ == 3) || (typ == 4)
        Params = 0.001;
         lim = 0.1;
    end
    Al=1;
    Algorithms={'interior-point', 'trust-region-reflective', 'sqp', 'active-set'};
    options = optimoptions(@fmincon,'Algorithm',char(Algorithms(Al)),...
            'DiffMaxChange', 0.02, ...
            'DiffMinChange', 1e-10, ...
            'Display', 'off', ...
            'MaxFunEvals',1000, ...
            'MaxIter',1000,....
            'TolFun', 1e-10, ...
            'TolCon', 1e-10, ...
            'TolX', 1e-10);
    [~]= fmincon(@fun10, Params,[],[],[],[],-lim,lim,[[],[]],options);
    out.type = out_test(1).type;
    out.r2_aver = out_test(1).rsquare_average;
    out.b_all(1,1) = out_test(1).parameters(2);
    for i = 1:size(ys,2)
        out.r2(i,1) = out_test(i).rsquare;
        out.a(i,1) = out_test(i).parameters(1);
        out.b(i,1) = out_test(i).parameters(2);
```

```
        try
            out.c(i,1) = out_test(i).parameters(3);
        catch
        end
        for j = 1:size(ys,1)
            out.CFD(j,i) = ys(j,i);
            if (typ == 1)
                out.calculated(j,i) = out_test(i).parameters(1) * xs(j,i) ^
                out_test(i).parameters(2);
            elseif (typ == 2)
                out.calculated(j,i) = out_test(i).parameters(1) * xs(j,i) ^
                out_test(i).parameters(2) + out_test(i).parameters(3);
            elseif (typ == 3)
                out.calculated(j,i) = out_test(i).parameters(1) * exp (xs(j,i) *
                out_test(i).parameters(2));
            elseif (typ == 4)
                out.calculated(j,i) = out_test(i).parameters(1) * exp (xs(j,i) *
                out_test(i).parameters(2)) + out_test(i).parameters(3);
            end
        end
    end
end
```

Function for finding parameters with individual power exponent, with parallel processing

```
function [out] = raw_calc_1D(par1, par2)
global Geometry depen indep;
ci = [0.05,0.05,0,0];
cw = [0.35,1,0.35,1];
depen_n = depen(1:size(depen,2)-1);
cat = str2double(depen(size(depen,2)));
indep1 = indep(1:size(indep,2)-1);
s = size(par1,2);
counter = 1;
out =
struct('Title',cell(2,s),'dependant',[],'Independent_1',[],'type',[],'rsquare',[],'Parameters',[],
'Geometry', [], 'Ci', [], 'Cw', []);
fitresult = cell( 1, 1 );
gof = struct( 'sse', cell( 1, 1 ), 'rsquare', [], 'dfe', [], 'adjrsquare', [], 'rmse', [] );
ft = fittype( 'power1' );
parfor i = 1:s
    opts = fitoptions( 'Method', 'NonlinearLeastSquares' );
    opts.Algorithm = 'Levenberg-Marquardt';
    opts.DiffMaxChange = 0.2;
    opts.DiffMinChange = 1e-20;
    opts.Display = 'Off';
    opts.MaxFunEvals = 10000;
    opts.MaxIter = 10000;
    opts.StartPoint = [0 0 0];
    opts.TolFun = 1e-20;
    opts.TolX = 1e-20;
    [xData, yData] = prepareCurveData( par2(:,i), par1(:,i) );
    [fitresult, gof] = fit( xData, yData, ft );
    out(counter,i).Title = [depen_n, ' vs. ',indep1];
    out(counter,i).dependant = depen_n;
    out(counter,i).Independent_1 = indep1;
```

```
        out(counter,i).type = formula(fitresult);
        out(counter,i).rsquare = gof.rsquare;
        out(counter,i).Parameters = coeffvalues(fitresult);
        out(counter,i).Geometry = char(Geometry(1,i));
        out(counter,i).Ci = ci(cat);
        out(counter,i).Cw = cw(cat);
    end
    counter = counter + 1;
    end
```

Function for finding parameters for two dependent variables and individual power exponent –with parallel processing–

```
function [out] = raw_calc_2D(par1, par2, par4)
global Geometry dep indep3 indep
ci = 0.05;
cw = 0.35;
dep_n = dep(1:size(dep,2)-1);
indep1 = indep;
indep1 = indep1(1:size(indep1,2)-1);
indep3_n = indep3(1:size(indep3,2)-1);
s = size(par1,2);
fitresult = cell( 1, 1 );
counter = 1;
gof = struct( 'sse', cell( 1, 1 ), 'rsquare', [], 'dfe', [], 'adjrsquare', [], 'rmse', [] );
out =
struct('Title',[],'dependant',[],'Independent_1',[],'Independent_2',[],'type',[],'rsquare',[],'Par
ameters',[], 'Geometry', [], 'Ci', [], 'Cw', [], 'calculated', [], 'original', []);
ft = fittype( 'a * x ^ b * y ^ c', 'independent', {'x', 'y'}, 'dependent', 'z' );
parfor i = 1:s
    warning off;
    opts = fitoptions( 'Method', 'NonlinearLeastSquares');
    opts.DiffMaxChange = 0.2;
    opts.DiffMinChange = 1e-20;
    opts.Display = 'Off';
    opts.MaxFunEvals = 100000;
    opts.MaxIter = 100000;
    opts.StartPoint = [0 0 0];
    opts.Algorithm = 'Levenberg-Marquardt';
    opts.TolFun = 1e-25;
    opts.TolX = 1e-25;
    [xData, yData, zData] = prepareSurfaceData( par2(:,i), par4(:,i), par1(:,i));
    [fitresult, gof] = fit( [xData, yData], zData, ft,opts );
    out(counter,i).Title = [dep_n, ' vs. ',indep1, ' & ',indep3_n];
```

```
    out(counter,i).dependant = dep_n;
    out(counter,i).Independent_1 = indep1;
    out(counter,i).Independent_2 = indep3_n;
    out(counter,i).type = formula(ft);
    out(counter,i).rsquare = gof.rsquare;
    out(counter,i).Parameters = coeffvalues(fitresult);
    out(counter,i).Geometry = char( Geometry (1,i) );
    out(counter,i).Ci = ci;
    out(counter,i).Cw = cw;
    out(counter,i).original = zData;
    out(counter,i).calculated = fitresult([xData, yData]);
end
r2 = 0;
r2min = 1;
count = 0;
rms = 0;
for i = 1:s
    r2 = r2 + out(1,i).rsquare;
    rms = rms + out(1,i).rsquare^2;
    r2min = min (r2min, out(1,i).rsquare);
    count = count + 1;
end
r2 = r2 / count;
rms = sqrt(rms / count);
if r2min < 0.9
    display(['For a,', dep_n, ' ', indep1, ' ', indep3_n, ' ','r2 = ',num2str(r2,'%.6g'),
    ' rms = ',num2str(rms,'%.6g'), ' min r2 = ',num2str(r2min,'%.6g')]);
end
r2 = 0;
r2min = 1;
count = 0;
rms = 0;
end
```

Function for trimming result tables

```
function [out] = trim(input1, input2, input3)
row = 1;
trimmed(row,:) = input1(row,:);
row = row + 1;
for i = 2:size(input1,1)
    if (input1{i,input2} > input3)
        trimmed(row,:) = input1(i,:);
        row = row + 1;
    end
end
out = trimmed;
end
```

Subroutine for calculating correlations between calculated parameters and geometry's characteristics

```
ci = [0.05,0.05,0,0];
cw = [0.35,1,0.35,1];
for c1 = 1:size(Dep1,2)
    for i = 1:size(InDep1,2)
        for d = 1:4
            for k = 1:size(Type1,2)
                for l = 1:size(InDep3,2)
                    dep = [Dep1{c1}, num2str(d)];
                    indep = [InDep1{i}, num2str(d)];
                    typ = Type1{k};
                    par = parameters.(dep).(indep).(typ)(1,:);
                    var_n = [InDep3{l}, num2str(d)];
                    var = eval(var_n);
                    var = var(1,:);
                    [param.(dep).(indep).(typ).a.(var_n)] = calc(var,par);
                    param.(dep).(indep).(typ).a.(var_n).Title = ['a for ',
                    Dep1{c1}, '-', InDep1{i},
                    '-', Type1{k}, '-', num2str(ci(d)), '-', num2str(cw(d)), ' vs.
                    ',InDep3{l}];
                    param.(dep).(indep).(typ).a.(var_n).dependent =
                    Dep1{c1};
                    param.(dep).(indep).(typ).a.(var_n).independent_1 =
                    InDep1{i};
                    param.(dep).(indep).(typ).a.(var_n).quality =
                    general_1D.(dep).(indep).(typ).r2_aver;
                    param.(dep).(indep).(typ).a.(var_n).Based = InDep3{l};
                    param.(dep).(indep).(typ).a.(var_n).Ci = ci(d);
                    param.(dep).(indep).(typ).a.(var_n).Cw = cw(d);
                    if k == 2
                        par = parameters.(dep).(indep).(typ)(2,:);
                        [param.(dep).(indep).(typ).(var_n).c] =
```

```
                calc(var,par);
                param.(dep).(indep).(typ).(var_n).c.Title = ['c
                for ', Dep1{c1}, '-',
                InDep1{i}, '-', Type1{k}, '-', num2str(ci(d)), '-',
                num2str(cw(d)), ' vs. ', InDep3{l}];
                param.(dep).(indep).(typ).(var_n).c.dependent =
                Dep1{c1};
                param.(dep).(indep).(typ).(var_n).c.
                independent_1 = InDep1{i};
                param.(dep).(indep).(typ).(var_n).c.Ci = ci(d);
                param.(dep).(indep).(typ).(var_n).c.Cw = cw(d);
            end
        end
    end
  end
end
```

Function for exporting the fitted curves between calculated equations' parameters and independent characteristics, in tabular format

```
function [output] = export_param(data)
global Geometry Dep1 InDep1 Type1 InDep3;
ci = [0.05,0.05,0,0];
cw = [0.35,1,0.35,1];
clear Out1;
row = 2;
c = 1;
Out1{1,c} = 'Dependent';
c = c+1;
Out1{1,c} = 'Original dependent';
c = c+1;
Out1{1,c} = 'Original independaet';
c = c+1;
Out1{1,c} = 'Original equation';
c = c+1;
Out1{1,c} = 'Ci';
c = c+1;
Out1{1,c} = 'Cw';
c = c+1;
Out1{1,c} = 'Original quality of fit';
c = c+1;
Out1{1,c} = 'Independent';
c = c+1;
Out1{1,c} = 'Equation';
c = c+1;
Out1{1,c} = 'R2';
c = c+1;
Out1{1,c} = 'a';
c = c+1;
Out1{1,c} = 'b';
c = c+1;
```

```
for c1 = 1:size(Dep1,2)
    for i = 1
        for d = 1:1
            for k = 1:size(Type1,2)
                for l = 1:size(InDep3,2)
                    c = 1;
                    dep = [Dep1{c1}, num2str(d)];
                    indep = [InDep1{i}, num2str(d)];
                    typ = Type1{k};
                    var_n = [InDep3{l}, num2str(d)];
                    Out1{row,c} = ['a for ', Dep1{c1}, '-', InDep1{i}, '-',
                    Type1{k}, '-',
                    num2str(ci(d)), '-', num2str(cw(d))];
                    c = c+1;
                    Out1{row,c} = Dep1{c1};
                    c = c+1;
                    Out1{row,c} = InDep1{i};
                    c = c+1;
                    Out1{row,c} = Type1{k};
                    c = c+1;
                    Out1{row,c} = ci(d);
                    c = c+1;
                    Out1{row,c} = cw(d);
                    c = c+1;
                    Out1{row,c} =
                    data.(dep).(indep).(typ).a.(var_n).quality;
                    c = c+1;
                    Out1{row,c} = InDep3{l};
                    c = c+1;
                    Out1{row,c} = 'a * x ^ b'
                    c = c+1;
                    Out1{row,c} =
                    data.(dep).(indep).(typ).a.(var_n).rsquare;
                    c = c+1;
```

```
                Out1{row,c} =
                data.(dep).(indep).(typ).a.(var_n).Parameters(1);
                c = c+1;
                Out1{row,c} =
                data.(dep).(indep).(typ).a.(var_n).Parameters(2);
                c = c+1;
                row = row + 1;
                try
                    data.(dep).(indep).(typ).c.rsquare;
                    c = 1;
                    Out1{row,c} = ['c for ', Dep1{c1}, '-',
                    InDep1{i}, '-', Type1{k}, '-',
                    num2str(ci(d)), '-', num2str(cw(d))];
                    c = c+1;
                    Out1{row,c} = InDep3{l};
                    c = c+1;
                    Out1{row,c} = 'a * x ^ b';
                    c = c+1;
                    Out1{row,c} =
                    data.(dep).(indep).(typ).c.(var_n).rsquare;
                    c = c+1;
                    Out1{row,c} = data.(dep).
                    (indep).(typ).c.(var_n).Parameters(1);
                    c = c+1;
                    Out1{row,c} = data.(dep).
                    (indep).(typ).c.(var_n).Parameters(2);
                    c = c+1;
                    row = row + 1;
                catch
                end
            end
        end
    end
end
```

```
end
[output] = Out1;
end
```

Function for exporting fitted curves' parameters in tabular format

```
function [output] = export_1D(data)
global Geometry Dep1 Flow Type;
clear Out1;
row = 2;
c = 1;
Out1{1,c} = 'Dependent';
c = c+1;
Out1{1,c} = 'Independent';
c = c+1;
Out1{1,c} = 'Equation';
c = c+1;
Out1{1,c} = 'Average R2';
c = c+1;
Out1{1,c} = 'b';
c = c+1;
for i = 1:size(Geometry,2)
    Out1{1,c} = ['R2 for ', char(Geometry(1,i))];
c = c+1;
    Out1{1,c} = ['a for ', char(Geometry(1,i))];
c = c+1;
    Out1{1,c} = ['c for ', char(Geometry(1,i))];
c = c+1;
end
for c1 = 1:size(Dep1,2)
    depen = Dep1{c1};
    for t = 1:4
        type = Type{t};
        for f = 1:size(Flow,2)
            indep = Flow{f};
            c = 1;
            Out1{row,c} = depen;
            c = c+1;
```

```
            Out1{row,c} = indep;
            c = c+1;
            Out1{row,c} = data.(depen).(indep).(type).type;
            c = c+1;
            Out1{row,c} = data.(depen).(indep).(type).r2_aver;
            c = c+1;
            Out1{row,c} = data.(depen).(indep).(type).b_all;
            c = c+1;
            for i = 1:size(Geometry,2)
                Out1{row,c} = data.(depen).(indep).(type).r2(i);
                c = c+1;
                Out1{row,c} = data.(depen).(indep).(type).a(i);
                c = c+1;
                try
                    Out1{row,c} = data.(depen).(indep).(type).c(i);
                catch
                end
                c = c + 1;
            end
            row = row + 1;
        end
    end
end
[output] = Out1;
end
```

Function for exporting fitted surfaces' parameters in tabular format

```
function [out1,out2,out3,out4] = export_2D(input1,input2)
global Geometry Dep1 Dep2 InDep2 InDep3 ;
s1 = size(Geometry,2);
ci = [0.05,0.05,0,0];
cw = [0.35,1,0.35,1];
s2 = 3;
row = 2;
c = 1;
Min1 = 1;
Min2 = 1;
Out1{1,c} = 'Dependant';
Out2{1,c} = Out1{1,c};
Out3{1,c} = Out1{1,c};
Out4{1,c} = Out1{1,c};
c = c+1;
Out1{1,c} = 'Independent 1';
Out2{1,c} = Out1{1,c};
Out3{1,c} = Out1{1,c};
Out4{1,c} = Out1{1,c};
c = c+1;
Out1{1,c} = 'Independent 2';
Out2{1,c} = Out1{1,c};
Out3{1,c} = Out1{1,c};
Out4{1,c} = Out1{1,c};
c = c+1;
Out1{1,c} = 'Original equation min R2';
Out2{1,c} = Out1{1,c};
Out3{1,c} = Out1{1,c};
Out4{1,c} = Out1{1,c};
c = c+1;
Out1{1,c} = 'Min R2';
Out2{1,c} = Out1{1,c};
```

```
Out3{1,c} = Out1{1,c};
Out4{1,c} = Out1{1,c};
c = c+1;
for i = 1:s1
    Out1{1,c} = char(Geometry(1,i));
Out2{1,c} = Out1{1,c};
Out3{1,c} = Out1{1,c};
Out4{1,c} = Out1{1,c};
c = c+1;
end
for d = 1
    for c1 = 1:size(Dep1,2)
        for i = 1
            depen = [Dep1{c1},num2str(d)];
            for ii = 1:size(InDep3,2)
                c = 1;
                indep3 = [InDep3{ii},num2str(d)];
                Out1{row,c} = input1.(depen).Re1.(indep3)(i,1).dependant;
                Out2{row,c} = Out1{row,c};
                Out3{row,c} = Out1{row,c};
                Out4{row,c} = Out1{row,c};
                c = c+1;
                Out1{row,c} =
                input1.(depen).Re1.(indep3)(i,1).Independent_1;
                Out2{row,c} = Out1{row,c};
                Out3{row,c} = Out1{row,c};
                Out4{row,c} = Out1{row,c};
                c = c+1;
                Out1{row,c} =
                input1.(depen).Re1.(indep3)(i,1).Independent_2;
                Out2{row,c} = Out1{row,c};
                Out3{row,c} = Out1{row,c};
                Out4{row,c} = Out1{row,c};
                c = c+3;
```

```
            for j = 1:s1
                Min2 =
                min(Min2,input1.(depen).Re1.(indep3)(i,j).rsquare);
                Min1 = min(Min1,input2.(depen).Re1(i,j).rsquare);
                Out1{row,c} =
                input1.(depen).Re1.(indep3)(i,j).Parameters(1);
                Out2{row,c} =
                input1.(depen).Re1.(indep3)(i,j).Parameters(2);
                Out3{row,c} =
                input1.(depen).Re1.(indep3)(i,j).Parameters(3);
                Out4{row,c} =
                input1.(depen).Re1.(indep3)(i,j).rsquare;
                c = c+1;
            end
            c = 4;
            Out1{row,c} = Min1;
            Out2{row,c} = Out1{row,c};
            Out3{row,c} = Out1{row,c};
            Out4{row,c} = Out1{row,c};
            Min1 = 1;
            c = c + 1;
            Out1{row,c} = Min2;
            Out2{row,c} = Out1{row,c};
            Out3{row,c} = Out1{row,c};
            Out4{row,c} = Out1{row,c};
            Min2 = 1;
            row = row + 1;
        end
    end
end
end
for d = 1
    for c1 = 1:size(Dep2,2)
        for i = 1
```

```
for n = 1:size(InDep2,2)
    indep = [InDep2{n},num2str(d)];
    depen = [Dep2{c1},num2str(d)];
    for ii = 1:size(InDep3,2)
        c = 1;
        indep3 = [InDep3{ii},num2str(d)];
        Out1{row,c} =
        input1.(depen).(indep).(indep3)(i,1).dependant;
        Out2{row,c} = Out1{row,c};
        Out3{row,c} = Out1{row,c};
        Out4{row,c} = Out1{row,c};
        c = c+1;
        Out1{row,c} =
        input1.(depen).(indep).(indep3)(i,1).Independent_1;
        Out2{row,c} = Out1{row,c};
        Out3{row,c} = Out1{row,c};
        Out4{row,c} = Out1{row,c};
        c = c+1;
        Out1{row,c} =
        input1.(depen).Re1.(indep3)(i,1).Independent_2;
        Out2{row,c} = Out1{row,c};
        Out3{row,c} = Out1{row,c};
        Out4{row,c} = Out1{row,c};
        c = c+3;
        for j = 1:s1
            Min1 =
            min(Min1,input2.(depen).(indep)(i,j).rsquare);
            Min2 = min(Min2,input1.(depen).(indep).
            (indep3)(i,j).rsquare);
            Out1{row,c} = input1.(depen).(indep).
            (indep3)(i,j).Parameters(1);
            Out2{row,c} = input1.(depen).(indep).
            (indep3)(i,j).Parameters(2);
            Out3{row,c} = input1.(depen).(indep).
```

```
                (indep3)(i,j).Parameters(3);
                Out4{row,c} = input1.(depen).(indep).
                (indep3)(i,j).rsquare;
                c = c+1;
            end
            c = 4;
            Out1{row,c} = Min1;
            Out2{row,c} = Out1{row,c};
            Out3{row,c} = Out1{row,c};
            Out4{row,c} = Out1{row,c};
            Min1 = 1;
            c = c + 1;
            Out1{row,c} = Min2;
            Out2{row,c} = Out1{row,c};
            Out3{row,c} = Out1{row,c};
            Out4{row,c} = Out1{row,c};
            Min2 = 1;
            row = row + 1;
        end
    end
  end
end
out1 = Out1;
out2 = Out2;
out3 = Out3;
out4 = Out4;
end
```